Precoding Schemes for Millimeter Wave Massive MIMO Systems

Prabhat Raj Gautam

The University of Leeds

School of Electronic and Electrical Engineering

Submitted in accordance with the requirements for the degree of Doctor of Philosophy

March, 2023

Declaration

The candidate confirms that the work submitted is his own and that appropriate credit has been given where reference has been made to the work of others. The material contained in the chapters of this thesis has been previously published in research articles written entirely by the author of this thesis who also appears as the lead author in all published papers. The research has been supervised and guided by Dr. Li Zhang who appears as the coauthor in all the published articles. All the materials included in this document are of the author's intellectual ownership.

The work in Chapter 2 of the thesis has appeared in publication as follows:

- P. R. Gautam and L. Zhang, "Hybrid Precoding for Millimeter Wave MIMO: Trace Optimization Approach," in *IEEE Access*, vol. 10, pp. 66874-66885, 2022.

The work in Chapter 3 of the thesis has appeared in publication as follows:

- P. R. Gautam and L. Zhang, "Hybrid Precoding for Partial-Full Mixed Connection mmWave MIMO," *2021 IEEE Statistical Signal Processing Workshop (SSP)*, 2021, pp. 271-275.

The work in Chapter 4 of the thesis has appeared in publication as follows:

- P. R. Gautam and L. Zhang, "Hybrid SLNR Precoding for Multi-user Millimeter Wave MIMO Systems," *2019 22nd International Symposium on Wireless Personal Multimedia Communications (WPMC)*, 2019, pp. 1-6.

The work in Chapter 5 of the thesis is based on the following submitted paper.

- P. R. Gautam, L. Zhang and P. Fan, "Hybrid MMSE Precoding for Millimeter

Wave MU-MISO via Trace Maximization,"in *IEEE Transactions on Wireless Communications*, Submitted.

The contribution of Prof. Pingzhi Fan: Prof. Fan reviewed the manuscript and provided his valuable suggestions to improve the manuscript.

Dedicated to my wife and my parents

Abstract

In an effort to cut high cost and power consumption of radio frequency (RF) chains, millimeter wave (mmWave) multiple input multiple output (MIMO) deploys hybrid architecture in which precoding is implemented as a combination of digital precoding and analog precoding, accomplished by using a smaller number of RF chains and a network of phase shifters respectively. The mmWave MIMO, which usually suffers from blockages, needs to be supported by Reconfigurable Intelligent Surface (RIS) to make communication possible. Along with the hybrid precoding in mmWave MIMO, the passive precoding of Reconfigurable Intelligent Surface (RIS) is investigated in a downlink RIS-assisted mmWave MIMO. The hybrid precoding and passive precoding are challenged by the unit modulus constraints on the elements of analog precoding matrix and passive precoding vector. The coupling of analog and digital precoders further complicates the hybrid precoding.

One of the approaches taken in proposed hybrid precoding algorithms is the use of alternating optimization in which analog precoder and digital precoder are optimized alternately keeping the other fixed. Analog precoder is determined by solving a semidefinite programming problem, and from the unconstrained least squares solution during each iteration. In another approach taken in the proposed methods, the hybrid precoding is split into separate analog and digital precoding subproblems. The analog precoding subproblems are simplified using some approximations, and solved by using iterative power method and employing a truncated singular value decomposition method in two different hybrid precoding algorithms. In the prooposed codebook-based precoder, analog precoder is constructed by choosing precoding vectors from a codebook to maximize signal-to-leakage-and-noise ratio (SLNR).

The passive precoding at the RIS in a single user MIMO is designed to minimize mean square error between the transmit signal and the estimate of received signal by using an iterative algorithm that solves the joint optimization problem of precoding, passive precoding and combiner. The problem of designing energy efficient RIS is solved by maximizing energy efficiency which is a joint optimization problem involving precoder, passive precoding matrix and power allocation matrix. The proposed hybrid precoding and passive precoding algorithms deliver very good performances and prove to be computationally efficient.

Acknowledgements

I take this opportunity to express my deepest sense of gratitude toward my supervisor Dr Li Zhang for her constant guidance and support throughout my PhD study and research. Her motivation and suggestions have been instrumental in shaping my research and thesis.

My sincere thanks Dr. MiaoMiao Liu, then my senior lab mate at ICAPNET, for helping me get started with my PhD. I would like to acknowledge my wife, Suraksha Neupane for always believing in me, and being my pillar of support. I could not have successfully completed my PhD without her.

Contents

List of Figures

List of Abbreviations

ADC	Analog-to-digital converter
ADMM	Alternating direction method of multipliers
AO	Alternating optimization
AoA	Angle of arrival
AoD	Angle of departure
AP	Access point
BCD	Block Coordinate Descent
BS	Base station
BER	Bit error rate
CCI	Co-channel interference
CDF	Cumulative distribution function
CSI	Channel state information
DAC	Digital-to-analog converter
DFT	Discrete Fourier Transform
EVD	Eigenvalue Decomposition
FC	Fully connected
FPGA	Field programmable gate array
GEVD	Generalized Eigenvalue Decomposition
IFFT	Inverse Fast Fourier Transform
KKT	Karush-Kuhn Tucker
LNA	Low Noise Amplifier
LoS	Line of sight
MBCD	Modified Block Coordinate Descent

mmWave	Millimeter wave
MO	Manifold optimization
MSE	Mean square error
MMSE	Minimum mean square error
MS	Mobile station
MIMO	Multiple Input Multiple Output
MU-MIMO	Multi-user Multiple Input Multiple Output
MU-MISO	Multi-user Multiple Input Single Output
OFDM	Orthogonal frequency division multiplexing
OMP	Orthogonal Matching Pursuit
PC	Partially connected
PC	Partial-Full mixed connection
QoS	Quality of Service
RF	Radio Frequency
RIS	Reconfigurable Intelligent Surface
RTHI	Residual Transceiver Hardware Impairment
s.t.	subject to
SDP	Semidefinite programming
SDP	Semidefinite relaxation
SIC	Successive interference cancellation
SNR	Signal-to-noise ratio
SINR	Signal-to-interference-and-noise ratio
SLNR	Signal-to-leakage-and-noise ratio
SVD	Singular Value Decomposition
THz	Tera Hertz
ULA	Uniform Linear Array
UPA	Uniform Planar Array
ZF	Zero-forcing

Notations

x	scalar
$\mathbf{x}$	vector
$\mathbf{X}$	matrix
$i:j$	all the integers from i to j ,
	i.e., $i, i+1, \ldots, j-1, j$
$\mathbf{X}_{i,j}$	$(i,j)^{th}$ element of $\mathbf{X}$
$\mathbf{X}_{\cdot j}$	the j^{th} column of $\mathbf{X}$
$\mathbf{X}_{i\cdot}$	the i^{th} row of $\mathbf{X}$
$\mathbf{X}_{i^c,j}$	the j^{th} column of $\mathbf{X}$ with i^{th} row removed
$\mathbf{X}_{i,j^c}$	the i^{th} row of matrix $\mathbf{X}$ with j^{th} column removed
$\mathbf{X}_{a:b,m:n}$	submatrix of $\mathbf{X}$ with rows a to b, and columns
	m to n
$\mathbf{X}_{:,m:n}$	submatrix of $\mathbf{X}$ with all rows, and columns m to n
$\mathbf{X}_{a:b,:}$	submatrix of $\mathbf{X}$ with rows a to b, and all columns
$\exp(.)$	exponential operator
$\exp(\mathbf{X})$	a matrix whose $(i,j)^{th}$ entry is $\exp(\mathbf{X}_{i,j})$
$[a_{ij}]_{mn}$	$m \times n$ matrix whose $(i,j)^{th}$ element is a_{ij}
$\mathbf{x}_i$	i^{th} element of vector $\mathbf{x}$
$\lvert\mathbf{x}\rvert$	2-norm of $\mathbf{x}$
$\lVert\mathbf{X}\rVert_F$	Frobenius norm of $\mathbf{X}$
$\mathbf{X} \in \mathbf{H}_p$	$\mathbf{X}$ lies in the cone of Hermitian matrices
	of dimension p
$rank(\mathbf{X})$	rank of matrix $\mathbf{X}$

$min(.,\ldots,.)$	minimum of the arguments
$\mathbf{X} \succ \mathbf{0}$	$\mathbf{X}$ is a positive definite matrix
$\mathbf{X} \succeq \mathbf{0}$	$\mathbf{X}$ is a positive semidefinite matrix
$(.)^T$	transpose
$(.)^*$	conjugate
$(.)^{-1}$	inverse
$(.)^H$	Hermitian transpose
$(.)^\dagger$	pseudoinverse
$\odot$	Hadamard product of two matrices
$\mathbf{I}_N$	$N \times N$ identity matrix
$\mathbf{0}_N$	$N \times N$ null matrix
$\mathbf{1}_{m\times n}$	$m \times n$ matrix having all 1s
$\mathbf{DIAG}\,(a_1,\ldots,a_n)$	diagonal matrix with $a_1,\ldots,a_n$ as its diagonal elements
$\mathbf{diag}\,(\mathbf{X})$	column vector corresponding to the diagonal of $\mathbf{X}$
$\mathbf{BLKDIAG}\,(\mathbf{A}_1,\ldots,\mathbf{A}_n)$	block diagonal matrix with $\mathbf{A}_1,\ldots,\mathbf{A}_n$ on its diagonal
$\mathbb{R}$	set of real numbers
$\mathbb{R}_+$	set of positive real numbers
$\Re(.)$	the real part of
$\mathcal{O}$	standard big-O notation
$\mathbb{E}[.]$	expectation operator
$\sim$	has the probability distribution of
$\triangleq$	is defined as
$\mathcal{CN}(\boldsymbol{\mu}, \mathbf{C})$	complex Gaussian vector with mean $\boldsymbol{\mu}$ and covariance matrix $\mathbf{C}$.

Chapter 1

An Introduction to Millimeter Wave MIMO and Precoding

1.1 Background and Motivation

Over the past decade, the number of users having access to mobile communication services has increased by leaps and bounds all over the world. The use of smart phones and smart devices which use cellular data is on the rise and so is the demand for seamless high speed data rates. It has been predicted that the mobile data usage will increase by more than thousand-folds in a decade's time [1]. To meet such dilating demands of cellular data rates, more spectrum needs to be put into use. All of the current mobile communication services operate within the frequency range of 300 MHz-3 GHz, known as sub-3 GHz band. Unfortunately, most of the spectrum in the sub-3 GHz band is already in use [1].

Spectrum refarming was believed to free up significant spectrum to be used for cellular communication. However, one such attempt at spectrum refarming, the reassigning of terrestrial TV spectrum to other broadband access failed to free up more than 80 MHz, that too at high cost of shifting the occupants [2]. Employing smaller cells such as femtocells can increase capacity per geographic area linearly with the number of cells, but not enough to fulfill the capacity required to accommodate gargantuan

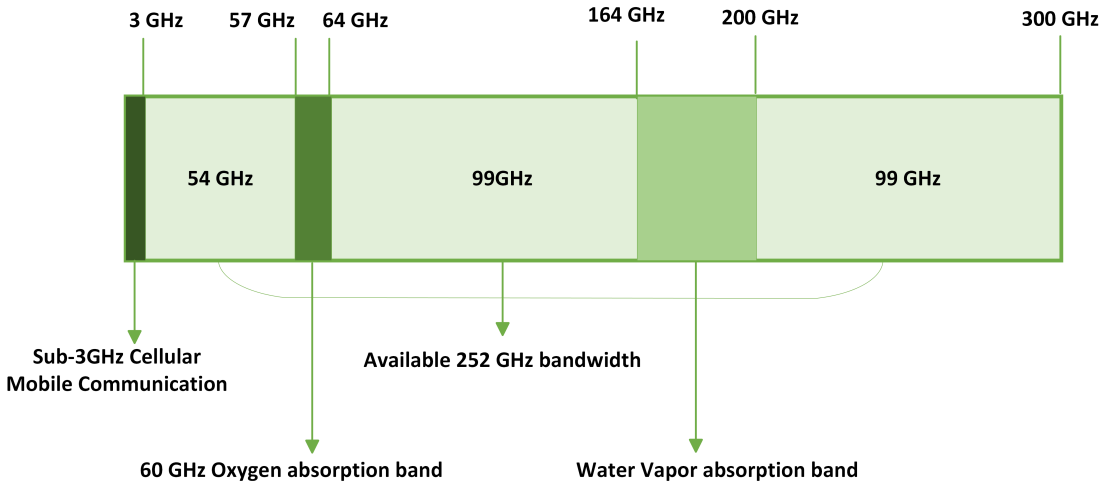

Figure 1.1: mmWave spectrum [1]

increase in mobile data traffic [1]. In short, it is impossible to squeeze out more spectrum for cellular communications from sub-3 GHz band and the current cellular spectrum would fall quite short to satisfy the mobile data need of the *not-so-distant* future. On the other hand, there is a huge spectrum in 3 GHz-300 GHz range which is mostly unused. The 3–30 GHz band, known as the super high frequency (SHF) band and 30–300 GHz spectrum, known as the extremely high frequency (EHF) or millimeter-wave band share similar propagation characteristics. Hence, the 3 GHz-300 GHz spectrum whose wavelength vary from 1 mm to 100 mm is collectively referred to as millimeter wave (mmWave) band [1]. mmWave communication offers large unused bandwidth that provides the future wireless communication technology a key to unleash the potential of achieving very high data rates in order of tens of gigabits-per-second [2–8].

mmWave communication has been attracting a lot of interest from academia and industry alike as an alternative for future cellular wireless communications. Studies have been done to understand the propagation characteristics of 28 GHz and 38 GHz frequencies in [9]. The mmWave frequencies, owing to their smaller wavelengths, are more sensitive to blockages and suffer from huge attenuation due to absorption or scattering by gases and rain particles, compared to the microwave frequencies [10, 11]. The measurements have shown that path loss of mmWave frequencies varies with distance and non-line-of-sight communication is feasible [2]. The measurements

in [9] show that path-loss exponent varied from 1.68 to 2.55 in LOS propagation and 4.58 to 5.76 in non-line-of-sight case. The studies have shown that for distances up to 200 m, the path-loss in mmWave frequencies is similar to that in microwave frequencies after considering additional beamforming gain [12].

On the other hand, the high path-loss suffered by mmWave frequencies can be reimbursed by employing massive multiple input multiple output (MIMO) systems which furnish large antenna array gain [2, 4, 13–15]. Thus, the union of mmWave communication with massive MIMO, termed as mmWave massive MIMO, has manifested itself as an encouraging prospect for cellular wireless systems. Moreover, mmWave massive MIMO antenna array can be accommodated in a small packing area because of smaller antenna size [4].

The most challenging hurdle faced by mmWave systems is expensive and high power consuming mixed signal components, mainly the analog-to-digital converters (ADCs) and digital-to-analog converters (DACs). In the traditional microwave systems, every antenna is connected to a high-rate ADC/DAC . With current semi-conductor technology, it is impossible for mmWave system to have similar architecture, keeping implementation budget in check [2]. Thus, the millimeter wave (mmWave) MIMO can not be implemented with conventional MIMO architectures, at least with the current advancement in semiconductor technology [1]. Hence, the fully digital precoding or channel estimation techniques implemented in conventional MIMO systems can not be applied to mmWave massive MIMO as the architecture is going to be different. Since very large antenna arrays are deployed at the base station (BS) and the mobile station (MS), the transmitter and receiver both need to design precoding and combining matrices that are huge in size. The huge MIMO system also makes precoding and channel estimation more complex. The precoding techniques in mmWave massive MIMO is an active research area and has been garnering a lot of attention.

1.2 Millimeter Wave Channel Model

1.2.1 Clustered Channel Model

The existing models for mmWave channels such as the channel models standardized for IEEE 802.11ad indoor 60 GHz channels, are based on Saleh-Valenzuela clustered channel model [16]. In clustered channel model, scatterers and reflectors that contribute to multiple paths are grouped into several clusters. Each cluster ricochets a series of paths [17]. The channel matrix is taken to be sum total of the contributions of a number of scatterers, each contributing a number of propagation paths [18]. The clustered channel model describes the paths as arriving in clusters with each cluster associated with some distribution on the delay, power and angles of arrival and departure. Clustering can be the outcome of reflections from surfaces, scattering from objects, diffraction from the small openings and the transmission through soft partitions [17]. Physically, the clusters correspond to different macro-level paths, and the angle and delay spreads within each cluster capture the scattering along these paths [12].

We consider a system with N_t transmit antennas and N_r receive antennas. We assume there are N_c clusters between the transmitter and the receiver; N_{p_i} is the number of paths in i^{th} cluster; the $i\ell^{th}$ path which has a complex gain of $\alpha_{i\ell}$ makes an angle of $\phi_{i\ell}^t$ with transmit array and an angle of $\phi_{i\ell}^r$ with the receive array. The subscript "$i\ell$" indicates a parameter associated with ℓ^{th} path in i^{th} cluster. The angles are measured relative to the horizontal axis. The multipath model can be used to define channel matrix $\mathbf{H}$ [17, 19] as

$$\mathbf{H}(t,f) = \sqrt{\frac{N_t N_r}{\sum_i N_{p_i}}} \sum_{i=1}^{N_c} \sum_{\ell=1}^{N_{p_i}} \alpha_{i\ell} e^{-j2\pi\tau_{i\ell}f} e^{j2\pi\nu_{i\ell}t} \mathbf{a}_r(\phi_{i\ell}^r)\mathbf{a}_t(\phi_{i\ell}^t)^H, \tag{1.1}$$

where $\sqrt{\frac{N_t N_r}{\sum_i N_{p_i}}}$ is the normalization factor, f is carrier frequency, $\nu_{i\ell}$ is the Doppler shift associated with the $i\ell^{th}$ path, $\tau_{i\ell}$ is the delay associated with the $i\ell^{th}$ path and $\mathbf{a}_r(\phi_{i\ell}^r)$ and $\mathbf{a}_t(\phi_{i\ell}^t)$ are the array steering vectors of the receive and transmit

antenna arrays respectively. The Doppler shifts, $\{\nu_{i\ell}\}_{\ell=1}^{N_{p_i}}, i = 1, \ldots, N_c$ incorporate the channel variation in time, whereas the path delays, $\{\tau_{i\ell}\}_{\ell=1}^{N_{p_i}}, i = 1, \ldots, N_c$ embody the channel variation in frequency [20]. In the 3D-channel model, the array steering vectors are functions of both the azimuth angle ϕ and elevation angle θ [12], so the channel matrix is given by

$$\mathbf{H}(t,f) = \sqrt{\frac{N_t N_r}{\sum_i N_{p_i}}} \sum_{i=1}^{N_c} \sum_{\ell=1}^{N_{p_i}} \alpha_{i\ell} e^{-j2\pi\tau_{i\ell}f} e^{j2\pi\nu_{i\ell}t} \mathbf{a}_r(\phi_{i\ell}^r, \theta_{i\ell}^r) \mathbf{a}_t(\phi_{i\ell}^t, \theta_{i\ell}^t)^H. \tag{1.2}$$

If it is assumed that the channel is slowly varying during signal duration of interest T, the Doppler shifts associated with all the paths are small, *i.e.*, $\nu_{i\ell}T \ll 1 \ \forall i, \ell$, $\ell = 1, \ldots, N_{p_i}$ and $i = 1, \ldots, N_c$. We can then approximately write (1.2) as

$$\mathbf{H}(f) = \sqrt{\frac{N_t N_r}{\sum_i N_{p_i}}} \sum_{i=1}^{N_c} \sum_{\ell=1}^{N_{p_i}} \alpha_{i\ell} e^{-j2\pi\tau_{i\ell}f} \mathbf{a}_r(\phi_{i\ell}^r, \theta_{i\ell}^r) \mathbf{a}_t(\phi_{i\ell}^t, \theta_{\ell}^t)^H. \tag{1.3}$$

If it is further assumed that the bandwidth of the input W is considerably smaller than the coherence bandwidth of the channel so that $W\tau_{i\ell} \ll 1 \ \forall i, \ell$, $\ell = 1, \ldots, N_{p_i}$ and $i = 1, \ldots, N_c$, the expression for narrowband model for channel matrix is obtained as

$$\mathbf{H}(f) = \sqrt{\frac{N_t N_r}{\sum_i N_{p_i}}} \sum_{i=1}^{N_c} \sum_{\ell=1}^{N_{p_i}} \alpha_{i\ell} e^{-j2\pi\tau_{i\ell}f} \mathbf{a}_r(\phi_{i\ell}^r, \theta_{i\ell}^r) \mathbf{a}_t(\phi_{i\ell}^t, \theta_{i\ell}^t)^H. \tag{1.4}$$

1.2.2 Millimeter Wave Wideband MIMO OFDM Channel

For the data transmission in frequency-selective channel, MIMO-Orthogonal Frequency Division Multiplexing (OFDM) is considered. It is assumed that the discrete-time channel comprises of multiple taps, corresponding to N_c different clusters. The discrete-time channel impulse response is given by [21, 22]

$$\mathbf{H}(n) = \sum_{i=0}^{N_c-1} \mathbf{H}_i(n)\delta(n-i), \tag{1.5}$$

where n is the discrete time index which corresponds to symbol period, $\delta(n)$ is Kronecker delta, and $\mathbf{H}_i(n)$ is the channel matrix associated with the i^{th} tap. Generally, the channel remains constant over many symbol periods because of the coherence of the channel which allows us to replace $\mathbf{H}_i(n)$ by $\mathbf{H}_i$, for simplicity [22]. The i^{th} matrix tap $\mathbf{H}_i$ is given by

$$\mathbf{H}_i = \sqrt{\frac{N_t N_r}{\sum_i N_{p_i}}} \sum_{\ell=1}^{N_{p_i}} \alpha_{i\ell} \mathbf{a}_r(\phi_{i\ell}^r, \theta_{i\ell}^r) \mathbf{a}_t(\phi_{i\ell}^t, \theta_{i\ell}^t)^H. \tag{1.6}$$

An OFDM system with S_c subcarriers is considered for transmission. Cyclic prefix of length C_p needs to be added to the transmit data in OFDM which occupies a fraction $\frac{C_p}{S_c + C_p}$ of the total time [17], and $C_p \geq N_c$. Thus, the number of subcarriers is chosen such that $S_c \gg N_c$, so the loss of transmission time and power is minimized. But the largest value S_c can take, is limited by the time-varying nature of the wireless channel [17]. The equivalent channel for the s^{th} subcarrier is obtained by performing S_c-point Discrete Fourier Transform (DFT) on channel impulse response [23] as

$$\mathbf{H}[s] = \frac{1}{\sqrt{S_c}} \sum_{i=0}^{N_c-1} \mathbf{H}_i e^{(-j\frac{2\pi}{S_c} si)}, \quad s = 0, \ldots, S_c - 1. \tag{1.7}$$

On substituting the value of $\mathbf{H}_i$ from (1.6), the expression for s^{th} OFDM subcarrier is acquired as

$$\mathbf{H}[s] = \sqrt{\frac{N_t N_r}{S_c \sum_i N_{p_i}}} \sum_{i=0}^{N_c-1} \sum_{\ell=1}^{N_{p_i}} \alpha_{i\ell} e^{(-j\frac{2\pi}{S_c} si)} \mathbf{a}_r(\phi_{i\ell}^r, \theta_{i\ell}^r) \mathbf{a}_t(\phi_{i\ell}^t, \theta_{i\ell}^t)^H, \quad s = 0, \ldots, S_c - 1. \tag{1.8}$$

1.2.3 Array Response Vector

If uniform planar array (UPA) of size $N_y \times N_z$ (N_y antenna elements along y-axis, and N_z along z-axis) is placed along yz-plane, the array response vector is given by

[23]

$$\mathbf{a}(\phi,\theta)=\frac{1}{\sqrt{N_yN_z}}\Big[1\ \ldots\ e^{j\zeta d(y\sin\phi\sin\theta+z\cos\theta)}\ \ldots\ e^{j\zeta d((N_y-1)\sin\phi\sin\theta+(N_z-1)\cos\theta)}\Big]^T, \tag{1.9}$$

where $\zeta=\frac{2\pi}{\lambda}$, λ being the carrier wavelength, d is the distance between antenna elements, and $0\leq y<N_y$ and $0\leq z<N_z$ are the antenna element indices. $N_yN_z=N$ is the total number of antenna elements in the array. If uniform linear array (ULA) is placed along y-axis, $N_z=1$ so that $N_y=N$. The array response vector of ULA can be obtained by setting $z=0$ in (1.9) as

$$\mathbf{a}(\phi,\theta)=\frac{1}{\sqrt{N}}\Big[1\quad e^{j\zeta d(\sin\phi\sin\theta)}\ \ldots\ e^{j\zeta d((N-1)\sin\phi\sin\theta)}\Big]^T. \tag{1.10}$$

The array response vector for an ULA is usually described only in terms of azimuth angle ignoring the elevation angle in literature as

$$\mathbf{a}(\phi))=\frac{1}{\sqrt{N}}\left[1\quad e^{j\zeta d\sin\phi}\ \ldots\ e^{j(N_t-1)\zeta d\sin\phi}\right]^T. \tag{1.11}$$

1.3 Millimeter Wave Massive MIMO architecture

As pointed out earlier, hardware constraints do not allow mmWave massive MIMO to be architecturally similar to conventional MIMO. In conventional MIMO, all the signal processing is performed digitally on the transmit signal, and the digitally processed signal is passesd through DACs and radio frequency (RF) chains before transmission through the channel. Each RF chain consists of frequency mixer, power amplifier and low noise amplifier. Each antenna in conventional MIMO is connected to a dedicated RF chain and ADC/DAC. High rate ADCs/DACs and RF chains, power amplifiers in particular, operating at millimeter wave frequency are expensive and operate on high power. Dedicating a single RF chain and ADC/DAC for each antenna element in mmWave massive MIMO would escalate the power consumption and installation cost to an unmanageable situation [12].

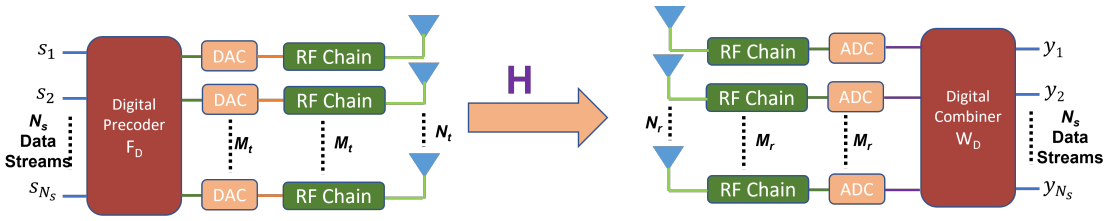

Figure 1.2: Conventional MIMO architecture

Restricted by the hardware constraints, signal processing in mmWave systems have been proposed to be divided in both analog and digital domains. This has given rise to hybrid architecture for mmWave massive MIMO where digital processing is performed using a limited number of RF chains which is very small compared to the number of antennas. Adoption of hybrid structure helps reduce the implementation cost and power consumption. The hybrid architecture can take one of the two forms, *viz.*, fully connected structure and partially connected structure, and will be explained shortly in the following section.

1.4 Precoding in mmWave MIMO and a Brief Review of Existing Works

Spatial multiplexing allows the transmission of multiple data streams simultaneously in the same channel through different antennas, so the multiplexing gain amplifies the system throughput [24]. If the channel state information (CSI) is available at the transmitter, some pre-processing can be performed on the symbols before transmission to transmit the symbols along the best spatial directions depending upon the type of performance criterion [24, 25]. A data stream is projected onto a beamforming vector before sending it spatially over the channel in beamforming [26]. This concept of beamforming is expanded to transmit multiple data streams spatially in linear precoding, thus making linear precoder intrinsically a form of multi-mode beamformer [25, 26]. Linear precoding multiplies the transmit data symbols by a precoding matrix that exploits the channel information to build vigor against the deformities introduced by the channel [27]. The purpose of precoding is to enable the transmit signal combat the interference and the noise it encounters

during transmission. Combining, which is similar to precoding, refers to the post-processing performed on the received signal so that the signal is correctly decoded. In conventional MIMO, the precoding (combining) is performed digitally at baseband. In mmWave MIMO, precoding (combining) is performed in both digital and analog domains termed as hybrid precoding (combining).

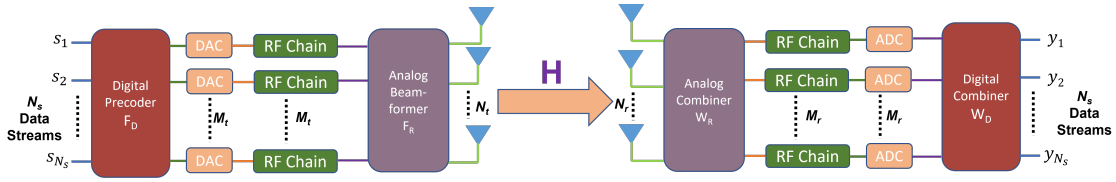

Figure 1.3: Hybrid mmWave MIMO architecture with M_{t} RF chains at BS and M_{r} RF chains at MS

The transmit symbols are first precoded digitally at baseband using a small number of RF chains and then analog precoding is applied before transmission. Such a hybrid mmWave MIMO architecture based on analog-digital precoding is shown in Figure 1.3. In the figure, $N_s \leq M_t < N_t$ and $N_s \leq M_r < N_r$. In the case where $N_s > 1$, multiplexing is possible so that multi-stream data to a single user, and multi-user MIMO both are supported. The special case where $N_s = M_r = M_t = 1$ implies application of analog beamforming only [12].

Several ways like phase shifters, switches, inverters and lenses have been studied to implement analog precoding. However, the use of phase shifters remains the most preferred approach in most of the works [18, 28–30]. The inverters and switches are favored in place of phase shifter network [31, 32] despite lower performance for lower power consumption. Hybrid architectures with phase shifter networks use phase shifters which can take one of the quantized phase values. The quantization level of the phases that a phase shifter supports, determines its power consumption [12]; higher the resolution, higher the power consumption.

If the phase shifters are used to realize analog precoding, all entries of analog precoding matrix need to satisfy unit amplitude constraint as phase shifters allow only the altering of phases, not the amplitudes. The hybrid structure may be fully connected or partially connected. Each RF chain is connected to all antennas in a fully connected structure (see Figure 1.4), whereas each RF chain is connected to

only a sub-set of antennas in partially connected structure (see Figure 1.5). While the complexity of a fully connected structure is high, it tenders full beamforming gain for each RF chain. On the other hand, the partially connected structure offers reduced complexity but at the cost of reduced beamforming gain [8].

The implementation of hybrid architecture in mmWave MIMO renders the direct use of conventional precoding schemes impossible. New algorithms need to be developed as the precoding matrix, as we will see later in section 1.6, is a product of analog precoding matrix and baseband precoding matrix, each of them having their own constraints.

The authors of [18] formulate the hybrid precoding problem as matrix factorization problem, and propose a hybrid precoder to solve it using Orthogonal Matching Pursuit (OMP). The authors in [33] and [34] consider multi-user scenario and aim to minimize the sum of mean squared error (MSE) for all users. Both [33] and [34] propose OMP-based hybrid minimum mean squared error (MMSE) precoders to minimize the sum-MSE for all users. The OMP-based hybrid precoders choose analog precoding vectors from a set of candidate vectors or a codebook. They are low on complexity but also come with low performance. Also depending on codebook to construct analog precoding matrix are the hybrid precoders in [30, 35], all of which consider a multi-user setting. In [30], the analog precoder and combiners are jointly chosen to maximize the received power.

In [36], Rusu *et al.* present various low complexity solutions to design the hybrid precoders for point-to-point MIMO with a view to approach the fully digital precoder. Of those various hybrid precoders in [36], hybrid precoder called *Hybrid Design by Least Squares Relaxation* (HD-LSR) exhibits very good performance. The HD-LSR algorithm uses heuristic relaxation based on least squares to update each entry of analog precoder. Sohrabi *et al.* [37] consider both point-to-point MIMO and multi-user multiple-input single-output (MU-MISO) systems, and propose hybrid precoding algorithms based on heuristic design.

It is shown in [37] that the minimum number of RF chains required to achieve the

performance of fully digital precoder is twice the number of data streams. On the other hand, Payami *et al.* [38] present how the hybrid precoder can be designed in such case to score the performance of a fully digital precoder. The authors of [38] prove that when number of RF chains is equal to number of data streams, the performance of fully digital precoder can be reached if two phase shifters and an adder are available for each RF chain. In [38], hybrid precoder is proposed that utilizes the properties of the singular vectors of the channel matrix to give asymptotically optimal solution.

Zhai *et al.* [39] propose an alternating optimization method to solve the problem of uplink sum rate maximization by splitting it into three subproblems. Yu *et al.* [40] present different alternating minimization algorithms based on manifold optimization (MO), semidefinite relaxation (SDR), and by enforcing orthogonality constraint on the digital precoder. In [41], the low complexity hybrid precoders are presented for the FC and PC architectures utilizing majorization-minimization and minorization-maximization structures respectively. Qiao *et al.* [42] break down the hybrid precoding problem for point-to-point MIMO into quadratically constrained quadratic programming (QCQP) subproblem and least-squares subproblem with constant-modulus constraint. The authors [42] present three alternating optimization (AO) algorithms, *viz.*, a) SDR-AO based on SDR, b) ADMM-AO based on alternating direction method of multipliers for the case when the number of transmit antennas is much larger than that of receive antennas or number of data streams is small, and c) ACMF-AO based on analytical constant modulus factorization for the case when RF chains and data streams are equal in number. Arora *et. al.* [41] consider fully connected and partially connected architectures, and propose separate low complexity algorithms based on majorization-minorization and minorization-majorization respectively.

In [43], analog precoder is determined first using iterative procedure involving generalized eigenvector decomposition (GEVD), and the digital precoder is derived with the fixed analog precoder. In [44], MO-based algorithm is proposed to minimize sum mean squared error (MSE). In an attempt to strike a balance between good

performance and power consumption, Feng *et al.* [45] adopt a phase-shifter network consisting of a combination of high-resolution phase shifters and low-resolution phase-shifters, and present hybrid precoding algorithms for both the dynamic and fixed connections between phase-shifter network and antennas.

1.5 A Brief Introduction to some conventional precoders

1.5.1 Eigenmode Precoder

While transmitting the signal $\mathbf{s} \in \mathbb{C}^{N_s \times 1}$, such that $\mathbb{E}[\mathbf{s}\mathbf{s}^H] = \mathbf{I}$, through the MIMO channel $\mathbf{H} \in \mathbb{C}^{N_r \times N_t}$, it is multiplied by precoder $\mathbf{F} \in \mathbb{C}^{N_t \times N_s}$ at the transmitter, and the received signal is multiplied by combiner $\mathbf{W} \in \mathbb{C}^{N_r \times N_s}$ at the receiver to get $\mathbf{y} \in \mathbb{C}^{N_s \times 1}$. Thus, the transmission can be described by the equation

$$\mathbf{y} = \sqrt{\rho}\mathbf{W}^H\mathbf{H}\mathbf{F}\mathbf{s} + \mathbf{W}^H\mathbf{n}, \tag{1.12}$$

where $\mathbf{n} \in \mathbb{C}^{N_r \times 1}$, $\mathbf{n} \sim \mathcal{CN}(\mathbf{0}, \sigma_n^2\mathbf{I})$ is the noise. It is possible to decompose the channel $\mathbf{H}$ into r independent parallel additive noise channels [46], where $r = rank(\mathbf{H}) \leq min(N_r, N_t)$. It is assumed that $N_s \leq r$. If we take $\mathbf{F} = \mathbf{V}_{:,1:N_s}$ and $\mathbf{W} = \mathbf{U}_{:,1:N_s}$, where $\mathbf{H} = \mathbf{U}\mathbf{\Sigma}\mathbf{V}^H$ is the singular value decomposition (SVD) of the channel, resulting in the parallel eigenmode channels as

$$\mathbf{y} = \sqrt{\rho}\mathbf{\Sigma}_{1:N_s,1:N_s}\mathbf{s} + \tilde{\mathbf{n}}, \tag{1.13}$$

where $\mathbf{\Sigma}_{1:N_s,1:N_s} = \mathrm{DIAG}(\sigma_1, \sigma_2, \ldots, \sigma_{N_s})$ and $\tilde{\mathbf{n}} = \mathbf{W}^H\mathbf{n}$. The channel decomposition into N_s parallel channels reduces the receiver signal processing into only scalar rather than complex joint detection and decoding [47].

1.5.2 Zero Forcing Precoder

We consider the MIMO transmission where a base station (BS) is serving K single-antenna mobile stations (MSs). The signal $\mathbf{s} = [s_1, \ldots, s_K], \mathbf{s} \in \mathbb{C}^{K\times 1}$ such that $\mathbb{E}[\mathbf{s}\mathbf{s}^H] = \mathbf{I}$, where s_k is the symbol intended for the k^{th} MS, is transmitted through the MIMO channel $\mathbf{H} \in \mathbb{C}^{K\times N_t}$. $\mathbf{H}_{k\cdot}$ is the channel from the BS to the k^{th} MS, and it is assumed that $K \leq N_t$. $\mathbf{F}_{\text{ZF}} \in \mathbb{C}^{N_t\times K}$ is the zero forcing precoder at the transmitter. The received signal $\mathbf{y} \in \mathbb{C}^{K\times 1}$ at K MSs, where $\mathbf{y}_k$ is the received symbol at the k^{th} MS, is given by

$$\mathbf{y} = \sqrt{\rho}\mathbf{H}\mathbf{F}_{\text{ZF}}\mathbf{s} + \mathbf{n}, \tag{1.14}$$

The ZF precoder $\mathbf{F}_{\text{ZF}}$ aims to diagonalize $\mathbf{H}\mathbf{F}_{\text{ZF}}$. Assuming $\mathbf{H}$ is full row-rank matrix, $\mathbf{F}_{\text{ZF}}$ is designed by normalizing $\mathbf{F}_{\text{ZF}_{un}}$ to have norm K, where $\mathbf{F}_{\text{ZF}_{un}}$ is the right pseudoinverse of $\mathbf{H}$ [48],

$$\mathbf{F}_{\text{ZF}_{un}} = \mathbf{H}^H \left(\mathbf{H}\mathbf{H}^H\right)^{-1}. \tag{1.15}$$

The ZF precoder $\mathbf{F}_{\text{ZF}}$ splits MIMO channel into K non-interfering channels, allowing scalar decoding on each of the channels. The k^{th} symbol is detected by projecting $\mathbf{y}$ onto the direction closest to $\mathbf{H}_{k\cdot}$ within the subspace orthogonal to the one spanned by the set of vectors $\mathbf{H}_{m\cdot}, m \neq k$. The performance of ZF precoder is adversely affected if channel matrix is badly-conditioned [48].

1.5.3 Minimum Mean Square Error Precoder

We consider minimum mean square error (MMSE) precoder in a similar setting as the ZF precoder. The MMSE precoder $\mathbf{F}_{\text{MMSE}}$ aims at minimizing,

$$\mathbb{E}\left[|\mathbf{y} - \mathbf{s}|^2\right], \quad \text{where} \tag{1.16a}$$

$$\mathbf{y} = \sqrt{\rho}\mathbf{H}\mathbf{F}_{\text{MMSE}}\mathbf{s} + \mathbf{n} \tag{1.16b}$$

$\mathbf{F}_{\text{MMSE}}$ is determined by normalizing the unnormalized MMSE precoder $\tilde{\mathbf{F}}_{\text{MMSE}}$ as

$$\mathbf{F}_{\text{MMSE}} = \beta\tilde{\mathbf{F}}_{\text{MMSE}}, \quad \text{where} \tag{1.17a}$$

$$\tilde{\mathbf{F}}_{\text{MMSE}} = \left(\mathbf{H}^H\mathbf{H} + \frac{K\sigma_n^2}{\rho}\right)^{-1}\mathbf{H}^H, \quad \text{and} \tag{1.17b}$$

$$\beta = \sqrt{\frac{K}{\mathbf{Tr}(\tilde{\mathbf{F}}_{\text{MMSE}}\tilde{\mathbf{F}}_{\text{MMSE}}^H)}}. \tag{1.17c}$$

1.6 Analog precoding with a network of phase shifters

In this section, we discuss how analog precoding is accomplished using a network of phase shifters in both fully-connected (FC) and partially-connected (PC) hybrid architectures. In hybrid architecture, the transmit signal is first digitally precoded and the digitally precoded signal is fed into analog precoder. The transmit signal $\mathbf{s} = [s_1, \ldots, s_{N_s}]^T$ is an N_s-length vector which is precoded by digital precoder $\mathbf{F}_{\text{D}} \in \mathbb{C}^{M_t \times N_s}$ into signal $\tilde{\mathbf{s}} = \mathbf{F}_{\text{D}}\mathbf{s} = [\tilde{s}_1, \ldots, \tilde{s}_{N_s}]^T$, which is an M_t-length vector. The i^{th} signal emerging from digital precoder is given by the product of the i^{th} row of $\mathbf{F}_{\text{D}}$ and $\mathbf{s}$ as

$$\tilde{s}_i = \mathbf{F}_{\text{D}_i.}\mathbf{s} \tag{1.18}$$

The phase shift produced by the phase-shifter connected between RF chain 'i' and antenna 'm' is denoted by $e^{j\psi_{m,i}}$ where $1 \leq i \leq N_t$, $1 \leq m \leq M_t$ as shown in Figure 1.4 and Figure 1.5. We discuss analog precoding in context of FC and PC architectures separately.

1.6.1 Analog precoding in fully-connected architecture

The signal emanating from the i^{th} RF chain is split into N_t branches to feed into N_t antennas. At each branch, the symbol goes through different phase shifts. Before transmitting the signal through m^{th} antenna, the signals arriving from different RF

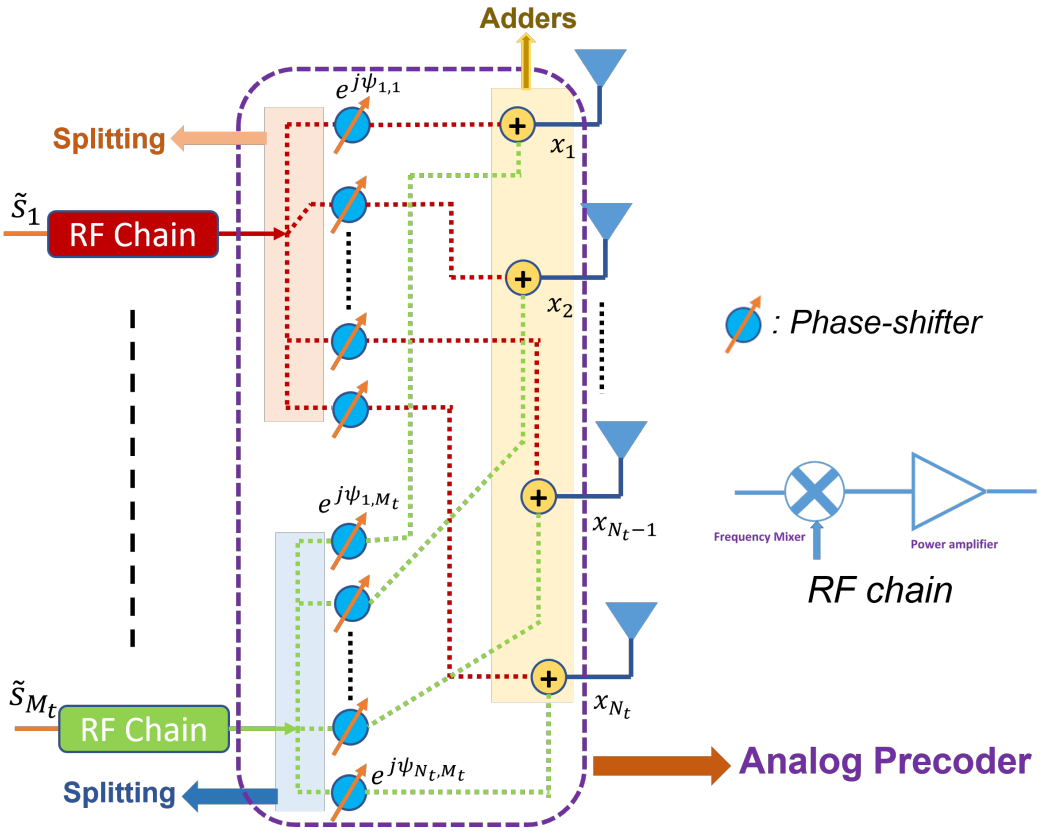

Figure 1.4: Analog precoder realized with splitters, a network of phase shifters and adders in fully connected hybrid structure

chains are summed up. Thus, the signal at the m^{th} antenna is

$$\begin{aligned} x_m &= \tilde{s}_1 e^{j\psi_{m,1}} + \cdots + \tilde{s}_i e^{j\psi_{m,i}} + \cdots + \tilde{s}_{M_t} e^{j\psi_{m,M_t}} \\ &= \left[e^{j\psi_{m,1}}, \ldots, e^{j\psi_{m,i}}, \ldots, e^{j\psi_{m,M_t}}\right] \left[\tilde{s}_1, \ldots, \tilde{s}_i, \ldots, \tilde{s}_{M_t}\right]^T \\ &= \left[e^{j\psi_{m,1}}, \ldots, e^{j\psi_{m,i}}, \ldots, e^{j\psi_{m,M_t}}\right] \tilde{\mathbf{s}} \\ &= \left[e^{j\psi_{m,1}}, \ldots, e^{j\psi_{m,i}}, \ldots, e^{j\psi_{m,M_t}}\right] \mathbf{F}_{\mathrm{D}}\mathbf{s}. \end{aligned}$$

Thus, the transmitted signal through N_t antennas is given by

$$\begin{aligned} \mathbf{x} &= \left[x_1, x_2, \ldots, x_{N_t}\right]^T \\ &= \begin{bmatrix} e^{j\psi_{1,1}} & e^{j\psi_{1,2}} & \ldots & e^{j\psi_{1,M_t}} \\ e^{j\psi_{2,1}} & e^{j\psi_{2,2}} & \ldots & e^{j\psi_{2,M_t}} \\ \vdots & \vdots & \ddots & \vdots \\ e^{j\psi_{N_t,1}} & e^{j\psi_{N_t,2}} & \ldots & e^{j\psi_{N_t,M_t}} \end{bmatrix} \mathbf{F}_{\mathrm{D}}\mathbf{s}. \end{aligned}$$

The analog precoder $\mathbf{F}_{\mathrm{R}}$ is defined as

$$\mathbf{F}_{\mathrm{R}} = \begin{bmatrix} e^{j\psi_{1,1}} & e^{j\psi_{1,2}} & \dots & e^{j\psi_{1,M_t}} \\ e^{j\psi_{2,1}} & e^{j\psi_{2,2}} & \dots & e^{j\psi_{2,M_t}} \\ \vdots & \vdots & \ddots & \vdots \\ e^{j\psi_{N_t,1}} & e^{j\psi_{N_t,2}} & \dots & e^{j\psi_{N_t,M_t}} \end{bmatrix} \tag{1.19}$$

Thus, the transmitted signal $\mathbf{x}$ is

$$\mathbf{x} = \mathbf{F}_{\mathrm{R}}\mathbf{F}_{\mathrm{D}}\mathbf{s}. \tag{1.20}$$

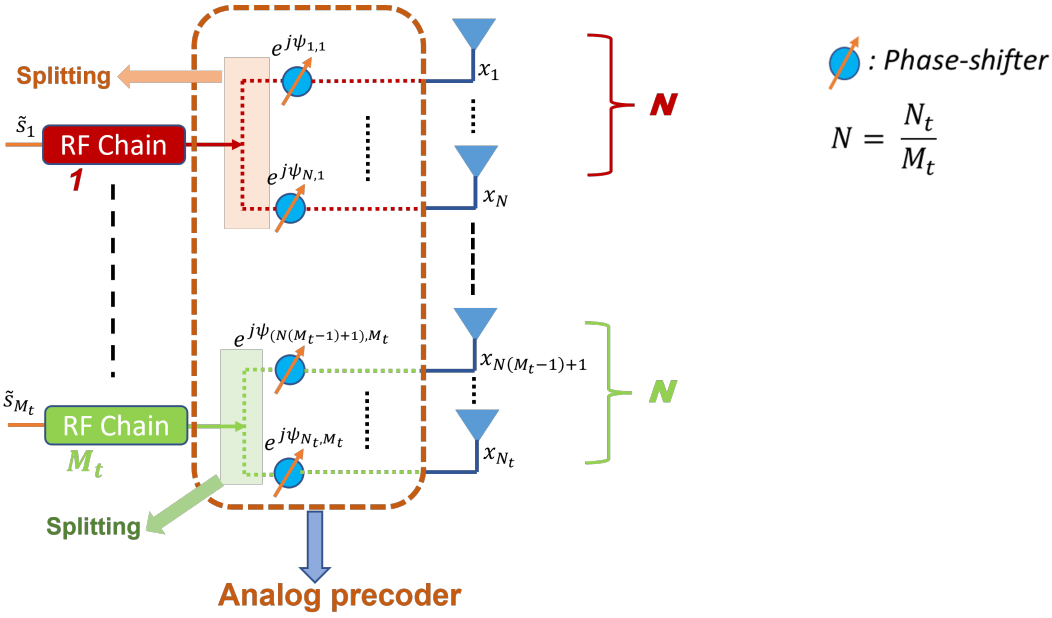

Figure 1.5: Analog precoder realized with splitters and a network of phase shifters in partially connected hybrid structure

1.6.2 Analog precoding in partially-connected architecture

The signal emanating from the i^{th} RF chain is split into $N = \frac{N_t}{M_t}$ branches and fed into N antennas of i^{th} subgroup of antennas after applying different phase shifts at

different branches. The signal transmitted by the m^{th} subgroup of antennas is

$$\begin{aligned}
\mathbf{x}_m &= \left[\tilde{s}_m e^{j\psi_{(N(m-1)+1),m}}, \tilde{s}_m e^{j\psi_{N(m-1)+2),m}}, \ldots, \tilde{s}_m e^{j\psi_{Nm,m}}\right]^T, \qquad 1 \le m \le M_t \\
&= \begin{bmatrix} 0 & \ldots & 0 & e^{j\psi_{(N(m-1)+1),m}} & 0 & \ldots & 0 \\ 0 & \ldots & 0 & e^{j\psi_{(N(m-1)+2),m}} & 0 & \ldots & 0 \\ \vdots & \ddots & \vdots & \vdots & \vdots & \ddots & \vdots \\ 0 & \ldots & 0 & e^{j\psi_{Nm,m}} & 0 & \ldots & 0 \end{bmatrix} \left[\tilde{s}_1, \ldots, \tilde{s}_m, \ldots, \tilde{s}_{M_t}\right]^T \\
&= \begin{bmatrix} \mathbf{0} & \ldots & \mathbf{0} & \mathbf{f}_{\mathrm{R}}^m & \mathbf{0} & \ldots & \mathbf{0} \end{bmatrix} \tilde{\mathbf{s}} \\
&= \mathbf{F}_{\mathrm{R}}^m \mathbf{F}_{\mathrm{D}} \mathbf{s},
\end{aligned}$$

where $\mathbf{F}_{\mathrm{R}}^m \in \mathbb{C}^{N \times M_t}$ is a matrix in which all the elements are 0 except the m^{th} column $\mathbf{f}_{\mathrm{R}}^m$ given by

$$\mathbf{f}_{\mathrm{R}}^m = \begin{bmatrix} e^{j\psi_{(N(m-1)+1),m}} \\ e^{j\psi_{(N(m-1)+2),m}} \\ \vdots \\ e^{j\psi_{Nm,m}} \end{bmatrix}, \qquad 1 \le m \le M_t. \tag{1.21}$$

Thus, the signal transmitted through N_t antennas is given by

$$\begin{aligned}
\mathbf{x} &= \left[\mathbf{x}_1, \mathbf{x}_2, \ldots, \mathbf{x}_{M_t}\right]^T \\
&= \begin{bmatrix} \mathbf{F}_{\mathrm{R}}^1 \\ \mathbf{F}_{\mathrm{R}}^2 \\ \vdots \\ \mathbf{F}_{\mathrm{R}}^{M_t} \end{bmatrix} \mathbf{F}_{\mathrm{D}} \mathbf{s} \\
&= \begin{bmatrix} \mathbf{f}_{\mathrm{R}}^1 & \mathbf{0} & \mathbf{0} & \ldots & \mathbf{0} \\ \mathbf{0} & \mathbf{f}_{\mathrm{R}}^2 & \mathbf{0} & \ldots & \mathbf{0} \\ \vdots & \vdots & \vdots & \ddots & \vdots \\ \mathbf{0} & \mathbf{0} & \mathbf{0} & \ldots & \mathbf{f}_{\mathrm{R}}^{M_t} \end{bmatrix} \mathbf{F}_{\mathrm{D}} \mathbf{s} \\
&= \mathbf{F}_{\mathrm{R}} \mathbf{F}_{\mathrm{D}} \mathbf{s},
\end{aligned}$$

where the analog precoder $\mathbf{F}_{\mathrm{R}}$ is defined as

$$\mathbf{F}_{\mathrm{R}} = \begin{bmatrix} \mathbf{f}_{\mathrm{R}}^{1} & \mathbf{0} & \mathbf{0} & \dots & \mathbf{0} \\ \mathbf{0} & \mathbf{f}_{\mathrm{R}}^{2} & \mathbf{0} & \dots & \mathbf{0} \\ \vdots & \vdots & \vdots & \ddots & \vdots \\ \mathbf{0} & \mathbf{0} & \mathbf{0} & \dots & \mathbf{f}_{\mathrm{R}}^{M_t} \end{bmatrix} \tag{1.22}$$

The analog precoder $\mathbf{F}_{\mathrm{R}}$ has a block diagonal structure where each block is a column vector in case of PC architecture.

1.7 Reconfigurable Intelligent Surface (RIS) Aided Millimeter Wave Communication and RIS passive precoding

It is challenging to have a reliable communication in millimeter-wave as shadowing affects the average received power severely [49]. The user or receiver falling in the dead zone with no link to the transmitter can be a common phenomenon, especially in the dense urban areas [50]. In low-received power scenarios, the Reconfigurable Intelligent Surface (RIS) can function as centralized beamformer to increase channel gains [49]. An RIS can create a virtual line of sight (LoS) path between the BS and the receiver to elude the impediment between the BS and the receiver [49, 51] by re-radiating signal in the shape of a beam toward the receiver [52]. RISs can be placed on the walls, ceilings, building facades, rooftops, or any flat surface [53].

An RIS is a metasurface consisting of a number of elements capable of reflecting the incident signal *smartly* without the need for RF processing, decoding, encoding, or retransmission [51, 54, 55]. Controlling the way electromagnetic wave behaves by introducing changes in the phases only (nearly-passive RIS) or amplitudes and phases (active RIS) of the incident signals, RIS can engender a programmable, highly deterministic radio environments from highly probabilistic wireless environment [56–59]. Such an *intelligent* radio channel makes the transfer and processing of

information between transmitters and receivers more reliable [57, 60]. Most of the RISs considered in the literature are capable of introducing only the phase change to the impinging waves. The RISs have been envisaged to be operated by evaluating the phase shift coefficients at the BS based on the CSI, and controlling the RIS through a smart controller such as a field programmable gate array (FPGA) [53]. RISs are also known by the names, Intelligent Reflecting Surfaces or Large Intelligent Surfaces. The proper design of phase response of RIS can achieve useful signal enhancement and/or interference suppression to produce high-quality passive precoding [61]. Thus, design of phase shift coefficients of RIS is also called passive precoding design.

Ning *et al.* [62] consider an RIS-aided point-to-point MIMO, and propose to design passive precoding by sum-path-gain maximization (SPGM) with the view to maximize the sum of gains of different channel paths, or effectively the channel power. The SPGM problem is solved by alternating direction of method of multipliers (ADMM), and singular value decomposition (SVD) is performed on the equivalent channel subsequently to construct active precoder. Wang *et al.* [63] seek to jointly optimize the transmitter precoding vector and RIS phase-shifts by maximizing the received signal power in an mmWave MIMO environment assisted by multiple RISs. An optimal closed-form solution is obtained for single RIS case, whereas near-optimal analytical solution is derived for multi-RIS case by assuming near-orthogonality of different steering vectors.

In [64], authors jointly design the precoder at the access point (AP) and the phases of the RIS elements to maximize the weighted sum-rate in an RIS-aided MU-MISO downlink system by designing a solution based on fractional programming. Pan *et al.* [53] and Zhang *et al.* [65] also aim to maximize weighted sum-rate of all users through joint optimization. The authors in [53] consider a multi-cell MIMO with multi-antenna users, while [65] considers cell free MIMO with multi-antenna users and multiple RISs. The problem is solved by alternating optimization in both [53] and [65]. Fractional programming is used in [65] to sever the problem into multiple subproblems which are solved alternately. [53] optimizes the phase-shifts of RIS through majorization-minimization algorithm and complex circle manifold method.

Zhang *et al.* [66] and Wang *et al.* [50] both consider joint optimization of active and passive precoding in point-to-point MIMO aided by a single RIS. [66] alternately optimizes the transmit covariance matrix and the phase-shift coefficients of the RIS. [50] capitalizes on the structure of mmWave channel and reconstructs the complex joint optimization problem into a simpler problem which is solved by a manifold optimization algorithm. The authors adopt manifold based optimization method [67] to generate hybrid precoder.

Zhao *et al.* [68] jointly optimize the precoding at the AP and discrete phase shifts of the RIS with the aim of minimizing AP's transmit power constrained to the outage probability for the users. Liu *et al.* [69] decouples the joint symbol-level precoding and reflection coefficients design problem in MU-MISO systems, and solves the symbol-level precoding and the reflection coefficients design subproblems by using algorithms based on gradient-projection and Riemannian conjugate gradient respectively.

1.8 Channel State Information Acquisition

Channel state information (CSI) is required at the transmitter to perform precoding. CSI is acquired through channel estimation. Channel estimation which involves mathematical operations such as multiplication, inversion, eigenvalue decomposition (EVD), or singular value decomposition (SVD) is constrained by the high dimensional channel matrix resulting because of the large number of antennas used in mmWave MIMO [70]. Furthermore, there is also increased overhead on the pilot sequence, and channel estimation becomes exacting in mmWave MIMO as a result [71].

In the conventional pilot-based channel estimation method, the pilot symbols are generated at baseband and transmitted at certain prescribed times and frequencies that are known by the receiver. The receiver, having known the pilot symbols, frequencies and times of transmission, estimates the channel based on the received pilot symbols [72]. It is possible to estimate channel matrix in conventional MIMO in this way as there is an RF chain corresponding to each antenna which enables

the control over individual signal transmitted from each antenna [16]. However, the number of RF chains is much lower than the number of antennas in the hybrid architecture adopted by mmWave MIMO. Thus, the traditional channel estimation techniques can not be employed in mmWave MIMO as they require access to the baseband signals associated with each antenna which is not possible with hybrid architecture [16]. It is only possible to procure a low-dimensional signal from the RF chains instead of the signal of higher dimension, which makes CSI acquisition arduous in mmWave MIMO [71].

The studies and measurements have attested that scattering environment between the transmitter and receiver is sparse at mmWave frequencies, *i.e.*, mmWave channel involves paths that are limited to a few clusters in angular domain [71, 73]. The sparse nature of mmWave channels is verified by several studies which show that there are typically only 3-4 scattering clusters in dense-urban mmWave channels in non-line-of-sight (NLOS) environments [73]. The channel sparsity can be leveraged by constructing channel estimation as a sparse recovery problem and compressed sensing (CS) algorithms can be used to solve the estimation problem. CS algorithms exploit the sparsity of the mmWave channel to estimate it from the samples using considerably few measurements despite large channel matrix [16].

There are also CSI acquisition techniques that use "beam training" in which we find a pair of transmit and receive beams that produce the largest received power. The beam training, sometimes also called beam alignment, selects beams from pre-determined codebooks at both the transmitter and receiver [71, 74]. The beam training reduces the estimation of channel matrix in the dimension of number of antennas to the estimation of equivalent channel matrix in the dimension of number of RF chains [71]. Once the beam training is accomplished, we use the classical methods such as least squares or minimum mean square error estimation, to estimate the equivalent channel matrix with a small number of pilot symbols [71].

1.9 Challenges in practical implemention of hybrid precoding and passive precoding

The mmWave MIMO has not yet been implemented in practice. Most of the works on hybrid precoding including the work in this thesis disregard some of the practical scenarios. It is assumed that there is availability of perfect CSI at the transmitter. This is difficult to attain in practice, more so in case of mmWave MIMO where the size of channel matrix is large. The imperfect CSI will lead to hybrid precoders that can not meet the expected performances. There might be situations where the received signal is of extremely poor quality because hybrid precoder produces beam along a direction that does not align with the user. The hybrid precoders need to be robust to channel estimation errors.

One of the biggest practical challenges in implementing hybrid precoders comes from the analog precoder design. In order to reduce the number of RF chains, power amplifiers are placed before analog precoder. This creates a practical challenge where signals with unequal amplitudes and phases are combined in the analog precoder, resulting in signal dependent mismatch at the antenna ports and hence the significant power loss [75]. The analog precoder also suffers from insertion loss that can not be ignored [75]. Thus, the hybrid precoder designed without considering the implications of analog signal processing will produce performances with significant departure from theory [75].

The RF chains that perform amplification and down-conversion of signals operate at dynamic ranges of frequencies which are much higher than the operating frequencies of the baseband. The signal processing at baseband level is unable to remove the residual transceiver hardware impairments (RTHIs) arising from nonlinearities of the amplifier, quantization errors, In-phase/Quadrature (I/Q) imbalance, and mutual coupling between antenna ports [76]. As a result, the achievable rates in practice are far from those obtained in theory. In order to make cost-efficient systems, the practical mmWave MIMO systems would possibly use low quality circuits which are

more susceptible to RTHIs. The hybrid precoding design should be aware of the impact of RTHIs to prevent RTHIs from thwarting the design of commercially viable mmWave MIMO transceivers [76].

The implementation of RIS in mmWave MIMO further increases the overhead on channel estimation. We consider availability of full CSI at transmitter to design phase shift coefficients of RIS. One of the toughest question to answer is - how quickly can we update the phase shifts of RIS? In the situation of mobility transmission when the channels are varying rapidly, getting full CSI and tuning the phase shifts of RIS will be a Herculean task with severe implications on CSI acquisition overhead. Only partial or outdated CSI may be obtained, which results in the signal misalignment [77]. The passive precoding also needs to take channel estimation errors into consideration during design. The placement of RIS plays an important role in forming channel that can produce better communication [77]. Thus, determining the optimal position to place an RIS in order to maximize performance, also needs to studied before deploying RISs.

1.10 Objectives of Research

The 6G is conceived to support applications such as holographic projection, virtual and augmented reality (VAR), brain communication interface, teleportation, remote surgery, and so on [78]. These technologies would demand ultra-high data rates, ultra-high reliability, and ultra-low latency [53, 78]. The mmWave communication is one of the key technologies for future wireless and cellular communications which solves the issues of bandwidth crunch by tendering huge unused bandwidth. The mmWave communication that needs to be supported by massive MIMO needs to be complemented by hybrid architecture. Thus, mmWave MIMO channel estimation and precoding techniques need to be tailored according to the new hybrid architecture. The research in this work is focussed on the hybrid precoding techniques for mmWave MIMO.

The analog precoding and digital precoding problems are coupled, as the hybrid

precoder is evaluated as the product of analog precoder and digital precoder. Thus, determining the optimal hybrid precoder is a very difficult problem. Moreover, each element of the analog precoding matrix is constrained to satisfy unit amplitude constraint as the analog precoder is incapable of introducing amplitude variations to the signal it acts on, as it is implemented by phase shifters. The unit modulus constraint on the entries of analog precoding matrix is non-convex which adds more complications to the already difficult problem. In this research, the hybrid precoding problem is studied in single user and multiple user scenarios.

The general aim of hybrid precoding is to provide spectral and bit error rate (BER) performances close to the fully digital precoder with the use of a very small number of RF chains. There are state-of-art hybrid precoders that offer high performances. But they are accompanied by higher computational complexities. The objective of this research is to look not only for the high-performing hybrid precoding solutions, but also for the computationally efficient hybrid precoders. The computational efficiency is essential to meet the ultra-low latency requirements of the future wireless communication technology.

One of the key issues that needs to be sorted to make mmWave communication a reality is the blockages faced by mmWave signals. This can be accomplished by the deployment of RISs which will be one of the preeminent features of wireless communications of the future. The RISs also need to programmed to have phase-shift coefficients that deliver good performances. Thus, passive precoding is also one of the momentous research areas in the field of communications. The development of high-performing and computationally efficient passive precoding algorithms is another area, this research is riveted on.

1.11 Main Contributions

The main contributions of this thesis can be outlined as follows:

(i) Two hybrid precoding algorithms are proposed for point-to-point mmWave MIMO with fully connected hybrid architecture. The first algorithm is based

on alternating minimization, in which the analog precoder is computed by using a modified form of Block Coordinate Descent (BCD) algorithm and the digital precoder is calculated as a closed form solution derived using the method of Lagrange multipliers at each iteration. In the second algorithm, hybrid precoding is split into analog precoding and digital precoding subproblems. Analog precoder is first determined by using an iterative power method, and the digital precoder is evaluated as the closed form solution. Both the algorithms exhibit very good spectral and BER performances, and the complexity is also lower than that of the existing solutions. The second algorithm, in particular, has significantly lower complexity compared to the existing solutions. Even though both the algorithms are developed considering the narrowband channel, they are extended to work in wideband channel.

(ii) Two hybrid precoding algorithms are proposed, considering the point-to-point MIMO with the so-called "partial-full mixed connection" (PFMC) architecture which is a mixture of FC and PC architectures. The antennas and the RF chains are grouped in various subgroups in this architecture, and the RF chains of a particular subgroup are connected to all the antennas of that subgroup through phase shifters à la FC structure. The hybrid precoding problem for such an architecture is devised as the matrix factorization problem corresponding to the subgroups. The first algorithm is an alternating minimization based algorithm, whereas the second one is based on iterative power method. The first method works only in narrowband channel, while the second one can operate in both the narrowband and wideband channel. The simulation results show that the PFMC architecture delivers better energy efficiency compared to FC and PC architectures, and proposed algorithms offer better spectral and energy efficiency performances compared to existing algorithm.

(iii) Hybrid precoding algorithm is proposed for mmWave multiple user MIMO (MU-MIMO) to maximize signal-to-leakage-and-noise ratio (SLNR) for each user. The analog precoder is constructed by choosing the candidate vectors from a codebook. The proposed hybrid SLNR precoder exhibits better spectral

performances than the existing codebook based precoders. The achievable spectral efficiency is computed analytically in single path channels with infinite-resolution codebook.

(iv) The hybrid precoder is proposed for mmWave MU-MISO to minimize MSE. The analog precoding and digital precoding subproblems are separated. The analog precoder is determined by optimizing the lower bound of analog precoding subproblem which helps in reducing the complexity. The analog precoder is then determined by using a low complexity iterative method based on truncated SVD. The digital precoder is determined by minimizing the MSE with fixed analog precoder. The simulation results reveal that the performance of the proposed hybrid MMSE precoder is on a par with state-of-art algorithm in both the narrowband and wideband channels.

(v) An algorithm for the passive precoding in an RIS assisted point-to-point mmWave MIMO is proposed that aims to minimize the MSE between the transmit signal and the received signal. The fully digital precoding at the BS, passive precoding and the fully digital combining at the receiver are jointly determined in iterative fashion by the proposed algorithm. The hybrid precoder is determined from the fully digital precoder at the end. The performance analysis shows that the proposed algorithm produces very good spectral and BER performances in both narrowband and wideband channels.

(vi) An iterative algorithm is developed for maximizing the energy efficiency in an mmWave MU-MISO which is supported by distributed RISs. The energy efficiency maximization problem is simplified by the use of ZF precoder into a problem of joint optimization of passive precoding and power allocation matrix. The joint optimization problem is solved by alternating optimization approach, where the passive precoding is solved by a greedy algorithm and the power allocation is optimized by the method of Lagrange multipliers, at each iteration. Moreover, a computationally efficient scheme is developed to switch off some elements of RIS that leads to further augmentation of energy efficiency. The hybrid precoder is constructed finally from the fully digital

precoder. The impact of different parameters on energy efficiency is studied using simulations. The simulation results prove that the proposed algorithm delivers better performance than the existing method.

1.12 Organization of Thesis

The rest of the thesis is organized as follows. In Chapter 2, the hybrid precoding problem of a single user mmWave MIMO with FC architecture is considered and two algorithms are presented. The two hybrid precoding algorithms are put forward for the single user MIMO with PFMC architecture in Chapter 3. Considering the mmWave MU-MIMO, a codebook-based hybrid precoder is proposed that aims to maximize SLNR of each user in Chapter 4. In Chapter 5, a low complexity hybrid MMSE precoder is proffered to minimize MSE in mmWave MU-MISO. An algorithm for passive precoding to minimize MSE in an RIS assisted single user mmWave MIMO is proposed in Chapter 6. In Chapter 7, an iterative algorithm is presented that determines precoding at the BS, passive precoding and power allocation for energy efficiency maximization in RIS enhanced mmWave MU-MISO. The conclusions of the thesis and future directions of the research are presented in Chapter 8. It is followed by appendices and references.

1.13 List of publications

(i) Published papers

- P. R. Gautam and L. Zhang, "Hybrid SLNR Precoding for Multi-user Millimeter Wave MIMO Systems," *2019 22nd International Symposium on Wireless Personal Multimedia Communications (WPMC)*, 2019, pp. 1-6. (Winner of **Best Student Paper Award**.)
- P. R. Gautam and L. Zhang, "Hybrid Precoding for Partial-Full Mixed Connection mmWave MIMO," *2021 IEEE Statistical Signal Processing Workshop (SSP)*, 2021, pp. 271-275.

- P. R. Gautam and L. Zhang, "Hybrid Precoding for Millimeter Wave MIMO: Trace Optimization Approach," in *IEEE Access*, vol. 10, pp. 66874-66885, 2022.

(ii) Submitted paper

- P. R. Gautam, L. Zhang and P. Fan, "Hybrid MMSE Precoding for Millimeter Wave MU-MISO via Trace Maximization,"in *IEEE Transactions on Wireless Communications*.

(iii) Papers in preparation

- P. R. Gautam and L. Zhang, "MMSE-based Passive Precoding Design for Reconfigurable Intelligent Surface Aided Millimeter Wave MIMO".
- P. R. Gautam and L. Zhang, "Passive Precoding and Power Allocation for Energy-efficient Reconfigurable Intelligent Surface Enhanced Millimeter Wave MU-MISO".

Chapter 2

Hybrid Precoding in Point-to-Point mmWave MIMO

Ayach *et al.* [18] show that the hybrid precoder for point-to-point MIMO can be evaluated by minimizing the Euclidean distance between the optimum fully digital precoder and the hybrid precoder. The hybrid precoder is computed as the product of analog precoder and digital precoder and the computation of hybrid precoder poses a problem because each element of analog precoding matrix needs to satisfy unit modulus constraint which is non-convex.

Among the existing algorithms for point-to-point MIMO, SDR-AO [42], an SDR-based algorithm that is solved by convex optimization toolbox CVX [79], offers a very good performance but suffers from extremely high computational complexity. The vectorization of the original problem which is in matrix form converts it into a high dimensional problem and hence the complexity of the proposed method is extremely high. MO-AltMin [40], the MO-based method, offers very good performance but it also suffers from higher complexity because of the vectorization of problem.

In this chapter, hybrid precoding problem in narrrowband point-to-point mmWave MIMO channel is considered. Starting with the optimal fully digital precoder, the hybrid precoder is determined by minimizing the Frobenius norm of the difference of optimal precoder and the hybrid precoder, as proposed in [18]. The Frobenius norm

minimization problem is translated into trace optimization problem by replacing the Frobenius norm with equivalent trace form. The contributions made in this chapter are:

(i) An algorithm based on alternating minimization is developed where the objective function is optimized, keeping one of the digital precoder or analog precoder constant at a time. The optimal digital precoder that minimizes the objective function with the fixed analog precoder is computed using the method of Lagrange multipliers. As for the analog precoder determination problem with the fixed digital precoder, the problem is translated into semidefinite programming (SDP) problem by convex relaxation. The subproblem is similar to the standard SDP found in phasecut problem [80], but with some additional constraints. The subproblem can be solved by CVX [79]. However, the modified form of BCD algorithm [81] is used to solve the analog precoding subproblem, hence the hybrid precoding algorithm is referred to as MBCD-HP. The SDR-AO algorithm in [42] also converts the hybrid precoding problem into SDP problem and solves it by using CVX. However, there are significant differences in its approach and the proposed approach in MBCD-HP. SDR-AO converts the hybrid precoding problem into vector form and finally forms an SDP problem which adds a high complexity. However, in MBCD-HP the operations are carried out in matrix form without converting into vector form to convert precoding problem into an SDP problem which helps in restricting the complexity. To the best of author's knowledge, there has not been any prior work that utilizes such SDP based algorithms on hybrid precoding or similar problem directly in matrix form without converting the problem into vector form.

(ii) In another hybrid precoding algorithm, the hybrid precoding problem is decoupled into analog precoding and digital precoding subproblems by substituting the least squares solution for digital precoder with fixed analog precoder into the trace form of the original objective function. The expression is further simplified by making suitable assumptions about the orthogonality of the analog

precoder, and then the new analog precoding subproblem is formed by imposing the orthogonality constraint on the analog precoder. A simple algorithm is developed called Iterative Power Method- Hybrid Precoding (IPM-HP) based on iterative power method to solve for the optimal analog precoder. With the analog precoder computed, the digital precoder is determined by the least squares solution of the original objective function.

(iii) The two hybrid precoding algorithms are developed by considering narrowband channel model. The algorithms are further extended for wideband channel by considering OFDM.

(iv) The computational complexities of the proposed hybrid precoding algorithms are computed and compared with the existing algorithms. It is demonstrated through simulations that the proposed method MBCD-HP not only performs close to high performance precoders like MO-AltMin, HD-LSR and SDR-AO but also involves smaller complexity compared to the MO-AltMin and SDR-AO algorithms. The IPM-HP displays slightly lower performance but it entails significantly low complexity.

2.1 System Model

A single user mmWave MIMO downlink system is considered in which the transmitter is equipped with N_t transmit antennas and M_t RF chains, whereas the receiver has N_r receive antennas and M_r RF chains as shown in Figure 1.3. The number of data streams being transmitted is N_s. It is assumed that $N_s \leq M_t \leq N_t$, $N_s \leq M_r \leq N_r$. The fully-connected architecture is considered at both the transmitter and the receiver in which each RF chain is connected to all the antennas through a network of phase shifters.

At the transmitter, transmit signal $\mathbf{s}$ is precoded by the hybrid precoder $\mathbf{F} = \mathbf{F}_{\mathrm{R}}\mathbf{F}_{\mathrm{D}}$ before transmission which is a combination of baseband precoder $\mathbf{F}_{\mathrm{D}} \in \mathbb{C}^{M_t \times N_s}$ and the analog beamformer $\mathbf{F}_{\mathrm{R}} \in \mathbb{C}^{N_t \times M_t}$. At the receiver, the received signal is processed by the hybrid combiner $\mathbf{W} = \mathbf{W}_{\mathrm{R}}\mathbf{W}_{\mathrm{D}}$ where $\mathbf{W}_{\mathrm{R}} \in \mathbb{C}^{N_r \times M_r}$ is the analog

combiner and $\mathbf{W}_{\mathrm{D}} \in \mathbb{C}^{M_r \times N_s}$ is the digital combiner.

The analog beamformer and combiner are implemented using phase shifters which impose a constant unit amplitude constraint on each element of $\mathbf{F}_{\mathrm{R}}$ and $\mathbf{W}_{\mathrm{R}}$, *i.e.*, $|\mathbf{F}_{\mathrm{R}_{i,j}}| = 1$ and $|\mathbf{W}_{\mathrm{R}_{i,j}}| = 1$. All the transmit symbols are assumed to be independent of each other such that $\mathbb{E}\left[\mathbf{s}\mathbf{s}^H\right] = \frac{1}{N_s}\mathbf{I}_{N_s}$. The hybrid precoder $\mathbf{F}$ is constrained to satisfy total power constraint so that the transmit signal does not exceed the total power limit.

Narrow-band block-fading channel model is adopted. The received signal, after combining, is given by

$$\mathbf{y} = \sqrt{\rho}\mathbf{W}_{\mathrm{D}}^H\mathbf{W}_{\mathrm{R}}^H\mathbf{H}\mathbf{F}_{\mathrm{R}}\mathbf{F}_{\mathrm{D}}\mathbf{s} + \mathbf{W}_{\mathrm{D}}^H\mathbf{W}_{\mathrm{R}}^H\mathbf{n}, \tag{2.1}$$

where ρ is the average total transmit power. $\mathbf{H} \in \mathbb{C}^{N_r \times N_t}$ is the channel from the transmitter to the receiver and $\mathbf{n} \sim \mathcal{CN}(\mathbf{0}, \sigma^2\mathbf{I}_{N_r})$ is the $N_r \times 1$ complex noise vector.

2.2 Hybrid Precoding Problem for point-to-point mmWave MIMO

The mutual information achieved by Gaussian signaling over mmWave channel can be maximized if hybrid precoder is designed as [18]

$$\begin{aligned} \underset{\mathbf{F}_{\mathrm{R}},\mathbf{F}_{\mathrm{D}}}{\arg\min} \quad & \|\mathbf{F}_{\mathrm{opt}} - \mathbf{F}_{\mathrm{R}}\mathbf{F}_{\mathrm{D}}\|_F^2 && \text{(2.2a)} \\ \text{s.t.} \quad & \|\mathbf{F}_{\mathrm{R}}\mathbf{F}_{\mathrm{D}}\|_F^2 = N_s, && \text{(2.2b)} \\ & \left|\mathbf{F}_{\mathrm{R}_{i,j}}\right| = 1, \ \forall i,j, && \text{(2.2c)} \end{aligned}$$

where $\mathbf{F}_{\mathrm{opt}} \in \mathbb{C}^{N_t \times N_s}$ is the optimal fully digital precoder and (2.2b) is the transmit power constraint. The optimal precoder and combiner are the matrices containing the right singular vectors and the left singular vectors of the channel matrix respectively, corresponding to the N_s largest singular values. If the SVD of channel matrix is

$\mathbf{H} = \mathbf{U}\mathbf{S}\mathbf{V}^H$, the optimal precoder and combiner are formed of the leading N_s columns of $\mathbf{V}$ and $\mathbf{U}$ respectively. The design of combiner follows the similar procedure as that of the precoder design except that the combiner does not need to satisfy any power constraint. The non-convex nature of the second constraint (2.2c) makes it pretty difficult to solve and there is no known solution [18]. Hence the general trend is to decompose the hybrid precoding problem (2.2) into two separate subproblems to determine analog precoder and digital precoder separately. The objective function (2.2a) can be expressed in terms of trace as,

$$\begin{aligned}
&\|\mathbf{F}_{\text{opt}} - \mathbf{F}_{\text{R}}\mathbf{F}_{\text{D}}\|_F^2 \\
=&\mathbf{Tr}\left[\left(\mathbf{F}_{\text{opt}} - \mathbf{F}_{\text{R}}\mathbf{F}_{\text{D}}\right)\left(\mathbf{F}_{\text{opt}} - \mathbf{F}_{\text{R}}\mathbf{F}_{\text{D}}\right)^H\right] \\
=&\mathbf{Tr}\left[\mathbf{F}_{\text{opt}}\mathbf{F}_{\text{opt}}^H - \mathbf{F}_{\text{R}}\mathbf{F}_{\text{D}}\mathbf{F}_{\text{opt}}^H - \mathbf{F}_{\text{opt}}\mathbf{F}_{\text{D}}^H\mathbf{F}_{\text{R}}^H + \mathbf{F}_{\text{R}}\mathbf{F}_{\text{D}}\mathbf{F}_{\text{D}}^H\mathbf{F}_{\text{R}}^H\right].
\end{aligned}$$

If analog precoder $\mathbf{F}_{\text{R}}$ is known, the digital precoder $\mathbf{F}_{\text{D}}$ can be evaluated by solving the problem,

$$\begin{aligned}
\mathbf{F}_{\text{D}}^\star = \arg\min_{\mathbf{F}_{\text{D}}} \quad & \mathbf{Tr}\left[\mathbf{F}_{\text{opt}}\mathbf{F}_{\text{opt}}^H - \mathbf{F}_{\text{R}}\mathbf{F}_{\text{D}}\mathbf{F}_{\text{opt}}^H - \mathbf{F}_{\text{opt}}\mathbf{F}_{\text{D}}^H\mathbf{F}_{\text{R}}^H + \mathbf{F}_{\text{R}}\mathbf{F}_{\text{D}}\mathbf{F}_{\text{D}}^H\mathbf{F}_{\text{R}}^H\right] \\
\text{s.t.} \quad & \mathbf{Tr}\left(\mathbf{F}_{\text{D}}^H\mathbf{F}_{\text{R}}^H\mathbf{F}_{\text{R}}\mathbf{F}_{\text{D}}\right) = N_s,
\end{aligned} \tag{2.3}$$

To solve (2.3), the Lagrangian is formed as,

$$\begin{aligned}
\mathcal{L} =&\mathbf{Tr}\left[\mathbf{F}_{\text{opt}}\mathbf{F}_{\text{opt}}^H - \mathbf{F}_{\text{R}}\mathbf{F}_{\text{D}}\mathbf{F}_{\text{opt}}^H - \mathbf{F}_{\text{opt}}\mathbf{F}_{\text{D}}^H\mathbf{F}_{\text{R}}^H + \mathbf{F}_{\text{R}}\mathbf{F}_{\text{D}}\mathbf{F}_{\text{D}}^H\mathbf{F}_{\text{R}}^H\right] + \\
&\lambda\left[\mathbf{Tr}\left(\mathbf{F}_{\text{D}}^H\mathbf{F}_{\text{R}}^H\mathbf{F}_{\text{R}}\mathbf{F}_{\text{D}}\right) - N_s\right],
\end{aligned} \tag{2.4}$$

where $\lambda \in \mathbb{R}$ is the Lagrange multiplier that needs to be determined. Differentiating (2.4) w.r.t $\mathbf{F}_{\text{D}}$ and equating it to $\mathbf{0}$ gives

$$\mathbf{F}_{\text{D}} = \frac{1}{(1+\lambda)}\left(\mathbf{F}_{\text{R}}^H\mathbf{F}_{\text{R}}\right)^{-1}\mathbf{F}_{\text{R}}^H\mathbf{F}_{\text{opt}} = \beta\tilde{\mathbf{F}}_{\text{D}}, \quad \text{where} \tag{2.5a}$$

$$\tilde{\mathbf{F}}_{\text{D}} = \left(\mathbf{F}_{\text{R}}^H\mathbf{F}_{\text{R}}\right)^{-1}\mathbf{F}_{\text{R}}^H\mathbf{F}_{\text{opt}} = \mathbf{F}_{\text{R}}^\dagger\mathbf{F}_{\text{opt}} \tag{2.5b}$$

is the unnormalized digital precoder and $\beta = \frac{1}{(1+\lambda)}$ is the normalization factor. To determine the value of β, the derivative of (2.4) w.r.t λ is equated to 0, and the value of $\mathbf{F}_{\mathrm{D}}$ from (2.5a) is substituted in the resulting equation. The value of β is obtained as

$$\beta = \sqrt{\frac{N_s}{\mathbf{Tr}\left(\tilde{\mathbf{F}}_{\mathrm{D}}^{H}\mathbf{F}_{\mathrm{R}}^{H}\mathbf{F}_{\mathrm{R}}\tilde{\mathbf{F}}_{\mathrm{D}}\right)}} \ . \tag{2.6}$$

2.3 Hybrid Precoding Method Based on Modified Block Coordinate Descent (MBCD) Method

The first hybrid precoding method is based on alternating minimization technique in which digital precoder and analog precoder are alternately optimized, keeping the other fixed. Starting with a feasible initial value of analog precoder, the digital precoder is determined first, keeping the analog precoder fixed. The analog precoder is then designed, treating the digital precoder as a constant in the next stage. This procedure of determining digital precoder and analog precoder is repeated until convergence is attained.

2.3.1 Analog Precoder Design by MBCD Method

The authors in [40] (Lemma 1) prove that if the Euclidean distance between the optimal precoder and the unnormalized hybrid precoder is minimized, the normalization step performed at the end will still make the distance between the hybrid precoder and the optimal precoder sufficiently small. Hence, the power constraint in (2.4) can be discarded for the time being, and only the Euclidean distance between the optimal precoder and the unnormalized hybrid precoder can be minimized. The normalization of the digital precoder can be performed after the computation of the analog precoder and the unnormalized digital precoder. Hence, if the digital precoder is known, the analog precoder design subproblem can be restated as

$$\begin{aligned} \min_{\mathbf{F}_{\mathrm{R}}} \quad & \mathbf{Tr}\left[\mathbf{F}_{\mathrm{opt}}\mathbf{F}_{\mathrm{opt}}^{H} - \mathbf{F}_{\mathrm{R}}\tilde{\mathbf{F}}_{\mathrm{D}}\mathbf{F}_{\mathrm{opt}}^{H} - \mathbf{F}_{\mathrm{opt}}\tilde{\mathbf{F}}_{\mathrm{D}}^{H}\mathbf{F}_{\mathrm{R}}^{H} + \mathbf{F}_{\mathrm{R}}\tilde{\mathbf{F}}_{\mathrm{D}}\tilde{\mathbf{F}}_{\mathrm{D}}^{H}\mathbf{F}_{\mathrm{R}}^{H}\right] \\ \text{s.t.} \quad & \left|\mathbf{F}_{\mathrm{R}_{i,j}}\right| = 1, \ \forall i, j. \end{aligned} \tag{2.7}$$

Discarding the term containing only $\mathbf{F}_{\text{opt}}\mathbf{F}_{\text{opt}}^H$ which does not depend on $\mathbf{F}_{\text{R}}$, the analog precoding subproblem in (2.7) can be equivalently written as

$$\begin{aligned} &\min_{\mathbf{F}_{\text{R}}} \mathbf{Tr}\left[\mathbf{F}_{\text{R}}\tilde{\mathbf{F}}_{\text{D}}\tilde{\mathbf{F}}_{\text{D}}^H\mathbf{F}_{\text{R}}^H - \mathbf{F}_{\text{R}}\tilde{\mathbf{F}}_{\text{D}}\mathbf{F}_{\text{opt}}^H - \mathbf{F}_{\text{opt}}\tilde{\mathbf{F}}_{\text{D}}^H\mathbf{F}_{\text{R}}^H\right] \\ &\text{s.t.} \quad \left|\mathbf{F}_{\text{R}_{i,j}}\right| = 1, \ \forall i, j. \end{aligned} \tag{2.8}$$

To solve the optimization problem in (2.8), another optimization problem is introduced,

$$\min_{\tilde{\mathbf{F}}_{\text{R}}} \quad \mathbf{Tr}\left[\tilde{\mathbf{F}}_{\text{R}}^H\mathbf{M}\tilde{\mathbf{F}}_{\text{R}}\right], \quad \text{where} \tag{2.9a}$$

$$\mathbf{M} = \begin{bmatrix} \tilde{\mathbf{F}}_{\text{D}}\tilde{\mathbf{F}}_{\text{D}}^H & -\frac{1}{\sqrt{N_t}}\tilde{\mathbf{F}}_{\text{D}}\mathbf{F}_{\text{opt}}^H \\ -\frac{1}{\sqrt{N_t}}\mathbf{F}_{\text{opt}}\tilde{\mathbf{F}}_{\text{D}}^H & \mathbf{0} \end{bmatrix}, \tag{2.9b}$$

$$\tilde{\mathbf{F}}_{\text{R}} = \begin{bmatrix} \bar{\mathbf{F}}_{\text{R}}^H \\ \mathbf{I}_{\text{N}_\text{t}} \end{bmatrix}, \quad |\bar{\mathbf{F}}_{\text{R}}| = \frac{1}{\sqrt{N_t}}\mathbf{1}_{\text{N}_\text{t}\times\text{M}_\text{t}}. \tag{2.9c}$$

If the problem (2.9) is expanded, it can be easily seen that it is equivalent to problem (2.8) with $\mathbf{F}_{\text{R}} = \sqrt{N_t}\bar{\mathbf{F}}_{\text{R}}$. If the optimal solution to (2.9) is $\tilde{\bar{\mathbf{F}}}_{\text{R}}^\star = \left[\left(\bar{\mathbf{F}}_{\text{R}}^{\star H}\right)^T, \ \mathbf{I}_{\text{N}_\text{t}}\right]^T$, it is obvious that the optimal solution of (2.8) is $\mathbf{F}_{\text{R}}^\star = \sqrt{N_t}\bar{\mathbf{F}}_{\text{R}}^\star$. Thus, the problem (2.9) can be solved to determine the analog precoder. The Hermitian matrix,

$$\mathbf{X} = \tilde{\mathbf{F}}_{\text{R}}\tilde{\mathbf{F}}_{\text{R}}^H = \begin{bmatrix} \bar{\mathbf{F}}_{\text{R}}^H\bar{\mathbf{F}}_{\text{R}} & \bar{\mathbf{F}}_{\text{R}}^H \\ \bar{\mathbf{F}}_{\text{R}} & \mathbf{I}_{\text{N}_\text{t}} \end{bmatrix} \tag{2.10}$$

is defined. Since the i^{th} diagonal element of $\bar{\mathbf{F}}_{\text{R}}^H\bar{\mathbf{F}}_{\text{R}}$ is equal to the sum of squares of all the elements of the i^{th} column of $\bar{\mathbf{F}}_{\text{R}}$, it is evident that all the diagonal elements of $\bar{\mathbf{F}}_{\text{R}}^H\bar{\mathbf{F}}_{\text{R}}$ are equal to 1. Hence, it is easy to see that $\mathbf{diag}\left(\mathbf{X}\right) = \mathbf{1}_{m\times 1}$, where $m \triangleq (N_t + M_t)$. $q \triangleq 1 : M_t$ and $r \triangleq (M_t + 1) : (N_t + M_t)$ are also defined. Thus, the problem in (2.9) can be restated as

$$
\begin{aligned}
&\min_{\mathbf{X}\in\mathbf{H}_{\mathrm{m}}} \quad \mathbf{Tr}\left(\mathbf{MX}\right) \\
&\text{s.t.} \quad \mathbf{X} \succeq 0, \\
&\qquad \mathbf{diag}\left(\mathbf{X}\right) = \mathbf{1}_{m\times 1}, \\
&\qquad |\mathbf{X}_{r,q}| = \frac{1}{\sqrt{N_t}}\mathbf{1}_{\mathrm{N_t}\times\mathrm{M_t}} = \left|\mathbf{X}_{q,r}^{H}\right|, \quad \mathbf{X}_{r,r} = \mathbf{I}_{N_t}, \\
&\qquad \mathrm{rank}\left(\mathbf{X}\right) = N_t.
\end{aligned} \tag{2.11}
$$

Discarding the non-convex rank constraint to achieve convex relaxation,

$$
\begin{aligned}
&\min_{\mathbf{X}\in\mathbf{H}_{\mathrm{m}}} \quad \mathbf{Tr}\left(\mathbf{MX}\right) && \text{(2.12a)} \\
&\text{s.t.} \quad \mathbf{X} \succeq 0, && \text{(2.12b)} \\
&\qquad \mathbf{diag}\left(\mathbf{X}\right) = \mathbf{1}_{m\times 1}, && \text{(2.12c)} \\
&\qquad |\mathbf{X}_{r,q}| = \frac{1}{\sqrt{N_t}}\mathbf{1}_{\mathrm{N_t}\times\mathrm{M_t}} = \left|\mathbf{X}_{q,r}^{H}\right|, \quad \mathbf{X}_{r,r} = \mathbf{I}_{N_t}. && \text{(2.12d)}
\end{aligned}
$$

The problem (2.12) is an SDP in $\mathbf{X}$. The problem in (2.12) looks similar to phasecut, the phase retrieval problem formulated as an SDP after a tractable convex relaxation [80] except for the additional last constraint in (2.12d). The relaxation is tight only when the solution of problem (2.12) has rank N_t and matrix $\tilde{\mathbf{F}}_{\mathrm{R}}$ such that $\mathbf{X} = \tilde{\mathbf{F}}_{\mathrm{R}}\tilde{\mathbf{F}}_{\mathrm{R}}^{H}$ is an optimal solution of the problem (2.12).

Any of the numerous algorithms to solve phasecut problem can be used to determine the unknown $\mathbf{X}$ in (2.12). However, the constraint (2.12d) needs to be integrated in the chosen method as it does not exist in the standard phasecut problems. The BCD algorithm [81] is chosen and modified to incorporate the additional constraint (2.12d) to solve (2.12). An algorithm called *Modified Block Coordinate Descent* (MBCD) algorithm is proposed that takes account of the structure of $\mathbf{X}$. The proposed MBCD algorithm is summed up in Algorithm 2.1. The proposed MBCD algorithm is exactly same as the BCD algorithm [80] except for the step 9 that ensures the constraint (2.12d) is incorporated.

In the phase retrieval problem, the final aim is to find column vector $\mathbf{v}$ such that

$\mathbf{v}\mathbf{v}^H = \mathbf{X}$ which is usually determined by normalizing each entry of the leading SVD vector or eigenvector of matrix $\mathbf{X}$ to have a magnitude of 1 [80]. However, $\mathbf{X} = \tilde{\mathbf{F}}_{\mathrm{R}}\tilde{\mathbf{F}}_{\mathrm{R}}^H$ in the problem (2.12) where $\tilde{\mathbf{F}}_{\mathrm{R}}$ is a $(N_t + M_t) \times N_t$ matrix, not a vector. However, we can exploit the structure of $\mathbf{X}$ revealed in (2.10) to obtain $\bar{\mathbf{F}}_{\mathrm{R}}$ and hence, $\mathbf{F}_{\mathrm{R}}$ directly from $\mathbf{X}$ as perpetrated in step 5 of Algorithm 2.2. It can be observed from (2.10) that the submatrix corresponding to the last N_t rows and the first M_t columns of $\mathbf{X}$ is equal to $\bar{\mathbf{F}}_{\mathrm{R}}$. Thus, $\mathbf{F}_{\mathrm{R}} = \sqrt{N_t}\bar{\mathbf{F}}_{\mathrm{R}}$ can be directly computed from $\mathbf{X}$. The use of computationally expensive SVD operation on $\mathbf{X}$ can be circumvented in this way.

Algorithm 2.1 Modified Block Coordinate Descent (MBCD) Algorithm

Require: $\mathbf{M}$, M_t, feasible initial $n \times n$ matrix $\mathbf{X}^1$.

1: Choose $\nu > 0$ such that $\nu \to 0$ and integer $N > 1$.
2: **for** $k = 1, \ldots, N_{it}^i$ **do**
3: Pick $i \in [1, n]$.
4: Compute $\mathbf{Y} = \mathbf{X}_{i^c,i^c}^k \mathbf{M}_{i^c,i}$.
5: Compute $\zeta = \Re\left(\mathbf{Y}^H \mathbf{M}_{i^c,i}\right)$.
6: **if** $\zeta > 0$ **then**
$\mathbf{X}_{i^c,i}^{k+1} = \mathbf{X}_{i,i^c}^{k+1^H} = -\sqrt{\frac{1-\nu}{\zeta}}\mathbf{Y}$
7: **else**
$\mathbf{X}_{i^c,i}^{k+1} = \mathbf{X}_{i,i^c}^{k+1^H} = 0$
8: **end if**
9: $\mathbf{X}_{r,r}^{k+1} = \mathbf{I}_{N_t}$ and $\mathbf{X}_{r,q}^{k+1} = \mathbf{X}_{q,r}^{k+1^H} = \frac{1}{\sqrt{N_t}}\exp(j\angle\mathbf{X}_{r,q}^{k+1})$, where $q = 1 : M_t$ and $r = M_t + 1 : n$.
10: **end for**
11: **return** $\mathbf{X}$.

2.3.2 Hybrid Precoder Design via Alternating Minimization

In the proposed hybrid precoding method MBCD-HP, alternating minimization technique is used to determine hybrid precoder. Analog precoder is initialized with a feasible initial value of $\mathbf{F}_{\mathrm{R}}^{(0)}$. The iteration index k is set to 1. At each iteration k, digital precoder $\tilde{\mathbf{F}}_{\mathrm{D}}^k$ is determined as $\mathbf{F}_{\mathrm{R}}^{(k-1)^\dagger}\mathbf{F}_{\mathrm{opt}}$. $\mathbf{M}^k$ is determined using (2.9b) and the value of $\mathbf{F}_{\mathrm{R}}^{(k)}$ is updated using Algorithm 2.1. The iteration index k is increased by 1. The procedure of determining $\tilde{\mathbf{F}}_{\mathrm{D}}$ and $\mathbf{F}_{\mathrm{R}}$ alternately is repeated until the convergence or the maximum number of iterations is reached. The algorithm has been summarized in Algorithm 2.2.

Algorithm 2.2 Alternating minimization hybrid precoding algorithm based on Modified Block Coordinate Descent Method

Require: $\mathbf{F}_{\text{opt}}$, N_t, M_t.

1: Set initial $\mathbf{F}_{\text{R}}^{(0)}$ such that $\left|\mathbf{F}_{\text{R}}^{(0)}\right| = \mathbf{1}_{N_t \times M_t}$ and set $k = 1$.
2: **repeat**
3: Compute $\tilde{\mathbf{F}}_{\text{D}}^{(k)} = \mathbf{F}_{\text{R}}^{(k-1)^{\dagger}} \mathbf{F}_{\text{opt}}$.
4: Compute $\mathbf{M}^{(k)}$ using (2.9b) and determine $\mathbf{X}^{(k)}$ with the help of Algorithm 2.1.
5: Compute $\mathbf{F}_{\text{R}}^{(k)} = \sqrt{N_t}\mathbf{X}_{r,q}^{(k)}$ where $r = M_t + 1 : N_t + M_t$ and $q = 1 : M_t$.
6: $\delta^k = \left| f^{\,k} - f^{\,k-1} \right|$, where $f^{\,k} = \left\| \mathbf{F}_{\text{opt}} - \mathbf{F}_{\text{R}}^{(k)} \tilde{\mathbf{F}}_{\text{D}}^{(k)} \right\|_F^2$.
7: $k \leftarrow k + 1$.
8: **until** $\delta^k < \epsilon$ where $\epsilon \to 0$, or $k \geq max$, the maximum number of iterations.
9: Set $\mathbf{F}_{\text{R}} = \mathbf{F}_{\text{R}}^{(k)}$, $\tilde{\mathbf{F}}_{\text{D}} = \tilde{\mathbf{F}}_{\text{D}}^{(k)}$.
10: Calculate $\mathbf{F}_{\text{D}} = \beta \tilde{\mathbf{F}}_{\text{D}}$, where β is calculated using (2.6).
11: **return** $\mathbf{F} = \mathbf{F}_{\text{R}} \mathbf{F}_{\text{D}}$.

2.4 Hybrid Precoder Based on Iterative Power Method (IPM)

While using the MBCD-HP algorithm, the unconstrained digital precoder and analog precoder need to be computed using MBCD algorithm at each iteration which adds to the complexity. In a bid to reduce the complexity further, a hybrid precoder based on iterative power method is proposed that gets rid of the burden of computing digital precoder and analog precoder at each iteration. The expression for $\tilde{\mathbf{F}}_{\text{D}}$ from (2.5) is substituted in the objective function in (2.8), and is simplified with valid assumptions to obtain the analog precoding subproblem. The objective function in (2.8) can be written as

$$
\begin{aligned}
&\mathbf{Tr}\left[\mathbf{F}_{\text{R}}\tilde{\mathbf{F}}_{\text{D}}\tilde{\mathbf{F}}_{\text{D}}^{H}\mathbf{F}_{\text{R}}^{H} - \mathbf{F}_{\text{R}}\tilde{\mathbf{F}}_{\text{D}}\mathbf{F}_{\text{opt}}^{H} - \mathbf{F}_{\text{opt}}\tilde{\mathbf{F}}_{\text{D}}^{H}\mathbf{F}_{\text{R}}^{H}\right] \\
\overset{(a)}{\approx}&\mathbf{Tr}\left[\frac{1}{N_t^2}\mathbf{F}_{\text{R}}\mathbf{F}_{\text{R}}^{H}\mathbf{F}_{\text{opt}}\mathbf{F}_{\text{opt}}^{H}\mathbf{F}_{\text{R}}\mathbf{F}_{\text{R}}^{H} - \frac{1}{N_t}\mathbf{F}_{\text{R}}\mathbf{F}_{\text{R}}^{H}\mathbf{F}_{\text{opt}}\mathbf{F}_{\text{opt}}^{H} - \frac{1}{N_t}\mathbf{F}_{\text{opt}}\mathbf{F}_{\text{opt}}^{H}\mathbf{F}_{\text{R}}\mathbf{F}_{\text{R}}^{H}\right] \\
\overset{(b)}{\approx}&\frac{1}{N_t}\mathbf{Tr}\left[\mathbf{F}_{\text{R}}^{H}\mathbf{F}_{\text{opt}}\mathbf{F}_{\text{opt}}^{H}\mathbf{F}_{\text{R}}\right] - \mathbf{Tr}\left[\frac{1}{N_t}\mathbf{F}_{\text{R}}\mathbf{F}_{\text{R}}^{H}\mathbf{F}_{\text{opt}}\mathbf{F}_{\text{opt}}^{H} + \frac{1}{N_t}\mathbf{F}_{\text{opt}}\mathbf{F}_{\text{opt}}^{H}\mathbf{F}_{\text{R}}\mathbf{F}_{\text{R}}^{H}\right] \\
=&-\mathbf{Tr}\left[\frac{1}{N_t}\mathbf{F}_{\text{R}}\mathbf{F}_{\text{R}}^{H}\mathbf{F}_{\text{opt}}\mathbf{F}_{\text{opt}}^{H}\right],
\end{aligned}
$$

where the reasons behind (a): $\tilde{\mathbf{F}}_{\mathrm{D}} = \mathbf{F}_{\mathrm{R}}^{\dagger}\mathbf{F}_{\mathrm{opt}} \approx \frac{1}{N_t}\mathbf{F}_{\mathrm{R}}^{H}\mathbf{F}_{\mathrm{opt}}$ as $\mathbf{F}_{\mathrm{R}}^{H}\mathbf{F}_{\mathrm{R}} \approx N_t\mathbf{I}$ in mmWave MIMO as $N_t \to \infty$ [18], (b): $\mathbf{Tr}\left[\mathbf{AB}\right] = \mathbf{Tr}\left[\mathbf{BA}\right]$ and $\mathbf{F}_{\mathrm{R}}^{H}\mathbf{F}_{\mathrm{R}} \approx N_t\mathbf{I}$. Thus, the analog precoding subproblem can be equivalently written as

$$\max_{\mathbf{F}_{\mathrm{R}}} \quad \frac{1}{N_t}\mathbf{Tr}\left[\mathbf{F}_{\mathrm{R}}^{H}\left(\mathbf{F}_{\mathrm{opt}}\mathbf{F}_{\mathrm{opt}}^{H}\right)\mathbf{F}_{\mathrm{R}}\right]. \tag{2.13}$$

If $\bar{\mathbf{F}}_{\mathrm{R}} \triangleq \frac{1}{\sqrt{N_t}}\mathbf{F}_{\mathrm{R}}$, the analog precoding subproblem can be equivalently represented by

$$\max_{\bar{\mathbf{F}}_{\mathrm{R}}} \quad \mathbf{Tr}\left[\bar{\mathbf{F}}_{\mathrm{R}}^{H}\left(\mathbf{F}_{\mathrm{opt}}\mathbf{F}_{\mathrm{opt}}^{H}\right)\bar{\mathbf{F}}_{\mathrm{R}}\right] \tag{2.14a}$$

$$\text{s.t.} \qquad \left|\bar{\mathbf{F}}_{\mathrm{R}_{i,j}}\right| = \frac{1}{\sqrt{N_t}},\ \forall i,j, \tag{2.14b}$$

$$\bar{\mathbf{F}}_{\mathrm{R}}^{H}\bar{\mathbf{F}}_{\mathrm{R}} = \mathbf{I}_{\mathrm{M}_t}, \tag{2.14c}$$

where an extra orthogonal constraint (2.14c) on $\bar{\mathbf{F}}_{\mathrm{R}}$ have been added which implies the constraint $\mathbf{F}_{\mathrm{R}}^{H}\mathbf{F}_{\mathrm{R}} = N_t\mathbf{I}$ on $\mathbf{F}_{\mathrm{R}}$ which is a fair constraint in mmWave MIMO. If it were not for the constraint (2.14b) in problem (2.14), the solution would be given by the matrix containing the M_t leading eigenvectors of $\mathbf{F}_{\mathrm{opt}}\mathbf{F}_{\mathrm{opt}}^{H}$. So, a solution based on iterative power method is proposed to solve (2.14). Similar iterative power method is used in the computation of eigenvectors [82]. However, the proposed iterative power method is modified to make sure that the solution satisfies the constraint (2.14b) at each iteration.

In the proposed method based on iterative power method, $\bar{\mathbf{F}}_{\mathrm{R}}$ is initialized with a feasible $\bar{\mathbf{F}}_{\mathrm{R}}^{(0)}$, and iteration index k is set to 1. At each iteration k, a product matrix $\left(\mathbf{F}_{\mathrm{opt}}\mathbf{F}_{\mathrm{opt}}^{H}\right)\bar{\mathbf{F}}_{\mathrm{R}}^{(k-1)}$ is formed.It is made sure that the columns of the product matrix are orthogonal to each other, and also satisfy the constraint (2.14b) while producing $\bar{\mathbf{F}}_{\mathrm{R}}^{(k)}$. The iteration index k is increased by 1. This procedure is repeated until convergence or the maximum number of iterations is reached. The analog precoder $\mathbf{F}_{\mathrm{R}}$ is computed as $\mathbf{F}_{\mathrm{R}} = \sqrt{N_t}\bar{\mathbf{F}}_{\mathrm{R}}^{(k)}$ and $\mathbf{F}_{\mathrm{D}}$ can be determined using (2.5). The hybrid precoding algorithm based on iterative power method is given in Algorithm 2.3. Modified Gram-Schmidt (MGS) procedure [83] can be used to implement orthogonality

Algorithm 2.3 Iterative Power Method based hybrid precoding algorithm

Require: $\mathbf{F}_{\text{opt}}$, M_t.

1: Compute $\mathbf{M} = \mathbf{F}_{\text{opt}}\mathbf{F}_{\text{opt}}^{H}$.
2: Set initial $\bar{\mathbf{F}}_{\text{R}}^{(0)}$ such that $\left|\bar{\mathbf{F}}_{\text{R}}^{(0)}\right| = \frac{1}{\sqrt{N_t}}\mathbf{1}_{N_t \times M_t}$ and set $k = 1$.
3: **repeat**
4: Perform the adapted Modified Gram-Schmidt orthogonalization procedure on $\mathbf{M}\bar{\mathbf{F}}_{\text{R}}^{(k-1)}$ to compute $\bar{\mathbf{F}}_{\text{R}}^{(k)}$, using Algorithm 2.4.
5: $\delta^k = \left|f^{\,k} - f^{\,k-1}\right|$, where $f^{\,k} = \mathbf{Tr}\left[\bar{\mathbf{F}}_{\text{R}}^{(k)^H}\mathbf{M}\bar{\mathbf{F}}_{\text{R}}^{(k)}\right]$.
6: $k \leftarrow k + 1$.
7: **until** $\delta^k < \epsilon$ wher $\epsilon \to 0$, or $k \geq max$, the maximum number of iterations.
8: Set $\mathbf{F}_{\text{R}} = \sqrt{N_t}\bar{\mathbf{F}}_{\text{R}}^{(k)}$. Compute $\tilde{\mathbf{F}}_{\text{D}} = \mathbf{F}_{\text{R}}^{\dagger}\mathbf{F}_{\text{opt}}$.
9: Calculate $\mathbf{F}_{\text{D}} = \beta\tilde{\mathbf{F}}_{\text{D}}$, where β is calculated using (2.6).
10: **return** $\mathbf{F} = \mathbf{F}_{\text{R}}\mathbf{F}_{\text{D}}$.

constraint (2.14c) on $\bar{\mathbf{F}}_{\text{R}}$. However, the constraint on $\bar{\mathbf{F}}_{\text{R}}$ (2.14b) also needs to be accommodated. Hence, the MGS algorithm has been adapted to develop new algorithm called Adapted Modified Gram-Schmidt (AMGS) orthogonalization procedure which makes sure that each column of the output matrix $\mathbf{Q}_{m\times n}$ is normalized so that its each element has constant modulus of $\frac{1}{\sqrt{m}}$. The AMGS procedure is provided in Algorithm 2.4. Obviously, the analog precoder $\mathbf{F}_{\text{R}}$ computed using AMGS procedure is not going to be exactly orthogonal but only approximately orthogonal as the output matrix $\mathbf{Q}$ of Algorithm 2.4 is derived by extracting only the phases of an orthogonal matrix. However, it works as good substitute as there is no method to the author's knowledge that determines the matrix in which each element satisfies constant modulus constraint and the columns are orthogonal to each other from a given matrix.

Algorithm 2.4 Adapted Modified Gram-Schmidt (AMGS) Orthogonalization Procedure

Require: $\mathbf{X}_{m\times n}$.

1: Initialize $\mathbf{Q} = \mathbf{0}_{m\times n}$.
2: **for** $j = 1, \ldots, n$ **do**.
3: $\mathbf{v} = \mathbf{X}_{.j}$
4: **for** $i = 1, \ldots, j-1$ **do**
5: $r_{ij} = \mathbf{Q}_{.i}^{H}\mathbf{v}$
6: $\mathbf{v} = \mathbf{v} - r_{ij}\mathbf{Q}_{.i}$
7: **end for**
8: Compute $\mathbf{Q}_{.j} = \frac{1}{\sqrt{m}}\exp\left(j\angle\mathbf{v}\right)$.
9: **end for**
10: **return Q**

2.5 Hybrid Precoding for Wideband Channel

In the previous section, two hybrid precoding methods were proposed, considering narrowband mmWave channel. However, the mmWave channel equipped with the large bandwidth exhibits frequency selectivity and multi-path fading. OFDM is employed in the wideband channel, and hybrid precoders for mmWave MIMO-OFDM systems are proposed using the developments made for the narrowband channel. The mmWave MIMO-OFDM channel for the m^{th} subcarrier is given by (1.10).

In the conventional MIMO-OFDM, the digital precoding is performed for each subcarrier, which is followed by inverse fast Fourier Transform (IFFT) that sums all the subcarrier signals together. The mmWave MIMO-OFDM espouses similar procedure with the additional analog precoding succeeding the IFFT operation [40]. Hence, even though there are different digital precoding matrices for each subcarrier, the analog precoding matrix is common for all subcarriers. Hence, the received signal on the m^{th} subcarrier after combining process is given by

$$\mathbf{y}[m] = \sqrt{\rho}\mathbf{W}_{\mathrm{D}}^{H}[m]\mathbf{W}_{\mathrm{R}}^{H}\mathbf{H}[m]\mathbf{F}_{\mathrm{R}}\mathbf{F}_{\mathrm{D}}[m]\mathbf{s} + \mathbf{W}_{\mathrm{D}}^{H}[m]\mathbf{W}_{\mathrm{R}}^{H}\mathbf{n}. \tag{2.15}$$

The hybrid precoding problem for mmWave MIMO-OFDM can be written as [40, 84]

$$\begin{aligned} \min_{\mathbf{F}_{\mathrm{R}},\mathbf{F}_{\mathrm{D}}[m]} \quad & \sum_{m=0}^{S_c-1} \|\mathbf{F}_{\mathrm{opt}}[m] - \mathbf{F}_{\mathrm{R}}\mathbf{F}_{\mathrm{D}}[m]\|_F^2 \\ \text{s.t.} \quad & \|\mathbf{F}_{\mathrm{R}}\mathbf{F}_{\mathrm{D}}[m]\|_F^2 = N_s, \\ & \left|\mathbf{F}_{\mathrm{R}_{i,j}}\right| = 1, \ \forall i, j, \end{aligned} \tag{2.16}$$

where S_c is the number of subcarriers, $\mathbf{F}_{\mathrm{opt}}[m]$ is the optimal fully digital precoder for the m^{th} subcarrier and $\mathbf{F}_{\mathrm{D}}[m]$ is the digital part of the hybrid precoder for the m^{th} subcarrier.

2.5.1 Hybrid Precoder Based on Modified Block Coordinate Descent for mmWave MIMO-OFDM

For the MBCD-based algorithm, we can write the analog precoding problem for the MIMO-OFDM, similar to that in (2.8), as

$$\begin{aligned} \min_{\mathbf{F}_{\mathrm{R}}} \ & \sum_{m=0}^{S_c-1} \mathbf{Tr}\left[\mathbf{F}_{\mathrm{R}}\tilde{\mathbf{F}}_{\mathrm{D}}[m]\tilde{\mathbf{F}}_{\mathrm{D}}^{H}[m]\mathbf{F}_{\mathrm{R}}^{H} - \mathbf{F}_{\mathrm{R}}\tilde{\mathbf{F}}_{\mathrm{D}}[m]\mathbf{F}_{\mathrm{opt}}^{H}[m] - \mathbf{F}_{\mathrm{opt}}[m]\tilde{\mathbf{F}}_{\mathrm{D}}^{H}[m]\mathbf{F}_{\mathrm{R}}^{H}\right] \\ \text{s.t.} \quad & \left|\mathbf{F}_{\mathrm{R}_{i,j}}\right| = 1, \ \forall i,j. \end{aligned} \tag{2.17}$$

The objective function of the problem (2.17) can be written as

$$\begin{aligned} \mathbf{Tr}\Bigg[\mathbf{F}_{\mathrm{R}}\left(\sum_{m=0}^{S_c-1}\tilde{\mathbf{F}}_{\mathrm{D}}[m]\tilde{\mathbf{F}}_{\mathrm{D}}^{H}[m]\right)\mathbf{F}_{\mathrm{R}}^{H} - \mathbf{F}_{\mathrm{R}}\left(\sum_{m=0}^{S_c-1}\tilde{\mathbf{F}}_{\mathrm{D}}[m]\mathbf{F}_{\mathrm{opt}}^{H}[m]\right) - \\ \left(\sum_{m=0}^{S_c-1}\mathbf{F}_{\mathrm{opt}}[m]\tilde{\mathbf{F}}_{\mathrm{D}}^{H}[m]\right)\mathbf{F}_{\mathrm{R}}^{H}\Bigg]. \end{aligned} \tag{2.18}$$

Thus, the analog precoder for mmWave MIMO-OFDM has been translated into optimization problem similar to that for the narrowband channel in (2.8) and hence solved by the same alternating minimization algorithm as in Algorithm 2.2. At each iteration, matrix $\mathbf{M}$ and the unconstrained digital precoder matrix for the m^{th} subcarrier, $\tilde{\mathbf{F}}_{\mathrm{D}}[m]$ can be determined as

$$\mathbf{M} = \begin{bmatrix} \sum_s \tilde{\mathbf{F}}_{\mathrm{D}}[m]\tilde{\mathbf{F}}_{\mathrm{D}}^{H}[m] & -\frac{1}{\sqrt{N_t}}\sum_s \tilde{\mathbf{F}}_{\mathrm{D}}[m]\mathbf{F}_{\mathrm{opt}}^{H}[m] \\ -\frac{1}{\sqrt{N_t}}\sum_s \mathbf{F}_{\mathrm{opt}}[m]\tilde{\mathbf{F}}_{\mathrm{D}}^{H}[m] & \mathbf{0} \end{bmatrix} \tag{2.19a}$$

$$\tilde{\mathbf{F}}_{\mathrm{D}}[m] = \mathbf{F}_{\mathrm{R}}^{\dagger}\mathbf{F}_{\mathrm{opt}}[m] \tag{2.19b}$$

2.5.2 Hybrid Precoder Based on Iterative Power Method for mmWave MIMO-OFDM

The mmWave MIMO-OFDM analog precoding problem equivalent to its narrowband counterpart in (2.14) can be written as

$$\begin{aligned} \max_{\bar{\mathbf{F}}_{\mathrm{R}}} \quad & \sum_{m=0}^{S_c-1} \mathbf{Tr}\left[\bar{\mathbf{F}}_{\mathrm{R}}^{H}\left(\mathbf{F}_{\mathrm{opt}}[m]\mathbf{F}_{\mathrm{opt}}^{H}[m]\right)\bar{\mathbf{F}}_{\mathrm{R}}\right] \\ \text{s.t.} \quad & \text{(2.14b)} \quad \text{and} \quad \text{(2.14c)}, \end{aligned} \tag{2.20}$$

which is equivalent to

$$\begin{aligned} \max_{\bar{\mathbf{F}}_{\mathrm{R}}} \quad & \mathbf{Tr}\left[\bar{\mathbf{F}}_{\mathrm{R}}^{H}\left(\sum_{m=0}^{S_c-1}\mathbf{F}_{\mathrm{opt}}[m]\mathbf{F}_{\mathrm{opt}}^{H}[m]\right)\bar{\mathbf{F}}_{\mathrm{R}}\right] \\ \text{s.t.} \quad & \text{(2.14b)} \quad \text{and} \quad \text{(2.14c)}. \end{aligned} \tag{2.21}$$

We can solve for $\mathbf{F}_{\mathrm{R}} = \sqrt{N_t}\bar{\mathbf{F}}_{\mathrm{R}}$ by solving (2.21) using the Algorithm 2.3 where $\mathbf{M} = \sum_{m=0}^{S_c-1}\mathbf{F}_{\mathrm{opt}}[m]\mathbf{F}_{\mathrm{opt}}^{H}[m]$. The digital precoder and then the hybrid precoder for each subcarrier can be determined subsequently.

2.6 Complexity Analyses of the proposed methods

The complexity of the hybrid precoding algorithm is mainly governed by the computation of its analog precoder. The computational complexities of calculating analog precoder of the proposed methods are compared with several existing hybrid precoding algorithms. The complexities of the proposed algorithms in narrowband scenario are computed and listed in TABLE 2.1. All the algorithms under consideration require optimal fully digital optimal precoder, and hence the complexity incurred in computing optimal precoder is not included in the comparison. In TABLE 2.1, the complexities of several existing precoders HD-LSR, SSP, MO-AltMin and SDR-AO in narrowband case are also listed. The complexity of MO-AltMin has been sourced from [44], whereas the complexity of SSP has been derived from [42].

(i) ***Narrowband MBCD-HP*** : The complexity of narrowband MBCD-HP at

Table 2.1: COMPARISON OF COMPUTATIONAL COMPLEXITY OF DIFFERENT ALGORITHMS

Narrowband	
Algorithm	**Complexity**
HD-LSR [36]	$\mathcal{O}\left(N_{it}\left(N_t M_t^2 N_s + N_t M_t N_s\right)\right)$
SSP [18]	$\mathcal{O}\left(N_t^2 M_t N_s\right)$
MO-AltMin [40]	$N_{it}^o N_{it}^i \mathcal{O}\left(4N_t^2 M_t + 13 N_t M_t^2 + 3 N_t M_t + 8 M_t^3\right)$
SDR-AO [42]	$\mathcal{O}\left(N_{it}\left(M_t^7\left(N_t^7 + N_s^7\right) + M_t^3\left(N_t^3 + N_s^3\right)\right)\right)$
MBCD-HP	$N_{it}^o \mathcal{O}\left(N_{it}^i \left(N_t + M_t - 1\right)^2 + N_t^2 M_t + 2 N_t M_t N_s + M_t^2 N_s\right)$
IPM-HP	$\mathcal{O}\left(N_{it} N_t^2 M_t + N_t M_t^2 + N_t^2 N_s\right)$
Wideband	
Algorithm	**Complexity**
MBCD-HP	$N_{it}^o \mathcal{O}\left(N_{it}^i \left(N_t + M_t - 1\right)^2 + S_c(N_t^2 M_t + 2 N_t M_t N_s + M_t^2 N_s)\right)$
IPM-HP	$\mathcal{O}\left(N_{it} N_t^2 M_t + N_t M_t^2 + S_c N_t^2 N_s\right)$

each iteration k is mainly governed by

- *Computation of* $\mathbf{M}^{(k)}$: The product of $\tilde{\mathbf{F}}_{\mathrm{D}}^{(k)} \tilde{\mathbf{F}}_{\mathrm{D}}^{(k)^H}$ has a computational complexity of $\mathcal{O}\left(M_t^2 N_s\right)$, while determining the product $\mathbf{F}_{\mathrm{opt}} \tilde{\mathbf{F}}_{\mathrm{D}}^{(k)^H}$ brings the complexity of $\mathcal{O}\left(N_t M_t N_s\right)$. Thus, computation of $\mathbf{M}^{(k)}$ incurs the complexity of $\mathcal{O}\left(M_t^2 N_s + N_t M_t N_s\right)$.

- *MBCD algorithm* : The complexity of BCD algorithm can not be categorically evaluated [80]. However, the complexity of the modified BCD algorithm is estimated for the worst case scenario. The complexity of the modified BCD algorithm mainly depends on step 4 of the Algorithm 2.1 which has the complexity of $\mathcal{O}\left((n-1)^2\right)$. The size of matrix $\mathbf{M}^{(k)}$ which is the input to modified BCD algorithm is $N_t + M_t$ so that $n = N_t + M_t$ and the step 4 in Algorithm 2.1 is repeated N_{it}^i times.

- *Computation of* $\tilde{\mathbf{F}}_{\mathrm{D}}^{(k)}$: It involves pseudoinverse computation of $\mathbf{F}_{\mathrm{R}}^{(k-1)}$ and a matrix multiplication. The computation of pseudoinverse of $\mathbf{F}_{\mathrm{R}}^{(k-1)}$ involves a complexity of $\mathcal{O}\left(N_t^2 M_t\right)$ and the matrix multiplication $\mathbf{F}_{\mathrm{R}}^{(k-1)^\dagger} \mathbf{F}_{\mathrm{opt}}$ to generate $\tilde{\mathbf{F}}_{\mathrm{D}}^{(k)}$ encompasses the complexity of $\mathcal{O}\left(N_t M_t N_s\right)$, making its computational complexity $\mathcal{O}\left(N_t^2 M_t + N_t M_t N_s\right)$.

The above operations are repeated N_{it}^o times so that the complexity of MBCD-HP may be expressed as $N_{it}^o \mathcal{O}(N_{it}^i \left(N_t + M_t - 1\right)^2 + N_t^2 M_t + 2 N_t M_t N_s + M_t^2 N_s)$.

N_{it}^o and N_{it}^i represent the number of outer and inner iterations respectively.

(ii) ***Wideband MBCD-HP*** : The computational complexity of each iteration of wideband MBCD-HP is the sum of complexities involved in

- *Computation of* $\mathbf{M}^{(k)}$: The computation of $\sum_s \tilde{\mathbf{F}}_{\mathrm{D}}^{(k)}[s]\,\tilde{\mathbf{F}}_{\mathrm{D}}^{(k)}[s]^H$ and $\sum_s \mathbf{F}_{\mathrm{opt}}\tilde{\mathbf{F}}_{\mathrm{D}}^{(k)}[m]^H$ have the complexity of $S_c\mathcal{O}\left(M_t^2N_s\right)$ and $S_c\mathcal{O}\left(N_tM_tN_s\right)$ respectively, so the total complexity in computing $\mathbf{M}^{(k)}$ is $S_c\mathcal{O}\left(M_t^2N_s + N_tM_tN_s\right)$.

- *MBCD algorithm* : Similar to the narrowband case, the complexity of MBCD algorithm in wideband scenario is $N_{it}\mathcal{O}\left(\left(N_t + M_t - 1\right)^2\right)$ where N_{it} is number of iterations in MBCD algorithm.

- *Computation of* $\tilde{\mathbf{F}}_{\mathrm{D}}^{(k)}[m]$: It involves pseudoinverse computation of $\mathbf{F}_{\mathrm{R}}^{(k-1)}$ and S_c matrix multiplications. The computation of S_c matrix multiplications $\mathbf{F}_{\mathrm{R}}^{(k-1)^\dagger}\mathbf{F}_{\mathrm{opt}}[m]$ brings the complexity of $S_c\mathcal{O}\left(N_tM_tN_s\right)$, making its computational complexity $\mathcal{O}\left(N_t^2M_t + S_cN_tM_tN_s\right)$.

The above operations are repeated N_{it}^o times so that the complexity of MBCD-HP may be expressed as $N_{it}^o\mathcal{O}\left(N_{it}^i\left(N_t + M_t - 1\right)^2 + S_c(N_t^2M_t + 2N_tM_tN_s + M_t^2N_s)\right)$.

(iii) ***Narrowband IPM-HP*** : The complexity of narrowband IPM-HP is largely determined by

- *The computation of* $\mathbf{M}\bar{\mathbf{F}}_R^{(k-1)}$: The complexity involved in calculating the product $\mathbf{M}\bar{\mathbf{F}}_{\mathrm{R}}^{(k-1)}$ is $\mathcal{O}\left(N_t^2M_t\right)$.

- *The adapted MGS orthogonalization* : It is performed on $\mathbf{M}\bar{\mathbf{F}}_{\mathrm{R}}^{(k-1)}$ using Algorithm 2.4 at each iteration k. The computational complexity of the adapted MGS orthogonalization in the Algorithm 2.4 is dictated by step 4-step 6. Even though the Algorithm 2.4 differs slightly from the actual MGS algorithm in step 8, we can still consider the computational complexity of the actual MGS algorithm which is $\mathcal{O}\left(N_tM_t^2\right)$ [85] (Chapter 5.2.8).

The above operations are repeated N_{it} times. In addition, the computational complexity of $\mathcal{O}\left(N_t^2 N_s\right)$ is associated with computing $\mathbf{M}$. Thus, the total complexity of computing analog precoder in the IPM-HP alogorithm is $\mathcal{O}\left(N_{it}(N_t^2 M_t + N_t M_t^2) + N_t^2 N_s\right)$ where N_{it} is the number of iterations performed. Finally, determining $\mathbf{F}_{\mathrm{D}}$ brings about the complexity of $\mathcal{O}(N_t^2 M_t + N_t M_t N_s)$.

(iv) ***Wideband IPM-HP*** : The complexity involved in wideband IPM-HP is the result of

- *Computation of* $\mathbf{M}$: The computational complexity arising from the computation of $\mathbf{M}$ is $S_c\mathcal{O}\left(N_t^2 N_s\right)$ as it involves S_c multiplications between $N_t \times N_s$ matrix $\mathbf{F}_{\mathrm{opt}}[m]$ and $N_s \times N_t$ matrix $\mathbf{F}_{\mathrm{opt}}^H[m]$.
- *Computation of* $\mathbf{M}\bar{\mathbf{F}}_R^{(k-1)}$: The complexity involved in calculating the product $\mathbf{M}\bar{\mathbf{F}}_{\mathrm{R}}^{(k-1)}$ is $\mathcal{O}\left(N_t^2 M_t\right)$.
- *Adapted MGS orthogonalization* : The adapted MGS orthogonalization is performed on $\mathbf{M}\bar{\mathbf{F}}_{\mathrm{R}}^{(k-1)}$ which is of size $N_t \times M_t$, similar to the narrowband case. Thus, the complexity is also $\mathcal{O}\left(N_t M_t^2\right)$.

The last two operations are repeated N_{it} times. Thus, the total complexity of computing analog precoder in the IPM-HP alogorithm is $\mathcal{O}(N_{it}(N_t^2 M_t + N_t M_t^2) + N_t^2 N_s)$ where N_{it} is the number of iterations performed. Finally, determining $\mathbf{F}_{\mathrm{D}}[m]$ brings about the complexity of $S_c\mathcal{O}\left(N_t^2 M_t + N_t M_t N_s\right)$.

2.7 Performance Analysis

Point-to-point MIMO system with $N_t = 64$ antennas at the transmitter and $N_r = 16$ antennas at the receiver is considered to assess the performance of the proposed precoding methods. A clustered channel model is considered to model mmWave channel so as to capture its scattering nature mathematically. The narrowband and wideband downlink channel between the transmitter and the receiver are given by (1.4) and (1.8) respectively where $N_{p_i} = N_p \ \forall i$.

The channel parameters $N_c = 5$, $N_p = 10$, $\alpha_{i\ell} \sim \mathcal{CN}(0,1)$, as in [40] are considered. The AoDs and AoAs are taken to be Laplacian distributed with their mean angles uniformly distributed over $[0, 2\pi]$ and angular spread of 10 degrees. The antenna elements are separated by a distance of half wavelength. We define the signal-to-noise ratio (SNR) used in the plots as SNR $= \frac{\rho}{\sigma_n^2}$. The number of data streams N_s is considered 4 in all figures except Figure 2.3 and Figure 2.7 where N_s is varied. In all the figures, the number of RF chains at both the transmitter and receiver are considered equal to the number of data streams, *i.e.*, $M_t = M_r = N_s$. When SNR is not the varying parameter, it is taken as 0 dB. The fully digital precoding is taken as performance benchmark.

Table 2.2: PARAMETERS FOR SIMULATIONS

Parameters	**Narrowband**	**Wideband**
N_t	64	64
N_r	16	16
N_s	4	4
N_c	5	5
N_p	10	10
$\alpha_{i\ell}$	$\sim \mathcal{CN}(0,1)$	$\sim \mathcal{CN}(0,1)$
S_c	-	128

2.7.1 Narrowband Channel

Figure 2.1 shows the convergence behavior of the proposed MBCD-HP and IPM-HP algorithms averaged over 500 channel realizations. The objective function at the k^{th} iteration is defined as

$$f^{\,k} = \left\| \mathbf{F}_{\text{opt}} - \mathbf{F}_{\text{R}}^{(k)} \mathbf{F}_{\text{D}}^{(k)} \right\|_F^2 .$$

It can be seen that both MBCD-HP and IPM-HP converge monotonically.

The spectral and bit error rate (BER) performances of the proposed algorithms are compared against SSP [18], the existing high-performing methods like HD-LSR [36], MO-AltMin [40] and SDR-AO [42]. The spectral efficiency is computed as

$$\log_2 \left(I + \frac{\rho}{\sigma_n^2 N_s} \mathbf{W}^{\dagger} \mathbf{H} \mathbf{F} \mathbf{F}^H \mathbf{H}^H \mathbf{W} \right).$$

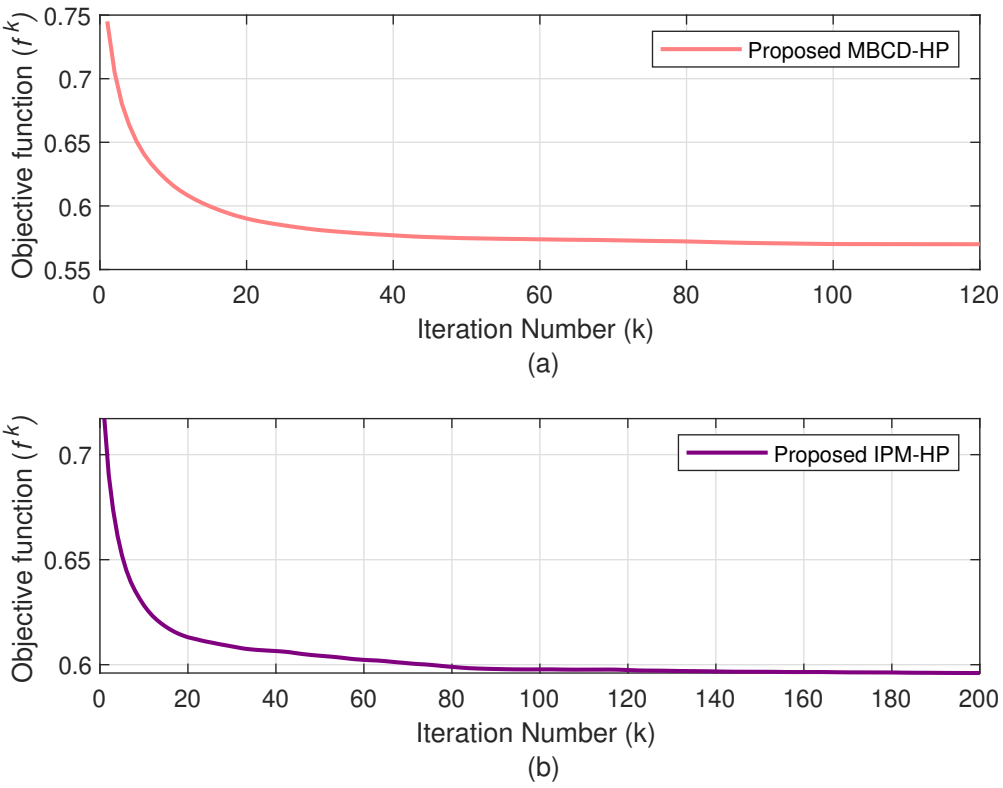

Figure 2.1: Convergence behavior of a) Proposed MBCD-HP a) Proposed IPM-HP in narrowband channel.

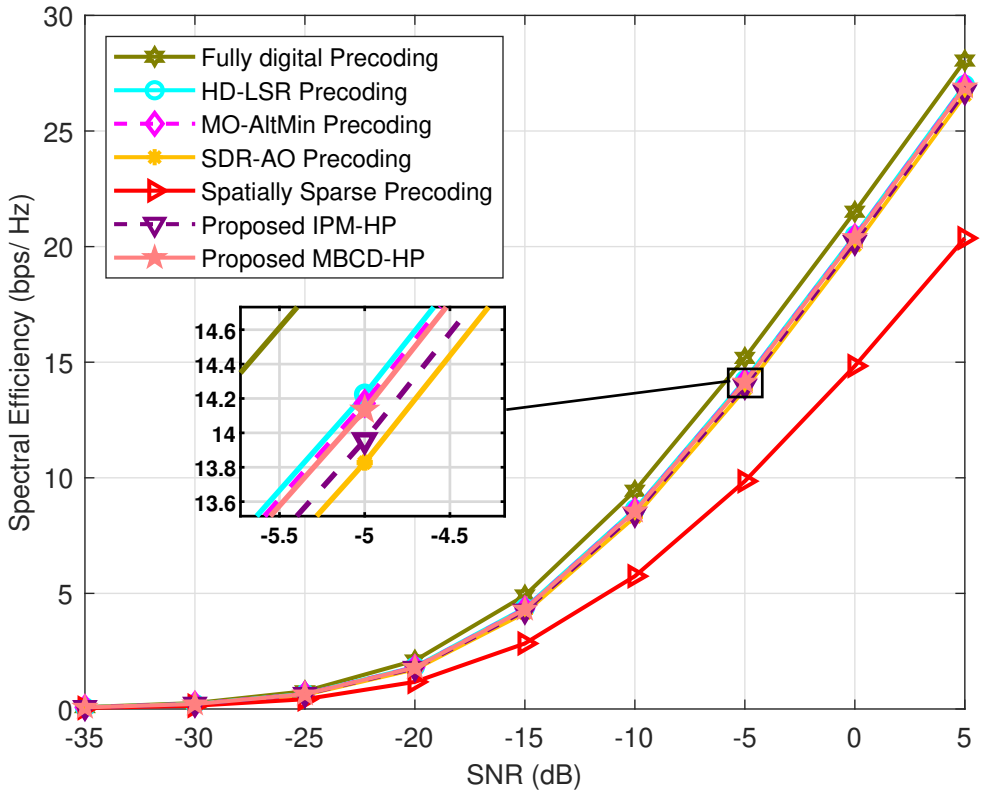

Figure 2.2: Spectral efficiency in narrowband channel as a function of SNR.

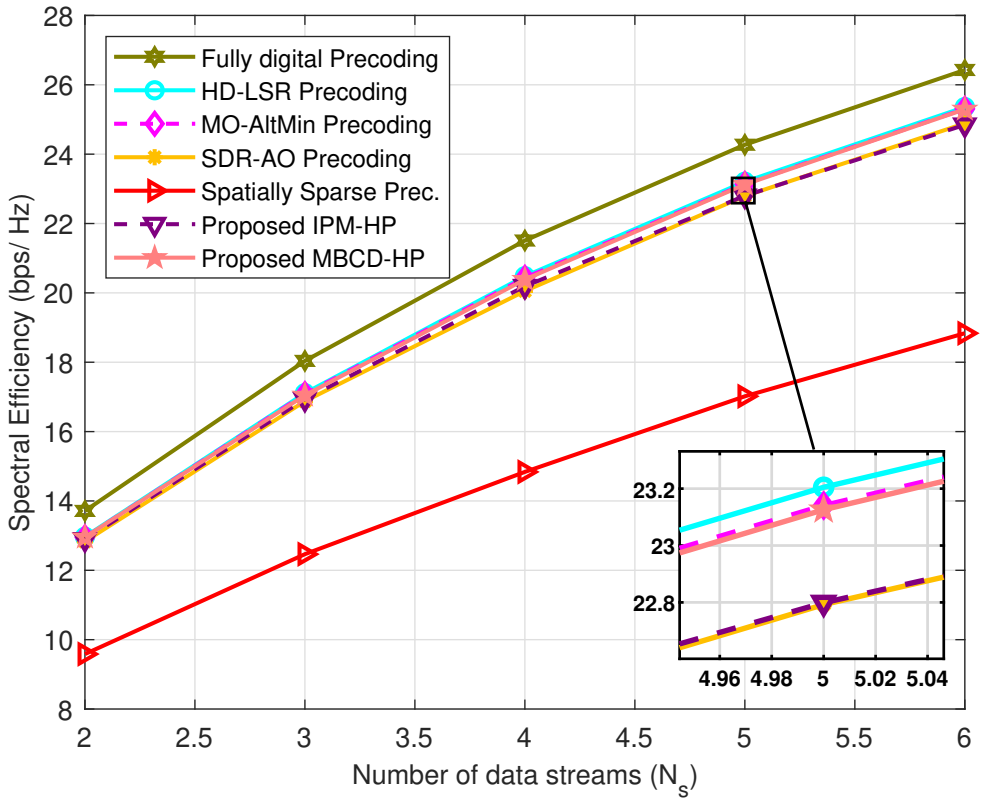

Figure 2.3: Spectral efficiency in narrowband channel as a function of number of data streams N_s.

In Figure 2.2 and Figure 2.3, the spectral performances of the proposed algorithms are examined with respect to other existing algorithms. The performance of MBCD-HP is very close to HD-LSR and MO-AltMin algorithms across all the values of SNR and N_s and clearly better than SDR-AO. IPM-HP, while slightly behind MBCD-HP, also performs better than SDR-AO. The spectral performance of IPM-HP is very close to HD-LSR, MO-AltMin and MBCD-HP at lower values of N_s but diverges slightly away at higher N_s.

In Figure 2.4, the BER performances of the proposed precoding methods are compared with the existing hybrid precoders. The BER performance of MBCD-HP is only behind performance of HD-LSR, and they both exhibit the best performances among all other precoders. The performances of SDR-AO, MO-AltMin and IPM-HP are similar with MO-AltMin showing the best performance among these three. However, the performance of SDR-AO gets better at higher SNR values. IPM-HP is slightly behind MO-AltMin and SDR-AO in BER performance, whereas SSP performs the

poorest across all SNR values.

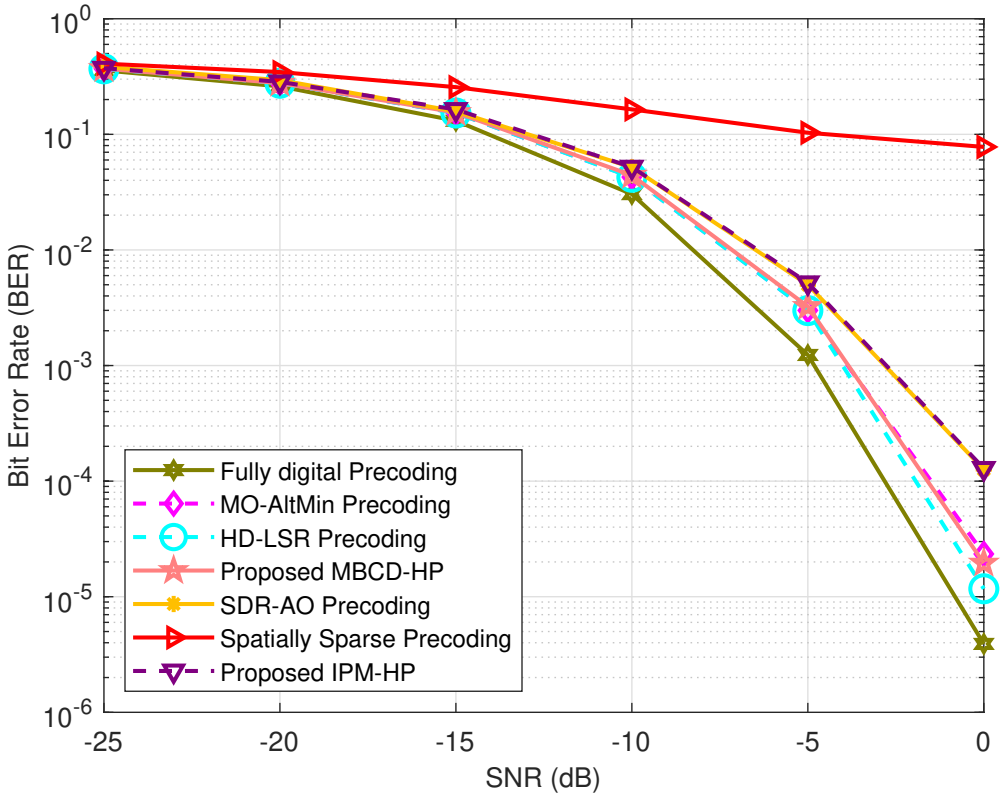

Figure 2.4: Bit Error Rate (BER) in narrowband channel as a function of SNR.

The Figure 2.5 shows how average run time of various algorithms vary versus the number of transmit antennas N_t. The plot for SDR-AO is produced in the inset to obtain an intelligible figure. All algorithms are run on 1.6 GHz Intel Core i5 PC with 8 GB RAM. It is evident that the convergence time of MBCD-HP is lower than that of MO-AltMin and very small compared to SDR-AO. For example at $N_t = 64$, the average run time are 45.08 seconds, 1.65 seconds, 0.9689 seconds, 0.0396 seconds, and 1.705 ms for SDR-AO, MO-AltMin, MBCD-HP, HD-LSR, and IPM-HP respectively. It is IPM-HP that proves to be the winner for having significantly lower convergence time compared to all the algorithms, including HD-LSR. HD-LSR comes with low complexity as well, however it is defined only for narrowband channel. The average run time increases with N_t for each of the algorithms. As far as average run time is concerned, SDR-AO is affected the most with the increase in N_t, followed by MO-AltMin. On the other hand, it is IPM-HP which is the least affected. As an instance, when N_t increases to 96, the average run time climbs to 152.3 seconds for

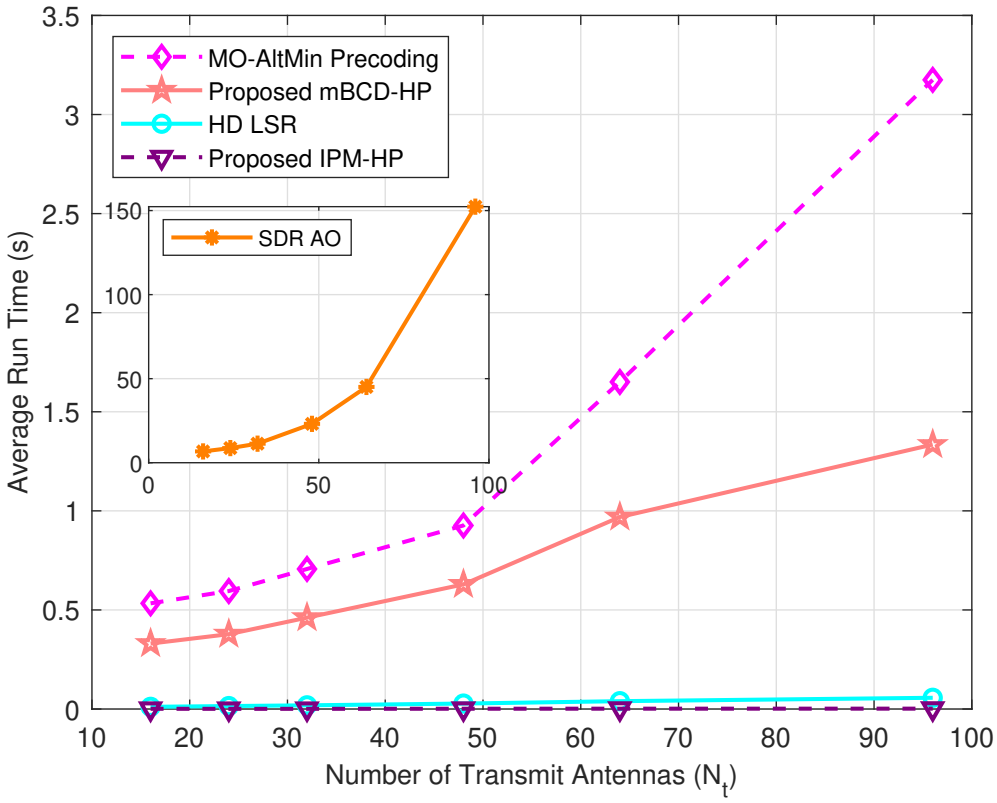

Figure 2.5: Average convergence times in narrowband channel for various precoding methods.

SDR-AO , 3.175 seconds for MO-AltMin , 1.335 seconds for MBCD-HP, 0.05673 seconds for HD-LSR , and 1.88 ms for IPM-HP. It is apparent that the computational complexity and hence the run time rises steeply for SDR-AO and MO-AltMin as N_t increases.

2.7.2 Wideband Channel

The number of subcarriers S_c for the wideband channel is taken as 128. The spectral performance of the proposed algorithms is compared against the fully digital precoding, the existing high-performing methods like MO-AltMin [40] and SDR-AO [42]. Since HD-LSR and SSP are designed only for narrowband channel case, they are not considered for comparison in wideband channel.

The spectral efficiency of the proposed algorithms are evaluated in wideband channel as compared to the existing methods in Figure 2.6 and Figure 2.7. The performances of all the algorithms are close throughout the values of SNR with MO-AltMin

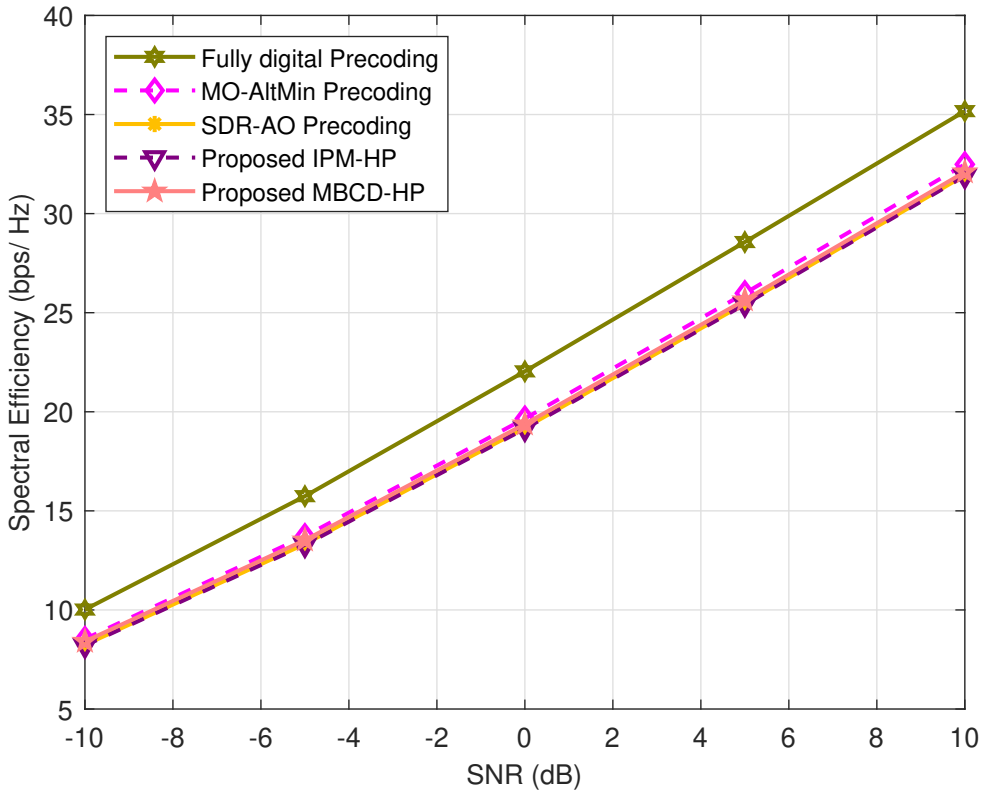

Figure 2.6: Spectral efficiency in wideband channel as a function of SNR.

performing the best, followed by MBCD-HP and SDR-AO. The performance of IPM-HP is behind all other methods. At lower values of N_s, MBCD-HP and SDR-AO are close in their performance, however MBCD-HP gets better at higher values of N_s. Similar to the case in narrowband channel, the spectral efficiency of IPM-HP deviates from those of other algorithms at higher values of N_s.

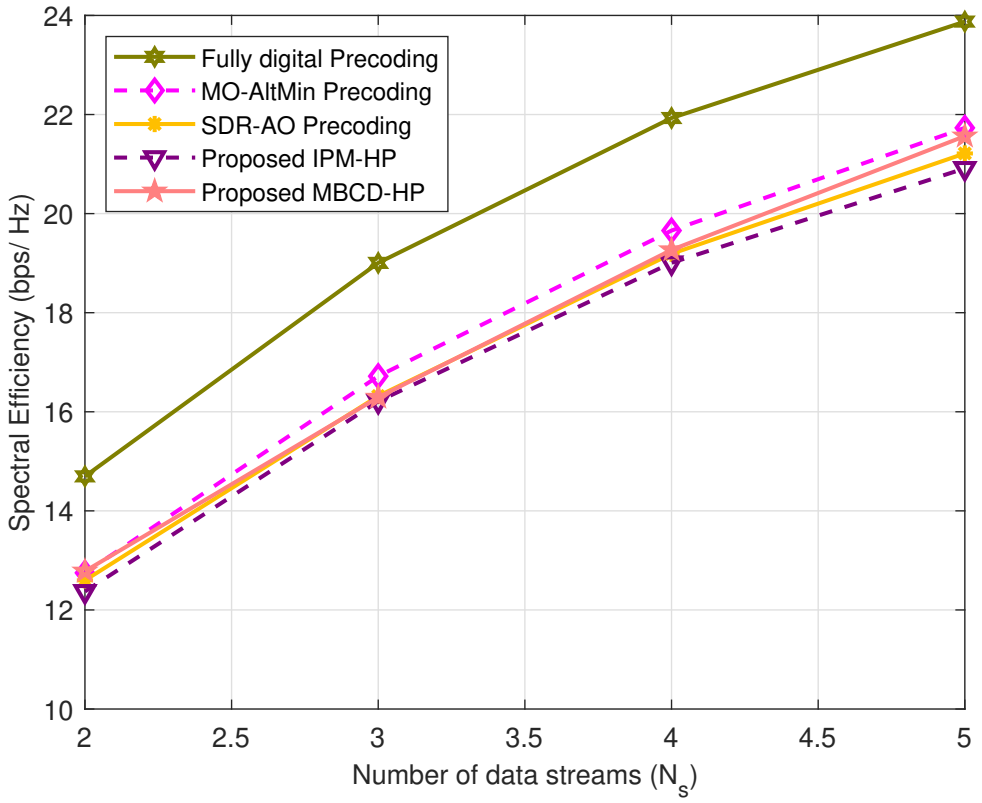

Figure 2.7: Spectral efficiency in wideband channel as a function of number of data streams N_s for $M_t = N_s$.

2.8 Summary

In this chapter, the hybrid precoding problem in narrowband point-to-point mmWave MIMO channel is considered. The hybrid precoding problem, which is a Frobenius norm minimization problem, is translated into trace minimization problem. Two algorithms are proposed to solve it. In the first method based on alternating minimization, the analog precoder and digital precoder are alternately determined, keeping the other constant to minimize the trace. The analog precoding subproblem with the fixed digital precoder is converted into an SDP problem and solved by BCD algorithm with suitable modifications. In the second method, the analog precoding and digital precoding subproblems are segregated by considering orthogonality of analog precoder. The analog precoding is further rephrased as a trace maximization problem and solved by an iterative power method by enforcing orthogonality constraint on the analog precoder. The adapted form of modified Gramm-Schmidt orthogonalization procedure is employed to impose orthogonality on the analog

precoder. The proposed methods are extended for wideband channel by considering OFDM. The proposed method based on modified BCD not only exhibits a good performance but also comes with lower computational complexity when compared to existing methods with comparable performances. The hybrid precoder based on iterative power method, in particular, has ridiculously low complexity compared to existing algorithms at the price of very small dent in performance.

Chapter 3

Energy-efficient Precoding in Point-to-Point mmWave MIMO

Among the two main kinds of hybrid architectures, PC and FC architectures, two hybrid precoding algorithms proposed in Chapter 2 considered FC architecture. The FC architecture comes with the added complexities introduced by the complex network of the phase shifters. The PC architecture, on the other hand, has reduced complexity but offers reduced beamforming gain and as a result, provides limited performance. The power consumption in the PC architecture is also lower than the FC architecture as the number of phase shifters is lesser by a factor of number of RF chains. In [86], an iterative procedure built on the concept of successive interference cancellation (SIC) is proposed for PC MIMO for a case where number of RF chains is equal to data streams. Yu *et. al.* [40] propose an alternating minimization algorithm based on semi-definite programming (SDP) as solution to hybrid precoding problem for PC MIMO.

Apart from FC and PC architectures, a new hybrid architecture was proposed in [87] that combines both FC and PC structures which we call *partial-full mixed connection* (PFMC). In the PFMC architecture, the RF chains and the antennas are organized into different subgroups. All the RF chains of each subgroup are connected to all the antennas of that particular subgroup through phase shifters. In this architecture,

each RF chain is connected to only a subset of antennas similar to PC architecture. However, PFMC architecture resembles FC architecture in regard to how RF chains of a particular subgroup are connected to the antennas of that particular subgroup.

Two hybrid precoders are presented in [87] for the PFMC architecture, one based on SIC and another based on matrix factorization. Chen *et al.* [88] consider an mmWave MIMO system with a PFMC architecture, which they call sub-array-connected architecture, in which each sub-array can have arbitrary number of RF chains and antennas. A hybrid precoding algorithm based on successive interference cancellation is proposed in [88] to enrich the energy efficiency. Feng *et al.* [89] adopt the PFMC architecture in an RIS-assisted mmWave MIMO, and present algorithm based on SIC that jointly optimizes hybrid precoder and passive precoding to maximize sum-rate for each subgroup.

In this chapter, the hybrid precoding for PFMC architecture is modeled as a matrix factorization problem for individual subgroups where the Euclidean distance between the submatrices of fully digital precoder and the hybrid precoder, corresponding to a subgroup is used as a cost function. Two hybrid precoders based on a) alternating minimization approach, and b) iterative power method introduced in Chapter 2, are proposed. The proposed hybrid precoders for the PFMC structure not only produce better energy efficiency and spectral performances than the SIC based precoder in [87], but also exhibit better energy efficiency compared to the existing precoders for FC and PC architectures.

3.1 System Model

A single user mmWave MIMO downlink system is considered with the transmitter connected to N_t transmit antennas and the receiver connected to N_r receive antennas. The mmWave transceiver system is similar to as shown in Figure 1.3. The transmitter and the receiver consist of M_t and M_r RF chains respectively. The transmitter is able to transmit N_s data streams such that $N_s \leq M_t \leq N_t$ and $N_s \leq M_r \leq N_r$. The PFMC architecture is considered at both the transmitter and the receiver. At the

transmitter, as shown in Figure 3.1, the RF chains and antennas are divided into S different subgroups with each subgroup 'i' having C_i RF chains and N_i antennas. Thus, $N_t = \sum_{i=1}^{S} N_i$ and $M_t = \sum_{i=1}^{S} C_i$. The number of paths traversed by a signal emanating from an RF chain is equal to N_t in FC architecture and $\frac{N_t}{M_t}$ in PC architecture. On the other hand, the average number of paths travelled by a signal emerging from an RF chain in PFMC architecture is $\frac{\sum_{i=1}^{S} C_i N_i}{\sum_{i=1}^{S} C_i}$ which is equal to $\frac{N_t}{S}$ when $C_i = C \ \forall \ i$. Thus, the complexity in terms of implementation of PFMC architecture lies in between the FC architecture and the PC architecture.

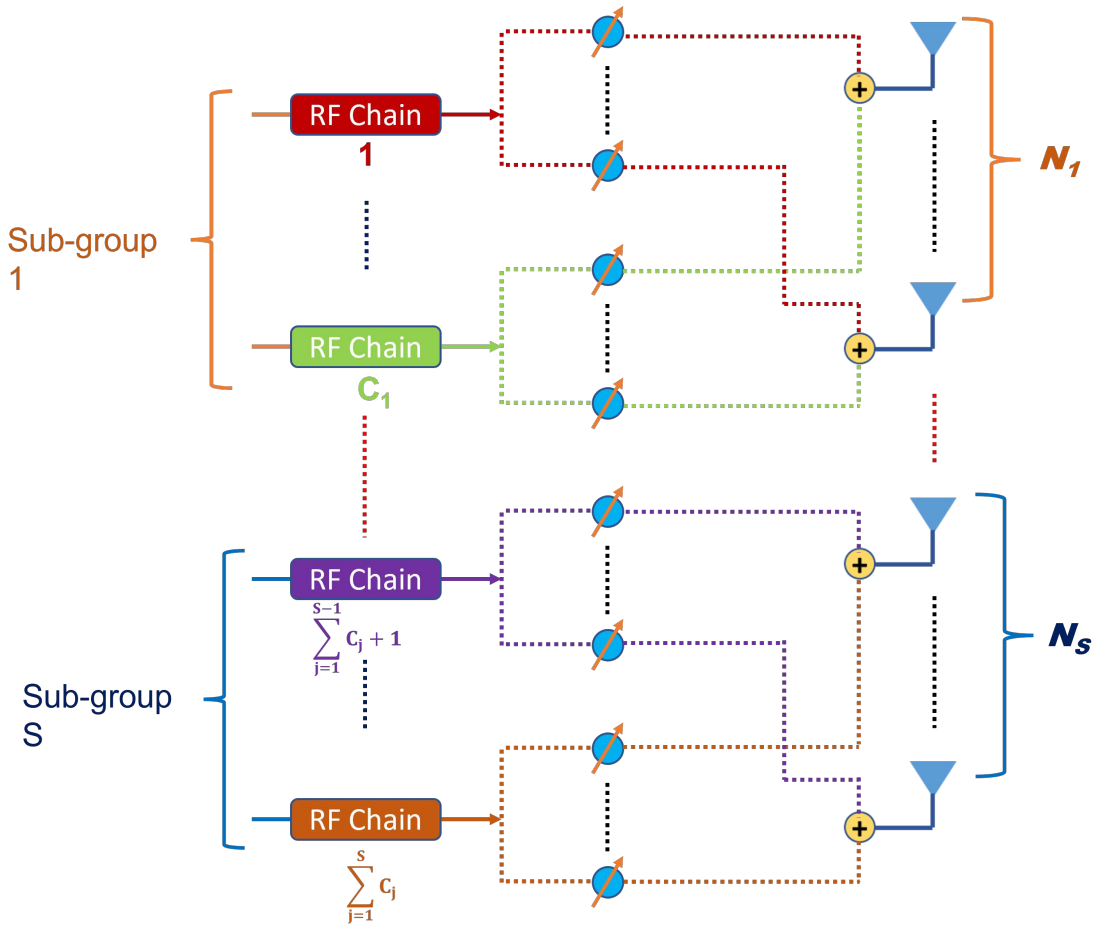

Figure 3.1: System diagram showing partial-full mixed connection.

The energy efficiency is defined as the ratio of spectral efficiency to the total power consumed [40] and thus the energy efficiency from BS's perspective is

$$\eta = \frac{Rate}{P_{com} + M_t P_{RF} + M_t P_{PA} + N_{PS} P_{PS}} \text{ bits/ Hz/ Joules,} \tag{3.1}$$

where P_{com} is the common power of transmitter, N_{PS} is the number of phase-shifters, whereas P_{RF}, P_{PA} and P_{PS} respectively represent the power of each RF chain, power amplifier and phase shifter. The number of phase-shifters in FC, PC and PFMC architectures are $N_t M_t$, N_t and $\sum_{i=1}^{S} C_i N_i$ respectively.

3.2 Problem Formulation

In this section, the modeling of hybrid precoder for the PFMC architecture will be performed. All the arguments about the hybrid precoder hold true for the hybrid combiner except the total power constraint. The analog precoding matrix $\mathbf{F}_{\mathrm{R}}$ has a block diagonal structure as

$$\mathbf{F}_{\mathrm{R}} = \begin{bmatrix} \mathbf{F}_{\mathrm{R}}^{1} & \mathbf{0} & \dots & \mathbf{0} \\ \mathbf{0} & \mathbf{F}_{\mathrm{R}}^{2} & \dots & \mathbf{0} \\ \vdots & \vdots & \ddots & \vdots \\ \mathbf{0} & \mathbf{0} & \dots & \mathbf{F}_{\mathrm{R}}^{S} \end{bmatrix}, \tag{3.2}$$

where $\mathbf{F}_{\mathrm{R}}^{i} \in \mathbb{C}^{N_i \times C_i},\ i = 1, \dots, S$ is the analog precoding submatrix corresponding to the i^{th} sub-group. The analog precoder is constructed using the network of phase shifters which, as a result, forces the non-zero element of $\mathbf{F}_{\mathrm{R}}$ to have a constant unit amplitude, *i.e.*, $|\mathbf{F}^{i}_{\mathrm{R}_{m,n}}| = 1\ \forall i$. Similar to Chapter 2, the optimal hybrid precoder can be constructed by minimizing the Euclidean distance between the optimal fully digital precoder and the hybrid precoder. Hence, the hybrid precoding design problem can be stated as

$$\begin{aligned} (\mathbf{F}_{\mathrm{R}}^{\star}, \mathbf{F}_{\mathrm{D}}^{\star}) = \underset{\mathbf{F}_{\mathrm{R}}, \mathbf{F}_{\mathrm{D}}}{\arg\min} \quad & \|\mathbf{F}_{\mathrm{opt}} - \mathbf{F}_{\mathrm{R}}\mathbf{F}_{\mathrm{D}}\|_F^2 \\ \text{s.t.} \quad & \|\mathbf{F}_{\mathrm{R}}\mathbf{F}_{\mathrm{D}}\|_F^2 = N_s, \\ & \mathbf{F}_{\mathrm{R}} = \mathbf{BLKDIAG}\left(\mathbf{F}_{\mathrm{R}}^{1}, \dots, \mathbf{F}_{\mathrm{R}}^{S}\right) \\ & |\mathbf{F}^{i}_{\mathrm{R}_{m,n}}| = 1, \quad 1 \le i \le S, \quad \forall m, n, \end{aligned} \tag{3.3}$$

where $\mathbf{F}_{\text{opt}}$ is the optimal fully digital precoder. The objective function (3.3) can be written as

$$\begin{aligned}\|\mathbf{F}_{\text{opt}} - \mathbf{F}_{\text{R}}\mathbf{F}_{\text{D}}\|_F^2 &= \sum_{i=1}^{S} \quad \left\|\mathbf{F}_{\text{opt}}^i - (\mathbf{F}_{\text{R}}\mathbf{F}_{\text{D}})^i\right\|_F^2 \\ &= \sum_{i=1}^{S} \quad \left\|\mathbf{F}_{\text{opt}}^i - \mathbf{F}_{\text{R}}^i\mathbf{F}_{\text{D}}^i\right\|_F^2,\end{aligned} \tag{3.4}$$

where $\mathbf{F}_{\text{opt}}^i$ and $(\mathbf{F}_{\text{R}}\mathbf{F}_{\text{D}})^i$ are the i^{th} submatrices corresponding to $\left(\sum_{j=1}^{i-1} N_j\right) + 1$ to $\sum_{j=1}^{i} N_j$ rows and all the columns of $\mathbf{F}_{\text{opt}}$ and $\mathbf{F}_{\text{R}}\mathbf{F}_{\text{D}}$ respectively, whereas $\mathbf{F}_{\text{D}}^i$ corresponds to $\left(\sum_{j=1}^{i-1} C_j\right) + 1$ to $\sum_{j=1}^{i} C_j$ rows and all the columns of $\mathbf{F}_{\text{D}}$. Thus, the hybrid precoding problem can be restated as

$$(\mathbf{F}_{\text{R}}^\star, \mathbf{F}_{\text{D}}^\star) = \underset{\mathbf{F}_{\text{R}}^i, \mathbf{F}_{\text{D}}^i}{\arg\min} \quad \sum_{i=1}^{S} \quad \left\|\mathbf{F}_{\text{opt}}^i - \mathbf{F}_{\text{R}}^i\mathbf{F}_{\text{D}}^i\right\|_F^2 \tag{3.5a}$$

$$\text{s.t.} \quad \|\mathbf{F}_{\text{R}}\mathbf{F}_{\text{D}}\|_F^2 = N_s, \tag{3.5b}$$

$$\mathbf{F}_{\text{R}} = \mathbf{BLKDIAG}\left(\mathbf{F}_{\text{R}}^1, \ldots, \mathbf{F}_{\text{R}}^S\right), \tag{3.5c}$$

$$|\mathbf{F}_{\text{R}_{m,n}}^i| = 1, \quad 1 \le i \le S, \quad \forall m, n. \tag{3.5d}$$

3.3 Proposed Hybrid Precoder Based on Alternating Minimization

It is assumed that $C_i \le N_s \ \forall i$, which is realistic because the high value of C_i is undesirable as it would mean high number of RF chains. A simple algorithm is developed based on alternating minimization to compute the hybrid precoder. In the first stage, solution to the problem

$$\begin{aligned}\mathbf{F}_{\text{R}_i}^\star = \underset{\mathbf{F}_{\text{R}}^i}{\arg\min} \quad & \left\|\mathbf{F}_{\text{opt}}^i - \mathbf{F}_{\text{R}}^i\mathbf{F}_{\text{D}}^i\right\|_F^2 \\ \text{s.t.} \quad & \left|\mathbf{F}_{\text{R}_{m,n}}^i\right| = 1, \quad 1 \le i \le S, \quad \forall m, n\end{aligned} \tag{3.6}$$

is determined. After all the optimal $\mathbf{F}_{\text{R}}^i, 1 \le i \le S$ are determined, $\mathbf{F}_{\text{R}}$ can be constructed as a block-diagonal matrix. Then, $\mathbf{F}_{\text{D}}$ is determined by solving (3.3)

with $\mathbf{F}_{\mathrm{R}}$ known. When $\mathbf{F}_{\mathrm{R}}$ is known, the solution of (3.3) for $\mathbf{F}_{\mathrm{D}}$ is the least squares solution multiplied by the normalization factor to satisfy power constraint,

$$\mathbf{F}_{\mathrm{D}} = \frac{\sqrt{N_s}}{\left\| \mathbf{F}_{\mathrm{R}} \mathbf{F}_{\mathrm{R}}^{\dagger} \mathbf{F}_{\mathrm{opt}} \right\|_F} \mathbf{F}_{\mathrm{R}}^{\dagger} \mathbf{F}_{\mathrm{opt}}. \tag{3.7}$$

Algorithm 3.1 Proposed Hybrid Precoding Algorithm Using Alternating Minimization Method

Require: $\mathbf{F}_{\mathrm{opt}}$, N_i, C_i, S.

1: Set $i = 1$.
2: **repeat**
3: Set $m = \sum_{j=1}^{i-1} N_j + 1$, $n = \sum_{j=1}^{i} N_j$.
4: Set $\mathbf{F}_{\mathrm{opt}}^{i} = \mathbf{F}_{\mathrm{opt}_{m:n,:}}$.
5: Initialize $\mathbf{F}_{\mathrm{R}}^{i(0)} = \exp(j\mathbf{\Theta})$, where $\mathbf{\Theta}$ is $N_i \times C_i$ matrix and $\mathbf{\Theta}_{i,j}$ are random phase angles, and set $k = 1$.
6: **repeat**
7: Compute $\mathbf{F}_{\mathrm{D}}^{i(k)} = \mathbf{F}_{\mathrm{R}}^{i(k-1)^{\dagger}} \mathbf{F}_{\mathrm{opt}}^{i}$.
8: Compute $\mathbf{F}_{\mathrm{D}}^{i(k)^{-}} = \mathbf{F}_{\mathrm{D}}^{i(k)^{H}} \left(\mathbf{F}_{\mathrm{D}}^{i(k)} \mathbf{F}_{\mathrm{D}}^{i(k)^{H}} + \epsilon \mathbf{I} \right)^{-1}$, where $\epsilon \to 0$.
9: Compute $\mathbf{F}_{\mathrm{R}}^{i(k)} = \exp\left(j \angle \left(\mathbf{F}_{\mathrm{opt}}^{i} \mathbf{F}_{\mathrm{D}}^{i(k)^{-}} \right) \right)$.
10: $k \leftarrow k + 1$.
11: **until** $\left| \mathrm{e}_i^k - \mathrm{e}_i^{k-1} \right| < tol$, where $\mathrm{e}_i^k = \left\| \mathbf{F}_{\mathrm{opt}}^{i} - \mathbf{F}_{\mathrm{R}}^{i(k)} \mathbf{F}_{\mathrm{D}}^{i(k)} \right\|_F^2$ and $tol \to 0$, or $k \geq iter_{\max}$, the maximum number of iterations.
12: Set $\mathbf{F}_{\mathrm{R}}^{i} = \mathbf{F}_{\mathrm{R}}^{i(k)}$, $\mathbf{F}_{\mathrm{D}}^{i} = \mathbf{F}_{\mathrm{D}}^{i(k)}$.
13: $i \leftarrow i + 1$.
14: **until** $i > S$.
15: Set $\mathbf{F}_{\mathrm{R}} = \mathbf{BLKDIAG}\left(\mathbf{F}_{\mathrm{R}}^{1}, \ldots, \mathbf{F}_{\mathrm{R}}^{S} \right)$.
16: Calculate $\mathbf{F}_{\mathrm{D}} = \frac{\sqrt{N_s}}{\left\| \mathbf{F}_{\mathrm{R}} \tilde{\mathbf{F}}_{\mathrm{D}} \right\|_F} \tilde{\mathbf{F}}_{\mathrm{D}}$, where $\tilde{\mathbf{F}}_{\mathrm{D}} = \mathbf{F}_{\mathrm{R}}^{\dagger} \mathbf{F}_{\mathrm{opt}}$ or $\tilde{\mathbf{F}}_{\mathrm{D}} = \left[\mathbf{F}_{\mathrm{D}}^{1^T}, \mathbf{F}_{\mathrm{D}}^{2^T}, \ldots, \mathbf{F}_{\mathrm{D}}^{S^T} \right]^T$.
17: **return** $\mathbf{F} = \mathbf{F}_{\mathrm{R}} \mathbf{F}_{\mathrm{D}}$.

Alternating minimization approach is taken to solve (3.6). Starting with a randomly initialized value of $\mathbf{F}_{\mathrm{R}}^{i}$, the objective function (3.6) is solved for $\mathbf{F}_{\mathrm{D}}^{i}$ with known $\mathbf{F}_{\mathrm{R}}^{i}$ in each iteration, which is $\mathbf{F}_{\mathrm{D}}^{i} = \mathbf{F}_{\mathrm{R}}^{i^{\dagger}} \mathbf{F}_{\mathrm{opt}}^{i}$.

In the next step, $\mathbf{F}_{\mathrm{R}}^{i}$ is determined with fixed $\mathbf{F}_{\mathrm{D}}^{i}$. The problem (3.6) is solved for unconstrained $\mathbf{F}_{\mathrm{R}}^{i}$ (without modulus constraint). The constrained $\mathbf{F}_{\mathrm{R}}^{i}$ is approximated by normalizing each element of unconstrained $\mathbf{F}_{\mathrm{R}}^{i}$ to have an unit amplitude, or equivalently extracting the phase values as

$$\mathbf{F}_{\mathrm{R}}^{i} = \exp\left(j \angle \left(\mathbf{F}_{\mathrm{opt}}^{i} \mathbf{F}_{\mathrm{D}}^{i^{-}} \right) \right), \tag{3.8}$$

where $\mathbf{F}_{\mathrm{D}}^{i^-} = \mathbf{F}_{\mathrm{D}}^{i^H}\left(\mathbf{F}_{\mathrm{D}}^{i}\mathbf{F}_{\mathrm{D}}^{i^H} + \epsilon\mathbf{I}\right)^{-1}, \epsilon \to 0$ is the right inverse of $\mathbf{F}_{\mathrm{D}}^{i}$, and $\mathbf{F}_{\mathrm{opt}}^{i}\mathbf{F}_{\mathrm{D}}^{i^-}$ is the solution of (3.6) for unconstrained $\mathbf{F}_{\mathrm{R}}^{i}$. This procedure of minimizing (3.6) alternately for $\mathbf{F}_{\mathrm{D}}^{i}$ and $\mathbf{F}_{\mathrm{R}}^{i}$ is repeated until the convergence is achieved. After $\mathbf{F}_{\mathrm{R}}$ is obtained by solving for each $\mathbf{F}_{\mathrm{R}}^{i}$, $\mathbf{F}_{\mathrm{D}}$ is determined using (3.7). Alternatively, $\mathbf{F}_{\mathrm{D}}$ can be constructed as $\mathbf{F}_{\mathrm{D}} = \frac{\sqrt{N_s}}{\left\|\mathbf{F}_{\mathrm{R}}\tilde{\mathbf{F}}_{\mathrm{D}}\right\|_F}\tilde{\mathbf{F}}_{\mathrm{D}}$, where $\tilde{\mathbf{F}}_{\mathrm{D}} = \left[\mathbf{F}_{\mathrm{D}}^{1^T}, \mathbf{F}_{\mathrm{D}}^{2^T}, \ldots, \mathbf{F}_{\mathrm{D}}^{S^T}\right]^T$. The proposed method is summarized in Algorithm 3.1. The proposed algorithm is similar, in spirit, to [90] which is used to solve phase recovery problems in which signals are retrieved from amplitude measurements. A similar method was proposed assuming unitary digital precoder for FC architecture in [36].

3.4 Proposed Hybrid Precoder Based on Iterative Power Method (IPM)

Using the relation obtained for the FC analog precoder in Section 2.4, the analog precoding problem for PFMC architecture can be correspondingly written as

$$\max_{\mathbf{F}_{\mathrm{R}}} \quad \mathbf{Tr}\left[\mathbf{F}_{\mathrm{R}}^{H}\left(\mathbf{F}_{\mathrm{opt}}\mathbf{F}_{\mathrm{opt}}^{H}\right)\mathbf{F}_{\mathrm{R}}\right] \tag{3.9a}$$

$$\text{s.t.} \quad \left|\mathbf{F}_{\mathrm{R}_{m,n}}^{i}\right| = 1, \quad 1 \le i \le S, \quad \forall m, n \tag{3.9b}$$

$$\mathbf{F}_{\mathrm{R}}^{H}\mathbf{F}_{\mathrm{R}} = N_t\mathbf{I}_{\mathrm{M}_t}. \tag{3.9c}$$

Taking the fact that $\mathbf{F}_{\mathrm{R}}$ is a block diagonal matrix into account, the objective function (3.9a) and the constraint (3.9c) can be equivalently written as

$$\sum_{i=1}^{S}\mathbf{Tr}\left[\mathbf{F}_{\mathrm{R}}^{i^H}\left(\mathbf{F}_{\mathrm{opt}}^{i}\mathbf{F}_{\mathrm{opt}}^{i^H}\right)\mathbf{F}_{\mathrm{R}}^{i}\right], \tag{3.10a}$$

$$\mathbf{F}_{\mathrm{R}}^{i^H}\mathbf{F}_{\mathrm{R}}^{i} = N_i\mathbf{I}_{\mathrm{C}_i}, \quad \forall i, \quad 1 \le i \le S. \tag{3.10b}$$

Thus, if $\bar{\mathbf{F}}_{\mathrm{R}}^{i} \triangleq \frac{1}{\sqrt{N_i}}\mathbf{F}_{\mathrm{R}}^{i}$, the analog precoding subproblem can be equivalently repre-

sented by

$$\max_{\bar{\mathbf{F}}_{\mathrm{R}}} \quad \sum_{i=1}^{S} N_i \mathbf{Tr}\left[\bar{\mathbf{F}}_{\mathrm{R}}^{i^H}\left(\mathbf{F}_{\mathrm{opt}}^{i}\mathbf{F}_{\mathrm{opt}}^{i^H}\right)\bar{\mathbf{F}}_{\mathrm{R}}^{i}\right] \tag{3.11a}$$

$$\text{s.t.} \quad \bar{\mathbf{F}}_{\mathrm{R}} = \mathbf{BLKDIAG}\left(\bar{\mathbf{F}}_{\mathrm{R}}^{1}, \ldots, \bar{\mathbf{F}}_{\mathrm{R}}^{S}\right) \tag{3.11b}$$

$$\left|\bar{\mathbf{F}}_{\mathrm{R}_{m,n}}^{i}\right| = \frac{1}{\sqrt{N_i}}, \ \forall i, \quad \forall m, n, \tag{3.11c}$$

$$\bar{\mathbf{F}}_{\mathrm{R}}^{i^H}\bar{\mathbf{F}}_{\mathrm{R}}^{i} = \mathbf{I}_{\mathrm{C}_i}, \quad 1 \leq i \leq S. \tag{3.11d}$$

The objective function (3.11a) is maximized when each of the $\mathbf{Tr}[\bar{\mathbf{F}}_{\mathrm{R}}^{i^H}(\mathbf{F}_{\mathrm{opt}}^{i}\mathbf{F}_{\mathrm{opt}}^{i^H})\bar{\mathbf{F}}_{\mathrm{R}}^{i}]$ is maximized, *i.e.*,

$$\begin{aligned} \max_{\bar{\mathbf{F}}_{\mathrm{R}}^{i}} \quad & \mathbf{Tr}\left[\bar{\mathbf{F}}_{\mathrm{R}}^{i^H}\left(\mathbf{F}_{\mathrm{opt}}^{i}\mathbf{F}_{\mathrm{opt}}^{i^H}\right)\bar{\mathbf{F}}_{\mathrm{R}}^{i}\right] \\ \text{s.t.} \quad & 3.11c \quad \text{and} \quad 3.11d. \end{aligned} \tag{3.12}$$

After computing $\bar{\mathbf{F}}_{\mathrm{R}}^{i}$, $1 \leq i \leq S$, $\mathbf{F}_{\mathrm{R}}^{i}$ is calculated as $\mathbf{F}_{\mathrm{R}}^{i} = \sqrt{N_i}\bar{\mathbf{F}}_{\mathrm{R}}^{i}$, and finally the analog precoder $\mathbf{F}_{\mathrm{R}}$ is constructed using (3.5c).

Algorithm 3.2 IPM-based hybrid precoding algorithm for PFMC architecture

Require: $\mathbf{F}_{\mathrm{opt}}$, M_t, S, $\{C_i\}_{i=1}^{i=S}$.
1: **for** $i = 1, 2, \ldots, S$ **do**
2: Compute $\mathbf{M} = \mathbf{F}_{\mathrm{opt}}^{i}\mathbf{F}_{\mathrm{opt}}^{i^H}$.
3: Set initial $\bar{\mathbf{F}}_{\mathrm{R}}^{i^{(0)}}$ such that $\left|\bar{\mathbf{F}}_{\mathrm{R}}^{i^{(0)}}\right| = \frac{1}{\sqrt{N_i}}\mathbf{1}_{N_i \times C_i}$ and set $k = 1$.
4: **repeat**
5: Perform the adapted Modified Gram-Schmidt orthogonalization procedure on $\mathbf{M}\bar{\mathbf{F}}_{\mathrm{R}}^{i^{(k-1)}}$ to compute $\bar{\mathbf{F}}_{\mathrm{R}}^{i^{(k)}}$, using Algorithm 2.4.
6: $\delta^k = \left|f^k - f^{k-1}\right|$, where $f^k = \mathbf{Tr}\left[\bar{\mathbf{F}}_{\mathrm{R}}^{i^{(k)^H}}\mathbf{M}\bar{\mathbf{F}}_{\mathrm{R}}^{i^{(k)}}\right]$.
7: $k \leftarrow k + 1$.
8: **until** $\delta^k < \epsilon$ where $\epsilon \to 0$, or $k \geq iter_{\max}$, the maximum number of iterations.
9: Set $\bar{\mathbf{F}}_{\mathrm{R}}^{i} = \bar{\mathbf{F}}_{\mathrm{R}}^{i^{(k)}}$.
10: **end for**
11: Set $\mathbf{F}_{\mathrm{R}}^{i} = \sqrt{N_i}\bar{\mathbf{F}}_{\mathrm{R}}^{i}$, and $\mathbf{F}_{\mathrm{R}} = \mathbf{BLKDIAG}\left(\mathbf{F}_{\mathrm{R}}^{1}, \ldots, \mathbf{F}_{\mathrm{R}}^{S}\right)$.
12: Calculate $\mathbf{F}_{\mathrm{D}}$, using (3.7).
13: **return** $\mathbf{F} = \mathbf{F}_{\mathrm{R}}\mathbf{F}_{\mathrm{D}}$.

3.5 Complexity Analyses of The Proposed Methods

(i) ***Alternating Minimization Based Hybrid Precoder*** : The complexity of computing the hybrid precoder is sum total of computing hybrid precoder corresponding to S different subgroups. The complexity related to the i^{th} subgroup can be computed as the sum of

- *Complexity of computing* $\mathbf{F}_D^i$: The complexities involved in calculating pseudoinverse of $\mathbf{F}_{\mathrm{R}}^i$ and the product $\mathbf{F}_{\mathrm{R}}^{i\dagger}\mathbf{F}_{\mathrm{opt}}^i$ are $\mathcal{O}\left(C_i N_i^2\right)$ and $\mathcal{O}\left(C_i N_i N_s\right)$ respectively, making the total complexity $\mathcal{O}\left(C_i N_i^2 + C_i N_i N_s\right)$.

- *Complexity of computing* $\mathbf{F}_D^{i^-}$: The computation of inverse of $C_i \times C_i$ matrix $\mathbf{F}_{\mathrm{D}}^i\mathbf{F}_{\mathrm{D}}^{iH} + \epsilon\mathbf{I}$ has a complexity $\mathcal{O}\left(C_i^3\right)$, and calculating the multiplication of $N_s \times C_i$ matrix $\mathbf{F}_{\mathrm{opt}}^i$ with $\mathbf{F}_{\mathrm{D}}^i\mathbf{F}_{\mathrm{D}}^{iH} + \epsilon\mathbf{I}$ adds a complexity of $\mathcal{O}\left(N_s C_i^2\right)$.

- *Complexity of computing* $\mathbf{F}_R^i$: The complexity mainly comes from the multiplication of $\mathbf{F}_{\mathrm{opt}}^i$ and $\mathbf{F}_{\mathrm{D}}^{i^-}$, which is $\mathcal{O}\left(N_i N_s C_i\right)$.

If N_{it}^i is the number of iterations required for computing i^{th} subgroup of the precoder, the total complexity is $\sum_{i=1}^{S} N_{it}^i \mathcal{O}(C_i N_i^2 + 2C_i N_i N_s + C_i^3 + N_s C_i^2)$.

(ii) ***IPM Based Hybrid Precoder*** : Following the developments in section 2.6, it can be easily deduced that the complexity of computing $\mathbf{F}_{\mathrm{R}}^i$ as $\mathcal{O}(N_{it}^i(N_i^2 C_i + N_i C_i^2) + N_i^2 N_s)$ where N_{it}^i is the number of iterations performed to compute $\mathbf{F}_{\mathrm{R}}^i$. Thus, the complexity of determining the analog precoder is $\sum_{i=1}^{S} \mathcal{O}(N_{it}^i(N_i^2 C_i + N_i C_i^2) + N_i^2 N_s)$. Finally, the total complexity of computing the hybrid precoder can be expressed as $\sum_{i=1}^{S} \mathcal{O}\left(N_{it}^i(N_i^2 C_i + N_i C_i^2) + N_i^2 N_s\right) + \mathcal{O}\left(N_t^2 M_t + N_t M_t N_s\right)$ by adding the complexity of computing $\mathbf{F}_{\mathrm{D}}$.

Table 3.1: PARAMETERS FOR SIMULATIONS

Parameters for simulations	**Values**
N_t	144
N_r	36
N_s	4
N_c	5
N_p	10
$\alpha_{i\ell}$	$\sim \mathcal{CN}(0,1)$
P_{com}	10 W
P_{RF}	100 mW
P_{PA}	100 mW
P_{PS}	10 mW

3.6 Performance Evaluation

Both the transmitter and the receiver are considered to have ULAs with $N_t = 144$ and $N_r = 36$. The antenna elements are separated by a distance of half wavelength. The clustered channel model given by (1.4) is used to model mmWave channel. The channel parameters $N_c = 5$, $N_{p_i} = N_p = 10\ \forall i$, $\alpha_{i\ell} \sim \mathcal{CN}(0,1)$. The azimuth AoDs and AoAs are Laplacian distributed with mean angles uniformly distributed over $[0, 2\pi]$ and having angular spread of 7.5 degrees. The signal-to-noise ratio (SNR) is defined as SNR $= \frac{P}{\sigma^2}$. We take $\mathrm{P}_{com} = 10$ W, $\mathrm{P}_{RF} = 100$ mW, $\mathrm{P}_{PA} = 100$ mW, $\mathrm{P}_{PS}=$ 10 mW [91]. The parameters have been summarized in Table 3.1. It is considered that $C_i = C$, $N_i = \frac{N_t}{S}\ \forall i = 1, \ldots, S$ to define the PFMC architecture.

The performances of the proposed hybrid precoders are compared against the fully digital precoder, spatially sparse precoder [18] which is a FC precoder, SIC-based hybridly connected precoder [87] and AltMin SDR precoder [40] which is a PC precoder. In the figures, the labels Altmin-HP and IPM-HP are used to represent the proposed alternating minimization based precoder and the IPM-based precoder respectively. To make a fair comparison, only precoding at the transmitter side is considered for all the precoders.

The Figure 3.2 shows that the spectral efficiencies of the proposed precoders for $C = 2$, $S = 4$ are better than AltMin SDR precoder and lower than the spatially sparse precoder. However, when C is increased to 4 and S is decreased to 2, keeping

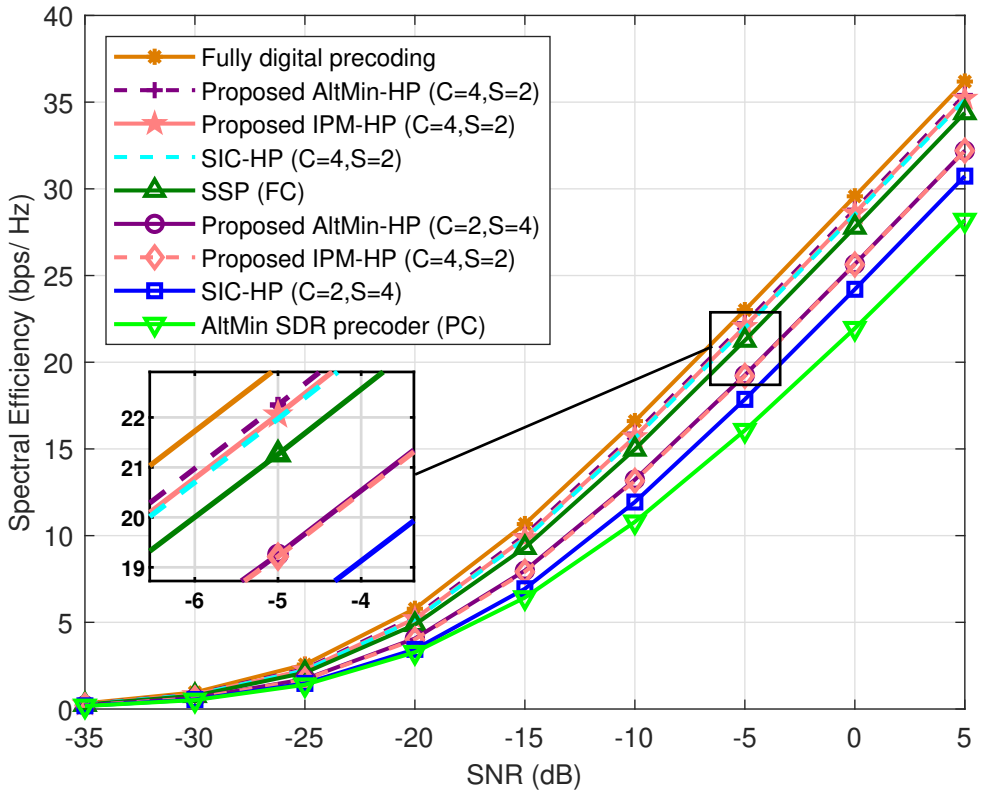

Figure 3.2: Spectral Efficiency vs. SNR, $N_s = 4$, $M_t = 8$.

M_t constant, the performances of the proposed hybrid precoders get even better than the spatially sparse precoder and come closer to the performance of fully digital precoder. In both these configurations, the proposed precoders' performances are superior to SIC-based hybridly connected precoder. Increasing C, keeping M_t constant will raise the spectral performance because the number of phase-shifters $\left(\sum_{i=1}^{S} C_i N_i = N_t C\right)$ also increases which adds to the beamforming gain.

The Figure 3.3 compares energy efficiency of various precoders. There are two separate plots for the proposed precoders, one with $C = 2$ and varying S, and the other with $S = 2$ and varying C. The Figure 3.3 shows that the proposed precoders exhibit the best energy efficiency among all the compared precoders when C is fixed and S is varied. As M_t is increased with fixed C, the energy efficiency of the proposed precoders increase first and then starts decreasing. At the beginning, the increase in rate because of increasing M_t exceeds the increase in power consumption of the RF chains. The rate can not increase beyond a point even after increasing M_t but the power consumption still increases, thereby finally causing a decline in the energy

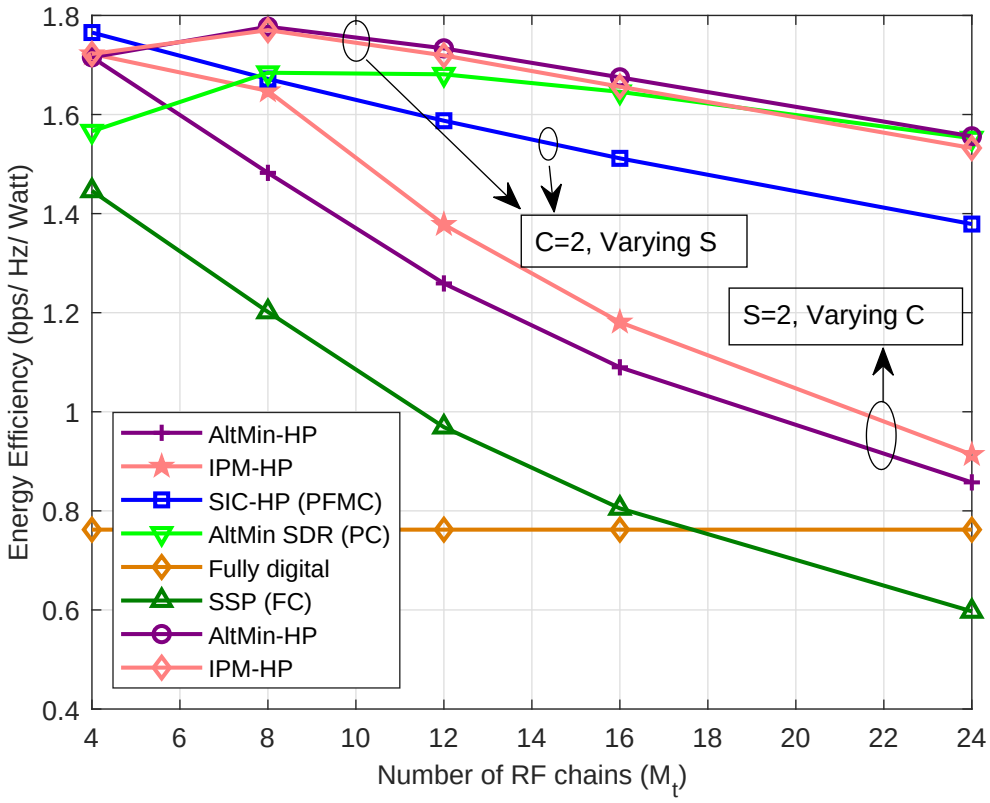

Figure 3.3: Energy Efficiency vs. the number of RF chains, $N_s = 4$, $SNR = 0$ dB.

efficiency. The energy efficiency of proposed precoders for varying C decreases with increasing M_t. In this case, the number of phase shifters is also increasing as it depends on the number of C which also causes growth in power consumption, and the increase in power consumption trumps the increase in rate. For the proposed precoders, the energy efficiency is better when S is varying when compared to PC architecture precoder for the most part before they become similar at very high M_t. This is because the increase in power consumption at larger M_t is higher than increase in rate. It should be noted that very high value of M_t is not desirable in mmWave MIMO.

3.7 Summary

This chapter investigates partial-full mixed connection (PFMC) architecture in mmWave MIMO. In PFMC architecture, the RF chains and the antennas are divided into various subgroups with full connection existing between the RF chains and the antennas of a particular subgroup. The hybrid precoding for the PFMC architecture

is established as a matrix factorization problem of all the sub-matrices corresponding to each subgroup of RF chains and antennas. Two algorithms are proposed to determine hybrid precoder for PFMC architecture MIMO, one based on alternating minimization and other based on IPM-HP proposed in Chapter 2. The proposed precoders are able to produce energy efficiency better than the precoders for FC and PC architectures and the existing precoder for the PFMC architecture.

Chapter 4

Codebook-based Precoding for Multi-user mmWave MIMO

In this chapter, MU-MIMO is considered, and a simple codebook-based precoding method is proposed. In MU-MIMO, the performance is impacted not only by noise, but also the interference from other users.

A two stage hybrid precoding method is proposed in [30] where analog precoding and combining vectors are jointly chosen from respective beamsteering codebooks to maximize received power for each user, and zero-forcing (ZF) precoding is performed on the equivalent baseband channel by inverting the equivalent channel. Ni *et. al.* [35] developed hybrid block diagonalization precoding-combining in which RF combiners are chosen from discrete Fourier transform (DFT) basis set, and RF beamforming matrix is constructed from the phases of the Hermitian transpose of the aggregate channel that includes the RF combiners. Finally block diagonalization precoding-combining is performed on the equivalent channel. Nguyen *et. al.* [34] presented an orthogonal matching pursuit (OMP)-based algorithm to minimize the sum mean squared error (sum-MSE) and an iterative method to minimize weighted sum-MSE. An OMP-based hybrid minimum mean squared error (MMSE) precoder is also proposed in [33]. Both these OMP-based MMSE precders [33, 34] use OMP to construct analog precoding matrix from the codebook.

The hybrid ZF precoder [30] necessitates that the equivalent channel matrix remains well-conditioned. Furthermore, hybrid ZF precoder and hybrid block diagonalization precoder [35] both do not take into account the impact of noise during the design. The OMP-based hybrid MMSE precoders [33, 34] are poor in performance. The contributions that we have made in this chapter are:

(i) A downlink mmWave MU-MIMO communication is considered where the number of RF chains in use is equal to the number of users, and hybrid precoder is designed by maximizing signal-to-leakage-and-noise ratio (SLNR). The reason behind choosing SLNR is that it also considers the influence of noise, and has proven to outperform zero-forcing solutions in traditional MU-MIMO [92]. The proposed precoder chooses the analog precoding vectors from the beamsteering codebook.

(ii) The spectral performance of the proposed hybrid precoder in single path channels is evaluated analytically.

(iii) The performance of the proposed hybrid precoding-analog combining scheme is compared with the fully digital precoding counterpart and the hybrid ZF precoding. Simulation results reveal that the proposed precoding method, with a smaller number of RF chains, achieves very good spectral efficiency which is better than the hybrid ZF precoding and comparable to the unconstrained digital SLNR precoding.

4.0.1 System Model

An mmWave MIMO downlink system is considered in which a BS equipped with N_t transmit antennas and M_t RF chains is serving K users or mobile stations (MSs) simultaneously. It is assumed that $M_t \geq K$, however, only K out of M_t RF chains would be used while communicating with K MSs. Each MS has N_r receive antennas and only one RF chain to support single data stream. The BS multiplexes K data streams, one data stream each for the K MSs.

At the BS, transmit signal is first passed through a baseband precoder $\mathbf{F}_{\mathrm{D}} =$

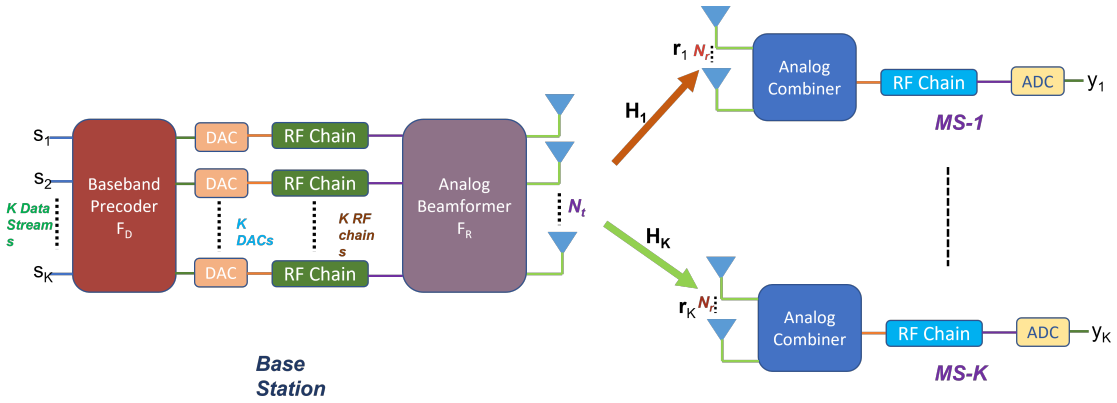

Figure 4.1: System diagram showing mmWave multi-user MIMO system with hybrid precoding at the transmitter and analog combining at the receiver.

$[\mathbf{F}_{\mathrm{D}\cdot 1}, \mathbf{F}_{\mathrm{D}\cdot 2}, ..., \mathbf{F}_{\mathrm{D}\cdot K}], \mathbf{F}_{\mathrm{D}} \in \mathbb{C}^{K\times K}$. $\mathbf{F}_{\mathrm{D}\cdot k} \in \mathbb{C}^{K\times 1}$ is the digital precoder for the k^{th} MS and corresponds to the k^{th} column of $\mathbf{F}_{\mathrm{D}}$. Then the digitally precoded signal is passed through the analog precoder $\mathbf{F}_{\mathrm{R}} \in \mathbb{C}^{N_t\times K}$. $\mathbf{F}_{\cdot k} = \mathbf{F}_{\mathrm{R}}\mathbf{F}_{\mathrm{D}\cdot k}$, $\mathbf{F}_{\cdot k} \in \mathbb{C}^{N_t\times 1}$ is the hybrid precoder for the k^{th} MS and has unit norm in order to satisfy the total power constraint.

The received signal at the k^{th} MS with narrow-band block-fading channel is given by

$$\mathbf{r}_k = \mathbf{H}_k\mathbf{F}_{\mathrm{R}}\mathbf{F}_{\mathrm{D}}\mathbf{s} + \mathbf{n}_k, \tag{4.1}$$

where $\mathbf{s} = [s_1, s_2, \ldots, s_K]^T$, $\mathbf{s} \in \mathbb{C}^{K\times 1}$ is the transmit signal and s_k is the symbol intended for the k^{th} MS. $\mathbf{H}_k \in \mathbb{C}^{N_r\times N_t}$ is the channel from the BS to the k^{th} MS and $\mathbf{n}_k \sim \mathcal{CN}(\mathbf{0}, \sigma_k^2\mathbf{I}_{N_r})$ is the $N_r \times 1$ complex noise vector. The transmit symbols for all the MSs are assumed to be independent of each other, *i.e.*, $\mathbb{E}[s_k s_k^*] = p_k$, $\mathbb{E}[s_i s_j^*] = 0$ for $i \neq j$, where p_k is the average power transmitted to the k^{th} user. Considering equal power distribution among different users, $p_k = \frac{P}{K}$ where P is the average total transmit power. The expression in (4.1) can be written as

$$\mathbf{r}_k = \mathbf{H}_k\mathbf{F}_{\cdot k}s_k + \mathbf{H}_k\sum_{\substack{m=1\\ m\neq k}}^{K}\mathbf{F}_{\cdot m}s_m + \mathbf{n}_k. \tag{4.2}$$

At the receiver of the k^{th} MS, the received signal $\mathbf{r}_k$ is acted upon by analog combiner

$\mathbf{w}_{r_k} \in \mathbb{C}^{N_r \times 1}$ to produce the processed received symbol y_k which is given by

$$y_k = \mathbf{w}_{r_k}^H \mathbf{H}_k \mathbf{F}_{\cdot k} s_k + \mathbf{w}_{r_k}^H \mathbf{H}_k \sum_{\substack{m=1 \\ m \neq k}}^{K} \mathbf{F}_{\cdot m} s_m + \mathbf{w}_{r_k}^H \mathbf{n}_k. \tag{4.3}$$

Each element of the analog combiner, $\mathbf{w}_{r_k}$ is realized through analog phase shifters. The second term on the right-hand side of (4.3), $\mathbf{w}_{r_k}^H \mathbf{H}_k \sum_{m=1, m\neq k}^{K} \mathbf{F}_{\cdot m} s_m$ is the interference due to other users and known as co-channel interference (CCI).

4.1 Problem Formulation

The signal-to-interference-and-noise ratio (SINR) for the k^{th} MS is defined as

$$\mathrm{SINR}_k = \frac{\left| \mathbf{w}_{\mathrm{r}_k}^H \mathbf{H}_k \mathbf{F}_{\cdot k} s_k \right|^2}{\sum\limits_{m=1, m\neq k}^{K} \left| \mathbf{w}_{\mathrm{r}_k}^H \mathbf{H}_k \mathbf{F}_{\cdot m} s_m \right|^2 + \mathbb{E}\left[\left| \mathbf{w}_{\mathrm{r}_k}^H \mathbf{n}_k \right|^2 \right]}. \tag{4.4}$$

The spectral efficiency for the k^{th} user is given by

$$\mathcal{R}_k = \log_2(1 + \mathrm{SINR}_k). \tag{4.5}$$

Then the sum-spectral efficiency of the system is $\mathcal{R}_{tot} = \sum_{k=1}^{K} \mathcal{R}_k$. One of the fundamental motivations of using a precoder is to maximize sum-spectral efficiency of the system which means maximizing SINR for each MS in MU-MIMO. In light of achieving this, precoding methods like zero-forcing (ZF) precoding and block-diagonalization aim to make CCI terms zero. This is because finding a precoder to maximize SINR_k for each MS_k, $k = 1, 2, ..., K$ poses a serious challenge due to K coupled vectors $\{\mathbf{F}_{\cdot k}\}_{k=1}^{K}$ [92, 93]. The authors of [92], in view of circumventing this issue, introduced another figure of merit called signal-to-leakage-and-noise ratio (SLNR) to find precoder. SLNR for the k^{th} MS is defined as

$$\mathrm{SLNR}_k = \frac{\left| \mathbf{H}_k \mathbf{F}_{\cdot k} s_k \right|^2}{\sum\limits_{m=1, m\neq k}^{K} \left| \mathbf{H}_m \mathbf{F}_{\cdot k} s_k \right|^2 + \mathbb{E}\left[\left| \mathbf{n}_k \right|^2 \right]}, \tag{4.6}$$

where $\sum_{m=1,m\neq k}^{K} |\mathbf{H}_m \mathbf{F}_{\cdot k} s_k|^2$ is the total power leaked from user k to all other users and is called *leakage* [92]. Thus, SLNR_k indicates the ratio of total useful power for user k to the sum of its interfering power on other users and noise. It can be seen that the expression for SLNR_k only involves precoding vector for the k^{th} MS unlike the case of SINR_k. Hence maximizing SLNR provides an elegant solution to the problem of determining the precoding vector as it is easy to arrive at a closed form solution.

4.2 Proposed Hybrid SLNR Precoding

SLNR is chosen as an optimizing criterion to determine precoding matrix at the BS. At first, each MS_k chooses its analog combiner $\mathbf{w}_{\text{r}_k}$ from MS beamforming codebook $\mathcal{W}_k$ that maximizes its received power, *i.e.*,

$$\mathbf{w}_{\text{r}_k}^{\star} = \underset{\mathbf{w}_{\text{r}_k} \in \mathcal{W}_k}{\arg\max}\, \mathbf{w}_{\text{r}_k}^H \mathbf{H}_k \mathbf{H}_k^H \mathbf{w}_{\text{r}_k}. \tag{4.7}$$

As in [18, 30], beamsteering codebook is used at the MS. The MS beamforming codebook is characterized by (B_θ, B_β) quantization bits. B_θ (B_β) bits quantify the uniform quantization of the azimuth (elevation) angles. That is, $\mathcal{W}_k$ contains the MS array response vectors $\mathbf{a}_r(\theta, \beta)$ for all combinations of θ and β , where $\theta \in \left\{ \frac{2\pi}{2^{B_\theta+1}},\ \frac{3.2\pi}{2^{B_\theta+1}}, ...,\ 2\pi - \frac{2\pi}{2^{B_\theta+1}} \right\}$ and $\beta \in \{-\frac{\pi}{2} + \frac{\pi}{2^{B_\beta+1}},\ -\frac{\pi}{2} + \frac{3.\pi}{2^{B_\beta+1}}, ...,\ \frac{\pi}{2} - \frac{\pi}{2^{B_\beta+1}}\}$ [18]. With the analog combiner for the k^{th} MS determined, an equivalent channel $\mathbf{h}_{\text{e}_k} \in \mathbb{C}^{1\times N_t}$ for each MS is defined as

$$\mathbf{h}_{\text{e}_k} = \mathbf{w}_{r_k}^H \mathbf{H}_k,\ k = 1, 2,\ \dots, K \tag{4.8}$$

so that the processed received symbol y_k in (4.3) can be equivalently written as

$$y_k = \mathbf{h}_{\text{e}_k} \mathbf{F}_{\cdot k} s_k + \mathbf{h}_{\text{e}_k} \sum_{\substack{m=1 \\ m\neq k}}^{K} \mathbf{F}_{\cdot m} s_m + z_k, \tag{4.9}$$

where $z_k = \mathbf{w}_{r_k}^H \mathbf{n}_k$ is the complex scalar representing the processed noise. Now at the BS, hybrid precoder is computed for each MS by maximizing SLNR for the effective channel for each of the K MSs. Now, SLNR for the equivalent channel to the k^{th} MS can be defined as

$$\mathrm{SLNR}_k = \frac{\frac{P}{K}\left|\mathbf{h}_{\mathrm{e}_k}\mathbf{F}_{\cdot k}\right|^2}{\frac{P}{K}\left|\tilde{\mathbf{H}}_{\mathrm{e}_k}\mathbf{F}_{\cdot k}\right|^2 + \mathbb{E}\left[|z_k|^2\right]}, \tag{4.10}$$

where $\frac{P}{K}$ is the power of the k^{th} symbol, *i.e.*, $|s_k|^2 = \frac{P}{K}$ and $\tilde{\mathbf{H}}_{\mathrm{e}_k} = \left[\mathbf{h}_{\mathrm{e}_1}^T,\ \mathbf{h}_{\mathrm{e}_2}^T,\ \ldots \mathbf{h}_{\mathrm{e}_{k-1}}^T,\ \mathbf{h}_{\mathrm{e}_{k+1}}^T,\ \ldots \mathbf{h}_{\mathrm{e}_K}^T\right]^T$ is $(K-1)\times N_t$ extended channel matrix that only excludes $\mathbf{h}_{\mathrm{e}_k}$. Noting $\mathbb{E}\left[|z_k|^2\right] = N_r\sigma_k^2$ and $|\mathbf{F}_{\cdot k}|^2 = 1$, and defining $\gamma_k = \frac{P}{K\sigma_k^2}$, we may simplify the expression for SLNR as

$$\mathrm{SLNR}_k = \frac{\mathbf{F}_{\cdot k}^H\left(\mathbf{h}_{\mathrm{e}_k}^H\mathbf{h}_{\mathrm{e}_k}\right)\mathbf{F}_{\cdot k}}{\mathbf{F}_{\cdot k}^H\left(\tilde{\mathbf{H}}_{\mathrm{e}_k}^H\tilde{\mathbf{H}}_{\mathrm{e}_k} + \frac{1}{\gamma_k}N_r\mathbf{I}_{\mathrm{N}_t}\right)\mathbf{F}_{\cdot k}}. \tag{4.11}$$

If $\mathbf{F}_{\cdot k}$ is calculated directly by maximizing the expression in (4.11), it would give the fully digital precoder which would require N_t RF chains. The precoder $\mathbf{F}_{\cdot k}$ that we want to determine is the combination of analog precoding matrix $\mathbf{F}_{\mathrm{R}}$ and the digital precoder $\mathbf{F}_{\mathrm{D}\cdot k}$ implemented using only K RF chains. Thus the task of designing precoder is split into two different stages, *viz.*, finding $\mathbf{F}_{\mathrm{R}}$ and finding $\mathbf{F}_{\mathrm{D}\cdot k}$. Similar to the MS, the BS employs a beamsteering codebook $\mathcal{F}$ with (B_ϕ, B_ψ) quantization bits and containing array response vectors of the BS for the uniformly quantized azimuth and elevation angles. The BS chooses the columns of analog precoder $\mathbf{F}_{\mathrm{R}}$, $\mathbf{F}_{\mathrm{R}\cdot k}$ from the precoding codebook $\mathcal{F}$ to maximize SLNR for the k^{th} equivalent channel, *i.e.*,

$$\mathbf{F}_{\mathrm{R}\cdot k}^{\star} = \underset{\mathbf{F}_{\mathrm{R}\cdot k}\in\mathcal{F}}{\arg\max}\ \frac{\mathbf{F}_{\mathrm{R}\cdot k}^H\left(\mathbf{h}_{\mathrm{e}_k}^H\mathbf{h}_{\mathrm{e}_k}\right)\mathbf{F}_{\mathrm{R}\cdot k}}{\mathbf{F}_{\mathrm{R}\cdot k}^H\left(\tilde{\mathbf{H}}_{\mathrm{e}_k}^H\tilde{\mathbf{H}}_{\mathrm{e}_k} + \frac{1}{\gamma_k}N_r\mathbf{I}_{\mathrm{N}_t}\right)\mathbf{F}_{\mathrm{R}\cdot k}}, k = 1, 2, ..., K. \tag{4.12}$$

Since the hybrid precoder is supposed to maximize SLNR, it is only natural that the columns of analog precoder are chosen from $\mathcal{F}$ which maximize SLNR. The BS, then, sets $\mathbf{F}_{\mathrm{R}} = \left[\mathbf{F}_{\mathrm{R}\cdot 1}^{\star}\ \mathbf{F}_{\mathrm{R}\cdot 2}^{\star}\ ...\ \mathbf{F}_{\mathrm{R}\cdot K}^{\star}\right]$. To design $\mathbf{F}_{\mathrm{D}\cdot k}$, the expression for SLNR is

first expanded as

$$\mathrm{SLNR}_k = \frac{\mathbf{F}_{\mathrm{D}.k}^H \left(\mathbf{F}_{\mathrm{R}}^H \mathbf{h}_{\mathrm{e}_k}^H \mathbf{h}_{\mathrm{e}_k} \mathbf{F}_{\mathrm{R}}\right) \mathbf{F}_{\mathrm{D}.k}}{\mathbf{F}_{\mathrm{D}.k}^H \mathbf{F}_{\mathrm{R}}^H \left(\tilde{\mathbf{H}}_{\mathrm{e}_k}^H \tilde{\mathbf{H}}_{\mathrm{e}_k} + \frac{1}{\gamma_k} N_r \mathbf{I}_{\mathrm{N}_t}\right) \mathbf{F}_{\mathrm{R}} \mathbf{F}_{\mathrm{D}.k}}. \tag{4.13}$$

If $\tilde{\mathbf{H}}_{\mathrm{eq}_k} \triangleq \tilde{\mathbf{H}}_{\mathrm{e}_k} \mathbf{F}_{\mathrm{R}}$ such that $\tilde{\mathbf{H}}_{\mathrm{eq}_k} \in \mathbb{C}^{(K-1)\times K}$, and $\mathbf{h}_{\mathrm{eq}_k} \triangleq \mathbf{h}_{\mathrm{e}_k} \mathbf{F}_{\mathrm{R}}$ such that $\mathbf{h}_{\mathrm{eq}_k} \in \mathbb{C}^{1\times K}$, the SLNR expression becomes

$$\mathrm{SLNR}_k = \frac{\mathbf{F}_{\mathrm{D}.k}^H \left(\mathbf{h}_{\mathrm{eq}_k}^H \mathbf{h}_{\mathrm{eq}_k}\right) \mathbf{F}_{\mathrm{D}.k}}{\mathbf{F}_{\mathrm{D}.k}^H \left(\tilde{\mathbf{H}}_{\mathrm{eq}_k}^H \tilde{\mathbf{H}}_{\mathrm{eq}_k} + \frac{1}{\gamma_k} N_r \mathbf{F}_{\mathrm{R}}^H \mathbf{F}_{\mathrm{R}}\right) \mathbf{F}_{\mathrm{D}.k}}. \tag{4.14}$$

The above expression for SLNR is the expression for *Rayleigh quotient* of the two Hermitian matrix pair $(\mathbf{h}_{\mathrm{eq}_k}^H \mathbf{h}_{\mathrm{eq}_k})$ and $(\tilde{\mathbf{H}}_{\mathrm{eq}_k}^H \tilde{\mathbf{H}}_{\mathrm{eq}_k} + \frac{1}{\gamma_k} N_r \mathbf{F}_{\mathrm{R}}^H \mathbf{F}_{\mathrm{R}})$, and hence determining $\mathbf{F}_{\mathrm{D}.k}$ boils down to a generalized eigenvalue problem. The digital part of the hybrid precoder for the k^{th} MS, $\mathbf{F}_{\mathrm{D}.k}$ is thus given by the generalized eigenvector corresponding to the largest generalized eigenvalue of the matrices $(\mathbf{h}_{\mathrm{eq}_k}^H \mathbf{h}_{\mathrm{eq}_k})$ and $(\tilde{\mathbf{H}}_{\mathrm{eq}_k}^H \tilde{\mathbf{H}}_{\mathrm{eq}_k} + \frac{1}{\gamma_k} N_r \mathbf{F}_{\mathrm{R}}^H \mathbf{F}_{\mathrm{R}})$. It is written in condensed form as

$$\mathbf{F}_{\mathrm{D}.k} \propto \text{max generalized eigenvector} \left(\mathbf{h}_{\mathrm{eq}_k}^H \mathbf{h}_{\mathrm{eq}_k}, \left(\tilde{\mathbf{H}}_{\mathrm{eq}_k}^H \tilde{\mathbf{H}}_{\mathrm{eq}_k} + \frac{1}{\gamma_k} N_r \mathbf{F}_{\mathrm{R}}^H \mathbf{F}_{\mathrm{R}}\right)\right). \tag{4.15}$$

The hybrid precoder $\mathbf{F}_{\cdot k}$ needs to be of unit norm to satisfy total power constraint. Hence the obtained $\mathbf{F}_{\mathrm{D}.k}$ from (4.15) is normalized so that $|\mathbf{F}_{\mathrm{R}} \mathbf{F}_{\mathrm{D}.k}|^2 = 1$. If a large number of antennas are used at the BS, $\mathbf{F}_{\mathrm{R}}^H \mathbf{F}_{\mathrm{R}} \approx N_t \mathbf{I}_{\mathrm{N}_t}$ [18]. In such case, $\left(\tilde{\mathbf{H}}_{\mathrm{eq}_k}^H \tilde{\mathbf{H}}_{\mathrm{eq}_k} + \frac{1}{\gamma_k} N_r \mathbf{F}_{\mathrm{R}}^H \mathbf{F}_{\mathrm{R}}\right)$ is guaranteed to be invertible and the expression in (4.15) reduces to a standard eigenvalue problem,

$$\mathbf{F}_{\mathrm{D}.k} \propto \text{max eigenvector} \left(\left(\tilde{\mathbf{H}}_{\mathrm{eq}_k}^H \tilde{\mathbf{H}}_{\mathrm{eq}_k} + \frac{1}{\gamma_k} N_r \mathbf{F}_{\mathrm{R}}^H \mathbf{F}_{\mathrm{R}}\right)^{-1} \mathbf{h}_{\mathrm{eq}_k}^H \mathbf{h}_{\mathrm{eq}_k}\right). \tag{4.16}$$

4.3 Performance Analysis in Single Path Channels with Infinite Resolution Codebook

Analyzing the spectral efficiency of hybrid precoding is non-trivial as it involves the combination of analog precoder and digital precoder. In this section, the performance of the proposed hybrid SLNR precoding will be analyzed in a single path channel with large number of BS antennas. Because mmWave channel is sparse and large antenna arrays are required for enough received power [30], this case holds significance. We assume perfect channel knowledge at the MS and the perfect effective channel knowledge at the BS. It is further assumed that infinite resolution codebooks are available at both the BS and the MS, *i.e.*, analog precoder and combiner can choose beamsteering vectors with continuous angles. Taking $N_{p_i} = 1$ and $N_c = L$ in (1.4), the channel from the BS to the k^{th} MS can be written as

$$\mathbf{H}_k = \sqrt{N_t N_r}\alpha^k \mathbf{a}_r^k(\phi_r^k)\mathbf{a}_t^k(\phi_t^k)^H, \tag{4.17}$$

where the symbols have their usual meanings with superscript 'k' representing relation with the channel to the k^{th} user, and subscripts 'r' and 't' denoting association with the receive and the transmit parameters respectively. Since it is a single path channel, the subscript ℓ has been dropped from all the parameters. For the sake of simplicity, ULAs are assumed to be deployed at the BS and the MSs, and hence only the azimuth AoAs and AoDs are considered. At first, MS_k chooses analog combiner to maximize received power as

$$\mathbf{w}_{\mathrm{r}_k}^{\star} = \underset{\mathbf{w}_{\mathrm{r}_k} \in \mathcal{W}_k}{\arg\max}\, \mathbf{w}_{\mathrm{r}_k}^H \mathbf{H}_k \mathbf{H}_k^H \mathbf{w}_{\mathrm{r}_k}. \tag{4.18}$$

Given the single path channel $\mathbf{H}_k$ and the choice of $\mathbf{w}_{\mathrm{r}_k}$ to take beamsteering vector of any angle, it is obvious that when $\mathbf{w}_{\mathrm{r}_k} = \sqrt{N_r}\mathbf{a}_r^k(\phi_r^k)$ the received power is maximized.

Hence, MS chooses $\mathbf{a}_r^k(\phi_r^k)$ as $\mathbf{w}_{\mathrm{r}_k}$. The effective channel to the k^{th} MS is given by

$$\begin{aligned}\mathbf{h}_{\mathrm{e}_k} &= \mathbf{w}_{r_k}^H \mathbf{H}_k \\ &= \sqrt{N_t} N_r \alpha^k \mathbf{a}_t^{k\,H}(\phi_t^k).\end{aligned} \tag{4.19}$$

Now, the BS decides upon the k^{th} column of analog precoder $\mathbf{F}_{\mathrm{R}}$ by solving

$$\mathbf{F}_{\mathrm{R}_{\cdot k}}^{\star} = \underset{\mathbf{F}_{\mathrm{R}_{\cdot k}} \in \mathcal{F}}{\arg\max} \frac{\mathbf{F}_{\mathrm{R}_{\cdot k}}^H \left(\mathbf{h}_{\mathrm{e}_k}^H \mathbf{h}_{\mathrm{e}_k}\right) \mathbf{F}_{\mathrm{R}_{\cdot k}}}{\mathbf{F}_{\mathrm{R}_{\cdot k}}^H \left(\tilde{\mathbf{H}}_{\mathrm{e}_k}^H \tilde{\mathbf{H}}_{\mathrm{e}_k} + \frac{1}{\gamma_k} N_r \mathbf{I}_{\mathrm{N}_t}\right) \mathbf{F}_{\mathrm{R}_{\cdot k}}}, \tag{4.20}$$

which upon substituting the values of $\mathbf{h}_{\mathrm{e}_k}$ and $\tilde{\mathbf{H}}_{\mathrm{e}_k}$ becomes

$$\mathbf{F}_{\mathrm{R}_{\cdot k}}^{\star} = \underset{\mathbf{F}_{\mathrm{R}_{\cdot k}} \in \mathcal{F}}{\arg\max} \frac{\mathbf{F}_{\mathrm{R}_{\cdot k}}^H \left(N_t N_r^2 \left|\alpha^k\right|^2 \mathbf{a}_t^k(\phi_t^k) \mathbf{a}_t^k(\phi_t^k)^H\right) \mathbf{F}_{\mathrm{R}_{\cdot k}}}{\mathbf{F}_{\mathrm{R}_{\cdot k}}^H \left(N_t N_r^2 \sum_{m=1, m\neq k}^{K} \left\{\left|\alpha^m\right|^2 \mathbf{a}_t^m(\phi_t^m) \mathbf{a}_t^m(\phi_t^m)^H\right\} + \frac{1}{\gamma_k} N_r \mathbf{I}_{\mathrm{N}_t}\right) \mathbf{F}_{\mathrm{R}_{\cdot k}}}. \tag{4.21}$$

If the number of antennas used (UPA or ULA) at the BS is large, it can be written that [94],

$$\lim_{N_t \to \infty} \sum_{\substack{m=1 \\ m\neq k}}^{K} \mathbf{a}_t^k(\phi_r^k)^H \mathbf{a}_t^m(\phi_r^m) = 0. \tag{4.22}$$

If $\mathbf{a}_t^k(\phi_t^k)$ is chosen as $\mathbf{F}_{\mathrm{R}_{\cdot k}}$, it will maximize the numerator in (4.21). At the same time, it will minimize the denominator in (4.21) following the relation in (4.5). Therefore, it is fair to say $\mathbf{a}_t^k(\phi_t^k)$ is the optimal $\mathbf{F}_{\mathrm{R}_{\cdot k}}$. Hence, the BS sets $\mathbf{F}_{\mathrm{R}} = \sqrt{N_t}\left[\mathbf{a}_t^1(\phi_t^1), \mathbf{a}_t^2(\phi_t^2), \ldots, \mathbf{a}_t^K(\phi_t^K)\right]$. The equivalent channel with analog combiner and analog precoder applied is

$$\mathbf{h}_{\mathrm{eq}_k} = \sqrt{N_t} N_r \alpha^k \mathbf{a}_t^k(\phi_t^k)^H \sqrt{N_t}\left[\mathbf{a}_t^1(\phi_t^1), \mathbf{a}_t^2(\phi_t^2), \ldots, \mathbf{a}_t^K(\phi_t^K)\right] \approx N_t N_r \alpha^k \mathbf{e}_k^H, \tag{4.23}$$

where $\mathbf{e}_k$ is a K-length column vector with 1 at k^{th} position and zero elsewhere. Further, we can write

$$\mathbf{h}_{\mathrm{eq}_k}^H \mathbf{h}_{\mathrm{eq}_k} = N_t^2 N_r^2 \mathbf{A}^k, \tag{4.24}$$

where $\mathbf{A}^k$ is a $K \times K$ matrix in which the element at the (k,k) position, $\mathbf{A}^k_{k,k} = \left|\alpha^k\right|^2$ while all other entries are zero. Also,

$$\tilde{\mathbf{H}}^H_{\mathrm{eq}_k}\tilde{\mathbf{H}}_{\mathrm{eq}_k} + \tfrac{1}{\gamma_k}N_r\mathbf{F}^H_{\mathrm{R}}\mathbf{F}_{\mathrm{R}} \approx N_t^2N_r^2\tilde{\mathbf{D}}_k + \tfrac{1}{\gamma_k}N_rN_t\mathbf{I}_{\mathrm{N}_t} = \mathbf{DIAG}\left(d_1, d_2, \ldots, d_K\right), \quad (4.25)$$

where $\tilde{\mathbf{D}}_k = \mathbf{DIAG}\left(\tilde{d}_1, \tilde{d}_2, \ldots, \tilde{d}_K\right)$ with $\tilde{d}_m = |\alpha^m|^2, m = 1, 2, \ldots, K$ and $m \neq k$, and $\tilde{d}_k = 0$. And, $d_m = N_t^2N_r^2|\alpha^m|^2 + \frac{1}{\gamma_k}N_tN_r, m = 1, 2, \ldots, K$ and $m \neq k$, and $d_k = \frac{1}{\gamma_k}N_tN_r$. Thus, the digital part of the k^{th} hybrid precoder is given by

$$\begin{aligned}
\mathbf{F}_{\mathrm{D}\cdot k} &\propto \text{max eigenvector}\left(\mathbf{DIAG}\left(\frac{1}{d_1}, \frac{1}{d_2}, ..., \frac{1}{d_K}\right) * N_tN_r\mathbf{A}^k\right) \\
&= \text{max eigenvector}\left(N_tN_r\mathbf{A}^k\tfrac{\gamma_k}{N_tN_r}\right) \\
&= \text{max eigenvector}\left(\gamma_k\mathbf{A}^k\right) \\
&= \mathbf{e}_k.
\end{aligned}$$

The obtained $\mathbf{F}_{\mathrm{D}\cdot k}$ should be normalized so that $\left|\mathbf{F}_{\mathrm{R}}\mathbf{F}_{\mathrm{D}\cdot k}\right|^2 = 1$. That is,

$$\mathbf{F}_{\mathrm{D}\cdot k} = \frac{\mathbf{e}_k}{|\mathbf{F}_{\mathrm{R}}\mathbf{e}_k|} = \frac{\mathbf{e}_k}{|\mathbf{F}_{\mathrm{R}\cdot k}|} = \frac{\mathbf{e}_k}{\sqrt{N_t}}. \quad (4.26)$$

The hybrid precoder for the k^{th} MS is $\mathbf{F}_{\cdot k} = \mathbf{F}_{\mathrm{R}}\frac{\mathbf{e}_k}{\sqrt{N_t}} = \frac{\mathbf{F}_{\mathrm{R}\cdot k}}{\sqrt{N_t}} = \mathbf{a}_t^k(\phi_t^k)$. Hence, it implies that in single path channel when $N_t \to \infty$, no SLNR precoding is required and beamsteering is sufficient. The achievable rate for the k^{th} user is given by

$$\mathcal{R}_k = \log_2\left(1 + \gamma_kN_tN_r\left|\alpha^k\right|^2\right). \quad (4.27)$$

4.4 Performance Analysis

The mmWave channel between BS and each MS is modeled using (1.4) with number of paths $L = 3$. UPA is employed at both the BS and the MS. The azimuth AoAs/AoDs are uniformly distributed in the range $[0, 2\pi]$, and the elevation AoAs/AoDs are uniformly distributed in the range $\left[-\frac{\pi}{2}, \frac{\pi}{2}\right]$ while the complex path gains, $\alpha_\ell^k \sim \mathcal{CN}(0, 1)$. The noise variance per receive antenna is assumed to be same for all users,

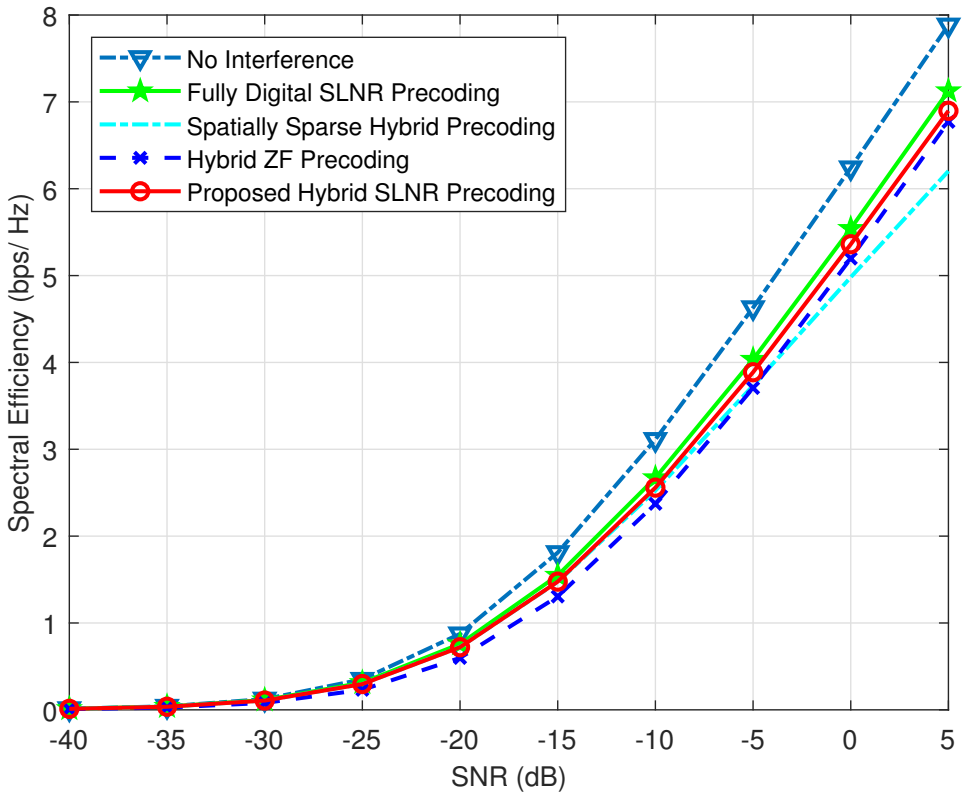

Figure 4.2: Achievable spectral efficiency in different precoding schemes.

i.e., $\sigma_1^2 = \sigma_2^2 = ... = \sigma_K^2 = \sigma^2$. The SNR used in the plots is defined as SNR $= \frac{P}{\sigma^2}$. The spectral efficiency plotted in the Figure 4.2, 4.5, 4.6 is defined as $\frac{1}{K}\mathbb{E}\left(\sum_{k=1}^{K} R_k\right)$. The SINR plotted in Figure 4.3 is defined as SINR $= \frac{1}{K}\sum_{k=1}^{K} \text{SINR}_k$. The sum spectral efficiency plotted in Figure 4.4 refers to the average total achievable rate, *i.e.*, $\mathbb{E}\left(\sum_{k=1}^{K} R_k\right)$. Unless it is a varying parameter, 8×8 BS UPA, 4×4 MS UPA, $K = 8$ and SNR $= 0$ dB are considered in all the figures.

The performance of the proposed hybrid SLNR precoder is compared with hybrid ZF precoder [30], no interference case (a hypothetical single user case which is used as a comparison benchmark), fully digital or unconstrained SLNR precoder and spatially sparse precoder [18] extended to maximize SLNR in MU-MIMO environment. Analog-only combining is considered at the MS in all the precoding schemes which ensures a fair comparison. Perfect channel knowledge is assumed at the MS and perfect effective channel knowledge at the BS. The beamsteering codebooks at the MS and the BS are assumed to be AoA/AoD codebooks, *i.e.*, $\mathcal{W}_k$ consists of array response vectors of the actual AoA's at the k^{th} MS and $\mathcal{F}$ consists of the array

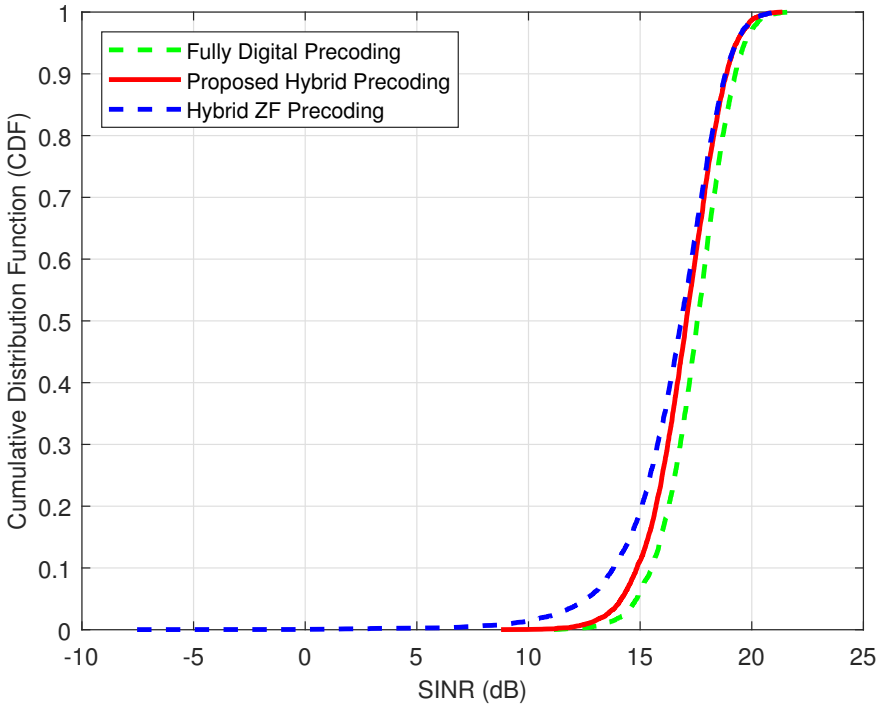

Figure 4.3: Cumulative distribution function (CDF) of SINR in different precoding schemes.

response vectors of the actual AoD's.

The spectral efficiency is plotted as a function of SNR and cumulative distribution function (CDF) of SINR respectively in Figure 4.2 and Figure 4.3. The proposed SLNR precoder clearly offers SINR and hence the achievable rate, quite close to fully digital precoder which establishes that the proposed precoder is capable of curbing the interference due to other users. The proposed precoder accomplishes a performance better than the hybrid ZF precoder.

Figure 4.4 depicts the effect of number of users on achievable sum-rates. The proposed precoder closely follows the sum-rate performance of the fully digital precoder, with its sum-rate increasing with K, while the sum-rate performance of hybrid ZF precoder satiates at high values of K. The hybrid ZF precoder is equivalent to the ZF precoder developed for a system with K transmit antennas and K MSs equipped with single antenna. In such a system, the sum-rate performance of the ZF precoder does not grow at higher number of users [34, 95]. The spatially sparse hybrid precoder tries to follow the fully digital precoder but falls quite short of both digital SLNR precoder and hybrid SLNR precoder.

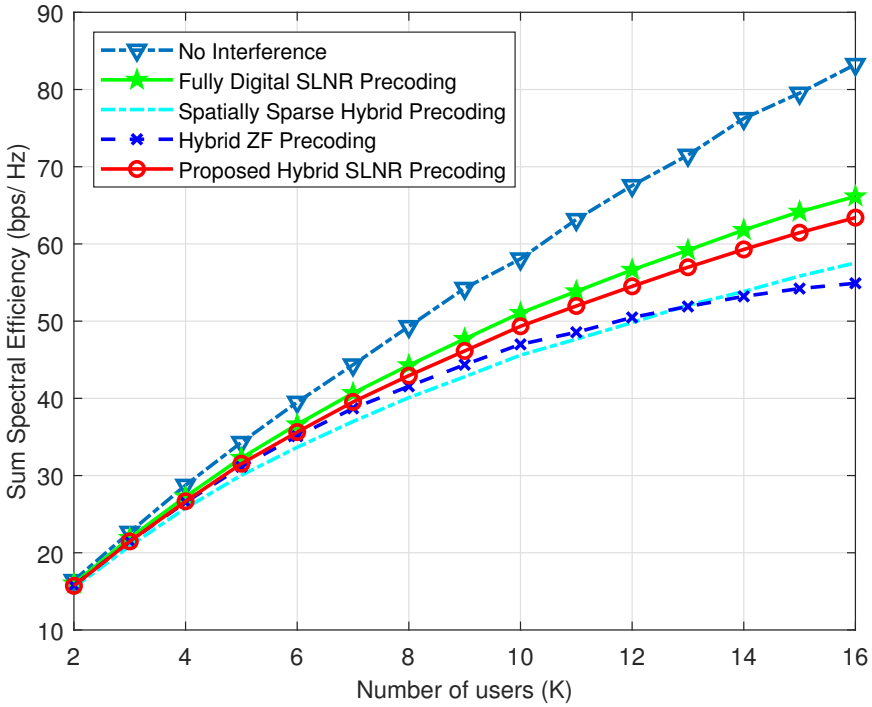

Figure 4.4: Achievable sum rates as a function of number of users in different precoding schemes.

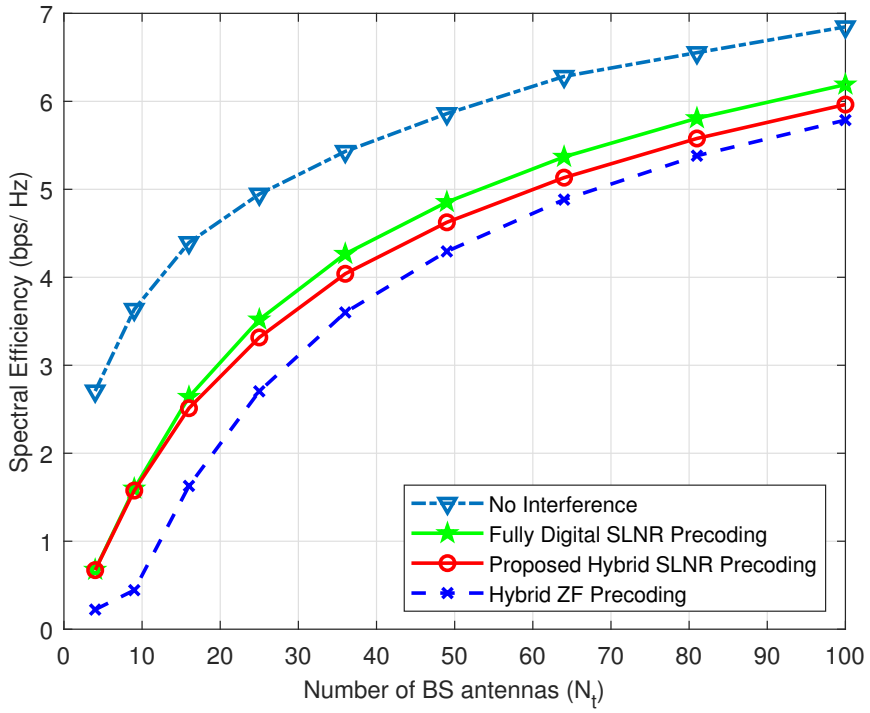

Figure 4.5: Achievable spectral efficiency as a function of number of BS antennas in different precoding schemes.

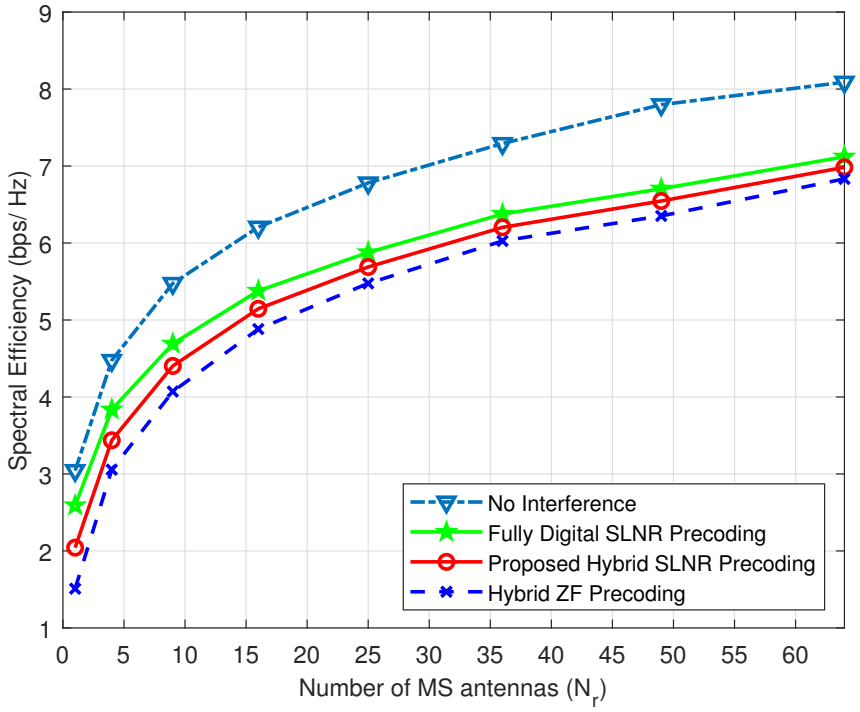

Figure 4.6: Achievable spectral efficiency as a function of number of MS antennas in different precoding schemes.

Figure 4.5 and Figure 4.6 portray the effect of N_t and N_r on achievable rates. With the growing number of N_t and N_r, the achievable spectral efficiency of the proposed SLNR precoder increases expectedly as there is a rise in array gain with the increase in N_t and N_r. However there is one glaring difference between two figures. In Figure 4.6, unlike at higher values of N_t in Figure 4.5, the proposed precoder does not narrow down the gap between its achievable rate and the no-interference rate at higher values of N_r. This can be attributed to the fact that the analog-only combiner employed at the MS is unable to combine the signals received at different antennas to maximize the received power.

4.5 Summary

In this chapter, a downlink multi-user massive MIMO scenario is considered, and a hybrid precoding scheme that maximizes signal-to-leakage-and-noise ratio (SLNR) is proposed. Each mobile station (MS) determines its analog combiner first, and then the base station (BS) constructs the analog precoder and the digital precoder of the

hybrid precoder in two separate stages to maximize the SLNR for each user. It is shown through simulations that the proposed hybrid SLNR-based precoder exhibits a performance close to the fully digital SLNR-based precoder despite using only a few number of RF chains.

Chapter 5

Hybrid MMSE Precoding for mmWave MU-MISO

In Chapter 4, codebook-based hybrid SLNR precoder was proposed for MU-MIMO. The problem with the codebook-based precoder is that the choice of analog precoding vectors from a codebook limits the performance. Moreover, the proposed precoder could utilize only as many RF chains as the number of users even if more RF chains were available. In this chapter, we ropose a hybrid precoder that eliminates the use of codebook and allows the use of RF chains more than the number of users for an MU-MISO system. The proposed hybrid precoder also avoids the need of computing optimal fully digital precoder for the determination of hybrid precoder unlike those proposed in Chapter 2, and can work in both narrowband and wideband channels. The contributions made in this chapter can be summarized as:

(i) With a view to minimize sum of MSE for all the users, the hybrid precoding problem for MU-MISO in narrowband channel is considered, which is solved in two stages. The digital part of the hybrid precoder can be easily determined in similar way to the conventional fully digital precoder, once the analog part of the hybrid precoder is fixed. The analog precoding problem is in the form of trace minimization of inverse of a Hermitian positive definite matrix [43, 44]. The lower bound of the trace function, which is in terms of reciprocal of trace

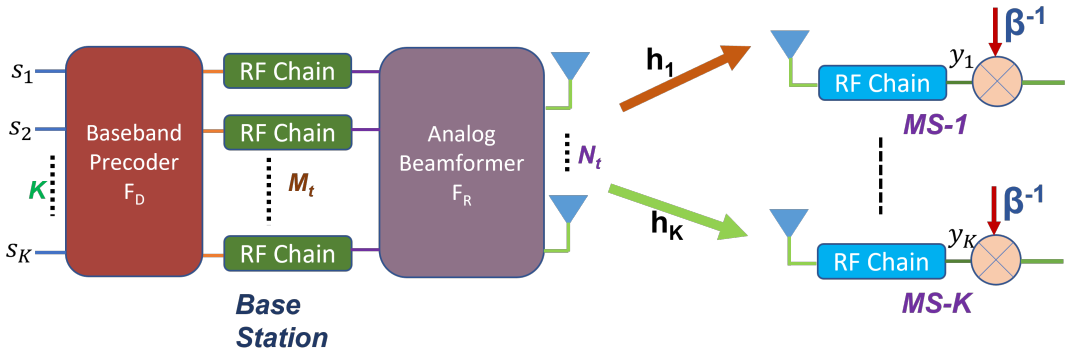

Figure 5.1: A downlink multi-user mmWave MISO system with hybrid precoding at the transmitter.

of a Hermitian positive definite matrix, is determined. In a bid to mitigate complexity, the lower bound of the objective function is minimized instead of directly minimizing the objective function.

(ii) The analog precoding problem is ultimately modeled as a trace maximization (TM) problem. Orthogonality constraint is enforced on analog precoder, and an iterative method relying on truncated singular value decomposition (SVD) is developed to construct the hybrid precoder which is called TM-HMP. The proposed precoder exhibits very good spectral and BER performances which are almost on par with the existing high-performing hybrid precoding method.

(iii) The hybrid precoding algorithm which is developed for narrowband channel is extended for wideband channel by considering OFDM. The proposed hybrid precoding algorithm performs equally well, if not better in wideband channel.

(iv) The complexity analysis of the proposed algorithm is also performed, and compared against the existing algorithms. The proposed method entails very low complexity and gives commendable performance even with quantized phase shifters of low resolution.

5.1 System Model

A multi-user mmWave MISO downlink system comprising of a BS with fully-connected architecture and K MSs as shown in Figure 5.1 is considered. The BS consists of N_t

transmit antennas and M_t RF chains, whereas each MS has a single receive antenna and a single RF chain. The total number of data streams being transmitted is K, one for each MS, and $K \leq M_t \leq N_t$.

At the BS, the transmit signal $\mathbf{s} = [s_1, s_2, \ldots, s_K]^T$, $\mathbf{s} \in \mathbb{C}^{K\times 1}$ is precoded by the hybrid precoder $\mathbf{F} = \mathbf{F}_\mathrm{R}\mathbf{F}_\mathrm{D}$ before transmission. $\mathbf{F}_\mathrm{D} \in \mathbb{C}^{M_t\times K}$ is the baseband digital precoder and $\mathbf{F}_\mathrm{R} \in \mathbb{C}^{N_t\times M_t}$ is the analog precoder. The transmit signal $\mathbf{s}$ is such that $\mathbb{E}\left[\mathbf{s}\mathbf{s}^H\right] = (P/K)\mathbf{I}_\mathrm{K}$, where P is the total transmit power. The unit amplitude constraint imposed on $\mathbf{F}_\mathrm{R}$ because of the use of phase shifters would mean that $|\mathbf{F}_{\mathrm{R}_{i,j}}| = 1$. We consider narrowband block-fading channel model so that we can write the received signal at the k^{th} MS as

$$y_k = \mathbf{h}_k\mathbf{F}_\mathrm{R}\mathbf{F}_\mathrm{D}\mathbf{s} + n_k,\ k = 1, 2, \ldots, K, \tag{5.1}$$

where $\mathbf{h}_k \in \mathbb{C}^{1\times N_t}$ is the channel to the k^{th} MS, $n_k \sim \mathcal{CN}(0, \sigma_n^2)$ is complex Gaussian noise. Organizing all the y_k, $k = 1, \ldots, K$ into a single vector we get

$$\mathbf{y} = \mathbf{H}\mathbf{F}_\mathrm{R}\mathbf{F}_\mathrm{D}\mathbf{s} + \mathbf{n}, \tag{5.2}$$

where $\mathbf{H} = \left[\mathbf{h}_1^T, \mathbf{h}_2^T, \ldots, \mathbf{h}_K^T\right]^T, \mathbf{H} \in \mathbb{C}^{K\times N_t}$ is the channel matrix and $\mathbf{n} \in \mathbb{C}^{K\times 1}, \mathbf{n} \sim \mathcal{CN}(\mathbf{0}, \sigma_n^2\mathbf{I})$ is the complex noise vector.

5.2 Problem Statement

As in [43, 44, 96], the precoder is designed by minimizing the sum of the modified MSE of the K users. Similar to [43, 97], the hybrid precoding problem can be stated as

$$\mathbf{F}_\mathrm{R}^\star, \mathbf{F}_\mathrm{D}^\star = \underset{\mathbf{F}_\mathrm{R},\mathbf{F}_\mathrm{D}}{\arg\min}\, \mathbb{E}\left[\left|\mathbf{s} - \beta^{-1}\mathbf{y}\right|^2\right] \tag{5.3a}$$

$$s.t. \qquad \|\mathbf{F}_\mathrm{R}\mathbf{F}_\mathrm{D}\|_F^2 = K \tag{5.3b}$$

$$|\mathbf{F}_{\mathrm{R}_{i,j}}| = 1,\ \forall i, j, \tag{5.3c}$$

where the parameter $\beta \in \mathbb{R}_+$. The reason for using modified MSE is the need to fulfill the transmit power constraint [96]. The use of the modified MSE means β^{-1} is used as scaling factor at all the receivers. The scaling factor β^{-1} serves the purpose of correcting the level of received signal to the desired signal level. The use of same β^{-1} at all the receivers or the modified MSE guarantees closed form solution for the digital part $\mathbf{F}_{\mathrm{D}}$ of the hybrid MMSE precoder if $\mathbf{F}_{\mathrm{R}}$ is known. This follows directly from the similar argument for the determination of conventional MMSE precoder [98].

The optimization problem of (5.3) is pretty difficult, especially because of the second constraint (5.3c) which is non-convex in nature. The problem becomes easier to solve if it is decomposed into two separate stages for determining analog precoder and digital precoder as in [43, 44]. If the analog precoder $\mathbf{F}_{\mathrm{R}}$ is available, the digital precoder that minimizes the objective function in (5.3a) can be easily determined using the method of Lagrange multipliers [43, 44] as,

$$\mathbf{F}_{\mathrm{D}} = \beta(\mathbf{F}_{\mathrm{R}}^H \mathbf{H}^H \mathbf{H} \mathbf{F}_{\mathrm{R}} + \mu \mathbf{F}_{\mathrm{R}}^H \mathbf{F}_{\mathrm{R}})^{-1} \mathbf{F}_{\mathrm{R}}^H \mathbf{H}^H = \beta \tilde{\mathbf{F}}_{\mathrm{D}}, \tag{5.4}$$

where $\mu = \frac{K\sigma_n^2}{P}$, $\tilde{\mathbf{F}}_{\mathrm{D}} = (\mathbf{F}_{\mathrm{R}}^H \mathbf{H}^H \mathbf{H} \mathbf{F}_{\mathrm{R}} + \mu \mathbf{F}_{\mathrm{R}}^H \mathbf{F}_{\mathrm{R}})^{-1} \mathbf{F}_{\mathrm{R}}^H \mathbf{H}^H$ is the unnormalized optimal digital precoder. Expanding (5.3a) after supplanting $\mathbf{y}$ with its expression (5.2), and replacing $\mathbf{F}_{\mathrm{D}}$ with the expression in (5.4) yields the optimization subproblem to determine analog precoder $\mathbf{F}_{\mathrm{R}}$ [43, 44],

$$\begin{aligned} \mathbf{F}_{\mathrm{R}}^{\star} = \underset{\mathbf{F}_{\mathrm{R}}}{\arg\min} \quad & \mathbf{Tr}[(\mathbf{I} + \mu^{-1} \mathbf{H} \mathbf{F}_{\mathrm{R}} \mathbf{F}_{\mathrm{R}}^H \mathbf{H}^H)^{-1}] \\ s.t. \quad & |\mathbf{F}_{\mathrm{R}_{i,j}}| = 1, \quad \forall i, j. \end{aligned} \tag{5.5}$$

The value of β is computed by substituting $\mathbf{F}_{\mathrm{D}} = \beta \tilde{\mathbf{F}}_{\mathrm{D}}$ in the constraint (5.3b) as

$$\beta = \sqrt{\frac{K}{\mathbf{Tr}(\mathbf{F}_{\mathrm{R}} \tilde{\mathbf{F}}_{\mathrm{D}} \tilde{\mathbf{F}}_{\mathrm{D}}^H \mathbf{F}_{\mathrm{R}}^H)}} \quad . \tag{5.6}$$

Thus, it can be seen that β is nothing but the normalization factor for the precoder.

5.3 Trace Maximization-based Hybrid MMSE Precoder (TM-HMP)

5.3.1 Analog Precoding as Trace Maximization Problem

The matrix inside the trace function in the objective function (5.5) is in terms of inverse of another matrix which makes the solution complicated. The objective function of (5.5) can be written as

$$\mathbf{Tr}\left[\left(\mathbf{I}+\mu^{-1}\mathbf{H}\mathbf{F}_{\mathrm{R}}\mathbf{F}_{\mathrm{R}}^{H}\mathbf{H}^{H}\right)^{-1}\right] \geq \frac{K^2}{\mathbf{Tr}\left(\mathbf{I}+\mu^{-1}\mathbf{H}\mathbf{F}_{\mathrm{R}}\mathbf{F}_{\mathrm{R}}^{H}\mathbf{H}^{H}\right)}.$$

The proof of this is provided in Appendix A. Instead of minimizing the objective function in (5.5), its lower bound is minimized to determine analog precoder $\mathbf{F}_{\mathrm{R}}$, which is equivalent to the optimization problem,

$$\mathbf{F}_{\mathrm{R}}^{\star} = \underset{\mathbf{F}_{\mathrm{R}}}{\arg\max} \quad \mathbf{Tr}\left(\mathbf{I}+\mu^{-1}\mathbf{H}\mathbf{F}_{\mathrm{R}}\mathbf{F}_{\mathrm{R}}^{H}\mathbf{H}^{H}\right) \tag{5.7}$$

The trace of $\mathbf{I}+\mu^{-1}\mathbf{H}\mathbf{F}_{\mathrm{R}}\mathbf{F}_{\mathrm{R}}^{H}\mathbf{H}^{H}$ is equal to the sum $\sum_{i=1}^{K}\lambda_i$, where $\{\lambda_i \mid \lambda_i \geq 1\}_{i=1}^{K}$ are its eigenvalues. On the other hand, the trace of $\left(\mathbf{I}+\mu^{-1}\mathbf{H}\mathbf{F}_{\mathrm{R}}\mathbf{F}_{\mathrm{R}}^{H}\mathbf{H}^{H}\right)^{-1}$ is equal to the sum, $\sum_{i=1}^{K}\lambda_i^{-1}$, where $0<\lambda_i^{-1}\leq 1\ \forall i=1,\ldots,K$. By choosing to maximize the objective function in (5.7), we are trying to determine $\mathbf{F}_{\mathrm{R}}$ so that it maximizes the sum of all λ_i's, which is possible only when λ_i's are increased. This means the values of λ_i^{-1}'s are decreased, and as a result diminishing the sum of λ_i^{-1}'s.

The objective function in (5.7) can be further simplified as

$$\begin{aligned} & \mathbf{Tr}\left(\mathbf{I}_K+\mu^{-1}\mathbf{H}\mathbf{F}_{\mathrm{R}}\mathbf{F}_{\mathrm{R}}^{H}\mathbf{H}^{H}\right) \\ \overset{(a)}{\approx} & \frac{K}{N_tM_t}\mathbf{Tr}\left(\mathbf{F}_{\mathrm{R}}^{H}\mathbf{F}_{\mathrm{R}}\right)+\mathbf{Tr}\left(\mu^{-1}\mathbf{F}_{\mathrm{R}}^{H}\mathbf{H}^{H}\mathbf{H}\mathbf{F}_{\mathrm{R}}\right) \\ = & \frac{K}{N_tM_t}\mathbf{Tr}\left[\mathbf{F}_{\mathrm{R}}^{H}\left(\mathbf{I}+\tau\mathbf{H}^{H}\mathbf{H}\right)\mathbf{F}_{\mathrm{R}}\right], \end{aligned}$$

where $\tau \triangleq \mu^{-1}\frac{N_tM_t}{K}$, and the reasons for (a) are $\mathbf{Tr}\left(\mathbf{I}_K\right)=K$, $\mathbf{F}_{\mathrm{R}}^{H}\mathbf{F}_{\mathrm{R}}\approx N_t\mathbf{I}_{M_t}$ so that

$\mathbf{Tr}\left(\mathbf{F}_{\mathrm{R}}^{H}\mathbf{F}_{\mathrm{R}}\right) \approx N_t\mathbf{Tr}\left(\mathbf{I}_{M_t}\right) = N_tM_t$ as $N_t \to \infty$ which is valid in mmWave MIMO [18]. Thus, the new optimization subproblem for analog precoding can be expressed as the trace maximization problem,

$$\mathbf{F}_{\mathrm{R}}^{\star} = \underset{\mathbf{F}_{\mathrm{R}}}{\arg\max} \quad \mathbf{Tr}\left[\mathbf{F}_{\mathrm{R}}^{H}\left(\mathbf{I} + \tau\mathbf{H}^{H}\mathbf{H}\right)\mathbf{F}_{\mathrm{R}}\right]. \tag{5.8}$$

Defining the new variable $\bar{\mathbf{F}}_{\mathrm{R}} \triangleq \frac{1}{\sqrt{N_t}}\mathbf{F}_{\mathrm{R}}$, the optimization subproblem for the determination of $\mathbf{F}_{\mathrm{R}}$ can be stated in terms of $\bar{\mathbf{F}}_{\mathrm{R}}$ as

$$\bar{\mathbf{F}}_{\mathrm{R}}^{\star} = \underset{\bar{\mathbf{F}}_{\mathrm{R}}}{\arg\max} \quad \mathbf{Tr}\left[\bar{\mathbf{F}}_{\mathrm{R}}^{H}\left(\mathbf{I} + \tau\mathbf{H}^{H}\mathbf{H}\right)\bar{\mathbf{F}}_{\mathrm{R}}\right] \tag{5.9a}$$

$$s.t. \quad \left(\bar{\mathbf{F}}_{\mathrm{R}}^{H}\bar{\mathbf{F}}_{\mathrm{R}}\right) = \mathbf{I}_{M_t} \tag{5.9b}$$

$$\left|\bar{\mathbf{F}}_{\mathrm{R}_{i,j}}\right| = \frac{1}{\sqrt{N_t}} \quad \forall i, j. \tag{5.9c}$$

If the solution to the problem in (5.9) is $\bar{\mathbf{F}}_{\mathrm{R}}^{\star}$, the analog precoder $\mathbf{F}_{\mathrm{R}}$ is computed as $\mathbf{F}_{\mathrm{R}} = \sqrt{N_t}\bar{\mathbf{F}}_{\mathrm{R}}^{\star}$. The constraint in (5.9b) enforces orthogonality on $\bar{\mathbf{F}}_{\mathrm{R}}$, which is equivalent to imposing $\mathbf{F}_{\mathrm{R}}^{H}\mathbf{F}_{\mathrm{R}} = N_t\mathbf{I}_{M_t}$. The objective function in (5.9a) came to fruition because $\mathbf{F}_{\mathrm{R}}^{H}\mathbf{F}_{\mathrm{R}} \approx N_t\mathbf{I}_{M_t}$, and hence adding this constraint in (5.9) is not unfounded. We leverage the orthogonality of $\mathbf{F}_{\mathrm{R}}$ to obtain the objective function in (5.9a) because it ensures that $\mathbf{I} + \nu\mathbf{H}^{H}\mathbf{H}$ is always a full rank matrix, and has its rank greater than that of $\mathbf{F}_{\mathrm{R}}$ in all cases. The matrix $\mathbf{I} + \nu\mathbf{H}^{H}\mathbf{H}$ can be replaced by just $\mathbf{H}^{H}\mathbf{H}$ for the case $M_t = K$.

5.3.2 The Proposed TM-HMP algorithm

An iterative method based on truncated singular value decomposition (SVD) is proposed to solve the problem (5.9). The matrix $\mathbf{I} + \tau\mathbf{H}^{H}\mathbf{H} \succ \mathbf{0}$, so the trace $\mathbf{Tr}\left[\bar{\mathbf{F}}_{\mathrm{R}}^{H}\left(\mathbf{I} + \tau\mathbf{H}^{H}\mathbf{H}\right)\bar{\mathbf{F}}_{\mathrm{R}}\right]$ is always real and positive. Thus, the objective function in (5.9a) can be replaced with $\left|\mathbf{Tr}\left[\bar{\mathbf{F}}_{\mathrm{R}}^{H}\left(\mathbf{I} + \tau\mathbf{H}^{H}\mathbf{H}\right)\bar{\mathbf{F}}_{\mathrm{R}}\right]\right|$ and maximized. Starting with a random initial value of $\bar{\mathbf{F}}_{\mathrm{R}}^{(0)}$, $\mathbf{A}^{(k)} = \bar{\mathbf{F}}_{\mathrm{R}}^{(k-1)^{H}}\left(\mathbf{I} + \tau\mathbf{H}^{H}\mathbf{H}\right)$ is defined where k is the iteration number starting from 1. At each iteration k, the matrix $\mathbf{D}^{(k)}$ is first

determined which is the solution to the problem,

$$\begin{aligned} &\arg\max_{\mathbf{D}^{(k)}} \ |\mathbf{Tr}(\mathbf{A}^{(k)}\mathbf{D}^{(k)})| \\ &s.t. \quad \mathbf{D}^{(k)^H}\mathbf{D}^{(k)} = \mathbf{I}_{M_t}. \end{aligned} \tag{5.10}$$

If $\mathbf{U}^{(k)}\mathbf{S}^{(k)}\mathbf{V}_t^{(k)^H}$ represents the truncated SVD of $\mathbf{A}^{(k)}$, the solution to the problem in (5.10), which is derived in Appendix B, is $\mathbf{D}^{(k)} = \mathbf{V}_t^{(k)}\mathbf{U}^{(k)^H}$. $\bar{\mathbf{F}}_{\mathrm{R}}^{(k)}$ is approximated by normalizing each element of the matrix $\mathbf{D}^{(k)}$ to have an amplitude of $\frac{1}{\sqrt{N_t}}$, the Step 6 of the Algorithm 5.1. In essence, the phase of each element of $\mathbf{D}^{(k)}$ is being extracted.

The iteration number is increased by 1 and the new value of $\mathbf{A}^{(k)}$ is determined. This procedure is repeated until the convergence is attained, or it reaches a fixed number of iterations. Finally, $\mathbf{F}_{\mathrm{R}}$ is computed as $\mathbf{F}_{\mathrm{R}} = \sqrt{N_t}\bar{\mathbf{F}}_{\mathrm{R}}$, and digital precoder $\mathbf{F}_{\mathrm{D}}$ is determined using (5.4). The proposed algorithm is summarized in Algorithm 5.1.

Algorithm 5.1 Hybrid MMSE Precoder Using SVD-based Iterative Trace Maximization Method

Require: $\mathbf{H}$, μ, M_t.

1: Initialize $\bar{\mathbf{F}}_{\mathrm{R}}^{(0)} = \frac{1}{\sqrt{N_t}}\exp(j\mathbf{\Theta})$, where $\mathbf{\Theta}$ is $N_t \times M_t$ matrix and $\mathbf{\Theta}_{i,j}$ are random phase angles, and set $k = 1$.
2: **repeat**
3: Compute $\mathbf{A}^{(k)} = \bar{\mathbf{F}}_{\mathrm{R}}^{(k-1)^H}\left(\mathbf{I} + \tau\mathbf{H}^H\mathbf{H}\right)$.
4: Compute truncated SVD of $\mathbf{A}^{(k)}$: $\mathbf{U}^{(k)}\mathbf{S}^{(k)}\mathbf{V}_t^{(k)^H}$.
5: Compute $\mathbf{D}^{(k)} = \mathbf{V}_t^{(k)}\mathbf{U}^{(k)^H}$.
6: Compute $\bar{\mathbf{F}}_{\mathrm{R}}^{(k)} = \frac{1}{\sqrt{N_t}}\exp\left(j\angle\left(\mathbf{D}^{(k)}\right)\right)$.
7: $k \leftarrow k + 1$.
8: **until** convergence, or $k \geq N_{iter}$, where N_{iter} is the maximum of number of iterations.
9: Compute $\mathbf{F}_{\mathrm{R}} = \sqrt{N_t}\bar{\mathbf{F}}_{\mathrm{R}}^{(k)}$.
10: Calculate $\mathbf{F}_{\mathrm{D}} = \beta(\mathbf{F}_{\mathrm{R}}^H\mathbf{H}^H\mathbf{H}\mathbf{F}_{\mathrm{R}} + \mu\mathbf{F}_{\mathrm{R}}^H\mathbf{F}_{\mathrm{R}})^{-1}\mathbf{F}_{\mathrm{R}}^H\mathbf{H}^H$.
11: **return** $\mathbf{F} = \mathbf{F}_{\mathrm{R}}\mathbf{F}_{\mathrm{D}}$.

5.3.3 Convergence of TM-HMP algorithm

Once the analog precoder is furnished, the digital part of the precoder is computed from the closed-form expression obtained using the method of Lagrange multipliers. It is guaranteed to minimize the original objective function, provided the analog

precoder is available. Hence, the convergence of the proposed hybrid precoding algorithm depends on the determination of the analog precoder alone.

In the proposed algorithm, we start with $\bar{\mathbf{F}}_{\mathrm{R}}^{(0)}$ as the initial value of $\bar{\mathbf{F}}_{\mathrm{R}}$. The next value of $\bar{\mathbf{F}}_{\mathrm{R}}$, $\bar{\mathbf{F}}_{\mathrm{R}}^{(1)}$ is calculated by normalizing each element of $\mathbf{D}^{(1)}$ to have an amplitude of $\frac{1}{\sqrt{N_t}}$, where $\mathbf{D}^{(1)}$ is the matrix that maximizes $\left|\mathbf{Tr}\left[\left\{\bar{\mathbf{F}}_{\mathrm{R}}^{(0)^H}\left(\mathbf{I}+\tau\mathbf{H}^H\mathbf{H}\right)\right\}\mathbf{D}^{(1)}\right]\right|$. As $\bar{\mathbf{F}}_{\mathrm{R}}^{(1)}$ is obtained from $\mathbf{D}^{(1)}$ by phase extraction, it can be intuitively said that $\bar{\mathbf{F}}_{\mathrm{R}}^{(1)}$ does not alter the direction of change of trace value brought by $\mathbf{D}^{(1)}$ from the trace value at $\bar{\mathbf{F}}_{\mathrm{R}}^{(0)}$. Thus, $\bar{\mathbf{F}}_{\mathrm{R}}^{(1)}$, the new value of $\bar{\mathbf{F}}_{\mathrm{R}}$ is an improvement from $\bar{\mathbf{F}}_{\mathrm{R}}^{(0)}$. As this procedure continues, the value of $\bar{\mathbf{F}}_{\mathrm{R}}$ gets closer to the optimal value with each successive value of $\bar{\mathbf{F}}_{\mathrm{R}}$ increasing the value of the objective function.

As far as the convergence of the algorithm is concerned in regard to the original objective function, it can not proved analytically that the proposed method ensures uniform decrease in the value of the objective function because, a) the lower bound of the objective function is minimized, b) the approximation $\mathbf{F}_{\mathrm{R}}^H\mathbf{F}_{\mathrm{R}} \approx N_t\mathbf{I}_{M_t}$ is used in the objective function c) the analog precoder is computed by extracting phase from the solution without any unit-modulus constraint. However, it will be shown empirically in section 5.6 that the proposed method converges, and is able to minimize the mean squared error (MSE) of all users. The MSE of the system is given by

$$\mathrm{MSE} = \frac{P}{K}\mathbf{Tr}\left[\mathbf{I} - \tilde{\mathbf{F}}_{\mathrm{D}}^H\mathbf{F}_{\mathrm{R}}^H\mathbf{H}^H - \mathbf{H}\mathbf{F}_{\mathrm{R}}\tilde{\mathbf{F}}_{\mathrm{D}} + \mathbf{H}\mathbf{F}_{\mathrm{R}}\tilde{\mathbf{F}}_{\mathrm{D}}\tilde{\mathbf{F}}_{\mathrm{D}}^H\mathbf{F}_{\mathrm{R}}^H\mathbf{H}^H + \beta^{-2}\sigma_n^2\mathbf{I}\right]. \quad (5.11)$$

5.4 Extension to Wideband Channel

In this section, it is shown how the proposed method can be easily extended to work in wideband channel. It is assumed that OFDM is applied to counter multi-path fading. IFFT is preceded by digital precoding, and followed by analog precoding. Thus, digital precoding is carried out for each sub-carrier unlike analog precoding which is common for all subcarriers.

The hybrid precoding problem is minimization of sum of MSEs for all the subcarriers

[44]. If $\mathbf{H}[m]$ is defined as $\mathbf{H}[m] = \left[\mathbf{h}_1^T[m], \ldots, \mathbf{h}_K^T[m]\right]^T$, analog precoder is thus determined by maximizing

$$\sum_{m=1}^{S_c} \mathbf{Tr}\left[\mathbf{F}_{\mathrm{R}}^H \left(\mathbf{I} + \tau \mathbf{H}[m]^H \mathbf{H}[m]\right) \mathbf{F}_{\mathrm{R}}\right] = \mathbf{Tr}\left[\mathbf{F}_{\mathrm{R}}^H \left(\mathbf{I} + \tau \sum_{m=1}^{S_c} \mathbf{H}[m]^H \mathbf{H}[m]\right) \mathbf{F}_{\mathrm{R}}\right],$$

where S_c is the total number of subcarriers. The analog precoding problem for wideband channel is similar to analog precoding subproblem in (5.7) and can be accomplished by the same algorithm. The digital part of the precoder for the m^{th} sub-carrier is calculated as

$$\mathbf{F}_{\mathrm{D}}[m] = \beta[m] \left(\mathbf{F}_{\mathrm{R}}^H \mathbf{H}[m]^H \mathbf{H}[m] \mathbf{F}_{\mathrm{R}} + \mu \mathbf{F}_{\mathrm{R}}^H \mathbf{F}_{\mathrm{R}}\right)^{-1} \mathbf{F}_{\mathrm{R}}^H \mathbf{H}[m]^H, \tag{5.12}$$

where $\beta[m]$ is the normalizing factor for the m^{th} sub-carrier calculated in similar way to (5.6).

5.5 Complexity Analysis of the proposed method

The computational complexity of the proposed hybrid precoder TM-HMP is computed, and compared with the complexities of existing hybrid precoders. In general, the computational complexity of evaluating digital precoder is same for all the hybrid MMSE precoders. Thus, the difference in complexities of different hybrid precoding methods is governed by the computation of analog precoder.

(i) *Narrowband TM-HMP*: The complexity of computing the analog part of Narrowband TM-HMP is mostly the sum of the complexities involved in

- *Computation of* $\mathbf{A}$: It requires multiplication between $M_t \times N_t$ matrix $\mathbf{F}_{\mathrm{R}}^H$ and $N_t \times N_t$ matrix $\mathbf{I} + \tau \mathbf{H}^H \mathbf{H}$ which brings complexity of $\mathcal{O}\left({N_t}^2 M_t\right)$.
- *Truncated SVD*: The truncated SVD of $M_t \times N_t$ matrix $\mathbf{A}$ entails complexity of $\mathcal{O}\left(N_t M_t^2\right)$.
- *Computation of* $\mathbf{D}$: It needs multiplication of $N_t \times M_t$ matrix $\mathbf{V}_t$ and $M_t \times M_t$ matrix $\mathbf{U}^H$, involving a complexity of $\mathcal{O}\left(N_t M_t^2\right)$.

All of these three operations are repeated during each iteration. In addition, multiplication with complexity of $\mathcal{O}\left({N_t}^2 K\right)$ is required to form $\mathbf{H}^H\mathbf{H}$. If N_{iter} is the number of iterations, total complexity of Narrowband TM-HMP is $\mathcal{O}\left({N_t}^2 K\right) + N_{iter}\mathcal{O}\left({N_t}^2 M_t + 2N_t M_t^2\right)$. The complexity in computing digital part of the precoder is $\mathcal{O}\left(KN_tM_t + 2M_t^2K + +{M_t}^2N_t + {M_t}^3\right)$.

(ii) *Wideband TM-HMP*: Compared to the Narrowband TM-HMP, the additional complexity in computing analog precoder for Wideband TM-HMP comes from the computation of $\sum_{m=1}^{S_c}\mathbf{H}\left[m\right]^H\mathbf{H}\left[m\right]$ which is $S_c\mathcal{O}\left({N_t}^2K\right)$. Thus, the total computational complexity in determining analog precoder of Wideband TM-HMP is $S_c\mathcal{O}\left({N_t}^2K\right) + N_{iter}\mathcal{O}\left({N_t}^2M_t + 2N_tM_t^2\right)$. The computational complexity of computing digital part of the precoder is $S_c\mathcal{O}(KN_tM_t + 2M_t^2K + +{M_t}^2N_t + {M_t}^3)$.

Table 5.1: COMPARISON OF COMPUTATIONAL COMPLEXITIES IN COMPUTING ANALOG PRECODER FOR DIFFERENT ALGORITHMS

Narrowband	
Algorithm	**Complexity**
HD-LSR [36]	$N_{iter}\mathcal{O}\left(N_tK^3 + N_tK^2\right)$
GEVD-HMP [43]	$N_{iter}\mathcal{O}\left(2{N_t}^2K + 5N_tK^2 + 3K^3 + N_q{N_t}^2\right)$
MO-HMP [44]	$N_{iter}\mathcal{O}\left(4{N_t}^2K + 13N_tK^2 + 3N_tK + 8K^3\right)$
TM-HMP	$\mathcal{O}\left({N_t}^2K\right) + N_{iter}\mathcal{O}\left({N_t}^2K + 2N_tK^2\right)$
Wideband	
MO-HMP [44]	$S_cN_{iter}\mathcal{O}\left(4{N_t}^2K + 13N_tK^2 + 3N_tK + 8K^3\right)$
TM-HMP	$S_c\mathcal{O}\left({N_t}^2K\right) + N_{iter}\mathcal{O}\left({N_t}^2K + 2N_tK^2\right)$

The complexities of computing analog part of GEVD-HMP and MO-HMP, sourced from [44] and the complexity of HD-LSR are listed in the Table 5.1 to compare against the computational complexity of the proposed TM-HMP for the case $M_t = K$. The typical value of N_q, appearing in the complexity of GEVD-HMP is around 10 [44]. The HD-LSR needs fully digital precoder to compute its hybrid precoder but the complexity in the Table 5.1 does not include the complexity required to determine fully digital precoder. With typically high value of N_t in mmWave MIMO, it can be clearly seen that the MO-HMP and GEVD-HMP are very high in complexity,

whereas HD-LSR and the proposed TM-HMP are very low in complexity. This will further be attested by the simulation results in Section 5.6.

5.6 Simulation Results

To evaluate the performance of the proposed method, a system in which the BS is equipped with ULA is considered. The values of different parameters taken in the simulations have been listed in Table 5.2. The AoDs are Laplacian distributed with mean angles uniformly distributed over $[0, 2\pi]$ and having angular spread of 10 degrees. The antenna elements are separated by a distance of half wavelength. The signal-to-noise ratio (SNR) used in the plots is defined as $\text{SNR} = \frac{P}{\sigma_n^2}$. We consider $M_t = K = 4$ in all the figures except Figure 5.5 where M_t is varying. However, $M_t = K+1 = 5$ for HHP [37] in all figures other than Figure 5.5 as minimum number of RF chains required to operate HHP is $K + 1$.

Table 5.2: PARAMETERS FOR SIMULATIONS

Parameters	**Narrowband**	**Wideband**
N_t	64	64
K	4	4
N_c	5	5
N_p	10	10
$\alpha_{i\ell}$	$\sim \mathcal{CN}(0, 1)$	$\sim \mathcal{CN}(0, 1)$
S_c	-	128

5.6.1 Narrowband Channel

The MSE of the proposed hybrid precoding method is plotted as a function of number of iterations in Figure 5.2 , averaged over 3000 channel realizations. It shows that the MSE decreases at each iteration, and is lower bounded. This proves the convergence of the proposed method.

In Figure 5.3 and Figure 5.4, the spectral efficiency and the BER performances of the proposed hybrid precoder in narrowband channel is compared with the performances of fully digital MMSE precoder, GEVD-HMP [43], MO-HMP [44], HD-LSR [36], HHP [37] and OMP-HMP [34].

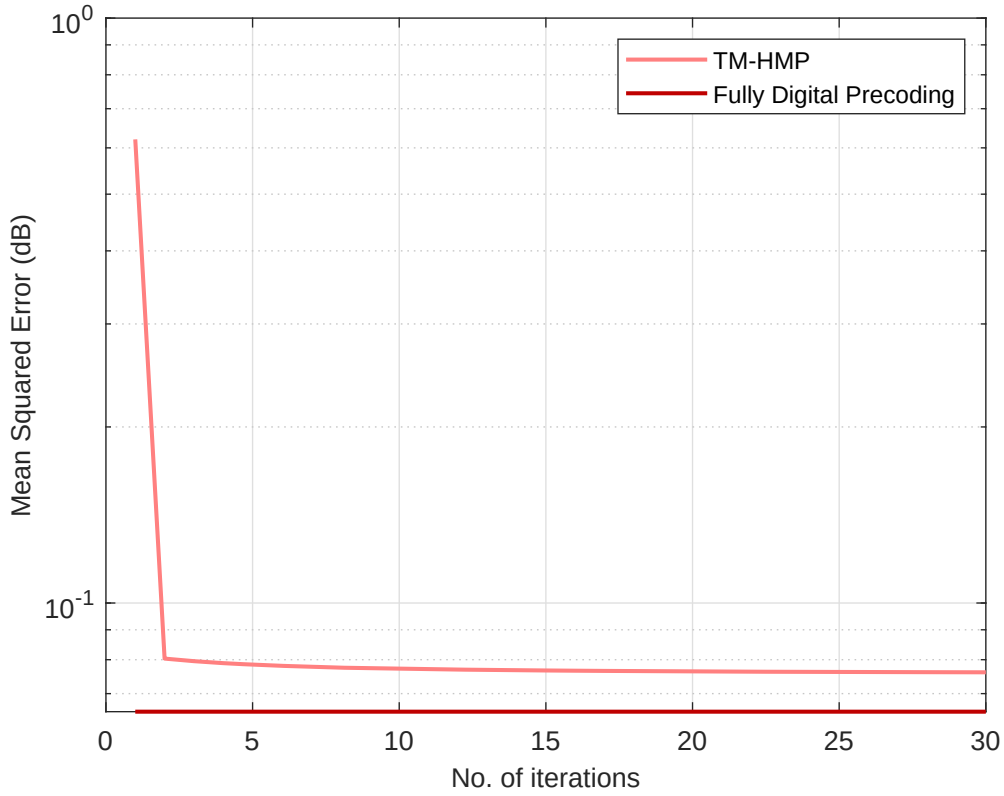

Figure 5.2: Convergence behavior of the proposed TM-HMP algorithm in narrowband channel for $SNR = 0$ dB, $M_t = K = 4$.

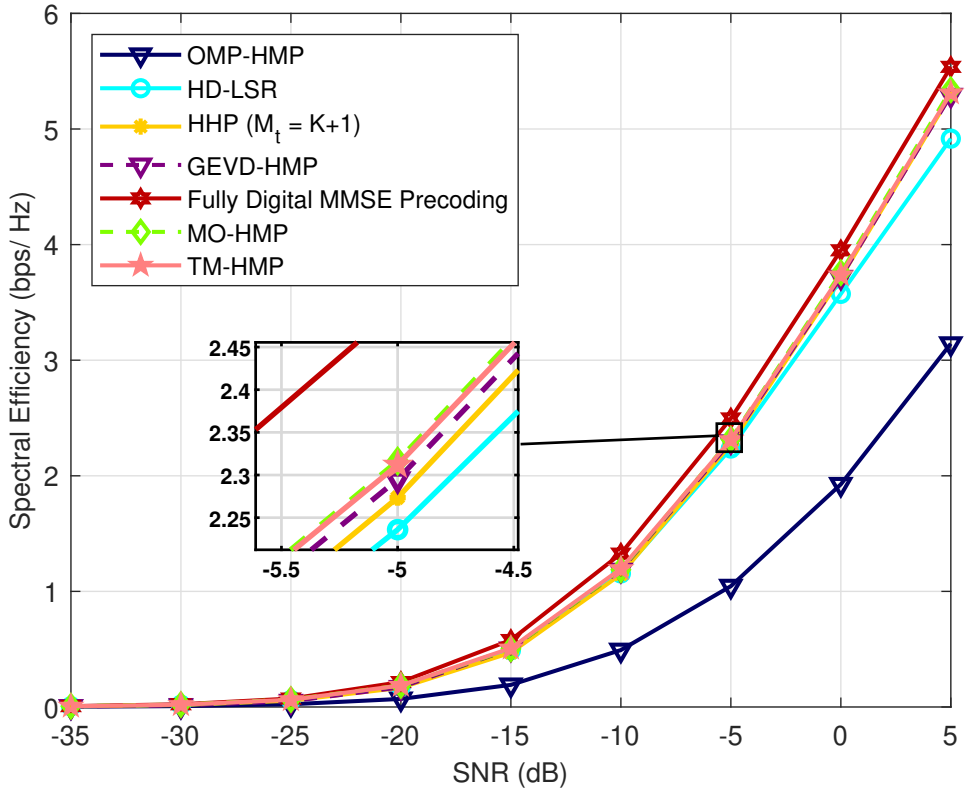

Figure 5.3: Spectral efficiency versus SNR in narrowband channel with $M_t = K = 4$.

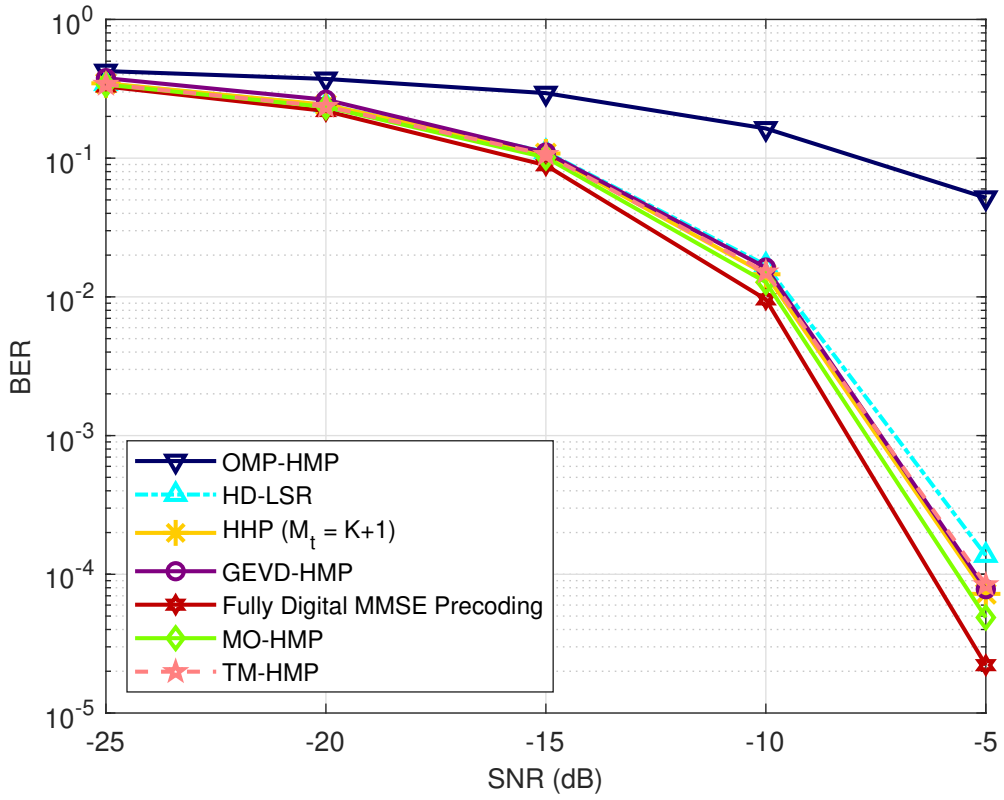

Figure 5.4: BER versus SNR in narrowband channel with $M_t = K = 4$.

It can be seen that the spectral performance of the proposed TM-HMP is almost the same as that of MO-HMP and better than all other compared precoders. The BER performance of TM-HMP is better than OMP-HMP and HD-LSR, and indistinguishable from those of GEVD-HMP and HHP. The TM-HMP lags behind MO-HMP by a small margin in BER performance.

In Figure 5.5, the spectral performance is compared as the number of RF chains is increased. The performance of TM-HMP is slightly lower than that of MO-HMP but better than others. As M_t is increased, the performances of MO-HMP, HD-LSR and TM-HMP improve before achieving the performance of the fully digital precoder at $M_t = 2K$. However, the performances of OMP-HMP, GEVD-HMP and HHP do not improve much even as M_t increases.

To have a numerical perspective on the computational complexities, the average run times of different hybrid precoders are plotted against N_t and K in Figure 5.6 and Figure 5.7 respectively. The computational times were calculated by executing the algorithms in MATLAB on a personal computer with Intel Core i5 1.6 GHz processor

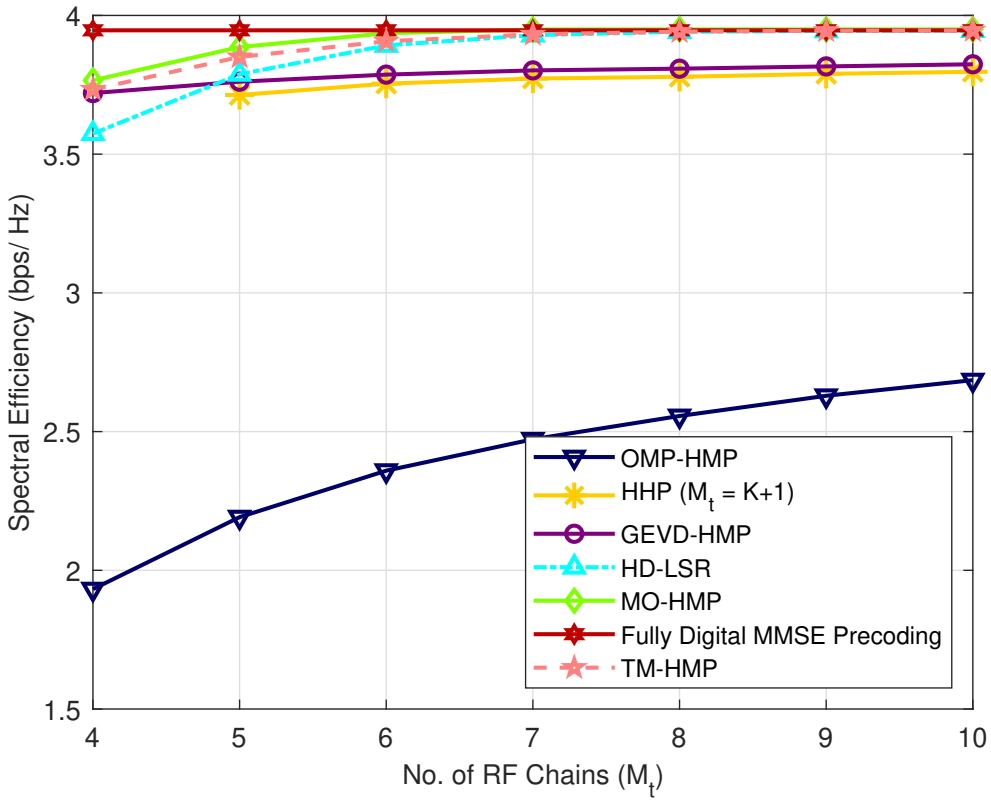

Figure 5.5: Spectral efficiency versus number of RF chains (M_t) in narrowband channel with $K = 4$.

and 8 GB RAM. In both figures, the curves corresponding to the HHP have been plotted in the insets to produce legible figures. The HHP has the largest run time among all the hybrid precoders, whereas the proposed TM-HMP has the lowest run time. Even when the N_t or K are increased, the average run time increases by small amount for the TM-HMP when the run times increase steeply for other hybrid precoders. The proposed TM-HMP clearly outshines all the hybrid precoders under comparison, as far as the average run time is concerned. The lesser average run time across the large range of values of N_t and K firmly establishes the lower computational complexity of TM-HMP.

The Figure 5.8 exhibits the effect of quantization of phase angles of the phase shifters on the spectral efficiency and the BER performance. It can be seen that the spectral and the BER performances of non-quantized continuous phase angles can almost be achieved with the phase shifters of quantization bits 4 which is practicable.

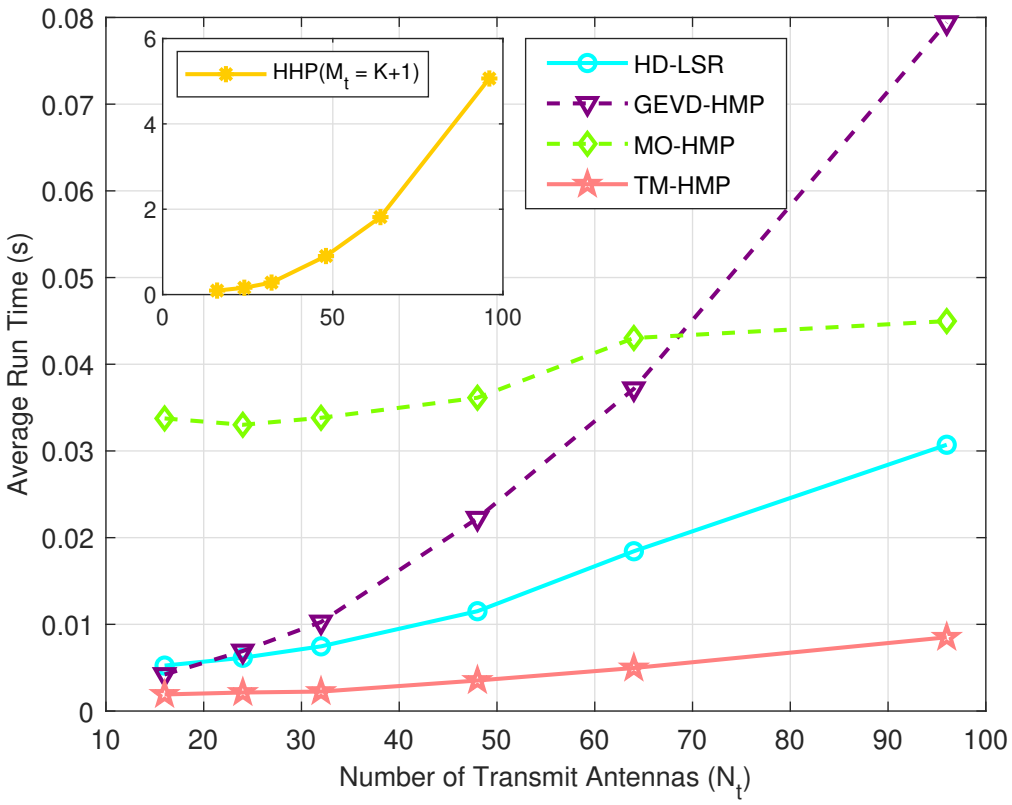

Figure 5.6: Average run time versus number of transmit antennas (N_t) in narrowband channel with $M_t = K = 4$.

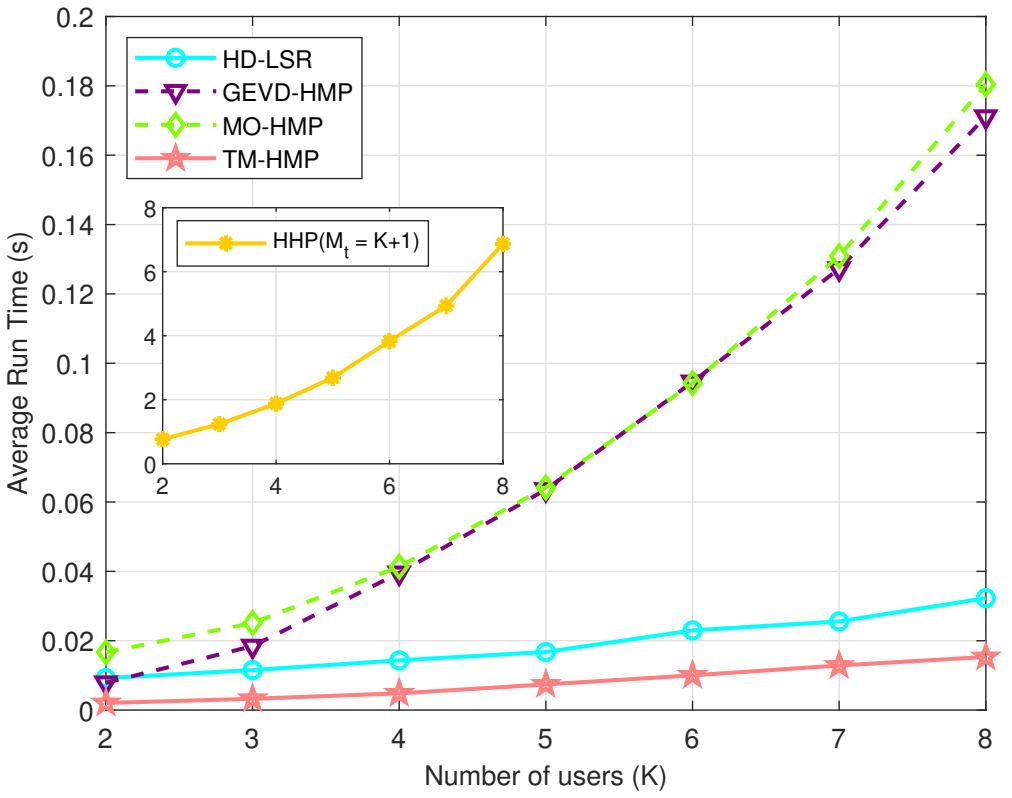

Figure 5.7: Average run time versus number of users (K) in narrowband channel with $M_t = K$.

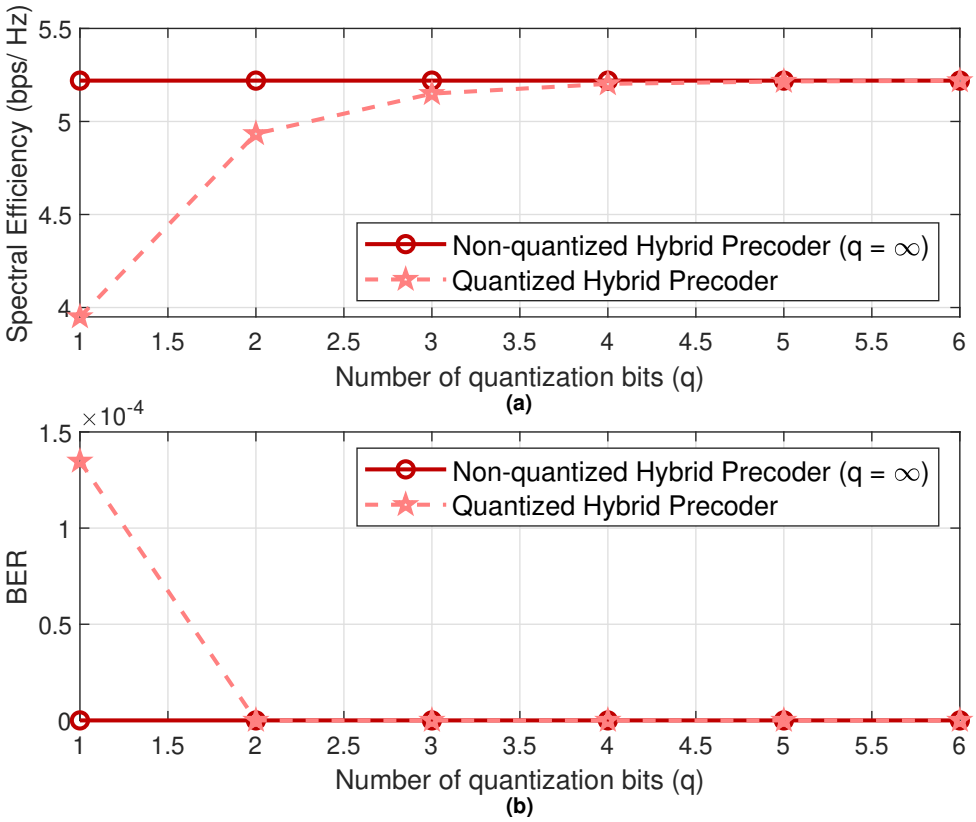

Figure 5.8: The effect of quantization bits of phase shifters on a)Spectral efficiency b)BER in narrowband channel.

5.6.2 Wideband Channel

The spectral performance, the BER performance, and the average run times of TM-HMP are compared with the fully digital precoder and MO-HMP for wideband channel. The Figure 5.9 shows that the wideband spectral performance of the proposed TM-HMP is quite close to the fully digital precoder even with $M_t = K$. The performance of TM-HMP is better than MO-HMP at lower SNR values, whereas the performances become similar at higher SNR values. In Figure 5.10, it can be seen that the BER performance of the proposed precoder is slightly better than the performance of MO-HMP at lower SNR, while the performance remains similar or marginally behind at the higher SNR. This establishes that the proposed hybrid precoding method performs finely even in the wideband scenario.

The average run times taken by different precoders are plotted versus N_t and K in Figure 5.11 and Figure 5.12 respectively, and TM-HMP is compared against the fully digital precoder and MO-HMP. MO-HMP has higher average run-time which

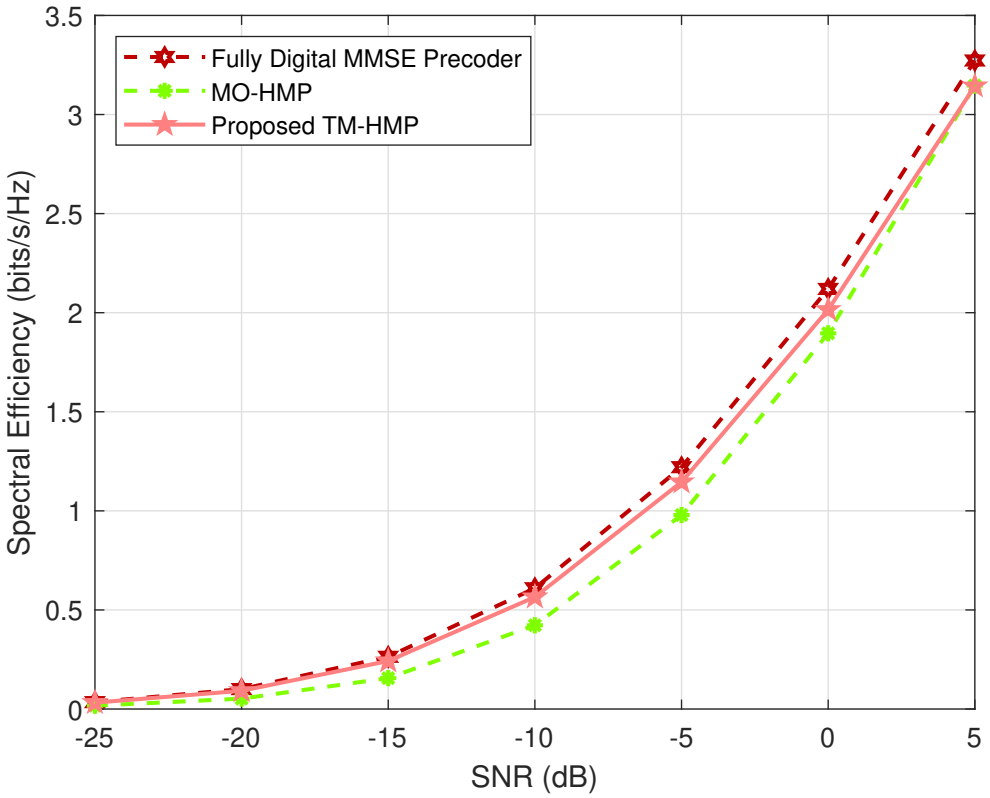

Figure 5.9: Spectral efficiency versus SNR in wideband channel with $M_t = K = 4$.

rises steeply with the increasing N_t and K. The average run-time of fully digital precoder is hugely worsened by increasing N_t, and less so by increasing K. On the other hand, TM-HMP exhibits very small average run time over the wide extent of values of N_t and K, and is less affected by increasing N_t or K. The interesting part is that the TM-HMP outperforms even the fully digital precoder. The analog precoder of the wideband TM-HMP has additional complexity only in computing $\sum_{m=1}^{S_c} \mathbf{H}[m]^H \mathbf{H}[m]$, as compared to the narrowband TM-HMP. The computation of digital precoder for each of the S_c subcarriers involves computation of inverse of $M_t \times M_t$ matrix. On the other hand, the fully digital MMSE precoder warrants the calculation of the digital precoder for each subcarrier which necessitates evaluation of inverse of $N_t \times N_t$ matrix. When the number of subcarriers S_c and N_t are high, it is possible that the computational complexity of the fully digital precoder exceeds the complexity incurred by the proposed method. This validates that the wideband TM-HMP has a very low computational complexity, like its narrowband counterpart.

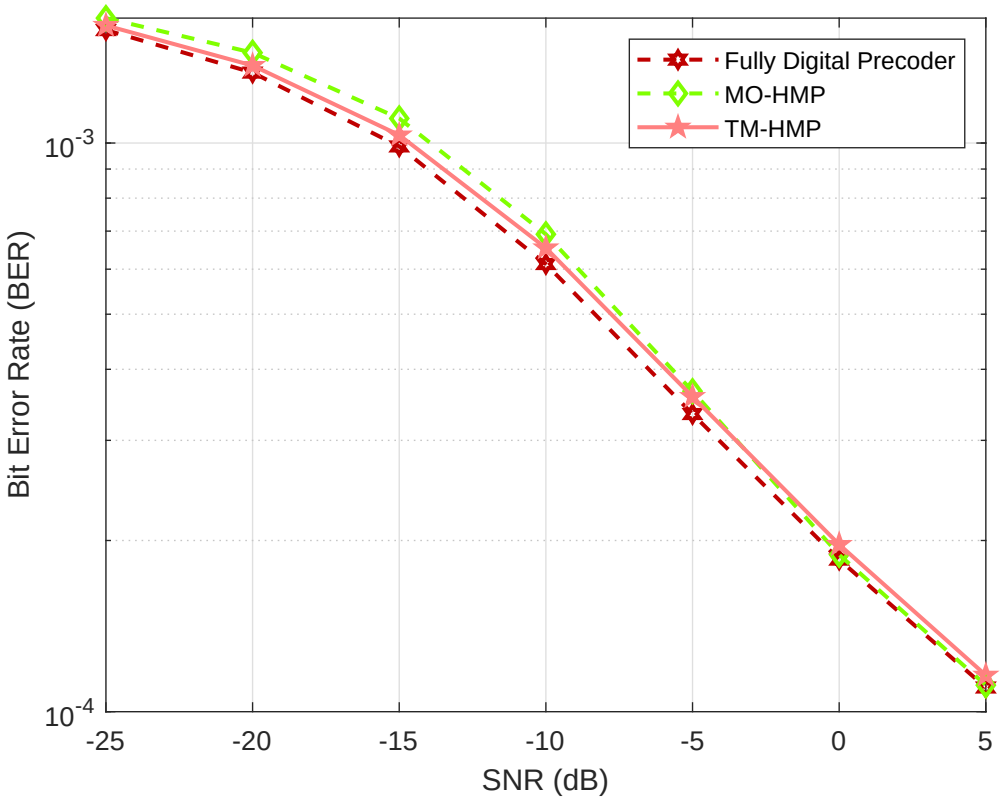

Figure 5.10: BER versus SNR in wideband channel with $M_t = K = 4$.

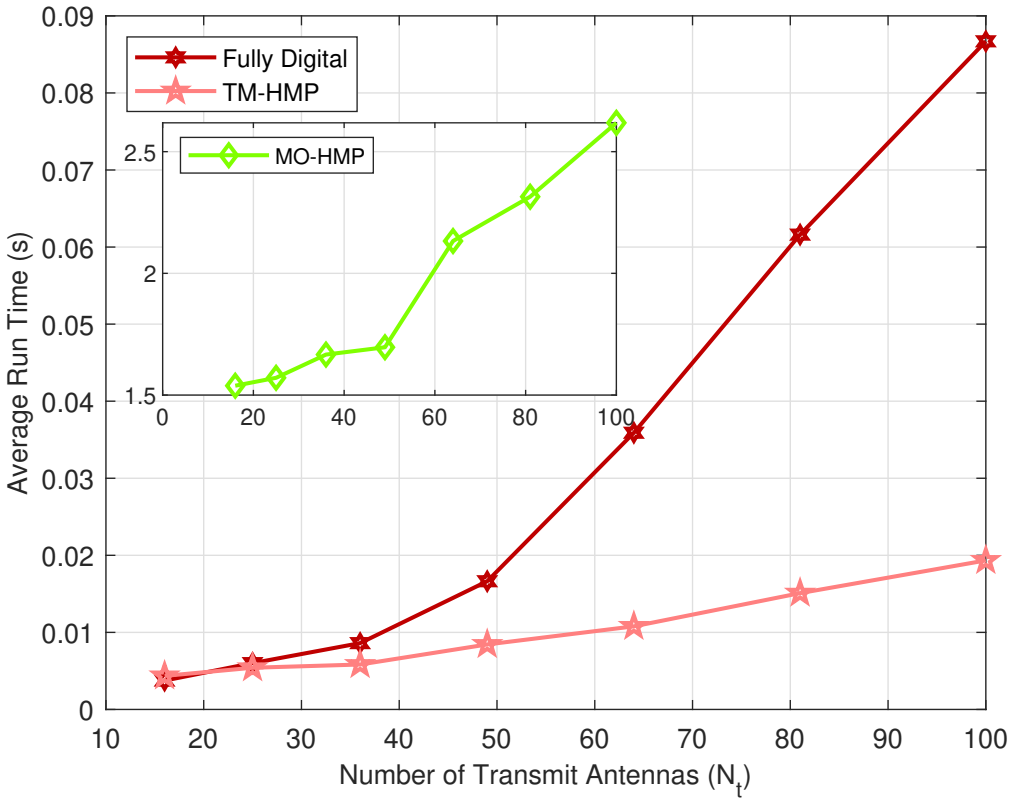

Figure 5.11: Average run time versus number of transmit antennas (N_t) in wideband channel with $M_t = K = 4$.

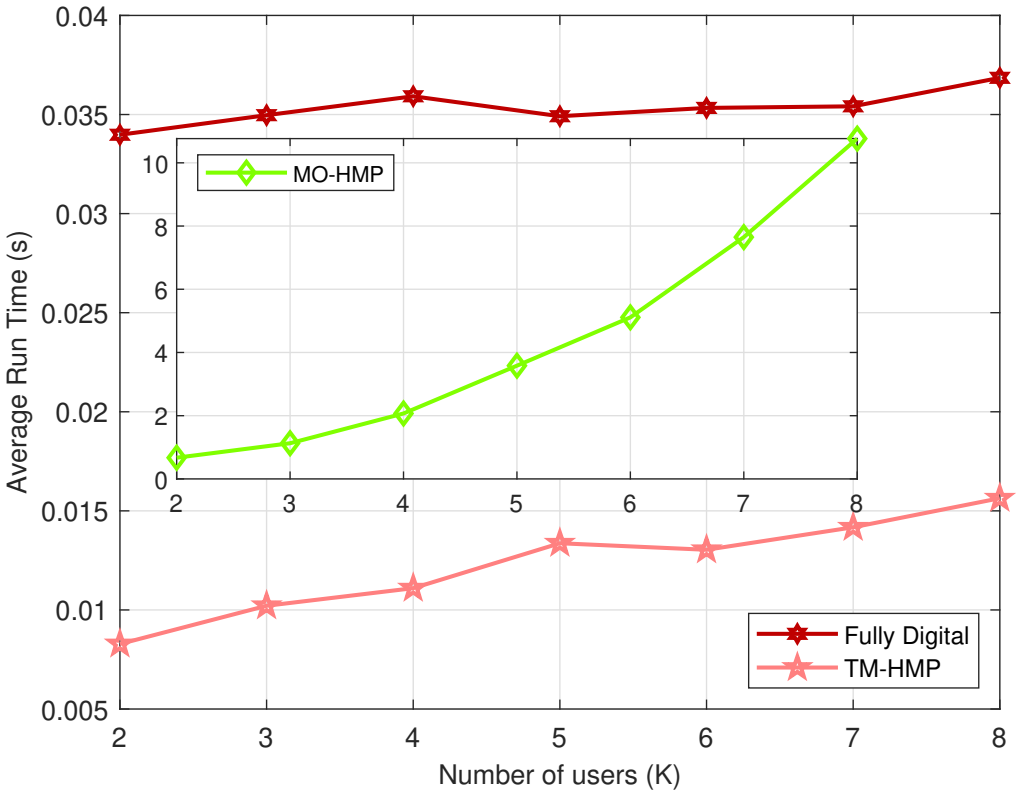

Figure 5.12: Average run time versus number of users (K) in wideband channel with $M_t = K$.

5.7 Summary

Considering narrowband channel model, a computationally-efficient hybrid precoding method based on minimizing the mean squared error for all users in downlink mmWave MU-MISO systems has been proposed. The problem of minimizing MSE is broken down into two separate stages to simplify the optimization problem. The analog precoder is evaluated by an iterative truncated SVD-based trace maximization procedure, and then the digital part of the precoder is computed for the fixed analog precoder. The proposed hybrid MMSE precoder produces the spectral and BER performances which are close to fully digital precoder and almost the same as the existing high performance hybrid precoders, but at much lower computational complexity. Further, it can be seen that the performance remains unaffected even while using quantized phase shifters with reasonable quantization bits. It is also shown that the proposed method can be extended to work in wideband channel. The simulation results manifest that the proposed method replicates its towering

narrowband channel performance in wideband channel by performing quite close to its fully digital counterpart. In short, the proposed hybrid precoder comes with very low complexity but with virtually no compromise in performance.

Chapter 6

MMSE-based Passive Precoding for RIS Aided mmWave MIMO

In this chapter, point-to-point mmWave MIMO is considered in which the link between the BS and the user is blocked by an obstacle. To establish a link between the BS and the user, an RIS is deployed. The RIS elements only provide phase alterations to the incoming signal, so the RIS phase shift coefficients are constrained to have unit amplitudes. An iterative procedure is developed in which phase shift coefficients of the RIS are jointly designed with the precoder and the combiner. The contributions made in this chapter can be summarized as

(i) Considering the narrowband channel, RIS phase shift matrix is designed with the aim to minimize the MSE between the transmit signal and the estimate of the received signal. The problem reduces to a quadratic problem in RIS phase shift vector which is equal to the diagonal of RIS phase shift matrix. The problem is in terms of precoding and combining matrices, which depend on RIS phase shift matrix. Thus, the problem can be solved to jointly determine RIS phase shift matrix, precoder and combiner. An iterative procedure is developed in which the solutions for each is computed in every iteration. In particular, the passive precoding subproblem is solved by extracting phases of the unconstrained solution. An equivalent optimization subproblem in RIS pas-

sive precoding vector is defined to determine the low complexity unconstrained solution. The hybrid precoder is determined from the fully digital precoder after the RIS phase shift matrix is computed.

(ii) The complexity analysis of the proposed algorithm is performed and compared against existing algorithms. Simulation results are generated to compare with existing solutions. Comparison with the existing solutions shows that the proposed method gives high-grade performance but entails lower complexity.

(iii) The algorithm developed for narrowband channel is extended for wideband channel with the application of MIMO-OFDM. The simulation results reveal that the proposed method offers very good performance in the wideband channel as well.

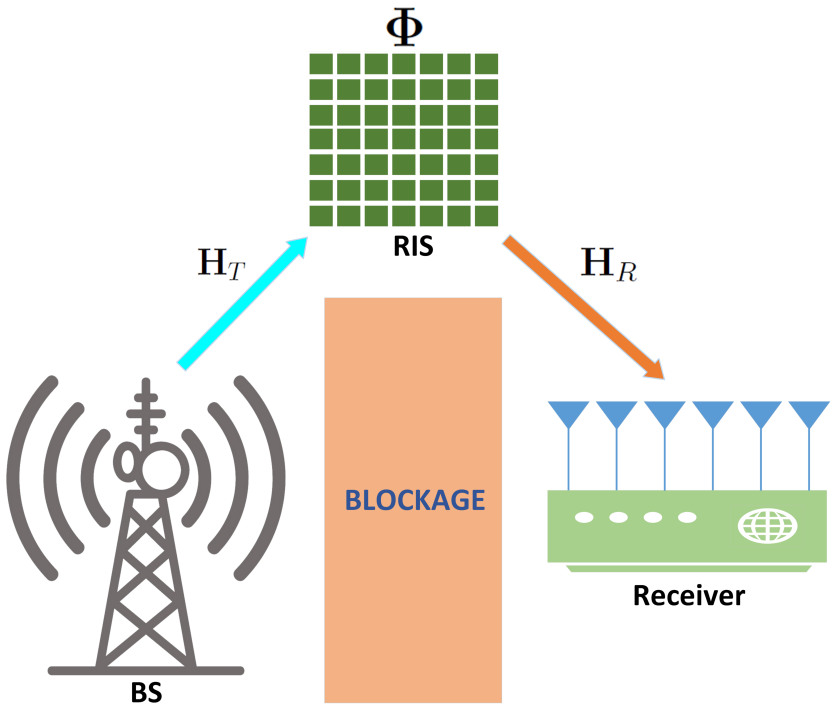

Figure 6.1: RIS-aided point-to-point mmWave MIMO

6.1 System Model

A downlink point-to-point mmWave MIMO having N_t antennas at the base station (BS) and N_r antennas at the receiver is considered, with the communication between the BS and the MS enhanced by an RIS with N_I elements. The precoding is

accomplished at the base station by a hybrid precoder $\mathbf{F}$ consisting of digital precoder $\mathbf{F}_{\mathrm{D}}, \mathbf{F}_{\mathrm{D}} \in \mathbb{C}^{M_t \times N_s}$ followed by analog precoder $\mathbf{F}_{\mathrm{R}}, \mathbf{F}_{\mathrm{R}} \in \mathbb{C}^{N_t \times M_t}$. At the receiver, combining is performed by a hybrid combiner $\mathbf{W} = \mathbf{W}_{\mathrm{R}}\mathbf{W}_{\mathrm{D}}$, where $\mathbf{W}_{\mathrm{R}} \in \mathbb{C}^{N_r \times M_r}$ and $\mathbf{W}_{\mathrm{D}} \in \mathbb{C}^{M_r \times N_s}$. $N_t \geq N_r \geq M_t \geq M_r \geq N_s$, where M_t and M_r are the number of RF chains at the BS and the receiver respectively. The channel between the BS and the RIS is $\mathbf{H}_{\mathrm{T}} \in \mathbb{C}^{N_I \times N_t}$, and the channel between RIS and the receiver is $\mathbf{H}_{\mathrm{R}} \in \mathbb{C}^{N_r \times N_I}$. It is assumed that no direct channel exists between the BS and the receiver. The signal impinging on the RIS is reflected after introducing phase shift $\boldsymbol{\phi}_i$ by i^{th} element of the RIS. The RIS phase shift matrix $\boldsymbol{\Phi} = \mathbf{DIAG}(\boldsymbol{\phi}_1, \boldsymbol{\phi}_2, \ldots, \boldsymbol{\phi}_{N_I})$. The equivalent channel between the BS and the receiver is given by

$$\mathbf{H} = \mathbf{H}_{\mathrm{R}}\boldsymbol{\Phi}\mathbf{H}_{\mathrm{T}}. \tag{6.1}$$

The received signal is acted upon by the combiner $\mathbf{W}$ to yield the estimate of the signal,

$$\mathbf{y} = \mathbf{W}^H\mathbf{H}\mathbf{F}\mathbf{s} + \mathbf{n}, \tag{6.2}$$

where $\mathbf{n} \in \mathbb{C}^{N_r \times 1}$ is noise vector such that $\mathbf{n} \sim \mathcal{CN}(\mathbf{0}, \sigma_n^2\mathbf{I})$. The channel between the BS and RIS, and the channel from the RIS to receiver are assumed narrowband and modeled by multi-path channel model.

6.2 Problem Statement

The phase shift matrix for the RIS $\boldsymbol{\Phi}$ and the precoder are determined in two different stages. $\boldsymbol{\Phi}$ is determined first, and then the hybrid precoder is computed once the $\boldsymbol{\Phi}$ is fixed. For the sake of simplicity, fully digital precoder $\mathbf{F}_{\mathrm{FD}}$ and fully digital combiner $\mathbf{W}_{\mathrm{FD}}$ are considered at both the transmitter and receiver to determine the phase shift matrix for the RIS.

6.2.1 Passive Precoding Problem

In this section, the problem for the determination of RIS phase-shift matrix, also known as passive precoding matrix, is defined. The RIS phase-shift matrix $\mathbf{\Phi}$ is determined by minimizing the MSE between the transmit signal $\mathbf{s}$ and the estimate of the transmit signal $\mathbf{y}$ at the receiver which is given by

$$\mathbb{E}\left[|\mathbf{s}-\mathbf{y}|^2\right]. \tag{6.3}$$

After substituting the expression for $\mathbf{y}$, the MSE can be written as

$$\begin{aligned}\text{MSE} = \mathbf{Tr}\big[&\mathbf{I}-\mathbf{W}_{\text{FD}}^H\mathbf{H}\mathbf{F}_{\text{FD}}-\mathbf{F}_{\text{FD}}^H\mathbf{H}^H\mathbf{W}_{\text{FD}}+\mathbf{W}_{\text{FD}}^H\mathbf{H}\mathbf{F}_{\text{FD}}\mathbf{F}_{\text{FD}}^H\mathbf{H}^H\mathbf{W}_{\text{FD}}+\\ &\sigma_n^2\mathbf{W}_{\text{FD}}^H\mathbf{W}_{\text{FD}}\big].\end{aligned} \tag{6.4}$$

The passive precoder that tries to minimize weighted mean square error (WMMSE) is proposed in [53] which converts the WMMSE problem in terms of passive precoding vector. Inspired by [53], we also express the MMSE problem in terms of passive precoding vector. Substituting $\mathbf{H}=\mathbf{H}_{\text{R}}\mathbf{\Phi}\mathbf{H}_{\text{T}}$ in the expression for MSE, and simplifying,

$$\begin{aligned}\text{MSE} &= \mathbf{Tr}\big[\mathbf{I}-\mathbf{W}_{\text{FD}}^H\mathbf{H}_{\text{R}}\mathbf{\Phi}\mathbf{H}_{\text{T}}\mathbf{F}_{\text{FD}}-\mathbf{F}_{\text{FD}}^H\mathbf{H}_{\text{T}}^H\mathbf{\Phi}^H\mathbf{H}_{\text{R}}^H\mathbf{W}_{\text{FD}}+\mathbf{W}_{\text{FD}}^H\mathbf{H}_{\text{R}}\mathbf{\Phi}\mathbf{H}_{\text{T}}\mathbf{F}_{\text{FD}}\\ &\qquad \mathbf{F}_{\text{FD}}^H\mathbf{H}_{\text{T}}^H\mathbf{\Phi}^H\mathbf{H}_{\text{R}}^H\mathbf{W}_{\text{FD}}+\sigma_n^2\mathbf{W}_{\text{FD}}^H\mathbf{W}_{\text{FD}}\big]\\ &= \mathbf{Tr}\big[\mathbf{\Phi}\left(\mathbf{H}_{\text{T}}\mathbf{F}_{\text{FD}}\mathbf{F}_{\text{FD}}^H\mathbf{H}_{\text{T}}^H\right)\mathbf{\Phi}^H\left(\mathbf{H}_{\text{R}}^H\mathbf{W}_{\text{FD}}\mathbf{W}_{\text{FD}}^H\mathbf{H}_{\text{R}}\right)-\mathbf{\Phi}\left(\mathbf{H}_{\text{T}}\mathbf{F}_{\text{FD}}\mathbf{W}_{\text{FD}}^H\mathbf{H}_{\text{R}}\right)\\ &\qquad -\left(\mathbf{H}_{\text{R}}^H\mathbf{W}_{\text{FD}}\mathbf{F}_{\text{FD}}^H\mathbf{H}_{\text{T}}^H\right)\mathbf{\Phi}^H\big]+\mathbf{Tr}\left[\mathbf{I}+\sigma_n^2\mathbf{W}_{\text{FD}}^H\mathbf{W}_{\text{FD}}\right]\\ &\overset{(a)}{=} \boldsymbol{\phi}\left(\mathbf{C}_1\odot\mathbf{C}_2^T\right)\boldsymbol{\phi}^H-\boldsymbol{\phi}\mathbf{t}-\mathbf{t}^H\boldsymbol{\phi}^H+\mathbf{Tr}\left[\mathbf{I}+\sigma_n^2\mathbf{W}_{\text{FD}}^H\mathbf{W}_{\text{FD}}\right]\\ &= \boldsymbol{\phi}\mathbf{C}\boldsymbol{\phi}^H-\boldsymbol{\phi}\mathbf{t}-\mathbf{t}^H\boldsymbol{\phi}^H+\mathbf{Tr}\left[\mathbf{I}\right]+\sigma_n^2\mathbf{Tr}\left[\mathbf{W}_{\text{FD}}^H\mathbf{W}_{\text{FD}}\right],\end{aligned}$$

where

$$\mathbf{C}_1 \triangleq \mathbf{H}_{\text{T}}\mathbf{F}_{\text{FD}}\mathbf{F}_{\text{FD}}^H\mathbf{H}_{\text{T}}^H, \tag{6.5a}$$

$$\mathbf{C}_2 \triangleq \mathbf{H}_{\text{R}}^H\mathbf{W}_{\text{FD}}\mathbf{W}_{\text{FD}}^H\mathbf{H}_{\text{R}}, \tag{6.5b}$$

$$\mathbf{t} \triangleq \mathbf{diag}\left(\mathbf{H}_{\text{T}}\mathbf{F}_{\text{FD}}\mathbf{W}_{\text{FD}}^H\mathbf{H}_{\text{R}}\right), \tag{6.5c}$$

$$\mathbf{C} \triangleq \mathbf{C}_1 \odot \mathbf{C}_2^T, \tag{6.5d}$$

$$\boldsymbol{\phi} \triangleq \mathbf{diag}\left(\boldsymbol{\Phi}\right), \boldsymbol{\phi} \in \mathbb{C}^{1\times N_I}, \tag{6.5e}$$

and the reason behind (a) is matrix identities $\mathbf{Tr}\left[\boldsymbol{\Phi}\mathbf{C}_1\boldsymbol{\Phi}^H\mathbf{C}_2\right] = \boldsymbol{\phi}\left(\mathbf{C}_1 \odot \mathbf{C}_2^T\right)\boldsymbol{\phi}^H$ and $\mathbf{Tr}\left[\boldsymbol{\Phi}\mathbf{T}\right] = \boldsymbol{\phi}\mathbf{diag}\left(\mathbf{T}\right)$ for the diagonal matrix $\boldsymbol{\Phi}$ [99]. Instead of $\boldsymbol{\Phi}$ itself, the expression for MSE is now in terms of row vector $\boldsymbol{\phi}$ that corresponds to the diagonal of the diagonal matrix $\boldsymbol{\Phi}$. The problem of determining optimal $\boldsymbol{\phi}$ and hence $\boldsymbol{\Phi}$, can be stated as

$$\boldsymbol{\phi}^\star = \arg\min_{\boldsymbol{\phi}} \quad \boldsymbol{\phi}\mathbf{C}\boldsymbol{\phi}^H - \boldsymbol{\phi}\mathbf{t} - \mathbf{t}^H\boldsymbol{\phi}^H + \left(N_s + \sigma_n^2 w\right) \tag{6.6a}$$

$$\text{s.t.} \quad |\boldsymbol{\phi}_i| = 1, \quad \forall i, \tag{6.6b}$$

where $w = \mathbf{Tr}\left[\mathbf{W}_{\text{FD}}^H\mathbf{W}_{\text{FD}}\right]$. The solution to the problem (6.6) is difficult because the constraint (6.6b) is non-convex, and there is no known optimal solution to the problem (6.6).

6.2.2 Hybrid Precoding Problem

A careful look at the optimization problem (6.6) shows that $\boldsymbol{\Phi}$ or $\boldsymbol{\phi}$ depend on $\mathbf{F}_{\text{FD}}$ and $\mathbf{W}_{\text{FD}}$. If there is a knowledge about channel matrix $\mathbf{H}$, the fully digital precoder for point-to-point MIMO can be calculated as

$$\mathbf{F}_{\text{FD}} = \mathbf{V}_{:,1:N_s}\boldsymbol{\Gamma}_{\text{FD}}, \quad \text{and} \tag{6.7a}$$

$$\boldsymbol{\Gamma}_{\text{FD}} = \mathbf{diag}(\sqrt{p_1}, \sqrt{p_2}, \ldots, \sqrt{p_{N_s}}), \tag{6.7b}$$

where $\mathbf{\Gamma}_{\text{FD}}$ is the power loading matrix, $\mathbf{H} = \mathbf{U}\mathbf{\Sigma}\mathbf{V}^H$ is the SVD of channel matrix $\mathbf{H}$, and $p_i, \forall i = 1, 2, \ldots, N_s$ is the power along the i^{th} data stream. The optimal $\mathbf{\Gamma}_{\text{FD}}$ is computed by the water-filling solution, whereas $\mathbf{\Gamma}_{\text{FD}} = \frac{P}{N_s}\mathbf{I}_{N_s}$ in case of equal power distribution, P being the maximum total transmit power. On the other hand, the fully digital combiner at the receiver is given by the MMSE combiner,

$$\mathbf{W}_{\text{FD}} = \left(\mathbf{H}\mathbf{F}_{\text{FD}}\mathbf{F}_{\text{FD}}^H\mathbf{H}^H + \sigma_n^2\mathbf{I}_{N_r}\right)^{-1}\mathbf{H}\mathbf{F}_{\text{FD}}. \tag{6.8}$$

The hybrid precoder is computed by minimizing the Euclidean distance from its fully digital counterpart $\mathbf{F}_{\text{FD}}$. $\mathbf{F}_{\text{R}}$ and $\mathbf{F}_{\text{D}}$ are determined in two separate stages. First, $\mathbf{F}_{\text{R}}$ is determined by solving the analog precoding subproblem (2.13). If $\mathbf{F}_{\text{R}}$ is known, $\mathbf{F}_{\text{D}}$ is computed using (2.5a). $\mathbf{F}_{\text{D}}$ can also be computed as the matrix containing right singular vectors corresponding to the leading N_s eigenvalues of the matrix $\mathbf{H}\mathbf{F}_{\text{R}}$.

6.3 Proposed Solution

$\mathbf{\Phi}$ can be determined by solving the problem (6.6). The objective function (6.6a) is dependent on the values of $\mathbf{F}_{\text{FD}}$ and $\mathbf{W}_{\text{FD}}$ which are given by (6.7a) and (6.8), and can be computed if $\mathbf{H}$ is known. Hence, $\mathbf{F}_{\text{FD}}$ and $\mathbf{W}_{\text{FD}}$ are themselves dependent on $\mathbf{\Phi}$ as the value of $\mathbf{H}$ is determined by $\mathbf{\Phi}$.

6.3.1 Passive precoding subproblem with known $\mathbf{F}_{\text{FD}}$ and $\mathbf{W}_{\text{FD}}$

There is no known optimal solution to the problem (6.6) to the best of author's knowledge. The problem (6.6) can be modeled as a Boolean quadratic programming problem. Boolean quadratic program is computationally difficult as it belongs to the class of NP-hard problems [100]. It is, however, possible to translate such problems into an SDP [100] after semidefinite relaxation [101]. But the solution is still computationally demanding.

$\boldsymbol{\phi}$ is determined by normalizing each element of the vector $\boldsymbol{\phi}_{uc}$, the optimal solution to the problem (6.6) without taking constraint (6.6b) into account, to have unit amplitude. Each element of $\boldsymbol{\phi}_{nc}$ are not constrained to satisfy unit modulus constraint. The unconstrained solution can be obtained by taking derivative of the objective function (6.6a) and equating it to zero. But it is in terms of $\mathbf{C}^{-1}$, and for $\mathbf{C}^{-1}$ to exist, $\mathbf{C}$ should be full-rank which can not be guaranteed.

To get around this problem, another optimization problem is considered,

$$\boldsymbol{\phi}^{\star} = \arg\min_{\boldsymbol{\phi}} \quad \boldsymbol{\phi}\left(\mathbf{C}+\mu\mathbf{I}\right)\boldsymbol{\phi}^{H} - \boldsymbol{\phi}\mathbf{t} - \mathbf{t}^{H}\boldsymbol{\phi}^{H} \tag{6.9a}$$

$$\text{s.t.} \quad |\boldsymbol{\phi}_{i}| = 1, \quad \forall i, \tag{6.9b}$$

where $\mu \in \mathbb{R}_{+}$. The unconstrained optimal solution to the problem (6.9) is obtained by taking derivative of the objective function (6.9a) with respect to $\boldsymbol{\phi}$ and equating it to 0 as

$$\boldsymbol{\phi}_{uc} = \mathbf{t}^{H}\left(\mathbf{C}+\mu\mathbf{I}\right)^{-1}, \tag{6.10}$$

where $\mathbf{C}+\mu\mathbf{I}$ is always a full-rank matrix. The objective function (6.9a) can be expanded as

$$\begin{aligned}
& \boldsymbol{\phi}\left(\mathbf{C}+\mu\mathbf{I}\right)\boldsymbol{\phi}^{H} - \boldsymbol{\phi}\mathbf{t} - \mathbf{t}^{H}\boldsymbol{\phi}^{H} \\
= \;& \boldsymbol{\phi}\mathbf{C}\boldsymbol{\phi}^{H} + \mu\boldsymbol{\phi}\boldsymbol{\phi}^{H} - \boldsymbol{\phi}\mathbf{t} - \mathbf{t}^{H}\boldsymbol{\phi}^{H} \\
= \;& \boldsymbol{\phi}\mathbf{C}\boldsymbol{\phi}^{H} + \mu\sum_{i=1}^{N_I}|\boldsymbol{\phi}_{i}|^{2} - \boldsymbol{\phi}\mathbf{t} - \mathbf{t}^{H}\boldsymbol{\phi}^{H} \\
= \;& \boldsymbol{\phi}\mathbf{C}\boldsymbol{\phi}^{H} + \mu N_I - \boldsymbol{\phi}\mathbf{t} - \mathbf{t}^{H}\boldsymbol{\phi}^{H}
\end{aligned}$$

The objective functions (6.6a) and (6.9a) are equivalent when

$$\mu = \tfrac{1}{N_I}\left(N_s + \sigma_n^2 w\right) \tag{6.11}$$

Thus, $\boldsymbol{\phi}$ is determined by normalizing each element of $\boldsymbol{\phi}_{uc}$ to have unit amplitude as

$$\boldsymbol{\phi} = \exp\left(j\angle\left(\mathbf{t}^{H}\left(\mathbf{C}+\mu\mathbf{I}\right)^{-1}\right)\right), \tag{6.12}$$

where μ is given by (6.11).

6.3.2 Passive precoding solution based on iterative method

Once $\boldsymbol{\phi}$ is calculated, $\mathbf{H}$ is known and both $\mathbf{F}_{\text{FD}}$ and $\mathbf{W}_{\text{FD}}$ can be computed. An iterative procedure is developed where $\boldsymbol{\phi}$ is initialized with a random value, so there is an initial value of $\mathbf{H}$. At each iteration, the SVD of $\mathbf{H}$ is performed, and the leading N_s right singular vectors serve as the solution for $\mathbf{F}_{\text{FD}}$, as in (6.7a). $\mathbf{W}_{\text{FD}}$ is computed using (6.8) as $\mathbf{H}$ and $\mathbf{F}_{\text{FD}}$ are known. Finally, $\boldsymbol{\phi}$ is determined using (6.12). This procedure is repeated until convergence is reached. The summary of the algorithm to determine $\boldsymbol{\phi}$ is presented in Algorithm 6.1.

Algorithm 6.1 MMSE-Based Passive Precoding Design Method

Require: $\mathbf{H}_{\text{T}}, \mathbf{H}_{\text{R}}, N_s, N_I, P$.

1: Choose initial value of $\boldsymbol{\phi}^{(0)}$ randomly such that $\left|\phi_i^{(0)}\right| = 1$ so that $\boldsymbol{\Phi}^{(0)} = \mathbf{diag}\left(\boldsymbol{\phi}^{(0)}\right)$ and $\mathbf{H}^{(0)} = \mathbf{H}_{\text{R}}\boldsymbol{\Phi}^{(0)}\mathbf{H}_{\text{T}}$.
2: Set $\epsilon = 10^{-4}$, a very small value, and set $k \leftarrow 1$.
3: **repeat**
4: Compute $\mathbf{F}_{\text{FD}}^{(k)}$, using (6.7a).
5: Compute $\mathbf{W}_{\text{FD}}^{(k)}$ using (6.8).
6: Compute $\boldsymbol{\phi}^{(k)}$ using (6.12). Set $\boldsymbol{\Phi}^{(k)} = \mathbf{DIAG}\left(\boldsymbol{\phi}^{(k)}\right)$.
7: Set $\mathbf{H}^{(k)} = \mathbf{H}_{\text{R}}\boldsymbol{\Phi}^{(k)}\mathbf{H}_{\text{T}}$.
8: Compute $\text{MSE}^{(k)}$ using (6.4).
9: Compute $\delta^{(k)} = \left|\text{MSE}^{(k)} - \text{MSE}^{(k-1)}\right|$.
10: Set $k \leftarrow k + 1$.
11: **until** $\delta^{(k)} < \epsilon$
12: $\boldsymbol{\Phi} = \boldsymbol{\Phi}^{(k)}$, $\mathbf{H} = \mathbf{H}^k$.
13: Compute $\mathbf{F}_{\text{FD}}^{(k)}$ using (6.7a) and compute $\mathbf{W}_{\text{FD}}$ using (6.8).
14: **return** $\boldsymbol{\Phi}, \mathbf{H}, \mathbf{F}_{\text{FD}}, \mathbf{W}_{\text{FD}}$.

6.3.3 Hybrid Precoding Solution

The analog precoder is determined using the Trace Maximization algorithm surmised in Algorithm 5.1 with $\mathbf{I} + \tau\mathbf{H}^H\mathbf{H}$ replaced by $\mathbf{F}_{\text{FD}}\mathbf{F}_{\text{FD}}^H$.

6.4 Extension to wideband channel

6.4.1 Passive Precoding for Wideband Channel

The proposed solution for passive precoding can also be applied in wideband scenario by considering transmission over frequency selective channels using MIMO-OFDM . If S_c is the number of subcarriers, the effective channel for the m^{th} subcarrier from transmitter to the receiver is given by

$$\mathbf{H}[m] = \mathbf{H}_{\text{R}}[m]\mathbf{\Phi}\mathbf{H}_{\text{T}}[m], \qquad m = 0, \ldots, S_c - 1, \tag{6.13}$$

where $\mathbf{H}_{\text{R}}[m]$ and $\mathbf{H}_{\text{T}}[m]$ are the frequency domain channel matrices for the RIS-receiver channel and transmitter-RIS channel respectively at m^{th} subcarrier. Following the developments made for narrowband channel, the MSE for wideband MIMO-OFDM can be written as the sum of MSEs for each subcarrier,

$$\begin{aligned}\text{MSE} = \sum_{m=0}^{S_c-1} \mathbf{Tr}\big[&\mathbf{I} - \mathbf{W}_{\text{FD}}[m]^H\mathbf{H}_{\text{R}}[m]\mathbf{\Phi}\mathbf{H}_{\text{T}}[m]\mathbf{F}_{\text{FD}}[m] - \mathbf{F}_{\text{FD}}[m]^H\mathbf{H}_{\text{T}}[m]^H\mathbf{\Phi}^H \\ &\mathbf{H}_{\text{R}}[m]^H\mathbf{W}_{\text{FD}}[m] + \mathbf{W}_{\text{FD}}[m]^H\mathbf{H}_{\text{R}}[m]\mathbf{\Phi}\mathbf{H}_{\text{T}}[m]\mathbf{F}_{\text{FD}}[m]\mathbf{F}_{\text{FD}}[m]^H \\ &\mathbf{H}_{\text{T}}[m]^H\mathbf{\Phi}^H\mathbf{H}_{\text{R}}[m]^H\mathbf{W}_{\text{FD}}[m] + \sigma_n^2\mathbf{W}_{\text{FD}}[m]^H\mathbf{W}_{\text{FD}}[m]\big].\end{aligned} \tag{6.14}$$

Similar to the case in narrowband channel, it can be simplified as

$$\boldsymbol{\phi} = \sum_{m=0}^{S_c-1} \boldsymbol{\phi}\mathbf{C}[m]\boldsymbol{\phi}^H - \boldsymbol{\phi}\mathbf{t}[m] - \mathbf{t}^H[m]\boldsymbol{\phi}^H + \left(N_s + \sigma_n^2 w[m]\right), \tag{6.15}$$

where

$$\mathbf{t}[m] \triangleq \mathbf{diag}\left(\mathbf{H}_{\text{T}}[m]\mathbf{F}_{\text{FD}}[m]\mathbf{W}_{\text{FD}}^H[m]\mathbf{H}_{\text{R}}[m]\right), \tag{6.16a}$$

$$\mathbf{C}[m] \triangleq \left(\mathbf{H}_{\text{T}}[m]\mathbf{F}_{\text{FD}}[m]\mathbf{F}_{\text{FD}}^H[m]\mathbf{H}_{\text{T}}^H[m]\right) \odot \left(\mathbf{H}_{\text{R}}^H[m]\mathbf{W}_{\text{FD}}[m]\mathbf{W}_{\text{FD}}^H[m]\mathbf{H}_{\text{R}}[m]\right)^T, \tag{6.16b}$$

$$w[m] \triangleq \mathbf{Tr}\left[\mathbf{W}_{\text{FD}}[m]^H\mathbf{W}_{\text{FD}}[m]\right] \tag{6.16c}$$

Thus, passive precoding problem for wideband channel can be written as

$$\boldsymbol{\phi}^{\star} = \arg\min_{\boldsymbol{\phi}} \quad \boldsymbol{\phi} \sum_{m=0}^{S_c-1} \mathbf{C}[m]\boldsymbol{\phi}^H - \boldsymbol{\phi} \sum_{m=0}^{S_c-1} \mathbf{t}[m] - \sum_{m=0}^{S_c-1} \mathbf{t}[m]^H \boldsymbol{\phi}^H + \left(S_c N_s + \sigma_n^2 \sum_{m=0}^{S_c-1} w[m] \right) \tag{6.17a}$$

$$\text{s.t.} \quad |\boldsymbol{\phi}_i| = 1, \quad \forall i, \tag{6.17b}$$

The problem is similar to the problem in narrowband channel and can be solved by similar iterative method. Using the results from narrowband case, $\mathbf{W}_{\text{FD}}[m]$ and $\mathbf{F}_{\text{FD}}[m]$ are calculated during each iteration as

$$\mathbf{W}_{\text{FD}}[m] = \left(\mathbf{H}[m]\mathbf{F}_{\text{FD}}[m]\mathbf{F}_{\text{FD}}[m]^H \mathbf{H}[m]^H + \sigma_n^2 \mathbf{I}_{N_s} \right)^{-1} \mathbf{H}[m]\mathbf{F}_{\text{FD}}[m], \quad \text{and} \tag{6.18a}$$

$$\mathbf{F}_{\text{FD}}[m] = \mathbf{V}[m]_{:,1:N_s} \boldsymbol{\Gamma}[m], \quad \forall m = 0, 1, \ldots, S_c - 1, \tag{6.18b}$$

where $\mathbf{V}[m]_{:,1:N_s}$ is the matrix containing the leading N_s singular values of $\mathbf{H}[m]$, and $\boldsymbol{\Gamma}[m]$ is the power loading matrix for the m^{th} subcarrier channel. $\boldsymbol{\phi}$ is calculated as

$$\boldsymbol{\phi} = \exp\left(j \angle \left(\mathbf{t}^H \left(\mathbf{C} + \mu \mathbf{I} \right)^{-1} \right) \right), \quad \text{where} \tag{6.19a}$$

$$\mu = \tfrac{1}{N_I} \left(S_c N_s + \sigma_n^2 \sum_{m=0}^{S_c-1} w[m] \right). \tag{6.19b}$$

6.4.2 Hybrid Precoding for Wideband Channel

The analog precoding subproblem for the wideband channel can be written in terms of $\bar{\mathbf{F}}_{\text{R}}$ as (2.21). Similar to narrowband case, $\mathbf{F}_{\text{R}}$ can be calculated as $\mathbf{F}_{\text{R}} = \sqrt{N_t}\bar{\mathbf{F}}_{\text{R}}$ by using the Algorithm 5.1, where $\sum_{m=0}^{S_c-1} \mathbf{F}_{\text{FD}}[m]\mathbf{F}_{\text{FD}}[m]^H$ replaces $\mathbf{I} + \tau \sum_{m=0}^{S_c-1} \mathbf{H}[m]^H \mathbf{H}[m]$.

Table 6.1: COMPARISON OF COMPUTATIONAL COMPLEXITIES OF DIFFERENT PASSIVE PRECODING ALGORITHMS

Narrowband	
Algorithm	**Complexity**
Proposed MMSE-PP	$N_{iter}^{PP}\mathcal{O}\left({N_r}^3+{N_I}^3+N_r{N_I}^2+N_rN_IN_t+{N_t}^2N_r+{N_r}^2N_t\right)$
T-SVD-PP [50]	$\mathcal{O}\left(N_t^2M_tN_s\right)$
AO-PP [66]	$N_{it}^oN_{it}^i\mathcal{O}\left(4N_t^2M_t+13N_tM_t^2+3N_tM_t+8M_t^3\right)$
SPGM-PP [62]	$\mathcal{O}\left(N_{it}\left(M_t^7\left(N_t^7+N_s^7\right)+M_t^3\left(N_t^3+N_s^3\right)\right)\right)$
WMMSE-PP [53]	$N_{it}^o\mathcal{O}\left(N_{it}^i\left(N_t+M_t-1\right)^2+N_t^2M_t+2N_tM_tN_s+M_t^2N_s\right)$
Wideband	
Algorithm	**Complexity**
Proposed MMSE-PP	$N_{iter}^{PP}\mathcal{O}\left(S_c{N_r}^3+S_cN_r{N_I}^2+S_cN_rN_IN_t+S_c{N_t}^2N_r+S_c{N_r}^2N_t+{N_I}^3\right)$
SPGM-PP	$\mathcal{O}\left(N_{it}N_t^2M_t+N_tM_t^2+S_cN_t^2N_s\right)$

6.5 Complexity Analysis of the proposed method

In this section, the computational complexity of the proposed method is evaluated. The complexity of the proposed method is calculated for narrowband channel, followed by the wideband channel.

6.5.1 Complexity Analysis of the proposed method in narrowband channel

The complexity of computing the IRS phase-shift matrix and the hybrid precoder are computed separately.

(i) *Computation of RIS phase-shift matrix* $\mathbf{\Phi}$:

- *Computation of* $\mathbf{F}_{\text{FD}}$: The evaluation of SVD of the $N_r \times N_t$ channel matrix governs the complexity, entailing a complexity of $\mathcal{O}({N_t}^2N_r+{N_r}^2N_t)$.
- *Computation of* $\mathbf{W}_{\text{FD}}$: The major complexity in computation comes from inverse operation of a $N_r \times N_r$ matrix which is $\mathcal{O}\left({N_r}^3\right)$.
- *Computation of* $\boldsymbol{\phi}$: The inverse of a $N_I \times N_I$ matrix that involves a complexity of $\mathcal{O}\left({N_I}^3\right)$ contributes mainly to the complexity.
- *Computation of channel matrix* $\mathbf{H}$: The computation of $\mathbf{H}$ requires a

multiplication between $N_r \times N_I$ matrix $\mathbf{H}_{\text{R}}$, $N_I \times N_I$ matrix $\mathbf{\Phi}$ and $N_I \times N_t$ matrix $\mathbf{H}_{\text{T}}$ which has a complexity of $\mathcal{O}\left({N_r}{N_I}^2 + N_r N_I N_t\right)$.

Each of these operations are repeated N_{iter}^{PP} times so that the total complexity of computing $\mathbf{\Phi}$ is $N_{iter}^{PP}\mathcal{O}\left({N_r}^3 + {N_I}^3 + {N_r}{N_I}^2 + N_r N_I N_t + {N_t}^2 N_r + {N_r}^2 N_t\right)$.

(ii) *Computation of hybrid precoder*: $\mathbf{F}_{\text{FD}}$ needs to be computed from $\mathbf{H}$ which entails a complexity of $\mathcal{O}({N_t}^2 N_r + {N_r}^2 N_t)$. Computing $\mathbf{F}_{\text{FD}}\mathbf{F}_{\text{FD}}^H$ has a complexity of $\mathcal{O}({N_t}^2 N_s)$. Following the computational complexity evaluation made in Chapter 5, it can be deduced that the computation of analog part of the precoder from $\mathbf{F}_{\text{FD}}$ comes with a complexity of $\mathcal{O}({N_t}^2 N_r + {N_r}^2 N_t) + \mathcal{O}({N_t}^2 N_s) + N_{iter}^{HP}\mathcal{O}({N_t}^2 M_t + 2N_t M_t^2)$, and the digital precoder with that of $\mathcal{O}(K N_t M_t + 2M_t^2 N_s + {M_t}^2 N_t + {M_t}^3)$, where N_{iter}^{HP} is the number of iterations performed.

6.5.2 Complexity Analysis of the proposed method in wideband channel

The complexity can be easily computed from the complexity of the narrowband couterpart.

(i) *Computation of RIS phase-shift matrix* $\mathbf{\Phi}$: The computation of $\mathbf{W}_{\text{FD}}[m]$ and $\mathbf{F}_{\text{FD}}[m]$ should be performed for S_c subcarriers. The channel matrix $\mathbf{H}[m]$ needs to be generated for S_c subcarriers. Thus, the complexity of computing phase-shift matrix $\mathbf{\Phi}$ is $N_{iter}^{PP}\mathcal{O}(S_c{N_r}^3 + S_c N_r {N_I}^2 + S_c N_r N_I N_t + S_c {N_t}^2 N_r + S_c {N_r}^2 N_t + {N_I}^3)$.

(ii) *Computation of hybrid precoder*: The complexity in computing analog precoder is $S_c\mathcal{O}({N_t}^2 N_r + {N_r}^2 N_t) + S_c\mathcal{O}({N_t}^2 N_s) + N_{iter}^{HP}\,\mathcal{O}({N_t}^2 M_t + 2N_t M_t^2)$. The digital precoder requires complexity of $S_c\mathcal{O}(N_s N_t M_t + 2M_t^2 N_s + {M_t}^2 N_t + {M_t}^3)$.

N_{it}^o and N_{it}^i in the Table 6.1 represent the number of outer and inner iterations respectively.

6.6 Performance Analysis

A point-to-point mmWave MIMO is considered in which BS, RIS and UE are placed at $(x_{_B}, 0, z_{_B})$, $(0, y_{_R}, z_{_R})$ and $(x_{_{Rx}}, y_{_{Rx}}, z_{_{Rx}})$ respectively, where $x_{_B} = 2\ m$, $z_{_B} = 10\ m$, $y_{_R} = 148\ m$, $z_{_R} = 10\ m$, $x_{_{Rx}} = 5\ m$, $y_{_{Rx}} = 150\ m$, $z_{_{Rx}} = 1.8\ m$. It is assumed that BS and the UE are both equipped with ULA having $N_t = 64$ and $N_r = 16$ antennas respectively, whereas the RIS utilizes square UPA with $N_I = N_I^y \times N_I^z$ elements. The number of RF chains at the BS and the UE are taken equal to N_s. The values of N_s and N_I are taken as 4 and 100 unless they are varying parameters. All the antenna elements are separated by a distance of half wavelength. The noise power $\sigma_n^2 = 90$ dBm. The BS-RIS and RIS-UE narrowband channels are modeled by (1.4), whereas (1.6) is used to model wideband channels with $N_{p_i} = 1$ and $N_c = L$. The number of paths in the BS-RIS link and RIS-UE link is chosen to be $L = 7$ including the line of sight (LOS) path. The complex gain of the LOS path is $\alpha_1 \sim \mathcal{CN}(0, 10^{-\kappa})$ where κ indicates the path loss given by [102]

$$\kappa = a + 10b\ log_{10}(d) + \xi, \tag{6.20}$$

where d denotes the distance between the transmitter and the receiver, and $\xi \sim \mathcal{N}(0, \sigma_\xi^2)$. The values $a = 61.4, b = 2$, and $\sigma_\xi = 5.8$ dB are taken based on the results from real-world measurements [102]. The performance of the proposed method is compared with sum-path gain maximization based passive precoding (SPGM) [62], and the high-performance methods like alternating optimization based passive precoding (AO) [66] and truncated SVD based passive precoding (T-SVD) [50] in narrowband channel, and with the SPGM in wideband scenario.

6.6.1 Narrowband Channel

In Figure 6.2, the spectral efficiency as a function of transmit power is plotted. The figure shows the performances of the proposed method and T-SVD with both the fully digital precoder and the hybrid precoder. The figure clearly shows that the proposed method performs better than T-SVD by a good margin, and the performance gap

with SPGM is huge. The proposed method performs almost the same as AO. It can be seen that performance similar to the fully digital precoder can be achieved with the hybrid precoder. The BER performance as a function of the transmit power in Figure 6.3 clearly shows the superiority of the proposed method over all other methods. The superior BER performance can be attributed to the fact that the proposed method designs $\mathbf{\Phi}$ by minimizing the MSE between the transmit signal and the received signal.

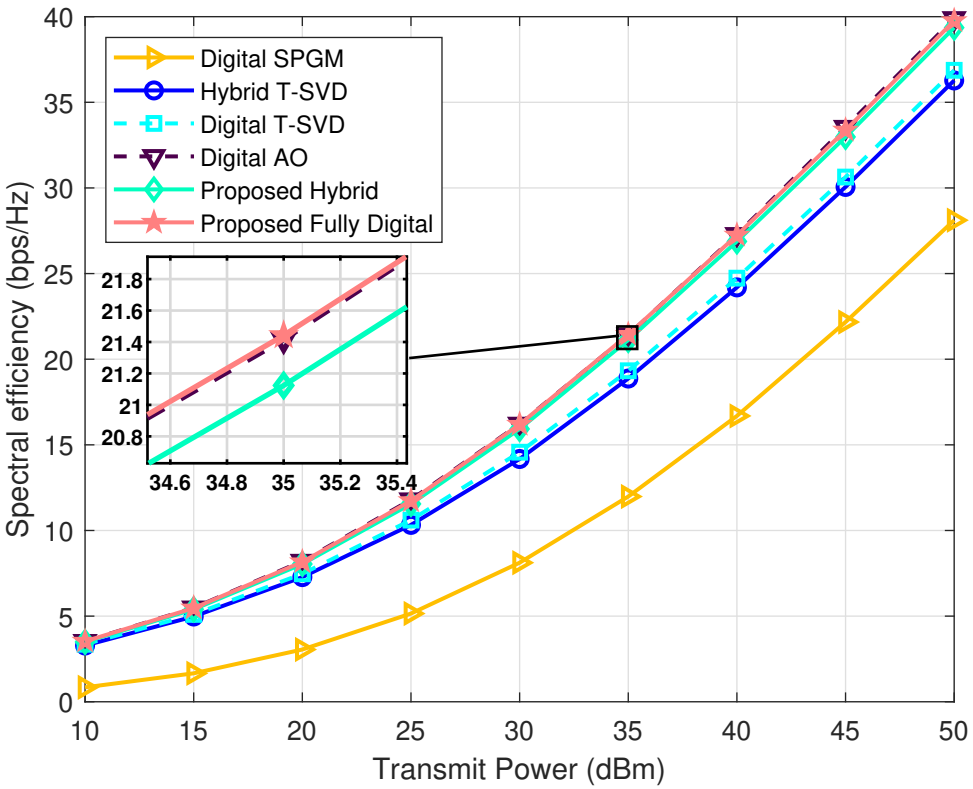

Figure 6.2: Spectral efficiency versus Transmit power, $N_I = 100$, $M_t = N_s = 4$.

When the spectral performance in Figure 6.4 is observed as N_I is varied, it can be seen that the spectral efficiency increases with N_I for all methods. The proposed method, along with AO-based method is clearly ahead of SPGM and T-SVD in spectral performance. This proves that the spectral performance in the proposed method is consistently very good for wide range of number of RIS elements. The spectral performances of the proposed method and AO-based method are almost the same. Another observation that can be made is that the difference in performances of the proposed method with the fully digital precoder and the hybrid precoder is not

significant. This proves that the hybrid precoder is able to emulate the performance of fully digital precoder successfully even with the minimum number of RF chains. It should be noted that the minimum number of RF chains required to multiplex N_s data streams is N_s.

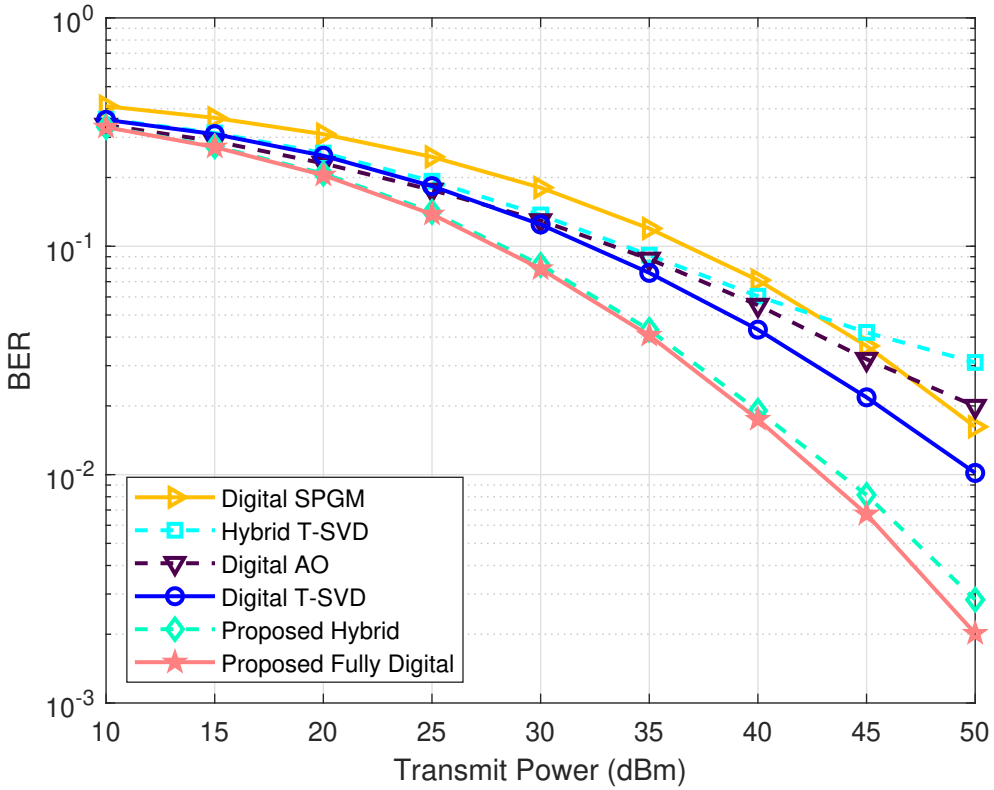

Figure 6.3: Bit error rate versus Transmit power, $N_I = 100$, $M_t = N_s = 4$.

The condition number of a channel is defined as

$$\zeta = \frac{\lambda_{max}}{\lambda_{min}}, \tag{6.21}$$

where λ_{max} and λ_{max} are the maximum and minimum singular values of the channel respectively. Since only N_s symbols are transmitted over $\mathbf{H}$, truncated condition number of the channel is considered. If $\lambda_1, \ldots, \lambda_{N_s}$ are the N_s largest singular values of the channel arranged in descending order, the truncated condition number of the channel is defined as [50]

$$\zeta_{tr} = \frac{\lambda_1}{\lambda_{N_s}}, \tag{6.22}$$

In Figure 6.5, the truncated condition number of the channel between the BS and

the UE is plotted. The truncated condition number in case of the AO-method is the largest at lower values of N_I but gets smaller with increasing N_I. It is still larger than those of SPGM and the proposed method even at higher N_I. The condition number of the channel with the proposed method has the lowest values, varying between 13 at $N_I = 36$ and 8 at $N_I = 256$. The condition number of the channel in case of the proposed method exhibits the least erratic plot across the wide range of N_I values. The channel with singular values that are spread less, or lower condition number have large capacity at high SNR, in general. The condition number closer to 1 is desirable as it makes the channel well-conditioned [17]. Thus, the Figure 6.5 attests that the proposed method produces more well-conditioned channel in comparison to other methods.

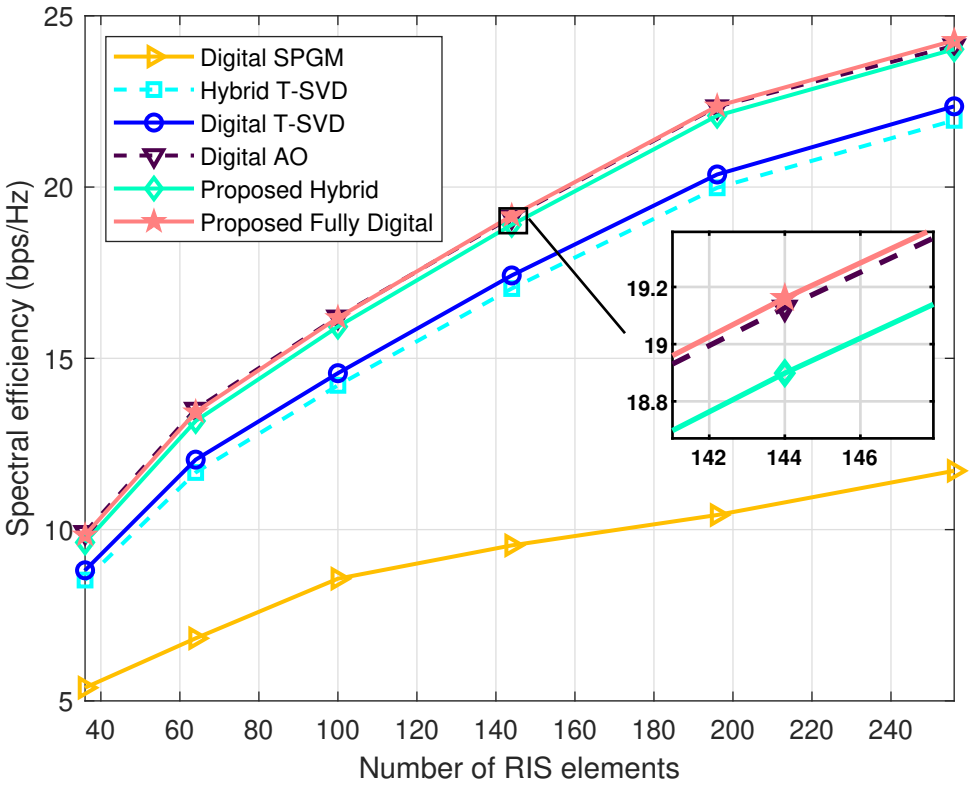

Figure 6.4: Spectral efficiency versus Transmit power, $P_t = 30$ dBm, $M_t = N_s = 4$.

To numerically compare the computational complexities of the various methods, the average runtimes of various methods are plotted as a function of N_I in Figure 6.6. All the algorithms are executed on MATLAB on a personal computer with Intel Core i5 1.6 GHz processor and 8 GB RAM. It can be observed that the average

runtime for the AO-method is the highest and those for the SPGM and the proposed method are the lowest. The average runtime for SPGM are smaller compared to the proposed method at lower values of N_I but as N_I increases the runtime for the proposed method gets lower than SPGM. Thus, it can be said that the proposed method is computationally-efficient, whereas the AO-method is computationally grueling.

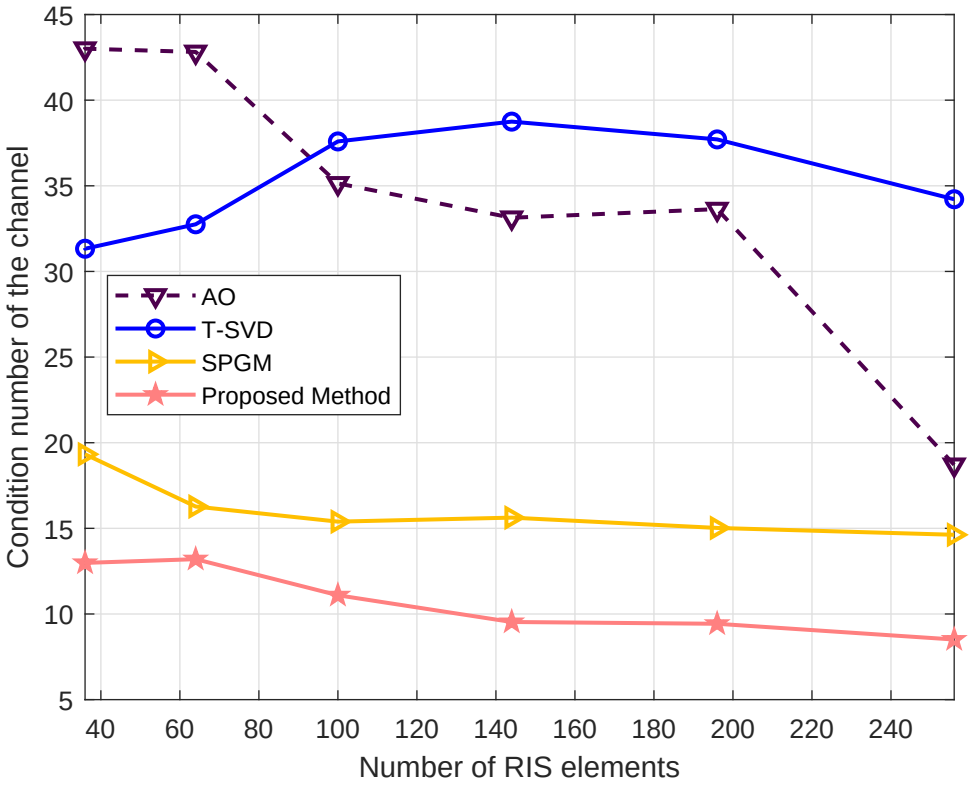

Figure 6.5: Condition number of the channel versus Number of RIS elements, $P_t = 50$ dBm, $N_s = 4$.

6.6.2 Wideband Channel

The spectral efficiency is plotted as a function of transmit power and number of RIS elements respectively in Figure 6.7 and Figure 6.9, whereas BER performance as a function of transmit power is plotted in Figure 6.8.

The proposed method emulates its superior narrowband performance in wideband scenario as well. The spectral and BER performances in Figure 6.7 and Figure 6.8 respectively depict that the proposed method is clearly performing very well and clearly ahead of the SPGM based method, whether it is fully digital precoder or

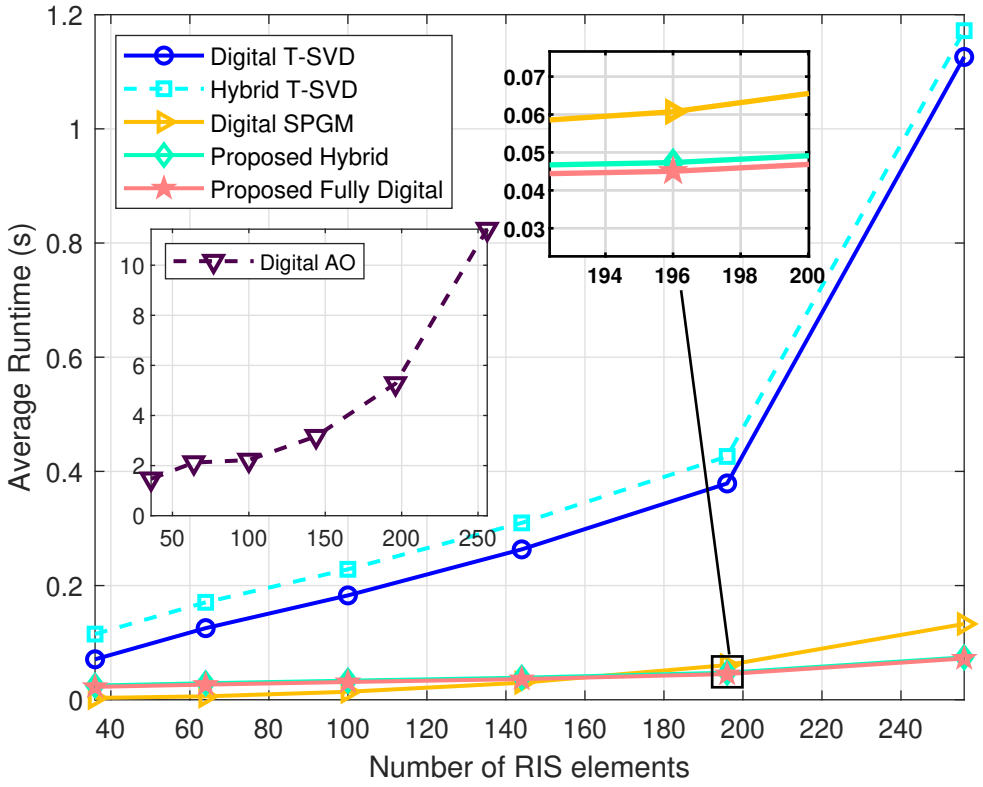

Figure 6.6: Average run time versus Number of RIS elements, $M_t = N_s = 4$.

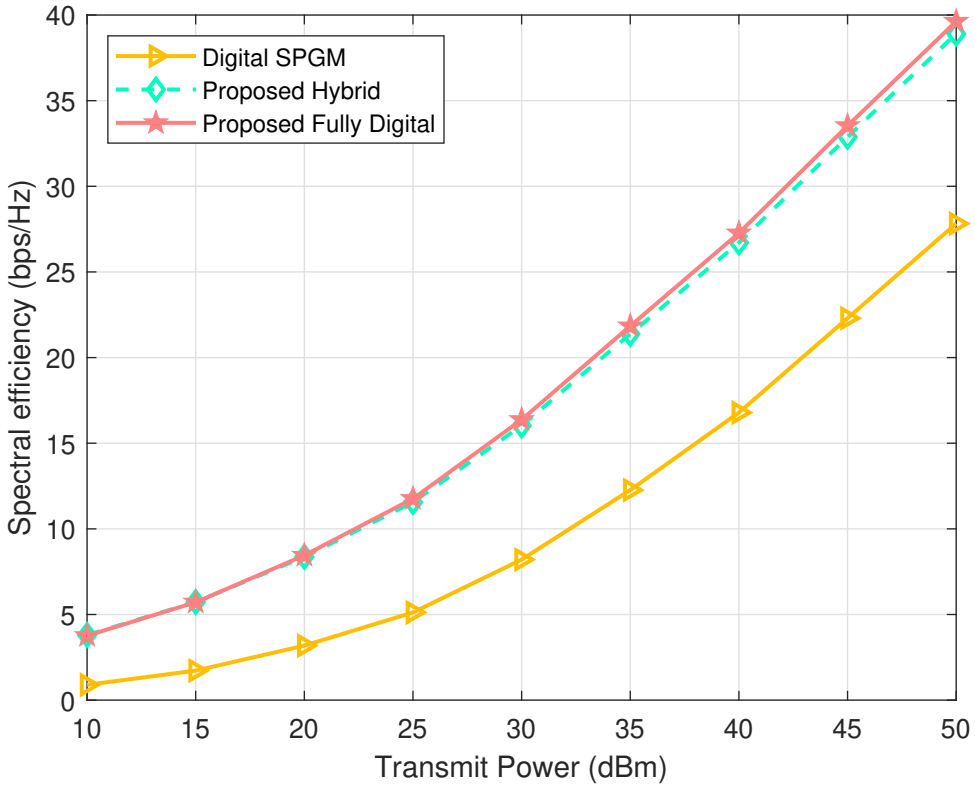

Figure 6.7: Spectral efficiency versus Transmit power, $N_I = 100$, $M_t = N_s = 4$.

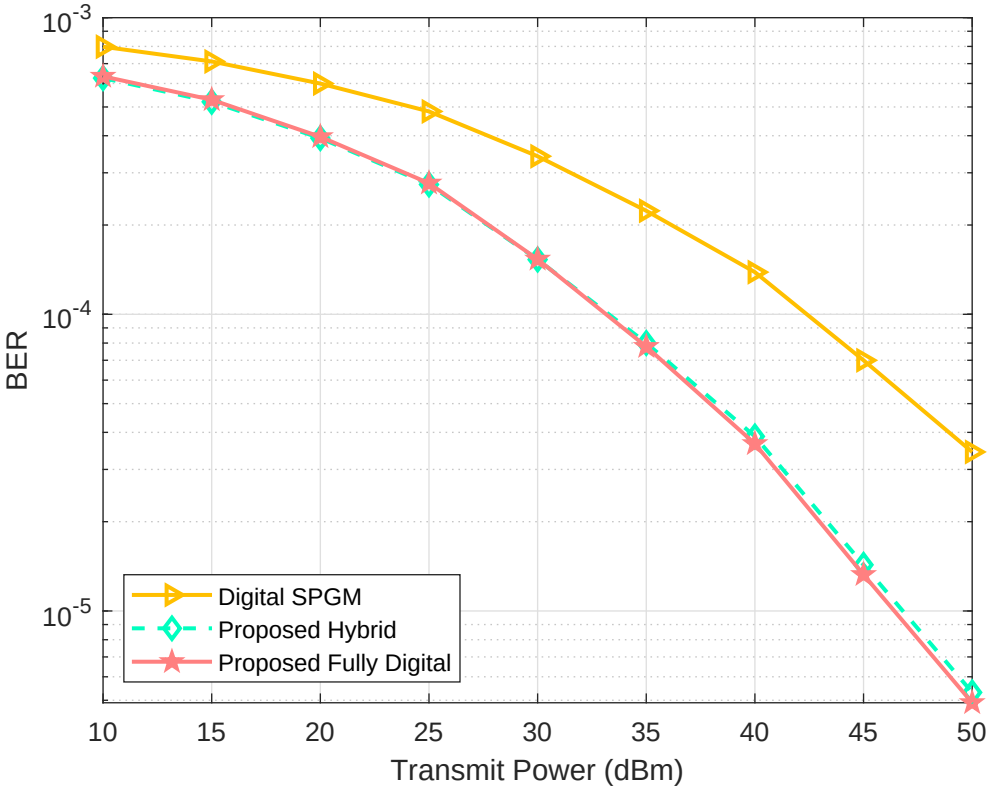

Figure 6.8: Bit error rate versus Transmit power, $N_I = 100$, $M_t = N_s = 4$.

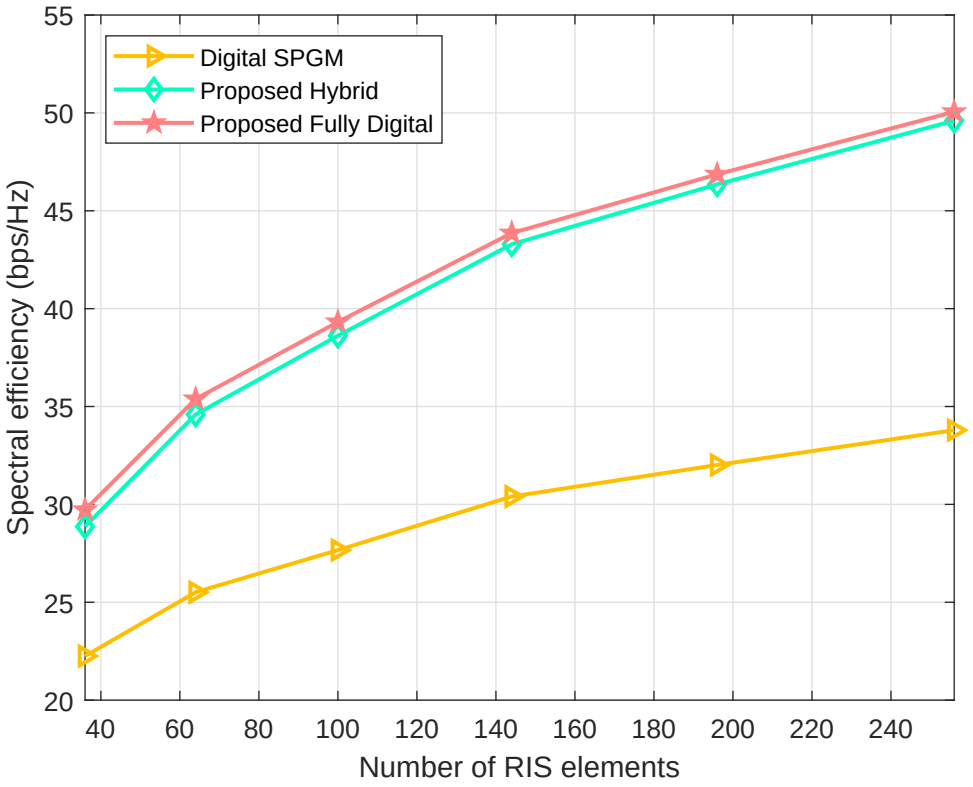

Figure 6.9: Spectral efficiency versus Transmit power, $P_t = 50$ dBm, $M_t = N_s = 4$.

hybrid precoder at the BS. The spectral efficiency plot against the number of RIS elements in Figure 6.9 shows that the performance gap between the proposed method and the SPGM method widens as the number of RIS elements grows. It establishes the proposed method's ability to design the RIS phase shift coefficients in such a way that the channel is programmed to extract the better performance.

6.7 Summary

An mmWave narrowband downlink MIMO is considered which is assisted by an RIS. The passive precoding at the RIS, the fully digital precoding at the BS and the fully digital combining at the receiver are jointly designed. The RIS phase shift matrix is designed to minimize the MSE between the transmit signal and the estimate of received signal in an iterative fashion. The RIS passive precoding vector is obtained by normalizing each element of the unconstrained solution vector of the equivalent MMSE passive precoding problem. The hybrid precoder and combiner are constructed once the passive precoding solution is obtained. The simulation results exhibit that proposed method produces spectral performance which is similar to the best of the state of art methods. In fact, the BER performance reveals that the proposed solution is much better than existing solutions, including the state of art methods. The proposed method is extended for wideband MIMO-OFDM where it echoes its excellent narrowband performance.

Chapter 7

Energy efficient Passive Precoding and Power Allocation for RIS Aided mmWave MU-MISO

Apart from the passive precoding techniques that seek to maximize spectral efficiency, there are also some works that look at energy efficiency of the system. Huang *et. al.* [103] propose an algorithm based on alternating maximization to maximize energy efficiency. In [103], two algorithms based on conjugate gradient search and sequential programming are presented to optimize the RIS phase shifts, and power allocated to different users is optimized by using Dinklebach method. Wu *et. al.* [104] aim to minimize transmit power through joint active and passive precoding design, subject to minimum SINR requirements at each user in both single user and multiple user MIMO communication assisted by an RIS with finite phase shifts. Yang *et. al.* [105] propose an iterative solution that utilizes successive convex approximation to optimize RIS phase shifts and precoding at the BS, while calculating the optimal power using a closed form solution to meet the goal of maximizing energy efficiency. In addition, the authors of [105] consider the dynamic turning on and off of RIS elements which is optimized through dual problem in case of a single user, and through low-complexity search method in multiple users. In this chapter, we consider a situation in which a BS is communicating with multiple users in mmWave channel.

The communication is facilitated through the distributed placement of RISs. We seek to design the precoder at the BS, power allocation to users and RIS phase shift coefficients to maximize energy efficiency of the system. The contributions that we have made can be outlined as

(i) The energy efficiency is maximized by designing the precoder at the BS, the RIS phase shift coefficients and the power allocated to each user. By choosing zero forcing (ZF) precoder, energy efficiency problem is simplified into design problem involving RIS phase shift matrix and power allocation only. The RIS phase shift coefficients and power allocated to each user are jointly optimized using alternating optimization technique. Specifically, passive precoding subproblem reduces into transmit power minimization subproblem which is translated into a boolean quadratic problem. The power allocation subproblem is solved by method of Lagrange multipliers using Karush-Kuhn-Tucker (KKT) conditions.

(ii) It is assumed that individual RIS elements can be switched off through the controller. To further push for energy efficient passive precoding, a computationally efficient strategy is proposed to switch off some of the RIS elements that leads to further enhancement in energy efficiency.

(iii) Simulations are performed to investigate how different parameters affect the energy efficiency with the proposed method. The performance of the proposed method is also compared with the existing solution. The comparison evinces that the proposed method outstrips the performance of the existing solution.

7.1 System Model

A downlink mmWave MU-MISO system is considered, with a base station serving K single-antenna users with the aid of R RISs. It is assumed that each element of the RIS can be switched off through controller, similar to [105]. The BS employs N_t transmit antennas, and each RIS has N_I elements. The transmit information signal $\mathbf{s} \in \mathbb{C}^{K\times 1}$, such that $\mathbb{E}\left[\mathbf{s}\mathbf{s}^H\right] = \mathbf{I}_K$, is precoded before transmission to produce

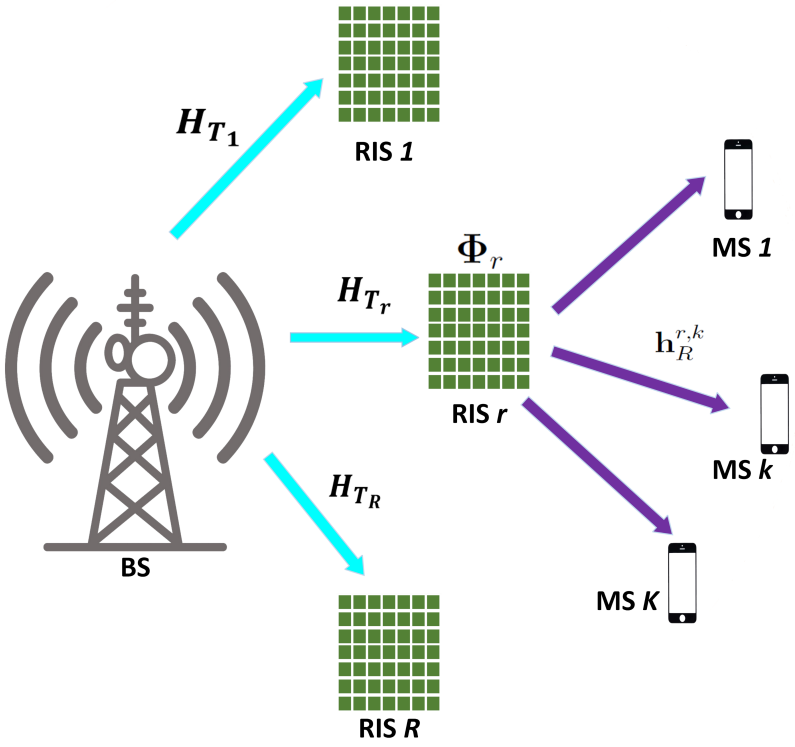

Figure 7.1: mmWave MU-MISO with distributed RIS-aided communication

transmitted signal as

$$\mathbf{x} = \sum_{k=1}^{K} \mathbf{F}_{\cdot\mathbf{k}} \sqrt{p_k} s_k = \mathbf{F}\mathbf{P}^{1/2}\mathbf{s}, \tag{7.1}$$

where s_k is the symbol intended for the k^{th} user, $\mathbf{F}$ is the precoder, $\mathbf{F}_{\cdot\mathbf{k}}$ is the k^{th} column of the precoder, and $\mathbf{P} = \mathbf{DIAG}(p_1, p_2, \ldots, p_K)$ is the power allocation matrix with p_k being the power for the k^{th} user. The transmit power constraint forces the total power of the transmitted signal to not exceed the maximum permitted power P_{max}, *i.e.*,

$$\mathbb{E}\left[|\mathbf{x}|^2\right] = \mathbf{Tr}\left[\mathbf{F}\mathbf{P}\mathbf{F}^H\right] \leq P_{max}. \tag{7.2}$$

There is no direct channel between the BS and the users. The received signal at the k^{th} MS is the sum of the signals received through various RISs,

$$y_k = \left(\sum_{r=1}^{R} \mathbf{h}_{\mathrm{R}}^{r,k} \mathbf{\Phi}_r \mathbf{H}_{\mathrm{T}_r}\right) \mathbf{x} + n_k = \left(\sum_{r=1}^{R} \mathbf{h}_{\mathrm{R}}^{r,k} \mathbf{\Phi}_r \mathbf{H}_{\mathrm{T}_r}\right) \mathbf{F}\mathbf{P}^{1/2}\mathbf{s} + n_k, \tag{7.3}$$

where $\mathbf{h}_{\mathrm{R}}^{r,k} \in \mathbb{C}^{1\times N_I}$ is the channel between the r^{th} RIS and the k^{th} MS, $\mathbf{\Phi}_r$ is a diagonal matrix with the phase shift coefficients of the r^{th} RIS along its diagonal, $\mathbf{H}_{\mathrm{T}_r} \in \mathbb{C}^{N_I\times N_t}$ is the channel between the BS and the r^{th} RIS, and $n_k \in \mathbb{C}$ is the noise

at the receiver of the k^{th} user. The receive vector can be formed by concatenating all y_ks vertically as $\mathbf{y} = [y_1, y_2, \ldots, y_K]^T$ which can be expressed as

$$\begin{aligned}
\mathbf{y} &= \begin{bmatrix} \sum_{r=1}^{R} \mathbf{h}_{\mathrm{R}}^{r,1} \mathbf{\Phi}_r \mathbf{H}_{\mathrm{T}_r} \\ \vdots \\ \sum_{r=1}^{R} \mathbf{h}_{\mathrm{R}}^{r,K} \mathbf{\Phi}_r \mathbf{H}_{\mathrm{T}_r} \end{bmatrix} \mathbf{F}\mathbf{P}^{1/2}\mathbf{s} + \mathbf{n} \\
&= \left\{ \sum_{r=1}^{R} \begin{bmatrix} \mathbf{h}_{\mathrm{R}}^{r,1} \\ \vdots \\ \mathbf{h}_{\mathrm{R}}^{r,K} \end{bmatrix} \mathbf{\Phi}_r \mathbf{H}_{\mathrm{T}_r} \right\} \mathbf{F}\mathbf{P}^{1/2}\mathbf{s} + \mathbf{n} \\
&= \left(\sum_{r=1}^{R} \mathbf{H}_{\mathrm{R}\cdot r} \mathbf{\Phi}_r \mathbf{H}_{\mathrm{T}_r} \right) \mathbf{F}\mathbf{P}^{1/2}\mathbf{s} + \mathbf{n} \\
&= \mathbf{H}_{\mathrm{R}} \mathbf{\Phi} \mathbf{H}_{\mathrm{T}} \mathbf{F}\mathbf{P}^{1/2}\mathbf{s} + \mathbf{n},
\end{aligned}$$

$$\text{where} \quad \mathbf{H}_{\mathrm{R}} = \left[\mathbf{H}_{\mathrm{R}\cdot 1}, \ldots, \mathbf{H}_{\mathrm{R}\cdot R}\right], \tag{7.4a}$$

$$\mathbf{\Phi} = \mathbf{BLKDIAG}\left(\mathbf{\Phi}_1, \ldots, \mathbf{\Phi}_R\right) = \mathbf{DIAG}\left(\boldsymbol{\phi}_1, \ldots, \boldsymbol{\phi}_{RN_I}\right), \tag{7.4b}$$

$$\mathbf{H}_{\mathrm{T}} = \left[\mathbf{H}_{\mathrm{T}_1}^T, \ldots, \mathbf{H}_{\mathrm{T}_R}^T\right]^T, \tag{7.4c}$$

$\mathbf{H}_{\mathrm{R}\cdot r}$ is the r^{th} column of $\mathbf{H}_{\mathrm{R}}$ and corresponds to the channel from r^{th} RIS to the K MSs.

7.1.1 Sum Rate and Power Consumption of the system

The total sum-rate of the system is

$$\mathcal{R}_{tot} = \sum_{k=1}^{K} log_2(1 + \mathrm{SINR_k}), \tag{7.5}$$

where $\mathrm{SINR_k}$ is the SINR at the k^{th} user given by

$$\mathrm{SINR}_k = \frac{|\mathbf{H}_{k\cdot}\mathbf{F}_{\cdot k}|^2 p_k}{\sum_{i=1, i\neq k}^{K} |\mathbf{H}_{i\cdot}\mathbf{F}_{\cdot i}|^2 p_i + \sigma_n^2}, \tag{7.6}$$

where $\mathbf{H}_{k\cdot} = \mathbf{h}_{\mathrm{R}}^{k}\mathbf{\Phi}\mathbf{H}_{\mathrm{T}}$ is the channel from the BS to the k^{th} MS where $\mathbf{h}_{\mathrm{R}}^{k} = \left[\mathbf{h}_{\mathrm{R}}^{1,k}, \ldots, \mathbf{h}_{\mathrm{R}}^{r,k}\right]$. Mathematically, the total power consumption of the system with hybrid architecture at the BS is

$$\mathcal{P}_{tot_{\mathrm{hy}}} = \nu^{-1}\mathbf{Tr}(\mathbf{FPF}^{H}) + P_{com} + P_{MS}K + P_{RF}M_t + P_{PA}M_t + P_{PS}N_{PS} + P_nN_I^{on}, \tag{7.7}$$

where, ν is the efficiency of the transmit power amplifier, P_{com} is the common power of the BS, P_{MS} is the circuit power consumed by each MS, P_{RF} is the power consumed by each RF chain, P_{PA} is the power consumed by each power amplifier, P_{PS} is the power consumed by each phase-shifter, P_n is the power consumed by each element of RIS, N_{PS} is the total number of phase-shifters, and N_I^{on} is the total number of RIS elements that are switched on. $N_I^{on} = RN_I$ when all the elements are switched on. If the conventional MIMO architecture exists at the BS so that fully digital precoding is possible, the number of RF chains, $M_t = N_t$ and $N_{PS} = 0$ so that the total power consumption of the system is

$$\mathcal{P}_{tot_{\mathrm{FD}}} = \nu^{-1}\mathbf{Tr}(\mathbf{FPF}^{H}) + P_{com} + P_{MS}K + (P_{RF} + P_{PA})N_t + P_nN_I^{on}. \tag{7.8}$$

7.2 Problem Statement

The energy efficiency of the system is defined as the ratio of total sum-rate to the total power consumption as,

$$\eta = \frac{\sum_{k=1}^{K} log_2(1 + \mathrm{SINR_k})}{\mathcal{P}_{tot}} \quad bits/Hz/Joule. \tag{7.9}$$

The energy efficiency depends on the choice of $\mathbf{\Phi}$, $\mathbf{F}$ and $\mathbf{P}$, so we design the precoder $\mathbf{F}$, $\mathbf{P}$ and $\mathbf{\Phi}$ to maximize the energy efficiency of the system subject to quality of service (QoS) constraint in terms of minimum guaranteed spectral efficiency $\mathcal{R}_{min_k}$ for the k^{th} user. Only the first term of the denominator depends on $\mathbf{F}$, $\mathbf{P}$ and $\mathbf{\Phi}$, so the rest of the terms is represented by $P_{rest} = P_{com} + P_{MS}K + P_{RF}M_t + P_{PA}M_t + P_{PS}N_{PS} + P_nN_I^{on}$ for simplicity.

7.2.1 Choice of Precoder

ZF precoder is chosen at the BS which is calculated as the right inverse of the equivalent channel. It is guaranteed to exist if $N_t \geq K$ and $RN_I \geq K$ [103]. Even though hybrid precoding is employed at the BS, fully digital precoder $\mathbf{F}_{\text{FD}}$ is considered at the BS to determine the RIS phase shift matrix for the sake of simplicity. The hybrid ZF precoder $\mathbf{F}$ will be computed from $\mathbf{F}_{\text{FD}}$ at the end. The fully digital ZF precoder is computed as

$$\mathbf{F}_{\text{FD}} = \mathbf{H}^{\dagger} = \mathbf{H}^{H} \left(\mathbf{H}\mathbf{H}^{H}\right)^{-1}. \tag{7.10}$$

The reason behind the choice of ZF precoder stems from the fact that application of ZF precoder makes interference zero and SINR for the k^{th} user reduces to the ratio of useful power to the noise power and hence sum rate looks like

$$\mathcal{R}_{tot} = \sum_{k=1}^{K} log_2 \left(1 + \frac{p_k}{\sigma_n^2}\right). \tag{7.11}$$

The precoder needs to satisfy transmit power constraint (7.2), which is accomplished through the appropriate choice of $\mathbf{P}$. Since the ZF precoder is used, the problem for determining $\mathbf{\Phi}$ and $\mathbf{P}$ to maximize energy efficiency can now be stated as

$$\mathbf{\Phi}, \mathbf{P} = \arg\max_{\mathbf{\Phi},\mathbf{P}} \frac{\sum_{k=1}^{K} log_2(1 + \frac{p_k}{\sigma_n^2})}{\nu^{-1}\mathbf{Tr}\left[\left(\mathbf{H}_{\text{R}}\mathbf{\Phi}\mathbf{H}_{\text{T}}\right)^{\dagger}\mathbf{P}\left(\mathbf{H}_{\text{R}}\mathbf{\Phi}\mathbf{H}_{\text{T}}\right)^{\dagger^H}\right] + P_{rest}} \tag{7.12a}$$

$$\text{s.t.} \quad p_k \geq \sigma_n^2 \left(2^{\mathcal{R}_{min_k}/10} - 1\right), \tag{7.12b}$$

$$\mathbf{Tr}\left[\left(\mathbf{H}_{\text{R}}\mathbf{\Phi}\mathbf{H}_{\text{T}}\right)^{\dagger}\mathbf{P}\left(\mathbf{H}_{\text{R}}\mathbf{\Phi}\mathbf{H}_{\text{T}}\right)^{\dagger^H}\right] \leq P_{max}, \tag{7.12c}$$

$$|\boldsymbol{\phi}_r| = 1 \quad \forall\ r = 1, 2, \ldots, RN_I, \tag{7.12d}$$

where the constraint (7.12b) represents the QoS constraint of user k with $\mathcal{R}_{min_k}$ being the minimum spectral efficiency of the k^{th} user. The constraints (7.12c) and (7.12d) represent the transmit power constraint and the constraints imposed by the

phase-only altering capability of the RIS respectively.

7.3 Maximization of Energy Efficiency

In this section, the problem (7.12) of maximizing energy efficiency is solved. It is not possible to optimize both $\mathbf{\Phi}$ and $\mathbf{P}$ at the same time. The route of alternating optimization [106, 107] is chosen where $\mathbf{\Phi}$ and $\mathbf{P}$ are optimized alternately in a series of iterations until convergence is achieved. We begin with optimization of $\mathbf{\Phi}$ for fixed $\mathbf{P}$, and follow it with optimization of $\mathbf{P}$ keeping $\mathbf{\Phi}$ fixed.

7.3.1 Passive Precoding for Energy Efficiency

The subproblem for determination of RIS phase-shift matrix or passive precoding matrix is defined when $\mathbf{P}$ is held constant. It can be seen that with fixed $\mathbf{P}$, maximizing the objective function (7.12a) is equivalent to minimizing the first term of the denominator. Hence if $\mathbf{P}$ is kept constant, the problem (7.12) reduces to passive precoding subproblem,

$$\mathbf{\Phi} = \arg\min_{\mathbf{\Phi}} \mathbf{Tr}\left[\left(\mathbf{H}_{\mathrm{R}}\mathbf{\Phi}\mathbf{H}_{\mathrm{T}}\right)^{\dagger}\mathbf{P}\left(\mathbf{H}_{\mathrm{R}}\mathbf{\Phi}\mathbf{H}_{\mathrm{T}}\right)^{\dagger^{H}}\right], \tag{7.13a}$$

$$\text{s.t.} \quad \mathbf{Tr}\left[\left(\mathbf{H}_{\mathrm{R}}\mathbf{\Phi}\mathbf{H}_{\mathrm{T}}\right)^{\dagger}\mathbf{P}\left(\mathbf{H}_{\mathrm{R}}\mathbf{\Phi}\mathbf{H}_{\mathrm{T}}\right)^{\dagger^{H}}\right] \leq P_{max}, \tag{7.13b}$$

$$|\phi_r| = 1 \quad \forall r = 1, 2, \ldots, RN_I. \tag{7.13c}$$

The objective function (7.13a) can be simplified as

$$\begin{aligned}
\mathbf{\Phi} &= \mathbf{Tr}\left[\left(\mathbf{H}_{\mathrm{R}}\mathbf{\Phi}\mathbf{H}_{\mathrm{T}}\right)^{\dagger}\mathbf{P}\left(\mathbf{H}_{\mathrm{R}}\mathbf{\Phi}\mathbf{H}_{\mathrm{T}}\right)^{\dagger^{H}}\right] \\
&\overset{(a)}{=} \mathbf{Tr}\left[\mathbf{H}_{\mathrm{T}}^{\dagger}\mathbf{\Phi}^{H}\mathbf{H}_{\mathrm{R}}^{\dagger}\mathbf{P}\mathbf{H}_{\mathrm{R}}^{H^{\dagger}}\mathbf{\Phi}\mathbf{H}_{\mathrm{T}}^{H^{\dagger}}\right] \\
&\overset{(b)}{=} \mathbf{Tr}\left[\mathbf{\Phi}^{H}\left(\mathbf{H}_{\mathrm{R}}^{H}\mathbf{P}^{-1}\mathbf{H}_{\mathrm{R}}\right)^{\dagger}\mathbf{\Phi}\left(\mathbf{H}_{\mathrm{T}}\mathbf{H}_{\mathrm{T}}^{H}\right)^{\dagger}\right] \\
&= \mathbf{Tr}\left[\mathbf{\Phi}^{H}\mathbf{C}_1\mathbf{\Phi}\mathbf{C}_2\right] \\
&\overset{(c)}{=} \boldsymbol{\phi}^{H}\mathbf{C}_1 \odot \mathbf{C}_2^{T}\boldsymbol{\phi} \\
&= \boldsymbol{\phi}^{H}\mathbf{C}\boldsymbol{\phi},
\end{aligned}$$

where (a) is possible because $(\mathbf{AB})^{\dagger} = \mathbf{B}^{\dagger}\mathbf{A}^{\dagger}$, $\mathbf{\Phi}^{\dagger} = \mathbf{\Phi}^{H}$, $(\mathbf{AB})^{\dagger^{H}} = (\mathbf{AB})^{H^{\dagger}} = \left(\mathbf{B}^{H}\mathbf{A}^{H}\right)^{\dagger}$; (b) is possible because $\mathbf{Tr}\left[\mathbf{AB}\right] = \mathbf{Tr}\left[\mathbf{BA}\right]$; $\mathbf{C}_1 = \left(\mathbf{H}_{\mathrm{R}}^{H}\mathbf{P}^{-1}\mathbf{H}_{\mathrm{R}}\right)^{\dagger}$, $\mathbf{C}_2 = \left(\mathbf{H}_{\mathrm{T}}\mathbf{H}_{\mathrm{T}}^{H}\right)^{\dagger}$; $\boldsymbol{\phi} = \mathbf{diag}\left(\mathbf{\Phi}\right)$ is a column vector; (c) is possible because of the matrix identity $\mathbf{Tr}\left[\mathbf{\Phi}\mathbf{C}_1\mathbf{\Phi}^{H}\mathbf{C}_2\right] = \boldsymbol{\phi}\left(\mathbf{C}_1 \odot \mathbf{C}_2^{T}\right)\boldsymbol{\phi}^{H}$ for the diagonal matrix $\mathbf{\Phi}$ [99] and $\mathbf{C} = \mathbf{C}_1 \odot \mathbf{C}_2^{T}$ is a Hermitian matrix. Thus, the passive precoding subproblem can be written as

$$\boldsymbol{\phi} = \arg\min_{\mathbf{\Phi}} \boldsymbol{\phi}^{H}\mathbf{C}\boldsymbol{\phi}, \tag{7.14a}$$

$$\text{s.t.} \quad \boldsymbol{\phi}^{H}\mathbf{C}\boldsymbol{\phi} \leq P_{max}, \tag{7.14b}$$

$$|\boldsymbol{\phi}_r| = 1 \quad \forall\ r = 1, 2, \ldots, RN_I. \tag{7.14c}$$

The optimization problem (7.14) needs to solved during each iteration of alternating optimization until convergence. We let go of the constraint (7.14b) and proceed with the alternating optimization. After the alternating optimization reaches convergence and there is a solution for $\mathbf{\Phi}$ and $\mathbf{P}$, we check if the constraint (7.13b) is satisfied. If only the constraint is satisfied, the solution is feasible. The objective function (7.14a) can be simplified as

$$\boldsymbol{\phi}^{H}\mathbf{C}\boldsymbol{\phi} = \sum_{i=1}^{RN_I}\left[\boldsymbol{\phi}_i^{*}\mathbf{C}_{i,i}\boldsymbol{\phi}_i + 2\Re\left(\boldsymbol{\phi}_i\sum_{\substack{j=1\\ j\neq i}}^{RN_I}\boldsymbol{\phi}_j^{*}\mathbf{C}_{j,i}\right)\right], \tag{7.15}$$

where $\mathbf{C}_{i,i}$ is a real quantity. Starting with an initial value of $\boldsymbol{\phi}$, $\boldsymbol{\phi}$ is determined by optimizing over its each element $\boldsymbol{\phi}_i$ at a time. The optimization problem over $\boldsymbol{\phi}_i$ can rewritten as

$$\begin{aligned} \boldsymbol{\phi}_i &= \arg\max_{\boldsymbol{\phi}_i} \Re\left(\boldsymbol{\phi}_i\sum_{j=1}^{RN_I}\boldsymbol{\phi}_j^{*}\mathbf{b}_j^{i}\right) \\ \text{s.t.} \quad & |\boldsymbol{\phi}_i| = 1, \quad \forall\ i = 1, 2, \ldots, RN_I, \end{aligned} \tag{7.16}$$

where $\mathbf{b}_j^i$ is the j^{th} element of $\mathbf{b}^i$ and given by

$$\mathbf{b}_j^i = \begin{cases} -\mathbf{C}_{j,i} & j \neq i \\ -\frac{1}{2}\mathbf{C}_{i,i} & j = i \end{cases} \tag{7.17}$$

The optimal solution to the problem (7.16) is obtained when

$$\boldsymbol{\phi}_i = \frac{\left(\sum_{j=1}^{RN_I} \boldsymbol{\phi}_j^* \mathbf{b}_j^i\right)^*}{\left|\sum_{j=1}^{RN_I} \boldsymbol{\phi}_j^* \mathbf{b}_j^i\right|}. \tag{7.18}$$

This greedy algorithm in phase for optimization of RIS phase shifts is similar to the greedy algorithm in [80].

Algorithm 7.1 Passive Precoding using Greedy Algorithm

Require: $\mathbf{C}, \boldsymbol{\phi}_{init}$.

Set $\delta = 1$, $\epsilon = 10^{-3}$, a very small value. Iteration index, m is set to 1.
while $\delta > \epsilon$ **do**
    for $i = 1$ to RN_I **do**
        Set $\mathbf{b}^i = -\mathbf{C}_{\cdot i}$
        Set $\mathbf{b}_i^i = \frac{1}{2}\mathbf{b}_i^i$
        Compute $\boldsymbol{\phi}_i^{(m)}$ using (7.18).
    end for
    Compute $\delta = \left|\boldsymbol{\phi}^{(m)} - \boldsymbol{\phi}^{(m-1)}\right|$.
    $m \leftarrow m + 1$.
end while
return $\boldsymbol{\phi}$.

7.3.2 Power optimization for energy efficiency

Once $\boldsymbol{\Phi}$ is obtained, the precoder can be determined from the equivalent channel using (7.10). The total transmit power can then be expressed as

$$\mathbf{Tr}\left[\mathbf{FPF}^H\right] = \sum_{k=1}^{K} |\mathbf{F}_{\cdot\mathbf{k}}|^2 p_k = \sum_{k=1}^{K} a_k p_k, \tag{7.19}$$

where $a_k \triangleq |\mathbf{F}_{\cdot\mathbf{k}}|^2$. The power optimization subproblem can be written as

$$\{p_k\}_{k=1}^{K} = \arg\max_{\{p_k\}_{k=1}^{K}} \frac{\sum_{k=1}^{K} log_2\left(1+\frac{p_k}{\sigma_n^2}\right)}{\nu^{-1}\sum_{k=1}^{K} a_k p_k + P_{rest}} \tag{7.20a}$$

$$\text{s.t.} \quad p_k \geq p_{min_k}, \tag{7.20b}$$

$$\sum_{k=1}^{K} a_k p_k \leq P_{max}, \tag{7.20c}$$

where $p_{min_k} \triangleq \sigma_n^2\left(2^{\mathcal{R}_{min_k}/10}-1\right)$. The following notations are used to make further computations tractable.

$$\mathcal{P}_T(p_k) \triangleq \nu^{-1}\sum_{k=1}^{K} a_k p_k + P_{rest}, \tag{7.21a}$$

$$\mathcal{R}(p_k) \triangleq \sum_{k=1}^{K} log_2\left(1+\frac{p_k}{\sigma_n^2}\right), \tag{7.21b}$$

$$f(p_k) = \frac{\mathcal{R}(p_k)}{\mathcal{P}_T(p_k)}. \tag{7.21c}$$

The power optimization subproblem is solved by using the method of Lagrange multipliers, similar to Algorithm 6 of [108]. The problem considered in [108] has slightly different constraints. The Kuhn-Tucker Lagrangian for problem (7.20) is formed as

$$\mathcal{L} = f(p_k) - \sum_{k=1}^{K} \mu_k\left(p_{min_k} - p_k\right) - \lambda\left(\sum_{k=1}^{K} a_k p_k - P_{max}\right), \tag{7.22}$$

where $\{\mu_k \in \mathbb{R}\}_{k=1}^{K}$ and $\lambda \in \mathbb{R}$ are Lagrange multipliers. The partial derivative of the Lagrangian with respect to p_k, λ and μ_k are

$$\frac{\partial \mathcal{L}}{\partial p_k} = \frac{\partial f(p_k)}{\partial p_k} + \mu_k - \lambda a_k \tag{7.23a}$$

$$\frac{\partial \mathcal{L}}{\partial \lambda} = -\left(\sum_{k=1}^{K} a_k p_k - P_{max}\right) \tag{7.23b}$$

$$\frac{\partial \mathcal{L}}{\partial \mu_k} = -\left(p_{min_k} - p_k\right), \quad \text{where} \tag{7.23c}$$

$$\frac{\partial f(p_k)}{\partial p_k} = \frac{1}{ln2} \cdot \frac{1}{p_k + \sigma_n^2} \cdot \frac{1}{\mathcal{P}_T(p_k)} - \frac{\nu^{-1} a_k \mathcal{R}(p_k)}{\mathcal{P}_T(p_k)^2}. \tag{7.23d}$$

The stationary point is obtained by equating (7.23a) to 0,

$$\frac{1}{ln2} \cdot \frac{1}{p_k + \sigma_n^2} \cdot \frac{1}{\mathcal{P}_T(p_k)} - \frac{\nu^{-1} a_k \mathcal{R}(p_k)}{\mathcal{P}_T(p_k)^2} + \mu_k - \lambda a_k = 0, \tag{7.24}$$

which is the first of Karush-Kuhn-Tucker (KKT) conditions [109]. It leads to

$$p_k = \frac{1}{ln2} \cdot \frac{\mathcal{P}_T(p_k)}{\mathcal{P}_T(p_k)^2 \{\lambda a_k - \mu_k\} + \nu^{-1} a_k \mathcal{R}(p_k)} - \sigma_n^2, \tag{7.25a}$$

$$\mu_k = \lambda a_k + \frac{\nu^{-1} a_k \mathcal{R}(p_k)}{\mathcal{P}_T(p_k)^2} - \frac{1}{ln2} \cdot \frac{1}{p_k + \sigma_n^2} \cdot \frac{1}{\mathcal{P}_T(p_k)}. \tag{7.25b}$$

The rest of the KKT conditions or the complementary slackness equations are

$$\mu_k \frac{\partial \mathcal{L}}{\partial \mu_k} = \mu_k \left(p_{min_k} - p_k\right) = 0 \tag{7.26a}$$

$$\lambda \frac{\partial \mathcal{L}}{\partial \lambda} = \lambda \left(\sum_{k=1}^{K} a_k p_k - P_{max}\right) = 0 \tag{7.26b}$$

$$p_k \frac{\partial \mathcal{L}}{\partial p_k} = p_k \left(\frac{\partial f(p_k)}{\partial p_k} + \mu_k - \lambda a_k\right) = 0 \tag{7.26c}$$

Substituting the value of $\frac{\partial f(p_k)}{\partial p_k}$ in (7.26c),

$$\lambda a_k p_k = \frac{1}{ln2} \cdot \frac{p_k}{p_k + \sigma_n^2} \cdot \frac{1}{\mathcal{P}_T(p_k)} - \frac{\nu^{-1} a_k \mathcal{R}(p_k)}{\mathcal{P}_T(p_k)^2} p_k + \mu_k p_k.$$

Taking $\sum_{k=1}^{K}$ on the both sides,

$$\lambda \sum_{k=1}^{K} a_k p_{_k} = \frac{1}{ln2} \cdot \frac{1}{\mathcal{P}_T\left(p_{_k}\right)} \sum_{k=1}^{K} \frac{p_{_k}}{p_{_k} + \sigma_n^2} - \frac{\nu^{-1}\mathcal{R}\left(p_{_k}\right)}{\mathcal{P}_T\left(p_{_k}\right)^2} \sum_{k=1}^{K} a_k p_{_k} + \sum_{k=1}^{K} \mu_k p_{_k}.$$

Substituting $\mu_k p_{_k} = \mu_k p_{min_k}$ and $\lambda \sum_{k=1}^{K} a_k p_{_k} = \lambda P_{max}$ from (7.26a) and (7.26b) respectively,

$$\lambda = \frac{1}{P_{max}} \left[\frac{1}{ln2} \cdot \frac{1}{\mathcal{P}_T\left(p_{_k}\right)} \sum_{k=1}^{K} \frac{p_{_k}}{p_{_k} + \sigma_n^2} - \frac{\nu^{-1}\mathcal{R}\left(p_{_k}\right)}{\mathcal{P}_T\left(p_{_k}\right)^2} \sum_{k=1}^{K} a_k p_{_k} + \sum_{k=1}^{K} \mu_k p_{min_k} \right] \quad (7.27)$$

The constraint (7.20b) ensures that $p_{_k}$ should at least have value p_{min_k} to ensure minimum spectral efficiency for the k^{th} user. In fact, this constraint can ignored during computation of $p_{_k}$. After computing $p_{_k}$, it can be made sure that $p_{_k}$ is at least p_{min_k}. Thus, we can just make $\mu_k = 0$ and develop an iterative algorithm to determine $\{p_{_k}\}_{k=1}^{K}$ using the developments so far which is summarized in Algorithm 7.2. The step 7 ensures $p_{_k}$ does not go below p_{min_k}. Similar approach is taken in [108].

Algorithm 7.2 Iterative power design

Require: $a_k, p_{min_k}, P_{max}, p_{init_k}, P_{rest}, \sigma_n^2, \nu$.

1: Set $\mu_k = 0$
2: Choose initial value of $p_k^0 = p_{init_k}$. Calculate $\mathcal{P}_{\mathrm{T}}^0\left(p_{_k}\right)$ using (7.21a) with $p_{_k} = p_k^0$.
3: Set $\epsilon = 10^{-4}$, a very small value, and set $i \leftarrow 1$.
4: **repeat**
5: Compute λ^i using (7.27).
6: Compute $p_{_k}^i$ using (7.25a).
7: If $p_{_k}^i < p_{min_k}$, set $p_{_k}^i = p_{min_k}$.
8: Compute $\delta^i = \sqrt{\sum_{k=1}^{K} \left|p_{_k}^i - p_{_k}^{i-1}\right|^2}$
9: Set $i \leftarrow i + 1$.
10: **until** $\delta^i < \epsilon$
11: **return** $p_{_k}$.

7.3.3 Alternating Optimization

An initial random value for $\mathbf{\Phi}$ is taken, so the equivalent channel $\mathbf{H} = \mathbf{H}_{\mathrm{R}}\mathbf{\Phi}\mathbf{H}_{\mathrm{T}}$. A valid initial value for $\mathbf{P}$ is calculated as

$$\mathbf{P} = p^0\mathbf{I}, \quad \text{where} \quad p^0 = \frac{P_{max}}{\mathbf{Tr}\left(\mathbf{H}^{\dagger}\mathbf{H}^{\dagger^H}\right)}, \tag{7.28}$$

which ensures that the transmit power is P_{max}. Then $\mathbf{\Phi}$ and $\{p_k\}_{k=1}^K$ are alternately optimized until $\{p_k\}_{k=1}^K$ converge. After convergence is attained, some of the RIS elements are strategically switch off which helps ratchet up energy efficiency. The details of the RIS On-Off strategy are given in next subsection. The alternating optimization algorithm to maximize the energy efficiency is summarized in Algorithm 7.3.

Algorithm 7.3 Alternating Optimization Based Algorithm for Energy Efficiency

Require: $\mathbf{H}_{\mathrm{R}}, \mathbf{H}_{\mathrm{T}}, p_{min_k}, P_{max}, P_{rest}, P_n, \sigma_n^2, \nu$.

1: Initialize $\mathbf{\Phi}$ with $\mathbf{\Phi}^{(0)} = \mathbf{DIAG}\left(\exp\left(j\boldsymbol{\psi}\right)\right)$, where $\boldsymbol{\psi}$ is an RN_I-length vector and $\boldsymbol{\psi}_j$ are random phase angles.
2: Initialize $\mathbf{P}$ with $\mathbf{P}^0$ calculated using (7.28).
3: Compute $\eta^{(0)}$ using (7.9). Set $\epsilon = 10^{-3}$, a very small value, and initialize iteration index $i \leftarrow 1$.
4: **repeat**
5: Compute $\mathbf{C} = \mathbf{C}_1^{(i)} \odot \mathbf{C}_2^T$, where $\mathbf{C}_1^{(i)} = \left(\mathbf{H}_{\mathrm{R}}^H\mathbf{P}^{(i-1)^{-1}}\mathbf{H}_{\mathrm{R}}\right)^{\dagger}$ and $\mathbf{C}_2 = \left(\mathbf{H}_{\mathrm{T}}\mathbf{H}_{\mathrm{T}}^H\right)^{\dagger}$.
6: Compute $\mathbf{\Phi}^{(i)} = \mathbf{DIAG}\left(\boldsymbol{\phi}^{(i)}\right)$ where $\boldsymbol{\phi}^{(i)}$ is calculated using Algorithm 7.1.
7: Compute $\{p_k\}_{k=1}^K$ using Algorithm 7.2. Set $\mathbf{P}^{(i)} = \mathbf{DIAG}\left(p_1, \ldots, p_k\right)$.
8: Compute $\eta^{(i)}$ using (7.9).
9: Compute $\delta^i = \left|\eta^{(i)} - \eta^{(i-1)}\right|$
10: Set $i \leftarrow i + 1$.
11: **until** $\delta^i < \epsilon$
12: Set $\mathbf{P} = \mathbf{P}^{(i)}$
13: Compute $\mathbf{F}_{\mathrm{FD}} = \mathbf{H}^{\dagger}$.
14: **if** $\mathbf{Tr}\left[\mathbf{F}_{\mathrm{FD}}\mathbf{P}\mathbf{F}_{\mathrm{FD}}^H\right] \leq P_{max}$ **then**
15: Compute $\mathbf{C} = \mathbf{C}_1 \odot \mathbf{C}_2^T$, where $\mathbf{C}_1 = \left(\mathbf{H}_{\mathrm{R}}^H\mathbf{P}^{-1}\mathbf{H}_{\mathrm{R}}\right)^{\dagger}$ and $\mathbf{C}_2 = \left(\mathbf{H}_{\mathrm{T}}\mathbf{H}_{\mathrm{T}}^H\right)^{\dagger}$.
16: Obtain $\mathbf{\Phi}$ and $\{p_k\}_{k=1}^K$ using Algorithm 7.4.
17: Obtain hybrid precoder $\mathbf{F}$ from $\mathbf{F}_{\mathrm{FD}}$ using Algorithm 7.5.
18: Calculate $\{p_k\}_{k=1}^K$ using Algorithm 7.4 with $\mathbf{F}$ as precoder.
19: **if** $\mathbf{Tr}\left[\mathbf{F}\mathbf{P}\mathbf{F}^H\right] \leq P_{max}$ **then**
20: **return** $\mathbf{\Phi}$ and $\mathbf{P} = \mathbf{DIAG}\left(p_1, \ldots, p_k\right)$.
21: **else** Declare infeasibility.
22: **end if**
23: **else** Declare infeasibility.
24: **end if**

7.3.4 RIS On-Off Strategy for Energy Efficiency using Low-complexity Algorithm

It is regarded that the individual elements of RISs can be switched on and off using a controller. After optimizing the RIS and power allocation for different users, we strategically switch off the RIS elements which, when switched off, augment the energy efficiency. If we set out to determine such RIS elements exhaustively, it would require to find new equivalent channel, ZF precoder, power allocation for each user, and finally determine the energy efficiency to check which RIS element is best suited to be switched off first. Then, the same procedure would need to be repeated to determine the second RIS element to switch off. In this section, a strategy is proposed to switch off the switches so as to increase energy efficiency in a computationally efficient way.

The determination of $\mathbf{\Phi}$ is accomplished by minimizing the transmit power (7.13a). To develop an order in which RIS elements are switched off, $\boldsymbol{\phi}_i$s are sorted in descending order in terms of their contribution to the term $\boldsymbol{\phi}^H\mathbf{C}\boldsymbol{\phi}$, which is an equivalent expression for transmit power of the system. It will be in the same order that the elements of the RIS will be switched off. To determine the contribution of each RIS element to the transmit power, we compute

$$d_i = \boldsymbol{\phi}_{-i}^H \mathbf{C}_{-i,-i} \boldsymbol{\phi}_{-i}, \tag{7.29}$$

where $\boldsymbol{\phi}_{-i}$ is the vector formed by removing i^{th} element from $\boldsymbol{\phi}$ and $\mathbf{C}_{-i,-i}$ is the matrix formed by removing i^{th} row and the i^{th} column from $\mathbf{C}$. The contribution of $\boldsymbol{\phi}_i$ to the transmit power is given by $\boldsymbol{\phi}^H\mathbf{C}\boldsymbol{\phi} - d_i$. Thus, RIS element '$i$' corresponding to the lowest d_i contributes the highest to the transmit power. Hence, if the $\boldsymbol{\phi}_i$s are arranged in ascending order in terms of the d_i values, $\boldsymbol{\phi}_i$s will be sorted in descending order in terms of contribution to the transmit power.

Now the order to switch off RIS elements is obtained. The energy efficiency, when the "*first in the queue*" element is switched off, is calculated. If it is greater than

the previous value of energy efficiency with all elements switched on, that element is switched off. Then we proceed to check if the energy efficiency increases when the "*next in the queue*" RIS element is switched off. If the energy efficiency increases we proceed to check for next RIS element else we do not switch off the element and stop the process of switching off the RIS elements. The RIS On-Off procedure is summarized in Algorithm 7.4.

Algorithm 7.4 RIS On-Off Strategy for Energy Efficiency

Require: $\mathbf{H}_{\mathrm{R}}, \mathbf{H}_{\mathrm{T}}, \mathbf{C}, p_{min_k}, \boldsymbol{\phi}, \{p_k\}_{k=1}^{K}, P_{max}, P_{rest}, P_n, \sigma_n^2, \nu$.

1: Set $\boldsymbol{\phi}^{(0)} = \boldsymbol{\phi}$ and $N_I^{on^{(0)}} = RN_I$.
2: Compute $d_i,\ i = 1, 2, \ldots, RN_I$ using (7.29).
3: Sort d_i in ascending order and store the sorting index order in $sort\_d$.
4: Set $\delta = 1$ and initialize iteration index $i \leftarrow 1$.
5: **while** $\delta > 0$ **do**
6: $\quad \ell = sort\_d(i)$
7: $\quad$ Set $\boldsymbol{\phi}^{(i)} = \boldsymbol{\phi}^{(i-1)}$ and set ℓ^{th} element of $\boldsymbol{\phi}^{(i)}$ to 0, *i.e.*, $\boldsymbol{\phi}_{\ell}^{(i)} = 0$.
8: $\quad$ Set $N_I^{on^{(i)}} = N_I^{on^{(i-1)}} - 1$.
9: $\quad$ Compute $\boldsymbol{\Phi}^{(i)} = \mathbf{DIAG}\left(\boldsymbol{\phi}^{(i)}\right)$ and $\mathbf{H}^{(i)} = \mathbf{H}_{\mathrm{R}}\boldsymbol{\Phi}^{(i)}\mathbf{H}_{\mathrm{T}}$.
10: $\quad \mathbf{F}^{(i)} = \mathbf{H}^{(i)^{\dagger}},\ a_k^{(i)} = \left|\mathbf{F}_{\cdot k}^{(i)}\right|^2$.
11: $\quad$ Compute $\left\{p_k^{(i)}\right\}_{k=1}^{K}$ using Algorithm 7.2. Set $\mathbf{P^{(i)}} = \mathbf{DIAG}\left(p_1^{(i)}, \ldots, p_K^{(i)}\right)$
12: $\quad$ If $\mathbf{Tr}\left[\mathbf{F}^{(i)}\mathbf{P}^{(i)}\mathbf{F}^{(i)^H}\right] > P_{max}$, go to step 17.
13: $\quad$ Compute $\eta^{(i)}$ using (7.9).
14: $\quad$ Compute $\delta = \eta^{(i)} - \eta^{(i-1)}$
15: $\quad$ Set $i \leftarrow i + 1$.
16: **end while**
17: Revert to the previous values of p_k, N_I^{on} and $\boldsymbol{\phi}$, *i.e.*, $\{p_k\}_{k=1}^{K} = \left\{p_k^{(i-1)}\right\}_{k=1}^{K}$, $\boldsymbol{\phi} = \boldsymbol{\phi}^{(i-1)}$
18: **return** $\{p_k\}_{k=1}^{K}$ and $\boldsymbol{\phi}$.

7.3.5 Hybrid Precoder from fully digital precoder

The hybrid precoder is computed by minimizing the Euclidean distance between the hybrid precoder and fully digital counterpart, $\mathbf{F}_{\text{FD}}$. The hybrid precoding problem [18] may be stated as

$$\underset{\mathbf{F}_{\mathrm{R}}, \mathbf{F}_{\mathrm{D}}}{\arg\min} \quad \|\mathbf{F}_{\text{FD}} - \mathbf{F}_{\mathrm{R}}\mathbf{F}_{\mathrm{D}}\|_F^2 \tag{7.30a}$$

$$\text{s.t.} \quad \left|\mathbf{F}_{\mathrm{R}_{i,j}}\right| = 1,\ \forall i, j. \tag{7.30b}$$

The precoding problem (7.30) does not have the transmit power constraint because it is satisfied through the choice of $\mathbf{P}$. $\mathbf{F}_{\mathrm{R}}$ and $\mathbf{F}_{\mathrm{D}}$ are determined in two separate stages. If $\mathbf{F}_{\mathrm{R}}$ is known, $\mathbf{F}_{\mathrm{D}}$ is computed as

$$\mathbf{F}_{\mathrm{D}} = (\mathbf{H}\mathbf{F}_{\mathrm{R}})^{\dagger}. \tag{7.31}$$

This makes sure that the digital part of the precoder inverts the equivalent channel. In fact, $\mathbf{F}_{\mathrm{D}}$ can also be computed as $\mathbf{F}_{\mathrm{D}} = \mathbf{F}_{\mathrm{R}}{}^{\dagger}\mathbf{F}_{\mathrm{FD}}$ which is substituted in the objective function (7.30) to get the analog precoding subproblem similar to (2.13) with $\mathbf{F}_{\mathrm{FD}}\mathbf{F}_{\mathrm{FD}}^{H}$ in place of $\mathbf{F}_{\mathrm{opt}}\mathbf{F}_{\mathrm{opt}}^{H}$. The iterative truncated SVD-based procedure described in Algorithm 5.1 is used with $\mathbf{I}+\tau\mathbf{H}^{H}\mathbf{H}$ replaced by $\mathbf{F}_{\mathrm{FD}}\mathbf{F}_{\mathrm{FD}}^{H}$. Algorithm 7.5 outlines the hybrid precoding method.

Algorithm 7.5 Hybrid Precoding Using SVD-based Iterative Trace Maximization Method

Require: $\mathbf{H}, \mathbf{F}_{\mathrm{FD}}, M_t$.

1: Compute $\mathbf{F}_{\mathrm{R}}$ using Algorithm 5.1
2: Calculate $\mathbf{F}_{\mathrm{D}}$, using (7.31).
3: **return** $\mathbf{F} = \mathbf{F}_{\mathrm{R}}\mathbf{F}_{\mathrm{D}}$.

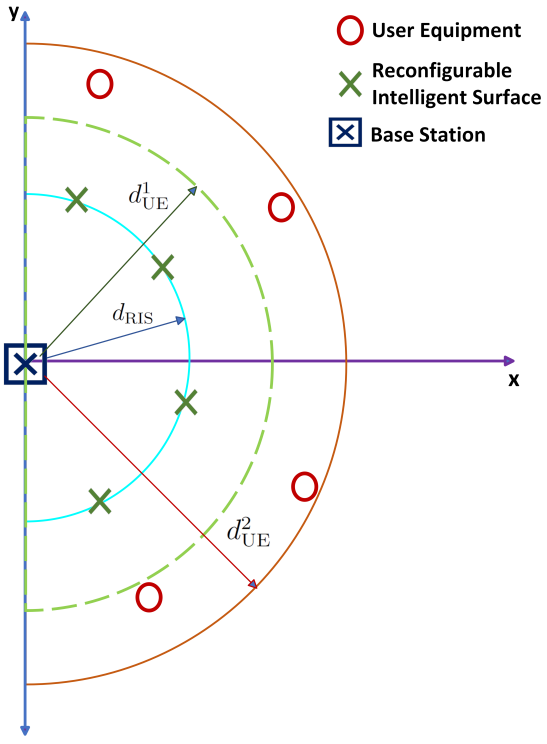

Figure 7.2: The arrangement of BS, RISs and UEs for performance analysis.

7.4 Performance Analysis

An mmWave MIMO with a single BS, R RISs and K single-antenna UEs is considered. The BS is placed at $(0, 0, z_{_B})$, where $z_{_B} = 10$ m. All the RISs are placed on the positive side of x-axis at a distance d_{RIS} m from the BS. The exact placement of the RISs, however, is chosen randomly. The UEs are randomly placed on the positive side of x-axis between the distance d^1_{UE} m and d^2_{UE} m from the BS such that $d^2_{\text{UE}} > d^1_{\text{UE}} > d_{\text{RIS}}$. We take $d^2_{\text{UE}} = 180$ m, $d^1_{\text{UE}} = 144$ m and $d_{\text{RIS}} = 80$ m. The topview of the arrangement of BS, RISs and UEs looks like Figure 7.2. The height of RIS is chosen to be 10 m, whereas the height of every UE is fixed to 1.8 m.

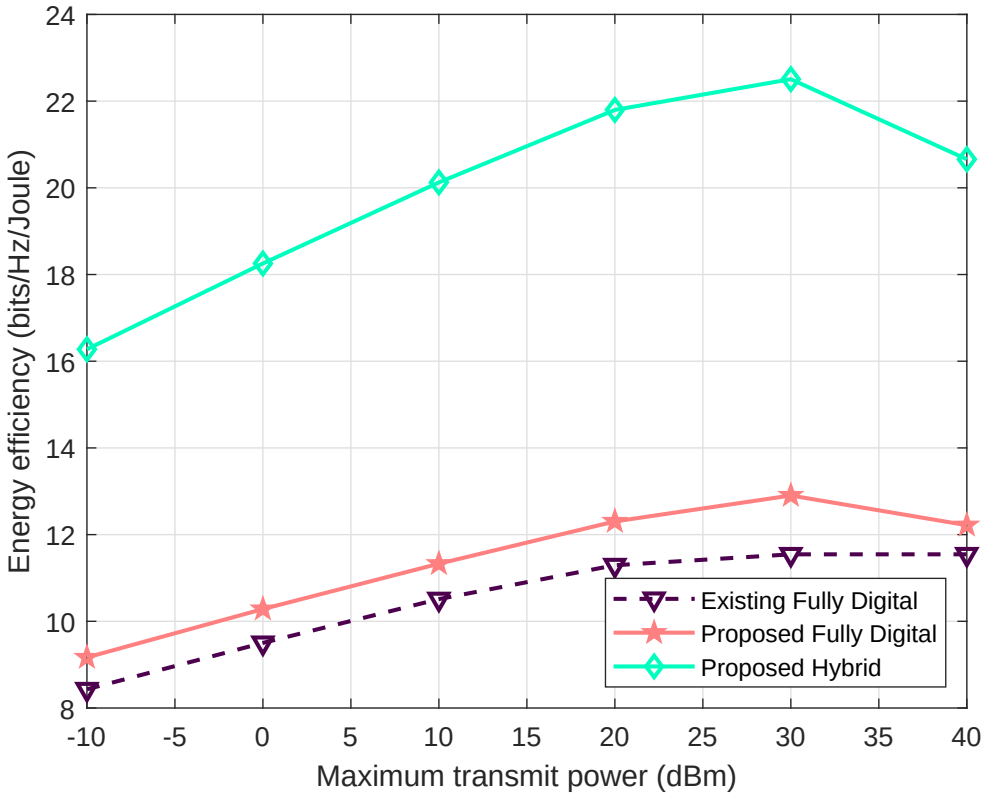

Figure 7.3: Energy efficiency versus Maximum transmit power, $\mathcal{R}_{min_k} = 3$ bps/Hz.

The BS is assumed to be equipped with ULA having $N_t = 64$ antennas, whereas the RIS utilizes square UPA with $N_I = N_I^y \times N_I^z$ antennas. The number of RF chains at the BS is taken equal to K. The values of K, R, N_I^y and N_I^z are taken as 8, 4, 6 and 6 respectively unless they are varying parameters. All the antenna elements are separated by a distance of half wavelength. The noise power $\sigma_n^2 = 90$

dBm. The channel from the BS to the RIS, and the channel from the RIS to the UE are considered narrowband which are modeled by (1.4) with $N_{p_i} = 1$ and $N_c = L$. All the parameters of the channel are taken same as those in Chapter 6.

The performances of the proposed method are compared with those of the existing one [103]. The curves for the proposed method are plotted with both the fully digital precoder and the proposed hybrid precoder, whereas the existing method with only the fully digital precoder. The energy efficiency and spectral efficiency performances as a function of maximum transmit power are portrayed in Figure 7.3 and Figure 7.4 respectively. The energy efficiency increases with maximum transmit power before gaining a maximum value and finally decreasing. With the increase in maximum transmit power, the BS can allocate more power to each user which naturally increases the spectral efficiency as proven by Figure 7.4 as well. This, however, comes with increase in transmit power which lowers energy efficiency once the growth in spectral efficiency is eclipsed by the increase in transmit power.

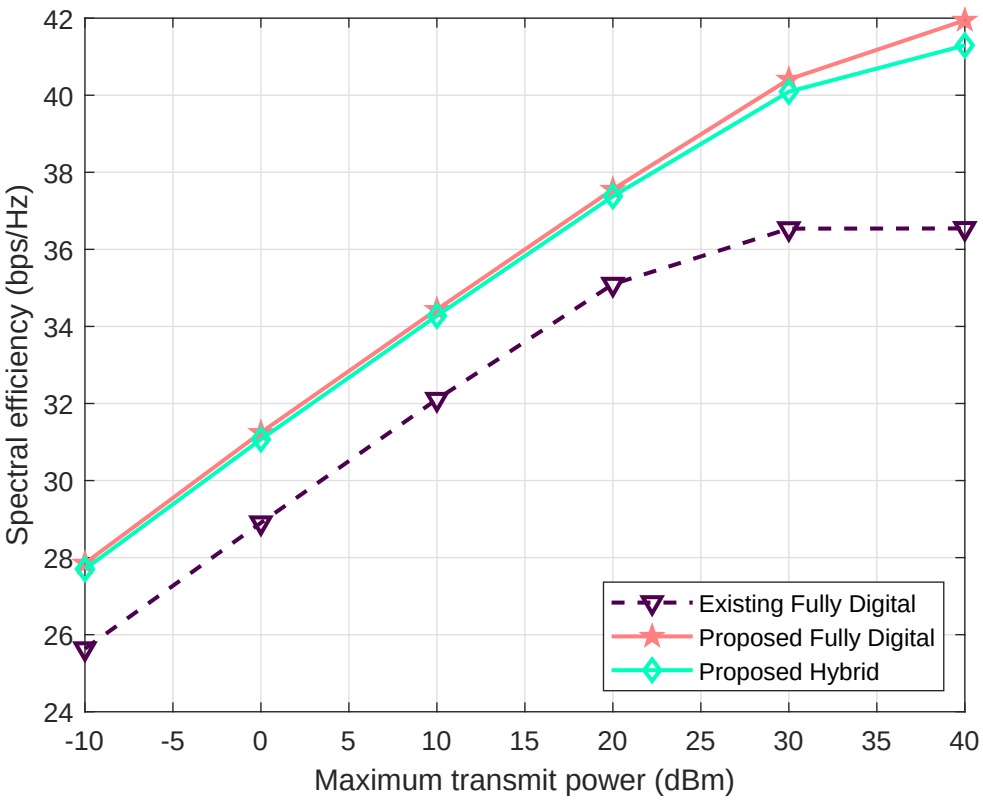

Figure 7.4: Spectral efficiency versus Maximum transmit power, $\mathcal{R}_{min_k} = 3$ bps/Hz.

The energy efficiency plot in Figure 7.5 shows that the energy efficiency increases

as the number of RISs grows. The energy efficiency slowly starts to decline after reaching the maximum. The higher number of RISs helps boost the spectral efficiency. But the power consumed is also higher with the larger number of RISs. The energy efficiency surges with the increasing number of RISs as long as the increase in spectral efficiency overcomes the increase in power consumed by the RISs.

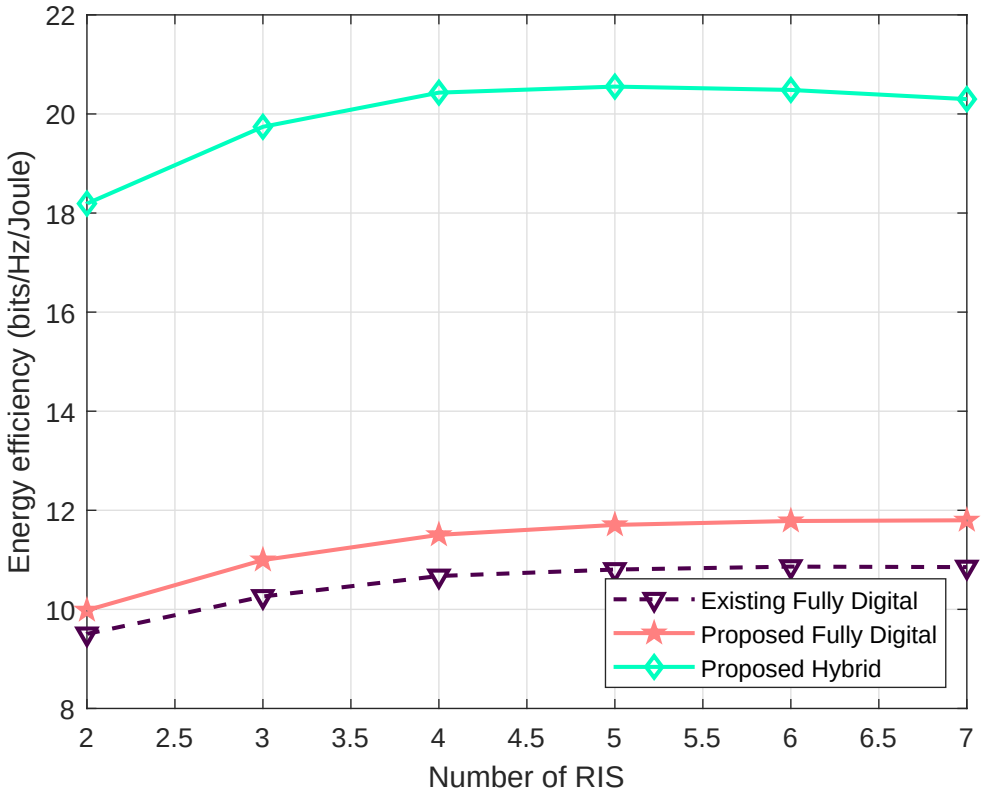

Figure 7.5: Energy efficiency versus Number of RISs, $P_{max} = 10$ dBm, $\mathcal{R}_{min_k} = 3$ bps/Hz.

The energy efficiency plot as a function of number of RIS elements per RIS in Figure 7.6 is similar to the Figure 7.5. The increase in the number of RIS elements per RIS helps enhance the spectral efficiency but the power consumed by the RISs also increases at the same time. As a result, the increase in energy efficiency is higher initially than the latter part of the plot.

The Figure 7.7 shows how energy efficiency varies when the QoS constraint in the form of minimum spectral efficiency $\mathcal{R}_{min_k}$ is increased. The minimum power required for each MS, p_{min_k} increases with $\mathcal{R}_{min_k}$. As long as the value of p_{min_k} is smaller enough, it does not have a say in the power allocated for each MS. But when p_{min_k}

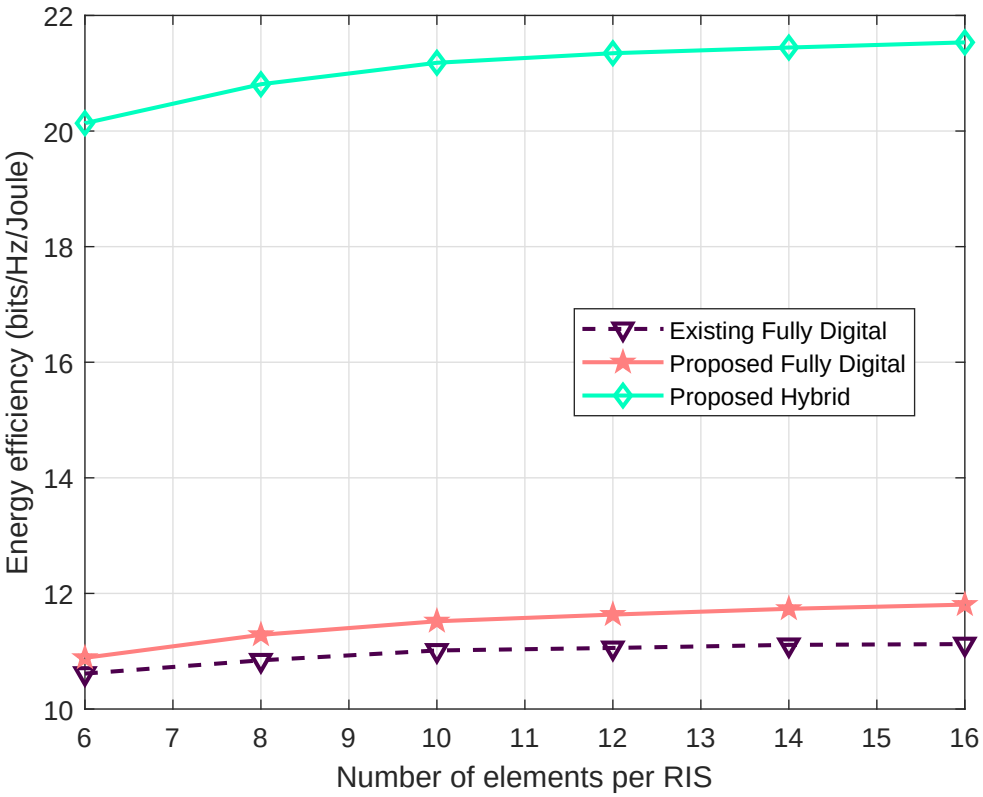

Figure 7.6: Energy efficiency versus Number of elements per each RIS, $P_{max} = 10$ dBm, $\mathcal{R}_{min_k} = 3$ bps/Hz.

reaches a large enough value, it dictates the power allocated for each MS. Hence, it increases the spectral efficiency while decreasing the energy efficiency on the other hand, at higher values of $\mathcal{R}_{min_k}$. Thus, when $\mathcal{R}_{min_k}$ increases from 36.17 bps/Hz to 38.18 bps/Hz, there is a sudden rise in spectral efficiency which comes at the cost of abrupt rise in power consumed, causing a dip in energy efficiency. The decline is more pronounced in existing method compared to the proposed solution.

The Figure 7.8 depicts the effect of the number of users on energy efficiency. There is an amplification in the sum spectral efficiency with the increase in number of users. The increase in power consumed by users is significantly lower than the increase in sum spectral efficiency, thus, increasing the energy efficiency with the number of users.

The increase in BS transmit antennas definitely enhances the spectral efficiency. But there is also an augmentation in the number of power amplifiers and the number of RF chains. There is no rise in the number of RF chains and power amplifiers where

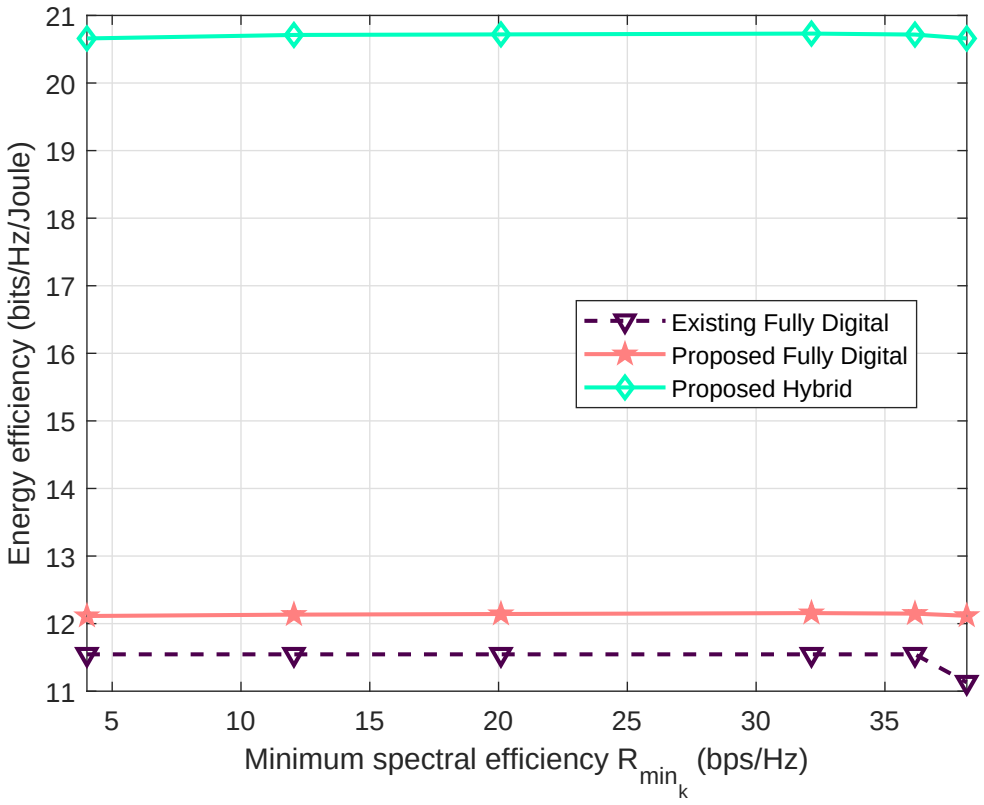

Figure 7.7: Energy efficiency versus Minimum rate for each user, $P_{max} = 40$ dBm.

hybrid precoding is applied but the number of phase shifters. The multiplication in the amount of power consumed by power amplifiers and RF chains outweighs the amplification of spectral efficiency in case of fully digital precoding. As a result, the energy efficiency decreases with the rising number of BS antennas. However, the energy efficiency in case of proposed solution with hybrid precoding fluctuates only within a small margin because there is an increase in spectral efficiency due to the rise of transmit antennas and the increase in power consumption is only due to phase shifters. From all the performance comparison plots, it can be deduced that the proposed method performs better than the existing method.

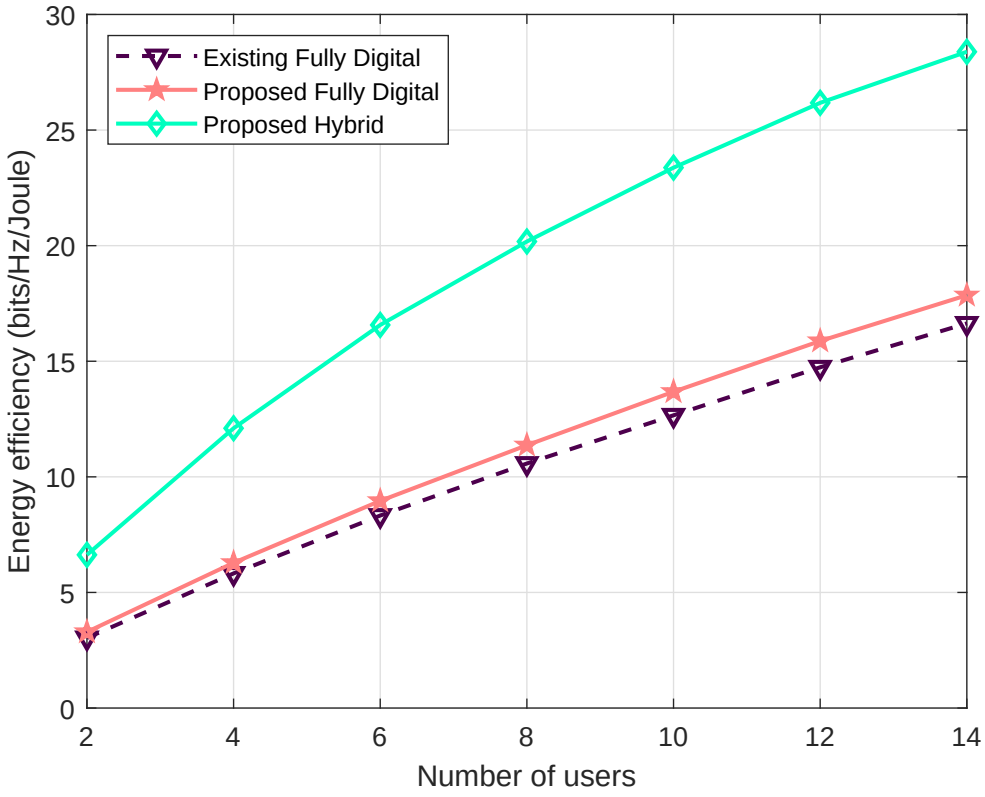

Figure 7.8: Energy efficiency versus Number of users, $P_{max} = 10$ dBm, $\mathcal{R}_{min_k} = 3$ bps/ Hz.

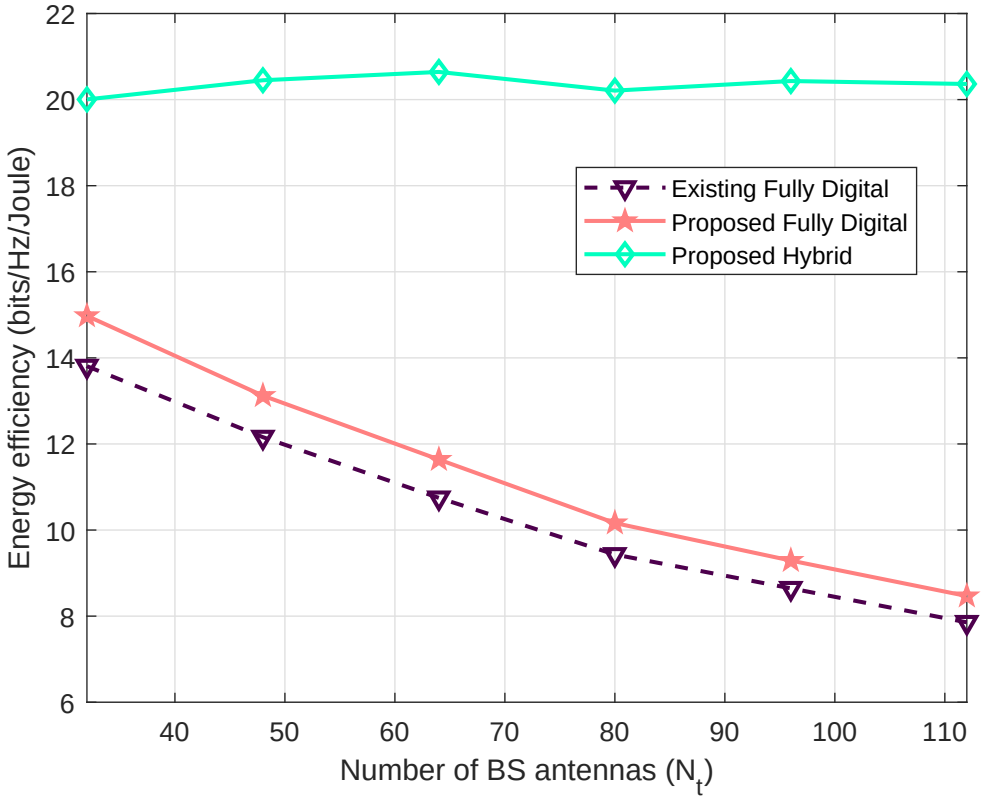

Figure 7.9: Energy efficiency versus Number of BS transmit antennas, $P_{max} = 10$ dBm, $\mathcal{R}_{min_k} = 3$ bps/ Hz.

7.5 Summary

In this chapter, an mmWave MU-MISO communication enhanced by the distributed RISs is considered, with the purpose of maximizing energy efficiency. The energy efficiency maximization problem is shrunk into a simplified problem of determining RIS phase shift coefficients and power allocated to the users with the use of ZF precoding at the BS. An algorithm that alternately optimizes RIS phase shift coefficients and the power allocation is proposed, opting for an alternating optimization route. A greedy algorithm in phase is used to determine RIS phase shift matrix, and an iterative algorithm based on the method of Lagrange multipliers using KKT conditions is developed to optimize power allocation matrix. Moreover, the energy efficiency is aggrandized by switching off some of the RIS elements by proposing a computationally efficacious RIS On-Off strategy. The impact of different parameters on energy efficiency is studied through simulations. The simulation results divulge that the proposed algorithm manages to achieve better energy efficiency as compared to the existing solution.

Chapter 8

Conclusions and Future Directions

8.1 Conclusions

In this thesis, a momentous topic of precoding techniques for mmWave MIMO has been explored. The mmWave MIMO will form an important component of future wireless communications, owing to its large unused bandwidth. The precoding, that allows multiplexing of several data streams, can help exploit the true benefit of MIMO communications. However, the hybrid architecture espoused by mmWave MIMO to make signal preprocessing feasible makes conventional fully digital precoding methods impertinent. This thesis has investigated the hybrid precoding that is challenged by the coupling of analog and digital precoders, and the unit modulus constraint on the elements of analog precoding matrix. There are some hybrid precoding algorithms that demonstrate high performances in both narrowband and wideband channels. However, the existing solutions are laden with high computational demand. With ultra-low latency being one of the integral features of the future wireless communications, it is imperative that the hybrid precoding solutions be not only good in performance but also computationally efficient. Thus, this thesis has concentrated in developing precoding solutions with high performance and low computational overhead.

The RIS will be another significant entity of future wireless communications, and will play a huge role in making mmWave communications, which will be severely impaired

by the blockages, a reality . The passive precoding at RIS is another important research topic that this thesis has addressed. The passive precoding problem is normally coupled with the precoding at the transmitter, giving rise to the joint active and passive precoding problem. In mmWave MIMO that embraces hybrid precoding, the problem gets more entangled but it can be eased by considering only fully digital precoder first and determining the hybrid precoder after settling on the passive precoding. The RIS obligates the passive precoding matrix to fulfill the unit amplitude contraint by its diagonal elements.

In Chapter 2, two hybrid precoding algorithms were proposed for point-to-point mmWave MIMO considering the narrowband channel. The first algorithm is an alternating minimization based algorithm MBCD-HP in which the analog precoding subproblem is cast as an SDP similar to phasecut, after convex relaxation. The analog precoding problem is solved by the MBCD method, making use of the additional constraints compared to the usual phasecut. The hybrid precoding problem is separated into analog precoding subproblem and digital precoding subproblem in the second precoding method IPM-HP. The analog precoding subproblem is solved by an iterative algorithm similar to power method used to determine the eigenvector matrix after enforcing orthogonality constraint on the analog precoder. The MBCD-HP algorithm produces very good spectral performance comparable to the state-of-art algorithms, and also comes with low complexity. The IPM-HP also produces good performance though slightly on the lower side compared to the MBCD-HP and the existing algorithms. However, IPM-HP comes with the benefit of extremely low complexity. Moreover, the proposed precoding methods can be extended to operate in wideband MIMO-OFDM channel. The good performances, coupled with low complexity and ability to operate on both narrowband and wideband channels make the proposed hybrid precoding algorithms promising.

In Chapter 3, the hybrid precoding for the PFMC architecture was established as a matrix factorization problem of all the sub-matrices corresponding to each subgroup of RF chains and antennas. Two algorithms were presented, one based on alternating minimization and the second one based on iterative power method.

The proposed precoders perform better than the existing precoder in terms of both the spectral efficiency and energy efficiency. With a properly chosen number of subgroups and the number of RF chains in each subgroup, it is possible to reap the benefit of performance of the FC architecture, while also lowering the complexity and the power consumption, an advantage of the PC structure. Thus, the PFMC architecture which provides the middle ground in terms of spectral performance and power consumption might be a better way forward for the mmWave MIMO architecture as far as the energy efficiency is concerned.

In Chapter 4, a hybrid SLNR-based precoder for downlink mmWave MU-MIMO systems was proposed. In the presented method, analog-only combiner is designed at MS first and then hybrid precoder is constructed at BS to maximize SLNR of the effective channel. The proposed scheme, while using a small number of RF chains, still produces spectral efficiency close to the fully-digital precoder and superior to those of existing codebook based precoders. In addition, the achievable spectral efficiency of the proposed precoder was evaluated for single path channel with infinite resolution codebook.

In Chapter 5, a computationally-efficient hybrid precoding method based on minimizing the MSE for all users in downlink mmWave MU-MISO systems was proposed considering narrowband channel. The problem of minimizing MSE was broken down into two separate stages to simplify the optimization problem. The analog precoder is evaluated by an iterative truncated SVD-based trace maximization procedure, and then the digital part of the precoder is computed for the fixed analog precoder. The proposed hybrid MMSE precoder produces the spectral and BER performances which are close to fully digital precoder and almost the same as the existing high performance hybrid precoders, but at much lower computational complexity. Further, it was seen that the performance remains unaffected even while using quantized phase shifters with reasonable quantization bits. It was also shown that the proposed method can be extended to work in wideband channel. The simulation results manifested that the proposed method replicates its towering narrowband channel performance in wideband channel by performing quite close to its fully digital coun-

terpart. In short, the proposed hybrid precoder comes with very low complexity but with virtually no compromise in performance.

In Chapter 6, passive precoding algorithm was devised to minimize the MSE between the transmit signal and the estimate of the received signal through iterative procedure by solving a joint optimization problem to determine fully digital precoder, passive precoding and fully digital combiner. The proposed algorithm replaces the passive precoding subproblem with an equivalent problem and extracts the phase of the unconstrained solution at each iteration. The hybrid precoder is determined after the solution for passive precoding is finalized. The spectral and BER performance analyses divulged that the proposed algorithm is better than the existing methods, while entailing lower complexity.

In Chapter 7, the precoding at the BS, passive precoding at the RIS and the power allocation to different users were designed to maximize energy efficiency of the system. The energy efficiency maximization problem was simplified by using ZF precoder which reduced the problem into finding passive precoding and power allocation only. The proposed iterative algorithm uses greedy algorithm to determine passive precoding matrix, and the method of Lagrange multipliers with KKT conditions to calculate power allocation at each iteration. In addition, a low complexity scheme was proposed to switch off some of the elements of RISs to further enhance energy efficiency. The impact of various parameters on energy efficiency was studied through simulations. The performance analysis proved that the proposed algorithm produces better performance than the existing solution.

In short, it can be concluded that the hybrid precoding algorithms can achieve the performances that are quite close to the performances of the fully digital precoding. The performance of the hybrid precoder is not affected significantly even with the use of quantized phase shifters of low resolution. While observing the performances of various passive precoding algorithms, it can be concluded that the passive precoding at RIS has a significant effect on the spectral, BER and energy efficiency performances. Thus, it is possible to program the channel between the transmitter and the receiver to have more reliable and better rate of communication with passive precoding.

8.2 Future Directions

The precoding is one of the important issues in the design of transceivers for mmWave MIMO. The low complexity hybrid precoding methods that deliver high performance are essential to address the expectations of future wireless communications. The following are a few suggestions for the future work that are very crucial.

(i) It has been assumed that the CSI available at the transmitter is perfect while determining precoder. The huge size of CSI in mmWave MIMO makes channel estimation prone to errors. Moreover, quantization errors, pilot contamination, feedback delays also add distortions to the CSI [110]. Thus, the availability of perfect CSI can rarely be realized in practice. Therefore, investigation on the development of hybrid precoding algorithms that are robust to CSI errors is a critical issue.

(ii) The energy efficiency of the mmWave systems can be improved by realizing the analog precoder using inverters and switches, or the use of partial-full mixed connection hybrid architecture. Once the type of hybrid architecture and the number of RF chains are fixed, the energy efficiency would depend on the number of active phase shifters. The best way to elevate energy efficiency would be to use minimal number of phase shifters that maintain the highest energy efficiency. Thus, another research direction would be to develop hybrid precoding methods that can dynamically determine the phase shifters that need to be switched off so that energy efficiency is maximized.

(iii) In the mmWave communication enhanced by RISs, one critical question is: *How should RISs be placed*? Should the RISs be placed near to the transmitter or the user? There is still a lot to research on the best positions to place RISs before arriving at the concrete answer. The answer to the question on the placement of RISs would help plan the deployment of RISs. Hence research toward finding out the answers pertaining to the placement of RISs needs attention.

(iv) Even though the extremely narrow and highly directional mmWave beams significantly reduce the information leakage from sidelobes, there is still possibility of eavesdropping along the mainlobe [111]. On the other hand, highly narrow beams make mmWaves prone to information leakage due to beam misalignment [112]. High susceptibility of mmWaves to blockages makes it easier for the eavesdroppers to block communications [113]. Thus, physical layer security is another important area of research in mmWave communications. The transmit precoding and passive precoding can be designed to ensure secure communication to maximize secrecy rate of the systems to stifle blocking [111], or reduce the prospects of eavesdropping [112].

The use of mmWave band in cellular communications in actual sense has not materialized yet, and the researchers have already been looking at the communications in TeraHertz (THz) band [114, 115] which includes the waves from 100 GHz-10 THz. The THz signals are also high frequency waves, hence suffer from huge path loss like mmWave signals. Thus, THz communication also needs to employ massive MIMO to make it a reality. The THz communications will embrace the hybrid MIMO architecture [116, 117] and RISs for the same reasons as mmWave communications [118]. Thus, the work accomplished in thesis will stay relevant even for the THz communications, and can be extended for different scenarios in THz communications.

Appendix A

Lower Bound of Trace of Inverse of a Matrix

If $\lambda_1 \geq \lambda_2 \geq \cdots \geq \lambda_n > 0$ are the n eigenvalues of a positive definite matrix $\mathbf{A} \in \mathbb{C}^{n\times n}$, the eigenvalues of its inverse $\mathbf{A}^{-1}$ are $0 < \lambda_1^{-1} \leq \lambda_2^{-1} \leq \cdots \leq \lambda_n^{-1}$. We can express the trace of $\mathbf{A}$ and trace of $\mathbf{A}^{-1}$ as

$$\mathbf{Tr}\left(\mathbf{A}\right) = \sum_{i=1}^{n} \lambda_i \tag{A.1a}$$

$$\mathbf{Tr}\left(\mathbf{A}^{-1}\right) = \sum_{i=1}^{n} \lambda_i^{-1}. \tag{A.1b}$$

The product of trace of $\mathbf{A}$ and trace of $\mathbf{A}^{-1}$ is

$$\mathbf{Tr}\left(\mathbf{A}\right)\mathbf{Tr}\left(\mathbf{A}^{-1}\right) = \left(\sum_{i=1}^{n} \lambda_i\right)\left(\sum_{i=1}^{n} \lambda_i^{-1}\right). \tag{A.2}$$

Since $\lambda_1, \lambda_2, \ldots, \lambda_n$ is a non-increasing sequence, and $\lambda_1^{-1}, \lambda_2^{-1}, \ldots, \lambda_n^{-1}$ is a non-decreasing sequence, we may write

$$\begin{aligned}\left(\sum_{i=1}^{n} \lambda_i\right)\left(\sum_{i=1}^{n} \lambda_i^{-1}\right) &\geq n\sum_{i=1}^{n} \lambda_i\lambda_i^{-1} \\ &= n^2,\end{aligned}$$

using Chebyshev inequality [119]. The equality is fulfilled when $\lambda_1 = \lambda_2 = \cdots = \lambda_n$. Hence,

$$\mathbf{Tr}\left(\mathbf{A}\right)\mathbf{Tr}\left(\mathbf{A}^{-1}\right) \geq n^2. \tag{A.3}$$

Since $\mathbf{Tr}\left(\mathbf{A}\right) > 0$, we may express the trace of $\mathbf{A}^{-1}$ as

$$\mathbf{Tr}\left(\mathbf{A}^{-1}\right) \geq \frac{n^2}{\mathbf{Tr}\left(\mathbf{A}\right)}, \tag{A.4}$$

with equality when all the eigenvalues of $\mathbf{A}$ are equal.

Appendix B

Trace Maximization Via Truncated SVD

We seek to determine matrix $\mathbf{D} \in \mathbb{C}^{N_t \times M_t}$ that solves the problem,

$$\begin{aligned} &\max_{\mathbf{D}} \ |\mathbf{Tr}(\mathbf{AD})| \\ &s.t. \ \ \mathbf{D}^H\mathbf{D} = \mathbf{I}_{M_t}, \end{aligned} \tag{B.1}$$

where $\mathbf{A}$ is $M_t \times N_t$ matrix. We will determine the maximum value of the $|\mathbf{Tr}\left(\mathbf{DA}\right)|$ and $\mathbf{D}$ that produces this maximum value subsequently. The SVD of matrix $\mathbf{A}$ is $\mathbf{A} = \mathbf{U\Sigma V}^H$, where $\mathbf{U} \in \mathbb{C}^{M_t \times M_t}, \mathbf{\Sigma} \in \mathbb{C}^{M_t \times N_t}$, and $\mathbf{V} \in \mathbb{C}^{N_t \times N_t}$. $\mathbf{U}$ and $\mathbf{V}$ are unitary matrices. We can write

$$\begin{aligned} |\mathbf{Tr}(\mathbf{AD})| &= |\mathbf{Tr}(\mathbf{U\Sigma V}^H\mathbf{D})| \\ &\overset{(a)}{=} |\mathbf{Tr}(\mathbf{\Sigma V}^H\mathbf{DU})| \\ &= |\mathbf{Tr}(\mathbf{\Sigma M})|, \end{aligned}$$

where $\mathbf{M} \triangleq \mathbf{V}^H\mathbf{D}\mathbf{U}$. We can easily show that $\mathbf{M} \in \mathbb{C}^{N_t \times M_t}$ is a semi-unitary matrix, *i.e.*, $\mathbf{M}^H\mathbf{M} = \mathbf{I}_{M_t}$ as

$$\begin{aligned}\mathbf{M}^H\mathbf{M} &= \mathbf{U}^H\mathbf{D}^H\mathbf{V}\mathbf{V}^H\mathbf{D}\mathbf{U} \\ &\overset{(a)}{=} \mathbf{U}^H\mathbf{D}^H\mathbf{D}\mathbf{U} \\ &\overset{(b)}{=} \mathbf{U}^H\mathbf{U} \\ &\overset{(c)}{=} \mathbf{I}_{M_t},\end{aligned}$$

where the reasons behind *(a)*, *(b)* and *(c)* are $\mathbf{V}$ is unitary matrix, $\mathbf{D}^H\mathbf{D} = \mathbf{I}_{M_t}$, and $\mathbf{U}$ is unitary matrix respectively. The matrix $\mathbf{\Sigma}_{:,1:M_t} = \mathbf{S}$, where $\mathbf{S} = \mathbf{diag}\left(\sigma_1, \ldots, \sigma_{M_t}\right)$ with $\sigma_1, \ldots, \sigma_{M_t}$ being the singular values of $\mathbf{A}$ and $\mathbf{\Sigma}_{:,(M_t+1):N_t} = \mathbf{0}$. Hence, the objective function in (B.1) can be written as

$$\begin{aligned}|\mathbf{Tr}(\mathbf{A}\mathbf{D})| = |\mathbf{Tr}(\mathbf{\Sigma}\mathbf{M})| &= \left|\sum_{i=1}^{M_t} \sigma_i m_{ii}\right| \\ &\overset{(a)}{\leq} \sum_{i=1}^{M_t} |\sigma_i m_{ii}| \\ &\overset{(b)}{=} \sum_{i=1}^{M_t} \sigma_i |m_{ii}|,\end{aligned}$$

where *(a)* is possible because for complex scalars a_i's $\left|\sum_{i=1}^{M_t} a_i\right| \leq \sum_{i=1}^{M_t} |a_i|$, the reason for *(b)* is the fact that $\sigma_i \geq 0, \forall i$ as they are the singular values of a matrix, and $m_{ii}, i = 1, \ldots, M_t$ are the diagonal elements of $\mathbf{M}$. Since $\mathbf{M}$ is a semi-unitary matrix, $|m_{ii}| \leq 1$. Thus,

$$|\mathbf{Tr}(\mathbf{A}\mathbf{D})| = |\mathbf{Tr}(\mathbf{\Sigma}\mathbf{M})| \leq \sum_{i=1}^{M_t} \sigma_i, \tag{B.2}$$

Hence, the maximum value of $|\mathbf{Tr}(\mathbf{A}\mathbf{D})|$ is $\sum_{i=1}^{M_t} \sigma_i$, which is attainable when $\mathbf{M}_{1:M_t,:} = \mathbf{I}_{M_t}$. This is possible when

$$\mathbf{D} = \mathbf{V}_t\mathbf{U}^H, \tag{B.3}$$

where $\mathbf{V}_t = \mathbf{V}_{:,1:M_t}$ is the truncated right singular matrix of $\mathbf{A}$, with only first M_t columns corresponding to M_t largest singular values. Thus, we do not need to have

full SVD of $\mathbf{A}$ to determine $\mathbf{D}$, but only the truncated SVD of $\mathbf{A}$, which involves lower complexity.

Bibliography

[1] Z. Pi and F. Khan, "An introduction to millimeter-wave mobile broadband systems," *IEEE Communications Magazine*, vol. 49, no. 6, pp. 101–107, June 2011.

[2] F. Boccardi, R. W. Heath, A. Lozano, T. L. Marzetta, and P. Popovski, "Five disruptive technology directions for 5G," *IEEE Communications Magazine*, vol. 52, no. 2, pp. 74–80, February 2014.

[3] W. H. Chin, Z. Fan, and R. Haines, "Emerging technologies and research challenges for 5G wireless networks," *IEEE Wireless Communications*, vol. 21, no. 2, pp. 106–112, 2014.

[4] A. L. Swindlehurst, E. Ayanoglu, P. Heydari, and F. Capolino, "Millimeter-wave massive MIMO: The next wireless revolution?" *IEEE Communications Magazine*, vol. 52, no. 9, pp. 56–62, Sep. 2014.

[5] T. S. Rappaport, J. N. Murdock, and F. Gutierrez, "State of the art in 60-ghz integrated circuits and systems for wireless communications," *Proceedings of the IEEE*, vol. 99, no. 8, pp. 1390–1436, 2011.

[6] S. Rangan, T. S. Rappaport, and E. Erkip, "Millimeter-wave cellular wireless networks: Potentials and challenges," *Proceedings of the IEEE*, vol. 102, no. 3, pp. 366–385, 2014.

[7] A. Ghosh, T. A. Thomas, M. C. Cudak, R. Ratasuk, P. Moorut, F. W. Vook, T. S. Rappaport, G. R. MacCartney, S. Sun, and S. Nie, "Millimeter-wave enhanced local area systems: A high-data-rate approach for future wireless

networks," *IEEE Journal on Selected Areas in Communications*, vol. 32, no. 6, pp. 1152–1163, 2014.

[8] S. Han, C. I, Z. Xu, and C. Rowell, "Large-scale antenna systems with hybrid analog and digital beamforming for millimeter wave 5G," *IEEE Communications Magazine*, vol. 53, no. 1, pp. 186–194, January 2015.

[9] T. S. Rappaport, S. Sun, R. Mayzus, H. Zhao, Y. Azar, K. Wang, G. N. Wong, J. K. Schulz, M. Samimi, and F. Gutierrez, "Millimeter wave mobile communications for 5G cellular: It will work!" *IEEE Access*, vol. 1, pp. 335–349, 2013.

[10] C.-X. Wang, F. Haider, X. Gao, X.-H. You, Y. Yang, D. Yuan, H. M. Aggoune, H. Haas, S. Fletcher, and E. Hepsaydir, "Cellular architecture and key technologies for 5g wireless communication networks," *IEEE Communications Magazine*, vol. 52, no. 2, pp. 122–130, 2014.

[11] T. E. Bogale and L. B. Le, "Beamforming for multiuser massive MIMO systems: Digital versus hybrid analog-digital," in *2014 IEEE Global Communications Conference*, 2014, pp. 4066–4071.

[12] R. W. Heath, N. González-Prelcic, S. Rangan, W. Roh, and A. M. Sayeed, "An overview of signal processing techniques for millimeter wave MIMO systems," *IEEE Journal of Selected Topics in Signal Processing*, vol. 10, no. 3, pp. 436–453, April 2016.

[13] F. Rusek, D. Persson, B. K. Lau, E. G. Larsson, T. L. Marzetta, O. Edfors, and F. Tufvesson, "Scaling up MIMO: Opportunities and challenges with very large arrays," *IEEE Signal Processing Magazine*, vol. 30, no. 1, pp. 40–60, Jan 2013.

[14] E. G. Larsson, O. Edfors, F. Tufvesson, and T. L. Marzetta, "Massive MIMO for next generation wireless systems," *IEEE Communications Magazine*, vol. 52, no. 2, pp. 186–195, February 2014.

[15] L. Lu, G. Y. Li, A. L. Swindlehurst, A. Ashikhmin, and R. Zhang, "An overview of massive MIMO: Benefits and challenges," *IEEE Journal of Selected Topics in Signal Processing*, vol. 8, no. 5, pp. 742–758, Oct 2014.

[16] Z. Marzi, D. Ramasamy, and U. Madhow, "Compressive channel estimation and tracking for large arrays in mm-wave picocells," *IEEE Journal of Selected Topics in Signal Processing*, vol. 10, no. 3, pp. 514–527, 2016.

[17] D. Tse and P. Viswanath, *Fundamentals of Wireless Communication*. New York, NY, USA: Cambridge University Press, 2005.

[18] O. E. Ayach, S. Rajagopal, S. Abu-Surra, Z. Pi, and R. W. Heath, "Spatially sparse precoding in millimeter wave MIMO systems," *IEEE Transactions on Wireless Communications*, vol. 13, no. 3, pp. 1499–1513, March 2014.

[19] A. M. Sayeed, "Deconstructing multiantenna fading channels," *IEEE Transactions on Signal Processing*, vol. 50, no. 10, pp. 2563–2579, Oct 2002.

[20] A. M. Sayeed, T. Sivanadyan, K. Liu, and S. Haykin, "Wireless communication and sensing in multipath environments using multi-antenna transceivers," in *Handbook on Array Processing and Sensor Networks*. Wiley Hoboken, NJ, USA, 2010, pp. 115–170.

[21] H. Bolcskei, M. Borgmann, and A. Paulraj, "Impact of the propagation environment on the performance of space-frequency coded MIMO-OFDM," *IEEE Journal on Selected Areas in Communications*, vol. 21, no. 3, pp. 427–439, 2003.

[22] A. Forenza, D. J. Love, and R. W. Heath, "Simplified spatial correlation models for clustered mimo channels with different array configurations," *IEEE Transactions on Vehicular Technology*, vol. 56, no. 4, pp. 1924–1934, 2007.

[23] Y.-P. Lin, "Hybrid mimo-ofdm beamforming for wideband mmwave channels without instantaneous feedback," *IEEE Transactions on Signal Processing*, vol. 66, no. 19, pp. 5142–5151, 2018.

[24] S. Sun, T. S. Rappaport, R. W. Heath, A. Nix, and S. Rangan, "MIMO for millimeter-wave wireless communications: beamforming, spatial multiplexing, or both?" *IEEE Communications Magazine*, vol. 52, no. 12, pp. 110–121, 2014.

[25] M. Vu and A. Paulraj, "MIMO wireless linear precoding," *IEEE Signal Processing Magazine*, vol. 24, no. 5, pp. 86–105, 2007.

[26] D. J. Love, R. W. Heath, V. K. N. Lau, D. Gesbert, B. D. Rao, and M. Andrews, "An overview of limited feedback in wireless communication systems," *IEEE Journal on Selected Areas in Communications*, vol. 26, no. 8, pp. 1341–1365, 2008.

[27] D. Love and R. Heath, "Multimode precoding for MIMO wireless systems," *IEEE Transactions on Signal Processing*, vol. 53, no. 10, pp. 3674–3687, 2005.

[28] A. Alkhateeb, O. E. Ayach, G. Leus, and R. W. Heath, "Hybrid precoding for millimeter wave cellular systems with partial channel knowledge," in *2013 Information Theory and Applications Workshop (ITA)*, Feb 2013, pp. 1–5.

[29] O. E. Ayach, R. W. Heath, S. Abu-Surra, S. Rajagopal, and Z. Pi, "Low complexity precoding for large millimeter wave MIMO systems," in *2012 IEEE International Conference on Communications (ICC)*, June 2012, pp. 3724–3729.

[30] A. Alkhateeb, G. Leus, and R. W. Heath, "Limited feedback hybrid precoding for multi-user millimeter wave systems," *IEEE Transactions on Wireless Communications*, vol. 14, no. 11, pp. 6481–6494, Nov 2015.

[31] X. Gao, L. Dai, Y. Sun, S. Han, and I. Chih-Lin, "Machine learning inspired energy-efficient hybrid precoding for mmwave massive MIMO systems," in *2017 IEEE International Conference on Communications (ICC)*, 2017, pp. 1–6.

[32] J.-C. Chen, "Constructive interference-based symbol-level precoding design for millimeter-wave massive multiuser MIMO systems with hardware-efficient hybrid precoding architecture," *IEEE Access*, vol. 9, pp. 18 393–18 401, 2021.

[33] M. Kim and Y. H. Lee, "MSE-based hybrid RF/baseband processing for millimeter-wave communication systems in MIMO interference channels," *IEEE*

Transactions on Vehicular Technology, vol. 64, no. 6, pp. 2714–2720, 2015.

[34] D. H. N. Nguyen, L. B. Le, T. Le-Ngoc, and R. W. Heath, "Hybrid MMSE precoding and combining designs for mmwave multiuser systems," *IEEE Access*, vol. 5, pp. 19 167–19 181, 2017.

[35] W. Ni and X. Dong, "Hybrid block diagonalization for massive multiuser MIMO systems," *IEEE Transactions on Communications*, vol. 64, no. 1, pp. 201–211, Jan 2016.

[36] C. Rusu, R. Mèndez-Rial, N. González-Prelcic, and R. W. Heath, "Low complexity hybrid precoding strategies for millimeter wave communication systems," *IEEE Transactions on Wireless Communications*, vol. 15, no. 12, pp. 8380–8393, 2016.

[37] F. Sohrabi and W. Yu, "Hybrid digital and analog beamforming design for large-scale antenna arrays," *IEEE Journal of Selected Topics in Signal Processing*, vol. 10, no. 3, pp. 501–513, 2016.

[38] S. Payami, M. Ghoraishi, and M. Dianati, "Hybrid beamforming for large antenna arrays with phase shifter selection," *IEEE Transactions on Wireless Communications*, vol. 15, no. 11, pp. 7258–7271, 2016.

[39] X. Zhai, Y. Cai, Q. Shi, M. Zhao, G. Y. Li, and B. Champagne, "Joint transceiver design with antenna selection for large-scale MU-MIMO mmWave systems," *IEEE Journal on Selected Areas in Communications*, vol. 35, no. 9, pp. 2085–2096, 2017.

[40] X. Yu, J. Shen, J. Zhang, and K. B. Letaief, "Alternating minimization algorithms for hybrid precoding in millimeter wave MIMO systems," *IEEE Journal of Selected Topics in Signal Processing*, vol. 10, no. 3, pp. 485–500, April 2016.

[41] A. Arora, C. G. Tsinos, B. S. M. R. Rao, S. Chatzinotas, and B. Ottersten, "Hybrid transceivers design for large-scale antenna arrays using majorization-

minimization algorithms," *IEEE Transactions on Signal Processing*, vol. 68, pp. 701–714, 2020.

[42] X. Qiao, Y. Zhang, M. Zhou, and L. Yang, "Alternating optimization based hybrid precoding strategies for millimeter wave MIMO systems," *IEEE Access*, vol. 8, pp. 113 078–113 089, 2020.

[43] J. Cong, T. Lin, and Y. Zhu, "Hybrid MMSE beamforming for multiuser millimeter-wave communication systems," *IEEE Communications Letters*, vol. 22, no. 11, pp. 2390–2393, 2018.

[44] T. Lin, J. Cong, Y. Zhu, J. Zhang, and K. Ben Letaief, "Hybrid beamforming for millimeter wave systems using the MMSE criterion," *IEEE Transactions on Communications*, vol. 67, no. 5, pp. 3693–3708, 2019.

[45] C. Feng, W. Shen, X. Gao, J. An, and L. Hanzo, "Dynamic hybrid precoding relying on twin- resolution phase shifters in millimeter- wave communication systems," *IEEE Transactions on Wireless Communications*, vol. 20, no. 2, pp. 812–826, 2021.

[46] T. M. Cover and J. A. Thomas, "Information theory and statistics," *Elements of information theory*, vol. 1, no. 1, pp. 279–335, 1991.

[47] E. Biglieri, R. Calderbank, A. Constantinides, A. Goldsmith, A. Paulraj, and H. V. Poor, *MIMO wireless communications*. Cambridge university press, 2007.

[48] B. Clerckx and C. Oestges, *MIMO wireless networks: channels, techniques and standards for multi-antenna, multi-user and multi-cell systems*. Academic Press, 2013.

[49] M. A. ElMossallamy, H. Zhang, L. Song, K. G. Seddik, Z. Han, and G. Y. Li, "Reconfigurable intelligent surfaces for wireless communications: Principles, challenges, and opportunities," *IEEE Transactions on Cognitive Communications and Networking*, vol. 6, no. 3, pp. 990–1002, 2020.

[50] P. Wang, J. Fang, L. Dai, and H. Li, "Joint transceiver and large intelligent surface design for massive MIMO mmwave systems," *IEEE Transactions on Wireless Communications*, vol. 20, no. 2, pp. 1052–1064, 2021.

[51] Q. Wu, S. Zhang, B. Zheng, C. You, and R. Zhang, "Intelligent reflecting surface-aided wireless communications: A tutorial," *IEEE Transactions on Communications*, vol. 69, no. 5, pp. 3313–3351, 2021.

[52] E. Bj"ørnson, O. "Øzdogan, and E. G. Larsson, "Reconfigurable intelligent surfaces: Three myths and two critical questions," *IEEE Communications Magazine*, vol. 58, no. 12, pp. 90–96, 2020.

[53] C. Pan, H. Ren, K. Wang, W. Xu, M. Elkashlan, A. Nallanathan, and L. Hanzo, "Multicell MIMO communications relying on intelligent reflecting surfaces," *IEEE Transactions on Wireless Communications*, vol. 19, no. 8, pp. 5218–5233, 2020.

[54] E. Basar, "Transmission through large intelligent surfaces: A new frontier in wireless communications," in *2019 European Conference on Networks and Communications (EuCNC)*, 2019, pp. 112–117.

[55] E. Basar, M. Di Renzo, J. De Rosny, M. Debbah, M.-S. Alouini, and R. Zhang, "Wireless communications through reconfigurable intelligent surfaces," *IEEE Access*, vol. 7, pp. 116 753–116 773, 2019.

[56] C. Liaskos, S. Nie, A. Tsioliaridou, A. Pitsillides, S. Ioannidis, and I. Akyildiz, "A new wireless communication paradigm through software-controlled metasurfaces," *IEEE Communications Magazine*, vol. 56, no. 9, pp. 162–169, 2018.

[57] M. D. Renzo, M. Debbah, D.-T. Phan-Huy, A. Zappone, M.-S. Alouini, C. Yuen, V. Sciancalepore, G. C. Alexandropoulos, J. Hoydis, H. Gacanin *et al.*, "Smart radio environments empowered by reconfigurable ai meta-surfaces: An idea whose time has come," *EURASIP Journal on Wireless Communications and Networking*, vol. 2019, no. 1, pp. 1–20, 2019.

[58] M. Di Renzo, K. Ntontin, J. Song, F. H. Danufane, X. Qian, F. Lazarakis, J. De Rosny, D.-T. Phan-Huy, O. Simeone, R. Zhang, M. Debbah, G. Lerosey, M. Fink, S. Tretyakov, and S. Shamai, "Reconfigurable intelligent surfaces vs. relaying: Differences, similarities, and performance comparison," *IEEE Open Journal of the Communications Society*, vol. 1, pp. 798–807, 2020.

[59] M. Di Renzo, A. Zappone, M. Debbah, M.-S. Alouini, C. Yuen, J. de Rosny, and S. Tretyakov, "Smart radio environments empowered by reconfigurable intelligent surfaces: How it works, state of research, and the road ahead," *IEEE Journal on Selected Areas in Communications*, vol. 38, no. 11, pp. 2450–2525, 2020.

[60] X. Yuan, Y.-J. A. Zhang, Y. Shi, W. Yan, and H. Liu, "Reconfigurable-intelligent-surface empowered wireless communications: Challenges and opportunities," *IEEE Wireless Communications*, vol. 28, no. 2, pp. 136–143, 2021.

[61] Q. Wu and R. Zhang, "Towards smart and reconfigurable environment: Intelligent reflecting surface aided wireless network," *IEEE Communications Magazine*, vol. 58, no. 1, pp. 106–112, 2020.

[62] B. Ning, Z. Chen, W. Chen, and J. Fang, "Beamforming optimization for intelligent reflecting surface assisted MIMO: A sum-path-gain maximization approach," *IEEE Wireless Communications Letters*, vol. 9, no. 7, pp. 1105–1109, 2020.

[63] P. Wang, J. Fang, X. Yuan, Z. Chen, and H. Li, "Intelligent reflecting surface-assisted millimeter wave communications: Joint active and passive precoding design," *IEEE Transactions on Vehicular Technology*, vol. 69, no. 12, pp. 14 960–14 973, 2020.

[64] H. Guo, Y.-C. Liang, J. Chen, and E. G. Larsson, "Weighted sum-rate maximization for reconfigurable intelligent surface aided wireless networks," *IEEE Transactions on Wireless Communications*, vol. 19, no. 5, pp. 3064–3076, 2020.

[65] Z. Zhang and L. Dai, "A joint precoding framework for wideband reconfigurable intelligent surface-aided cell-free network," *IEEE Transactions on Signal Processing*, vol. 69, pp. 4085–4101, 2021.

[66] S. Zhang and R. Zhang, "Capacity characterization for intelligent reflecting surface aided MIMO communication," *IEEE Journal on Selected Areas in Communications*, vol. 38, no. 8, pp. 1823–1838, 2020.

[67] H. Kasai, "Fast optimization algorithm on complex oblique manifold for hybrid precoding in millimeter wave mimo systems," in *2018 IEEE Global Conference on Signal and Information Processing (GlobalSIP)*, 2018, pp. 1266–1270.

[68] M.-M. Zhao, A. Liu, and R. Zhang, "Outage-constrained robust beamforming for intelligent reflecting surface aided wireless communication," *IEEE Transactions on Signal Processing*, vol. 69, pp. 1301–1316, 2021.

[69] R. Liu, M. Li, Q. Liu, and A. L. Swindlehurst, "Joint symbol-level precoding and reflecting designs for irs-enhanced mu-miso systems," *IEEE Transactions on Wireless Communications*, vol. 20, no. 2, pp. 798–811, 2021.

[70] H. Xie, F. Gao, and S. Jin, "An overview of low-rank channel estimation for massive mimo systems," *IEEE Access*, vol. 4, pp. 7313–7321, 2016.

[71] C. Qi, P. Dong, W. Ma, H. Zhang, Z. Zhang, and G. Y. Li, "Acquisition of channel state information for mmwave massive MIMO: Traditional and machine learning-based approaches," *Science China Information Sciences*, vol. 64, pp. 1–16, 2021.

[72] J. R. Hampton, *Channel estimation*. Cambridge University Press, 2013, p. 214–231.

[73] K. Hassan, M. Masarra, M. Zwingelstein, and I. Dayoub, "Channel estimation techniques for millimeter-wave communication systems: Achievements and challenges," *IEEE Open Journal of the Communications Society*, vol. 1, pp. 1336–1363, 2020.

[74] G. N. Reddy, C. Ravikumar, and A. Rajesh, "Literature review and research direction towards channel estimation and hybrid pre-coding in mmwave massive mimo communication systems," *Journal of Reliable Intelligent Environments*, pp. 1–20, 2022.

[75] V. Venkateswaran and R. Krishnan, "Hybrid analog and digital precoding: From practical RF system models to information theoretic bounds," in *2016 IEEE Globecom Workshops (GC Wkshps)*. IEEE, 2016, pp. 1–6.

[76] A. K. Papazafeiropoulos, G. K. Papageorgiou, O. Y. Kolawole, P. Kourtessis, S. Chatzinotas, J. M. Senior, M. Sellathurai, and T. Ratnarajah, "Towards the assessment of realistic hybrid precoding in millimeter wave mimo systems with hardware impairments," *IET Communications*, vol. 15, no. 12, pp. 1606–1619, 2021.

[77] Z. Chen, J. Tang, X. Y. Zhang, Q. Wu, G. Chen, and K.-K. Wong, "Robust hybrid beamforming design for multi-RIS assisted MIMO system with imperfect CSI," *IEEE Transactions on Wireless Communications*, 2022.

[78] F. Tariq, M. R. A. Khandaker, K.-K. Wong, M. A. Imran, M. Bennis, and M. Debbah, "A speculative study on 6G," *IEEE Wireless Communications*, vol. 27, no. 4, pp. 118–125, 2020.

[79] S. Boyd and L. Vandenberghe, *Convex Optimization*. Cambridge University Press, 2004.

[80] I. Waldspurger, A. d'Aspremont, and S. Mallat, "Phase recovery, MaxCut and complex semidefinite programming," *Math. Program.*, vol. 149, no. 1-2, pp. 47–81, 2015. [Online]. Available: https://doi.org/10.1007/s10107-013-0738-9

[81] Z. Wen, D. Goldfarb, and K. Scheinberg, "Block coordinate descent methods for semidefinite programming," in *Handbook on semidefinite, conic and polynomial optimization*. Springer, 2012, pp. 533–564.

[82] H. Rutishauser, "Computational aspects of F. L. Bauer's simultaneous iteration method." *Numerische Mathematik*, vol. 13, pp. 4–13, 1969. [Online].

Available: https://link.springer.com/article/10.1007/BF02165269

[83] Björck, Åke, "Numerics of Gram-Schmidt orthogonalization," *Linear Algebra and its Applications*, vol. 197-198, pp. 297–316, 1994. [Online]. Available: https://www.sciencedirect.com/science/article/pii/0024379594904936

[84] J. Lee and Y. H. Lee, "AF relaying for millimeter wave communication systems with hybrid rf/baseband mimo processing," in *2014 IEEE International Conference on Communications (ICC)*, 2014, pp. 5838–5842.

[85] G. H. Golub and C. F. Van Loan, *Matrix Computations*, 4th ed. The Johns Hopkins University Press, 2013.

[86] L. Dai, X. Gao, J. Quan, S. Han, and C. I, "Near-optimal hybrid analog and digital precoding for downlink mmwave massive MIMO systems," in *2015 IEEE International Conference on Communications (ICC)*, 2015, pp. 1334–1339.

[87] D. Zhang, Y. Wang, X. Li, and W. Xiang, "Hybridly connected structure for hybrid beamforming in mmwave massive MIMO systems," *IEEE Transactions on Communications*, vol. 66, no. 2, pp. 662–674, 2018.

[88] C. Feng, W. Shen, J. An, and L. Hanzo, "Joint hybrid and passive RIS-assisted beamforming for mmwave MIMO systems relying on dynamically configured subarrays," *IEEE Internet of Things Journal*, vol. 9, no. 15, pp. 13 913–13 926, 2022.

[89] ——, "Joint hybrid and passive RIS-assisted beamforming for mmwave MIMO systems relying on dynamically configured subarrays," *IEEE Internet of Things Journal*, vol. 9, no. 15, pp. 13 913–13 926, 2022.

[90] P. Netrapalli, P. Jain, and S. Sanghavi, "Phase retrieval using alternating minimization," *IEEE Transactions on Signal Processing*, vol. 63, no. 18, pp. 4814–4826, 2015.

[91] T. Rappaport, R. Heath, R. Daniels, and J. Murdock, *Millimeter wave wireless communications*. Prentice Hall, 2015.

[92] M. Sadek, A. Tarighat, and A. H. Sayed, "A leakage-based precoding scheme for downlink multi-user MIMO channels," *IEEE Transactions on Wireless Communications*, vol. 6, no. 5, pp. 1711–1721, May 2007.

[93] M. Schubert and H. Boche, "Solution of the multiuser downlink beamforming problem with individual SINR constraints," *IEEE Transactions on Vehicular Technology*, vol. 53, no. 1, pp. 18–28, Jan 2004.

[94] O. E. Ayach, R. W. Heath, S. Abu-Surra, S. Rajagopal, and Z. Pi, "The capacity optimality of beam steering in large millimeter wave MIMO systems," in *2012 IEEE 13th International Workshop on Signal Processing Advances in Wireless Communications (SPAWC)*, June 2012, pp. 100–104.

[95] C. Peel, B. Hochwald, and A. Swindlehurst, "A vector-perturbation technique for near-capacity multiantenna multiuser communication—part I: Channel inversion and regularization," *IEEE Transactions on Communications*, vol. 53, no. 1, pp. 195–202, 2005.

[96] V. Stankovic and M. Haardt, "Generalized design of multi-user MIMO precoding matrices," *IEEE Transactions on Wireless Communications*, vol. 7, no. 3, pp. 953–961, 2008.

[97] M. Joham, W. Utschick, and J. Nossek, "Linear transmit processing in MIMO communications systems," *IEEE Transactions on Signal Processing*, vol. 53, no. 8, pp. 2700–2712, 2005.

[98] J. Brehmer, G. Dietl, M. Joham, and W. Utschick, "Reduced-complexity linear and nonlinear precoding for frequency-selective MIMO channels," in *IEEE 60th Vehicular Technology Conference, 2004. VTC2004-Fall. 2004*, vol. 5, 2004, pp. 3684–3688 Vol. 5.

[99] X.-D. Zhang, *Matrix analysis and applications*. Cambridge University Press, 2017.

[100] L. Vandenberghe and S. Boyd, "Semidefinite programming," *SIAM Review*, vol. 38, no. 1, pp. 49–95, 1996. [Online]. Available:

https://doi.org/10.1137/1038003

[101] Z.-q. Luo, W.-k. Ma, A. M.-c. So, Y. Ye, and S. Zhang, "Semidefinite relaxation of quadratic optimization problems," *IEEE Signal Processing Magazine*, vol. 27, no. 3, pp. 20–34, 2010.

[102] M. R. Akdeniz, Y. Liu, M. K. Samimi, S. Sun, S. Rangan, T. S. Rappaport, and E. Erkip, "Millimeter wave channel modeling and cellular capacity evaluation," *IEEE Journal on Selected Areas in Communications*, vol. 32, no. 6, pp. 1164–1179, 2014.

[103] C. Huang, A. Zappone, G. C. Alexandropoulos, M. Debbah, and C. Yuen, "Reconfigurable intelligent surfaces for energy efficiency in wireless communication," *IEEE Transactions on Wireless Communications*, vol. 18, no. 8, pp. 4157–4170, 2019.

[104] Q. Wu and R. Zhang, "Beamforming optimization for wireless network aided by intelligent reflecting surface with discrete phase shifts," *IEEE Transactions on Communications*, vol. 68, no. 3, pp. 1838–1851, 2020.

[105] Z. Yang, M. Chen, W. Saad, W. Xu, M. Shikh-Bahaei, H. V. Poor, and S. Cui, "Energy-efficient wireless communications with distributed reconfigurable intelligent surfaces," *IEEE Transactions on Wireless Communications*, vol. 21, no. 1, pp. 665–679, 2022.

[106] I. Csiszár, "Information geonetry and alternating minimization procedures," *Statistics and decisions*, vol. 1, pp. 205–237, 1984.

[107] J. C. Bezdek and R. J. Hathaway, "Some notes on alternating optimization," in *Advances in Soft Computing — AFSS 2002*, N. R. Pal and M. Sugeno, Eds. Berlin, Heidelberg: Springer Berlin Heidelberg, 2002, pp. 288–300.

[108] A. Zappone, E. Jorswieck *et al.*, "Energy efficiency in wireless networks via fractional programming theory," *Foundations and Trends in Communications and Information Theory*, vol. 11, no. 3-4, pp. 185–396, 2015.

[109] H. W. Kuhn and A. W. Tucker, *Nonlinear Programming*. Basel: Springer Basel, 2014, pp. 247–258.

[110] M.-M. Zhao, Y. Cai, M.-J. Zhao, Y. Xu, and L. Hanzo, "Robust joint hybrid analog-digital transceiver design for full-duplex mmWave multicell systems," *IEEE Transactions on Communications*, vol. 68, no. 8, pp. 4788–4802, 2020.

[111] X. Lu, W. Yang, X. Guan, Q. Wu, and Y. Cai, "Robust and secure beamforming for intelligent reflecting surface aided mmwave MISO systems," *IEEE Wireless Communications Letters*, vol. 9, no. 12, pp. 2068–2072, 2020.

[112] J. Qiao and M.-S. Alouini, "Secure transmission for intelligent reflecting surface-assisted mmWave and terahertz systems," *IEEE Wireless Communications Letters*, vol. 9, no. 10, pp. 1743–1747, 2020.

[113] J. Qiao, C. Zhang, A. Dong, J. Bian, and M.-S. Alouini, "Securing intelligent reflecting surface assisted terahertz systems," *IEEE Transactions on Vehicular Technology*, vol. 71, no. 8, pp. 8519–8533, 2022.

[114] H. Elayan, O. Amin, R. M. Shubair, and M.-S. Alouini, "Terahertz communication: The opportunities of wireless technology beyond 5G," in *2018 International Conference on Advanced Communication Technologies and Networking (CommNet)*, 2018, pp. 1–5.

[115] H.-J. Song and T. Nagatsuma, "Present and future of terahertz communications," *IEEE Transactions on Terahertz Science and Technology*, vol. 1, no. 1, pp. 256–263, 2011.

[116] L. Yan, C. Han, and J. Yuan, "A dynamic array-of-subarrays architecture and hybrid precoding algorithms for terahertz wireless communications," *IEEE Journal on Selected Areas in Communications*, vol. 38, no. 9, pp. 2041–2056, 2020.

[117] ——, "Hybrid precoding for 6G terahertz communications: Performance evaluation and open problems," in *2020 2nd 6G Wireless Summit (6G SUMMIT)*, 2020, pp. 1–5.

[118] H. Sarieddeen, M.-S. Alouini, and T. Y. Al-Naffouri, "An overview of signal processing techniques for terahertz communications," *Proceedings of the IEEE*, vol. 109, no. 10, pp. 1628–1665, 2021.

[119] G. Hardy, J. Littlewood, and G. Pólya, *Inequalities*. Cambridge University Press, 1988.